Condensin and Chromatin Mediated X Chromosome Architecture in *Caenorhabditis elegans*

by

Alyssa C. Lau

A dissertation submitted in partial fulfillment
of the requirements for the degree of
Doctor of Philosophy
(Molecular, Cellular, and Developmental Biology)
in The University of Michigan
2016

Doctoral Committee:

Associate Professor Györgyi Csankovszki, Chair
Assistant Professor Laura Buttitta
Professor Kenneth M. Cadigan
Assistant Professor Sundeep Kalantry

This work is dedicated

to my family.

ACKNOWLEDGEMENTS

I would like to take this opportunity to first and foremost thank my mentor Dr. Györgyi Csankovszki, who has always been extremely encouraging and supportive. All of her training and guidance has allowed me to grow as a scientist and has prepared me for the next stage of my career. With her support, I have also had the opportunity to pursue a Master's degree in Bioinformatics and attend and present at scientific meetings. Her dedication to science, her students, and her family has been inspiring, and has motivated me throughout my Ph.D. career. I would also like to thank my committee members Dr. Ken Cadigan, Dr. Laura Buttitta, and Dr. Sundeep Kalantry. They have provided me with much kindness and their time, insights, and suggestions have helped develop my research.

Next, I would like to thank all the members of the lab for their invaluable help over the years. They have made my time in Michigan a fun and less stressful one. I especially want to thank, Margarita Sifuentes, my fellow Graduate Student and friend, when I joined the lab she made me feel welcomed and she has always made the lab environment fun and exciting. I want to also thank our lab manager and my friend, Betsy Brouhard. She is hard working, extremely organized, and always very helpful and has been a great support. Thank you to all the other members of the lab past and present, Dr. Jianhao Jiang, Jessica Trombley, Mike Davis, Elaine Otchere, Netta Golenberg,

Anna Cacciaglia and Dr. Laura Custer. Also I am glad I had the privilege to mentor such great undergrads, Jennifer Knister and Kevin Zhu. Additionally thanks to all the members of the Buttitta, Cadigan, Raymond, and Wierzbicki labs for borrowed regents and scientific input.

Finally, I could not have made it to where I am now without the love and support of my friends and family. Thanks to my long time college friends who made cell biology and biochemistry lectures enjoyable and exciting. Thanks to my loving boyfriend, Christian Blanke, for always lifting me up and supporting my dream of getting a Ph.D. even when I had to work late or go into lab on the weekends. Most of all I want to thank my caring Mom, she has been my biggest fan and I cannot thank her enough. She has always been there to support me, encourage me, and to push me to my fullest. She really is the greatest, most loving, and crazy (in a good way) mom a person could ask for. I would like to thank John, for all the support and encouragement. I also want to thank my Dad, he always told me to do what I love and he's always believed in me. I can't forget my sister, Theresa, although she's my younger sister I truly look up to her and I know she is going to be a great PT. I am so lucky to have her as a sister and best friend. And thank you to my Grandmother, who is so proud of me no matter what. Lastly, thanks to Juniper and Summer for always welcoming me with a wagging tail whenever I come home from work!

TABLE OF CONTENTS

LIST OF FIGURES

LIST OF TABLES

CHAPTER 1

Introduction

Some elements and ideas described in this chapter were published as Lau et al. (2015) in Frontiers in Genetics as “Condensin-mediated chromosome organization and gene regulation.” I wrote the manuscript and created all illustrations.

Sex determination and dosage compensation

Whether an animal becomes a male, a female, or a hermaphrodite has been studied for hundreds of years. In 335 B.C.E., Aristotle proposed that sex was determined by the amount of heat generated from the male partner, the more heat the greater chance of a male offspring [1]. Until the twentieth century, environmental factors such as temperature and nutrition were believed to be important in determining sex. These theories of sex determination remained until the discovery of sex chromosomes, in the early 1900s [2]. Studies analyzing male and female insect chromosomes uncovered that the female sex has XX sex chromosomes and the male sex has XY or XO chromosomes [3,4]. Aristotle’s theory was partially correct; in the case of some reptiles the temperature after fertilization determines the sex of the embryo [5]. However, analysis of additional species over the years has revealed that for most animals sex is determined by chromosomal differences.

Many species utilize a chromosome-based mechanism of sex determination. Males and females/hermaphrodites have chromosomal differences illustrated in the XX-XY, XX-XO, ZZ-ZW, or haploidploidy systems. Mammals, worms, and some insects are governed by the XX-XY or XX-XO system, in which the males are heterogametic (XY/XO) and females are homogametic (XX) [6,7]. Birds have ZZ-ZW chromosomes, and in this case females are heterogametic (ZW) and males are homogametic (ZZ) [6,7]. In other insects, such as bees and ants, the haploidploidy system is utilized. In this system males come from unfertilized eggs and are haploid, while the females come from fertilized eggs and are diploid [8]. These chromosome-based mechanisms rely on either a sex chromosome-linked gene or a chromosome counting mechanism to determine sex. In mammals, it is the presence or absence of the Y chromosome, specifically the Y-linked *SRY* gene, which triggers male development [9]. In birds two doses of the Z-linked gene DMRT1 is required for male development, however incomplete knockdown of DMRT1 does not abrogate male sexual development [10]. In other species there are chromosome-counting mechanisms whereby the cell can sense chromosome copy number based on one or more sex chromosome signal elements [11,12]. Additionally, some species use the ratio of the number of X chromosomes to the number of sets of autosomes to determine sex [12]. However, regardless of the exact mechanism, all chromosome-based mechanisms entail a difference in sex chromosome number between the males and females/hermaphrodites.

The chromosomal differences if left uncorrected puts one sex at a selective disadvantage. In addition to the in difference in sex chromosome number, there is an

imbalance between X-linked genes expression and autosomal expression within the heterogametic sex. This imbalance creates a natural aneuploidy and chromosomal aneuploidies are often not tolerated [13]. Therefore Ohno hypothesized that sex chromosome gene expression between the sexes must be balanced, as well as X to autosomal expression within a sex [14]. The mechanism that has evolved to correct this sex-linked gene expression imbalance is known as dosage compensation. Dosage compensation mechanisms are diverse between species. These strategies have been widely studied in the fruit fly *Drosophila melanogaster*, mammals, and the worm *Caenorhabditis elegans* (Figure 1.1). In fly dosage compensation, the single male X gets unregulated two fold. This process balances the X and autosomal expression within males and X-linked gene expression between the sexes [15,16]. Although highly debated, evidence suggests that in mammals and *C. elegans* upregulation of the X occurs in both males and females/hermaphrodites [17-22]. This upregulation balances X and autosomal expression in males however causes X hyperactivation in females/hermaphrodites. To prevent this X overexpression in females/hermaphrodites, one X is inactivated in mammalian females [23-25], while both X chromosomes in hermaphrodite *C. elegans* are downregulated two-fold [26,27]. In the next sections, I will briefly describe the dosage compensation strategies in *D. melanogaster*, mammals, and *C. elegans*.

X upregulation in *Drosophila melanogaster*

Drosophila dosage compensation is achieved by the male specific lethal (MSL) complex [28,29]. The MSL complex binds to the male X chromosome, concentrates

MOF acetyltransferase activity, and leads to increased H4K16ac on the hyperactive X (Figure 1.2) [28-30]. The MSL complex is composed of the proteins MSL1 (male-specific lethal 1), MSL2 (male-specific 2), MSL3 (male-specific 3), MLE (maleless), MOF (males absent on the first) and the non-coding RNAs roX1 (RNA on the X 1) and roX2 (RNA on the X 2) [31]. This complex binds and transcriptionally hyperactivates the single male X chromosome by two-fold [15,16]. The targeting of the MSL complex to the X chromosome starts with MSL1, a scaffolding protein, and MSL2, a RING finger protein, which bind to GA rich high-affinity sites known as chromatin entry sites (CES) [32-36]. MSL1 and MSL2 provide the scaffold for direct binding and recruitment of the remaining members of the MSL complex. The PEHE and C-terminal domains of the MSL1/MSL2 scaffold associate with the chromodomain protein MSL3 and histone acetyltransferase MOF [37,38]. The RNA helicase MLE associates with the other MSL subunits by binding and incorporating the non-coding roX RNAs [39]. Additionally, the two roX loci act as chromatin entry sites [40]. Once bound to the CES sites the complex spreads along the X chromosome, through the actions of both MOF and MSL3 [33,41].

A key MSL member that hyperacetylates the male X chromosome is the MYST family histone acetyltransferase MOF [42]. MOF specifically acetylates H4K16, which is enriched on the male X [42]. MOF is not only required to acetylate histone 4 lysine 16, its activity is also required for the interaction and recruitment of MSL1 and MSL3 [38]. In *Drosophila*, immunofluorescence and genome-wide mapping has shown that the distribution of H4K16ac is similar to the binding patterns of the MSL, associating preferentially with the X chromosome in males [43,44]. The binding profiles of H4K16ac

and MSL are unique, unlike many other factors that bind primarily at promoters to regulate gene expression; H4K16ac and MSL are enriched over active genes on the male X chromosome and accumulate towards the 3' end of coding regions [44-47]. These genes are in a transcriptionally active state and blocking transcription can severely reduce MSL binding to its target genes, suggesting that transcription triggers MSL activity on the X chromosome [48]. In addition to 3' end binding, MOF is detected at many promoters on the X, whereas on autosomes and in females MOF binds primarily at promoters and is depleted at the 3' end. A similar but broader binding pattern is observed with H4K16ac [46]. Therefore, in addition to its dosage compensation activity, MOF is thought to act as a genome-wide regulator of gene expression, while over members of the MSL complex only function in dosage compensation activity.

The fly MSL complex affects the three-dimensional structure of the male X chromosome. Biophysical studies support the idea that the acetylation of H4K16 loosens the nucleosome interactions, which leads to a more open nucleosome fiber, allowing for more accessible DNA [49,50]. Additionally the MSL complex has been shown to reduce the levels of negative supercoiling [51]. Both these activities cause chromatin decondensation on the male X chromosome, and facilitate transcription.

X chromosome hyperactivation and inactivation in mammals

In mammals, dosage compensation is thought to occur in two steps. It has been proposed that one mechanism upregulates expression 2-fold on the X chromosomes of both sexes to compensate for autosomal expression [14], and another mechanism

equalizes X-linked gene expression between the sexes by silencing one X in mammalian females [52]. Although evidence for X upregulation in mammals is relatively recent, the mechanism is well supported by microarray analysis and expression analysis of individual genes [17,18,20,22,53,54]. Microarray analysis in mammalian tissues shows that in both sexes X-linked gene expression is not at half the average autosomal expression, but rather expressed at approximately the same levels as autosomal genes [20,54]. Additionally, when considering the effects of the skewed gene content and regulation of the X chromosome, by excluding silent genes on the X chromosome, RNA-seq data supports the upregulation of expressed genes in mammals [18]. X upregulation is also evident when examining allele-specific ChIP-seq for RNA polymerase II (Pol II) and active chromatin marks along with RNA-seq data. There is enrichment of the active chromatin marks on the X chromosome and the relationship between active chromatin states and transcription is non-linear, implying that small changes in chromatin states can produce large changes in transcription or vise versa. This relationship is not X-specific suggesting that the chromatin processes required for X upregulation are used genome wide [22]. Similar to fly X upregulation, recent data has indicated that MOF-mediated H4K16ac may enhance transcription initiation in mammalian X upregulation. The depletion of MOF or MSL in mouse ES cells causes a decrease in expression of a group of X-linked genes and induces the long non-coding RNA *Xist* (X inactivation specific transcript). However instead of being distributed predominantly at the 3' end of X-linked genes, MOF and H4K16ac are enriched at the 5'

end [17]. This data supports a conserved role for the MSL complex to upregulate X-linked gene expression.

To prevent X hyperactivation in mammalian females and to balance transcription from the single X in males, one of the two X chromosome is inactivated [52]. The process of X chromosome inactivation (XCI) is more fully understood than the X upregulation mechanism. Similar to fly dosage compensation, X inactivation involves the initiation and spreading of inactivation along one X chromosome. X inactivation is initiated at a single site, the X inactivation center (XIC) [55]. X inactivation is achieved by the long non-coding RNA *Xist* (X inactivation specific transcript), which is expressed from the XIC [56,57]. In mice, the non-coding RNA *Tsix*, also located within the XIC, overlaps with *Xist* but is transcribed in the antisense direction. *Tsix* directly competes with *Xist* to repress *Xist* accumulation on the active X (Xa) [58]. After differentiation, *Xist* RNA is expressed from both X chromosomes but accumulates more on one X. Eventually *Xist* is expressed only from one X known as the inactive X chromosome (Xi), and coats this chromosome in *cis* [57,59,60]. This spreading of the X is followed by the exclusion of RNA Pol II and the recruitment of the Polycomb Repressor Complex 2 (PRC2) and PRC1 and mutations in PRC2 causes the derepression of X-linked genes [61-63]. PRC2 activity results in an accumulation H3K27me3 on the Xi, while PRC1 monoubiquitylates H2A on the Xi [64,65]. In addition to H3K27me3 and H2AUb1, the Xi possesses high levels of H4K20me1 and other repressive chromatin marks, while lacking acetylated forms of histone H4 [66,67]. Later on, the histone variant marcoH2A

is enriched [68] and DNA methylation is distributed on promoters of X-linked genes for long-term maintenance of the silent state (Figure 1.3) [69-71].

The heterochromatin marks on the Xi are thought to alter chromatin structure thereby impeding transcription. Fluorescence *in situ* hybridization (FISH) studies have revealed that silenced loci colocalize with H3K27me3 and are found within an internal, densely packed region of the Xi, lacking transcription factors, whereas genes that escape inactivation are found on the periphery of the Xi [61]. Studies have also shown that the Xa and Xi chromosomes have distinct shape and surface structure, with the Xi having a larger surface area to volume ratio [72,73]. *Xist* coating is not defined by specific sequences; instead by its proximity to the *Xist* transcription locus, suggesting that Xist spreads to new sites through its ability to modify the three-dimensional conformation of the X chromosome [74]. Lastly, in interphase the Xi is usually found close to the nuclear periphery, which suggests the X inactivation results in the formation of a repressive nuclear compartment which may contribute to stable gene silencing [61].

Up and downregulation of *C. elegans* X chromosomes

As in mammals, dosage compensation in *C. elegans* is believed to involve two mechanisms, an upregulation and a downregulation step [18,19,27]. In contrast to mammals, worms do not inactivate one X in hermaphrodites but instead downregulate both X chromosomes by two-fold [27]. The mechanism of X upregulation is currently unknown, but recently experimental evidence has emerged to support this hypothesis. Gene expression analysis has shown that the average gene expression level from a single male X is comparable to the average autosomal gene expression levels [18,19].

However, a recent study on different *Caenorhabditis* species found evidence both for and against the X upregulation hypothesis. When excluding genes repressed by X chromosome germline silencing, a process unrelated to dosage compensation, X and autosomal gene expression levels were equivalent in both males and females/hermaphrodites. However, when analyzing one-to-one orthologs located on the X and the autosome of the different species, the autosomal ortholog was more highly expressed compared to the X ortholog, arguing against X upregulation [75]. Global run on analysis (GRO-seq) of active transcription in wild type *C. elegans* hermaphrodites has also provided supporting evidence for X upregulation. In wild type hermaphrodite embryos, the average X-linked genes have engaged RNA polymerase II levels comparable to autosomal genes, implying that hermaphrodites are subjected to both upregulation and downregulation. In hermaphrodites lacking the downregulation mechanism, the X chromosomes have higher levels of engaged RNA Pol II compared to autosomes, suggesting that in the absence of X chromosome downregulation, the X chromosomes are indeed highly expressed [76]. A recent study proposed that the single male X chromosome interacts with nuclear pore proteins to achieve upregulation, however gene expression analysis was not performed [77]. Overall, evidence suggests that in the absence of the DCC on average, X-linked genes in *C. elegans* are expressed at a higher level than autosomal genes. In Chapter 4, I will provide further evidence and a possible mechanism for X upregulation in *C. elegans*.

The mechanism of X chromosome downregulation is better understood. To downregulate transcription by two, a complex of proteins, known as the dosage

compensation complex (DCC), binds along both hermaphrodite X chromosomes (Figure 1.4A) [27]. The DCC proteins were first discovered in genetic screens searching for sex-specific mutations [78-84], while additional proteins were found by biochemical interactions with the known DCC proteins [85,86]. The DCC contains two sub complexes, a five-subunit condensin complex, condensin I^{DC}, and an additional subcomplex containing at least another five associated proteins, made primarily of sex determination and dosage compensation (SDC) genes (Figure 1.4B) [26]. Condensin complexes function in mitosis and meiosis to segregate and compact chromosome [87]. Although similar to canonical condensins, condensin I^{DC} differs both in chromosome-specificity and cell cycle specificity [85,88]. Due to the close homology of condensin I^{DC} and the canonical condensins it has been hypothesized that DCC activity results in interphase X chromosome compaction. My work in Chapter 2 provides the first experimental evidence supporting this long standing hypothesis, that condensin I^{DC} is compacting X chromosomes and performs dosage compensation through functions shared wih the mitotic and meiotic condensins.

Similar to flies and mammals, the loading and spreading of the DCC is thought to occur by a two-step process. The additional subcomplex, specifically SDC-2, DPY-30, and SDC-3, is responsible for DCC binding specifically to the X chromosomes [89-91]. All DCC proteins are maternally loaded into the oocyte, except for SDC-2, which is expressed only in the hermaphrodite zygote [90,92,93]. SDC-2 is the first DCC protein to be expressed and bind the X; this initiates the assembly of all other DCC proteins, around the 30-cell stage [90]. In addition to SDC-2, SDC-3 and DPY-30 are required for

normal DCC binding on X [94,95]. Much like MSL binding to chromatin entry sites, the *C. elegans* DCC binds to primary binding sites, termed recruitment element on X (*rex*) sites which are partially defined by a 12 bp DNA sequence motif known as motif enriched on X (MEX). Then the DCC spreads in *cis* across the X chromosome to sites unable to recruit the DCC outside their native chromosome state; these sites are known as dependent on X (*dox*) sites (Figure 1.4C) [91,96]. However, not all *rex* sites contain the MEX motif and there are occurrences of the MEX motif on the X chromosome that are not bound by the DCC [96,97]. Thus, *rex* sites alone do not fully explain DCC targeting, and more recent studies have shown that changes in chromatin also contribute to DCC binding. It has been found that in order to restrict DCC binding to the X chromosome the histone variant HTZ-1 (H2A.Z) is required. In *htz-1* mutants, the DCC no longer localizes to only the X and spreads to autosomes [98]. In addition the sumoylation of SDC-3, and DPY-27 and DPY-28 (condensin I^{DC} subunits) are required for the stable interactions between the X targeting proteins and other DCC proteins and therefore overall DCC binding [99]. In Chapter 5, I discuss the respective contribution histone acetyltransferases have on DCC recruitment to the X chromosome.

How the DCC downregulates gene expression is not fully understood. However DCC mediated changes in chromatin structure can provide some insight. The dosage compensated X chromosome is enriched for H4K20me1 [100,101] and is depleted for H4K16ac compared to autosomes [101]. In addition to requiring the DCC, the enrichment of H4K20me1 requires the activities of the histone methyltransferases SET-1 and SET-4 [100,101], while the depletion of H4K16ac requires the histone

deacetylase SIR-2.1 as well as SET-1 and SET-4 [101]. This indicates that H4K20me1 levels influence H4K16ac levels in the context of dosage compensation. These results suggest that similar to flies and mammals, changes in chromatin structure play a large role in *C. elegans* dosage compensation.

Condensin-mediated chromosome organization and gene regulation

It has been long hypothesized that DCC activity results in interphase X chromosome compaction. My work is consistent with this long standing hypothesis suggesting that dosage compensated X chromosomes maintain some characteristics associated with condensed mitotic chromosomes. To provide a foundation for understanding how condensins function, I will focus on our current understanding of condensins' biological functions and molecular mechanisms that enable them to achieve both mitotic chromosome compaction which leads to gene repression.

Condensin complexes

Condensin complexes are highly conserved five subunit complexes essential for chromosome compaction and segregation in mitosis and meiosis [87]. While yeast has one complex, higher eukaryotes have two, condensins I and II. They consist of a pair of SMC2 and SMC4 subunits belonging to the SMC (structural maintenance of chromosomes) family of chromosomal ATPases and three unique CAP (chromosome-associated polypeptide) proteins. Condensin I contains CAP-D2, CAP-G, and CAP-H, while condensin II contains CAP-D3, CAP-G2, and CAP-H2 [102-104]. Uniquely, *C. elegans* has three condensin complexes, condensins I, II and an additional complex, condensin I^{DC}, which contributes exclusively to dosage compensation

[85,86,93,105,106] (Figure 1.5). Interestingly, condensin I^{DC} differs from condensin I complex by only one subunit: DPY-27 replaces SMC-4 [85,88]. Unlike condensins I and II, which compact and segregate all mitotic and meiotic chromosomes, condensin I^{DC} is X-specific resulting in gene repression in hermaphrodites. Due to the similarity of condensin I and I^{DC}, similar mechanisms have long been hypothesized to mediate chromosome compaction and dosage compensation [105].

Mitotic and meiotic defects in condensin mutants or knockdowns

In higher eukaryotes condensins I and II have different spatial and temporal localization patterns. Condensin I is cytoplasmic in interphase and accesses chromosomes only after nuclear envelope breakdown (NEBD) in prometaphase, while condensin II is predominantly nuclear and binds chromosomes as soon as condensation begins in prophase [103,107-110]. This suggests that chromosome condensation may occur in two-steps, first with condensin II in prophase and then with condensin I after NEBD. An exception is mouse embryonic stem cells, where condensin I is nuclear during interphase [111]. Furthermore, the global and regional localization of condensins I and II on mitotic chromosomes are different. In monocentric organisms, condensins I and II have non-overlapping distributions within the axis of each sister-chromatid arm, with condensin II enriched at the centromeres [102-104]. Similar differences were also found in *C. elegans*, a holocentric organism, in which microtubule attachment sites are scattered throughout the entire length of chromosomes. In *C. elegans*, condensin I associates with mitotic chromosomes in a diffuse discontinuous pattern, while condensin II is enriched at centromeres [85,107]. Differences in spatial

and temporal dynamics of condensins I and II are also present during meiosis ([85,107,112] Recent studies explored the genome-wide distribution of condensin complexes at high resolution. These studies have uncovered both unique and similar binding sites of condensins I and II [113-115].

Although the two mitotic condensins are structurally similar, this difference in localization suggests that they may play distinct roles in chromosome organization. Consistent with this idea, the depletion of condensin I or II alone results in distinct chromosomal defects, while the depletion of both condensins leads to more severe defects [102-104]. Condensin I facilitates lateral compaction of mitotic chromosomes, whereas condensin II primarily contributes to axial compaction [102,104,110,116]. The roles the two condensins play in mitosis varies among different eukaryotic species. For example, in *Xenopus laevis*, *S. pombe* and *S. cerevisiae*, condensin is required for mitotic chromosome condensation and mechanical stability [108,109,117-119]. Condensins also play critical roles in meiotic chromosome compaction and segregation [112,120]. During *C. elegans* meiosis, depletion of condensin I or II leads to an expansion of chromosome axis [88]. A study using *Xenopus laevis* egg extracts showed that a critical determinant of chromatid shape is the relative ratio of condensins I and II [110]. In other organisms, such as mammals and worms, condensin II plays a primary role in prophase condensation [85,102,121]. Interestingly, when both condensins are depleted in *Drosophila*, worms, mammals, and chicken DT40 cells, the primary defect appears to be anaphase chromatin bridging, rather than chromosome condensation [87]. This suggests that other factors may contribute to mitotic chromosome

condensation in addition to condensin. Because condensin is depleted throughout the cell cycle in these experiments, is it is difficult to differentiate between mitotic and interphase functions of condensins. The effects of the activities of condensin in mitosis may persist in interphase and vice versa.

Interphase defects in condensin mutants or knockdowns

Emerging evidence suggests that condensin complexes also contribute to a variety of interphase functions. It is believed that condensin II, rather than condensin I, plays a primary role in interphase, since condensin II is nuclear throughout the cell cycle, while condensin I is cytoplasmic in interphase [102,103,107,108,110]. In *Drosophila* ovarian nurse cells, condensin II disassembles polytene chromosomes into unpaired homologous chromosomes. This unpairing activity leads to interphase chromosome compaction [122-124]. In *Drosophila* cell lines, condensin-mediated interphase condensation is normally limited by the SCF^{Slimb} ubiquitin ligase. The condensin II subunit CAP-H2 is a Slimb target for ubiquitin-mediated degradation. Degradation of CAP-H2 inactivates condensin II, thereby preventing interphase chromatin reorganization. Inhibition of SCF^{Slimb} leads to CAP-H2 stabilization, resulting in chromosome unpairing and nuclear structural abnormalities [125]. This suggests that in interphase, condensin II activity is suppressed in order to prevent chromosome condensation and changes in nuclear organization. In addition, condensin II also regulates chromosome territory formation in multiple cell types. This conclusion is based on the finding that CAP-H2 promotes axial compaction and proper compartmentalization of the interphase nucleus into chromosome territories in both nurse cells and salivary

glands [126]. These findings suggest that the interphase function of condensin II is similar to its role in axial compaction of mitotic chromosomes.

Condensin subunits also play a role in regulation of cell-type specific gene expression. In mice, chromosome compaction by condensin II is required for T-cell development and maintenance of the quiescent state. Mutations in the condensin II subunit kleisin-β (CAP-H2) lead to open chromatin configuration and upregulation of normally silenced genes. After T-cell activation, chromatin decondenses and transcription is upregulated [127]. Similarly, murine CAP-G2 represses transcription during erythroid cell differentiation. During erythroid cell maturation nuclei gradually condense, mediated by condensin [128]. Condensin is also required for higher-order chromatin compaction and viability in ES cells. [111].

Yeast condensin has also been shown to play a role in interphase chromatin organization and RNA polymerase III-transcribed gene clustering. In budding and fission yeast, the three-dimensional organization of the genome is facilitated in part by condensin-mediated localization of RNA-polymerase III genes within the nucleus [129]. In budding yeast, tRNA genes are clustered at the nucleolus in a condensin-dependent manner. Mutations in yeast condensin subunits cause tRNA gene positioning defects and partially inhibit tRNA gene-mediated silencing [130], illustrating another connection between condensin-mediated genome organization and gene expression.

In the above examples, condensin either affected the entire genome, or a subset of genes scattered on different chromosomes. By contrast, my work has showed that in *C. elegans*, condensin I^{DC} causes chromosome-specific changes. Consistent with a role

in chromosome condensation, *C. elegans* condensin I^{DC} mediates compaction of dosage compensated X chromosomes in interphase. Condensin I^{DC}-bound X chromosomes are more compact than expected by DNA content, whereas mutations or depletions of condensin I^{DC} result in decompaction of X chromosome territories (These data will be discussed thoroughly in Chapter 2 [131]). These results are consistent with the model that reduction of X-linked gene expression occurs as a result of condensin I^{DC}-mediated changes in chromatin structure. However whether this condensation is a cause or consequence of transcriptional repression is unknown.

Condensin and chromatin mediated chromosome compaction

In addition to condensin-mediated condensation, histone modifications also influence chromatin compaction during mitosis and the structure of *C. elegans* dosage compensated X chromosomes. The similarity of chromatin modifications between mitotic chromosome and dosage compensated X chromosomes of *C. elegans* is consistent with X chromosome repression being mediated by mechanisms similar to mitotic chromosome condensation. On both mitotic chromosomes and interphase dosage compensated X chromosomes monomethylation of H4K20 is increased whereas acetylation of H4K16 is decreased (Figure 1.6) [100,101,132-134]. During cell cycle progression the levels of both the H4K20 methyltransferase, PR-SET-7, and H4K20me1 increase in G2, remain high in mitosis, and decrease in G1 [132,133]. Additionally, the depletion of PR-SET-7 leads to cell cycle defects, and mitotic and interphase chromosome decondensation [132], illustrating the importance of H4K20me1 in mitosis and chromosome compaction. By contrast, H4K16ac levels increase during S

phase and decrease during mitosis [133,134]. This data is consistent with findings that H4K20me1 antagonizes H4K16ac [89]. In yeast, H4K16ac deacetylation in mitosis is achieved by Hst2 (Sir2 homolog), which is recruited by histone H3 phosphorylated on serine 10 [134]. Deacetylation of H4K16ac leads to stronger interactions between H2A and H4 on neighboring nucleosomes, leading higher degree of condensation [134,135]. In mitosis, this cascade of histone modifications is proposed to drive chromatin hypercondensation, independently from condensin [134]. However it has been shown that mitotic condensin II subunits CAP-D3 and CAP-G2 are capable of binding H4K20me1, suggesting H4K20me1 may play a role in condensin II loading [136].

C. elegans interphase dosage compensated X chromosomes show similar changes in histone modifications: H4K20me1 is increased, whereas H4K16ac is decreased on X. The enrichment of H4K20me1 is regulated not only by the DCC but also the H4K20 monomethylase, SET-1 (PR-SET7 homolog), and the H4K20 di- and trimethylase, SET-4 (SUV4-20 homolog) [100,101]. The DCC also regulates SIR-2.1 (Sir2 homolog), which mediates the depletion of H4K16ac on X chromosomes [101]. My work shows that this cascade of histone modifications drives X chromatin condensation in a DCC- (therefore condensin-) dependent manner (This will be discussed thoroughly in Chapter 2 [131]). By contrast, in mitosis, these histone modifications are proposed to act independently of condensin [134]. These observations suggest that interphase dosage compensated X chromosomes maintain some characteristics associated with condensed mitotic chromosome.

Molecular mechanisms of condensin activity

The mechanisms by which condensin generates and maintains chromosome condensation in interphase and mitosis are highly debated and poorly understood. The biochemical mechanisms discussed below have been proposed to contribute to chromosome condensation. However, whether these activities contribute to condensin's interphase or mitotic functions, or both, is unknown.

The two SMC proteins of condensin are able to hydrolyze ATP and this activity is believed to be essential for regulating higher-order chromatin structure [87,137]. The SMC proteins also have the ability to reanneal complementary ssDNAs into dsDNAs [138], perhaps as a preparatory step for the formation of mitotic chromosomes (Figure 1.7). The best-characterized mechanism of mitotic condensin, detected in many eukaryotic species is the ability to introduce ATP-dependent positive supercoils into DNA *in vitro* [121,137,139-141]. Using closed circular DNA and in the presence of topoisomerase I, mitotic condensin I is able to supercoil the DNA with its DNA-stimulated ATPase activity [137]. This activity requires the entire five-unit complex. The SMC proteins alone do not have ATPase activity and cannot bind chromatin *in vitro* [140]. Positive supercoiling is proposed to facilitate topoisomerase II-mediated decatenation of the sister chromatids and lead to the formation of chiral loops. Higher order assemblies by condensin-condensin interactions can then compact the chromatin fiber (Figure 1.7) [142,143].

Phosphorylation of condensin's CAP subunits by the kinase CDK1 (cyclin-dependent kinase 1) is required to supercoil DNA and initiate mitotic chromosome

condensation *in vitro* [144,145]. By contrast, the supercoiling activity is not detected when the interphase form of condensin is incubated with circular DNA in the presence of ATP and topoisomerase I [144]. In fact, phosphorylation of condensin I at different sites, by a different kinase, CK2 (casein kinase 2), suppresses supercoiling activity during interphase [145]. This suggests that condensin I-mediated DNA supercoiling may not be involved in chromosome compaction during interphase. However it is not known whether condensin II-mediated supercoiling or additional molecular mechanisms drive interphase chromatin organization.

Alternatively, or in addition to supercoiling, condensin is proposed to entrap the chromatin fibers in a ring-like structure [146]. This hypothesis is based on condensin's resemblance to cohesin, both containing a pair of SMC proteins, forming a V-shape, and additional non-SMC proteins, proposed to close the ring (Figure 1.7). Cohesin is believed to hold pairs of the sister chromatids together by entrapping DNA from each chromatid within its ring-like structure [147]. A recent study on yeast minichromosomes provided evidence that condensin forms similar topological links by encircling DNA. Linearization of the minichromosome DNA or opening the condensin ring eliminated the association between the DNA and condensin [146]. While cohesion is believed to hold sister chromatids together, condensin is proposed to entrap different sections of the same DNA molecule, to facilitate condensation.

Condensin's ability to shape chromosomes is further illustrated by its localization to topologically associating domain (TAD) boundaries in interphase chromosomes. A TAD is a contiguous chromosomal region with high frequency of interactions between

sequences within the TAD, but few interactions with sequences outside the TAD. In interphase *Drosophila,* mouse and human ES cells, condensin II has been found to localize at high occupancy architectural protein binding sites (APBSs) located at the borders of TADs [115]. Localization of condensin II at TAD boundaries, together with its ability to entrap DNA, suggests a possible mechanisms for regulating interphase chromatin organization. Recent evidence in *C. elegans* has shown that the dosage compensated X chromosomes have many TAD boundaries that coincide with condensin I^{DC} high affinity binding sites. These TADS are lost in condensin I^{DC} mutants, suggesting that condensin I^{DC} packages the X chromosomes into TADs and regulates interphase chromatin organization [148]. Unlike interphase chromatin, which is partitioned into small sub-megabase TADs and large multi-megabase compartments [149], mitotic chromosomes do not exhibit chromosome compartments and TADs [150]. Instead it is believed that chromatin is linearly compacted into consecutive loops, potentially by SMC complexes, and then homogeneous axial compression leads to the formation of dense mitotic chromosomes [150]. Thus, there may be unique and overlapping mechanisms involved in condensin-mediated chromosome compaction in interphase and mitosis.

How does condensin regulate gene expression?

Which of these biochemical activities, if any, contribute to *C. elegans* dosage compensation is unknown. Mutations in the ATPase domains of DPY-27 and MIX-1 lead to dosage compensation defects [86,105], suggesting that the ATPase activity is required for dosage compensation. Whether condensin I^{DC} is able to reanneal single stranded DNA, supercoil DNA, or entrap chromatin fibers has not been investigated. It is

known that the condensin I^{DC} can reshape the X chromosome by forming TAD boundaries, but whether and how TAD formation contributes to gene expression regulation, is not known. In fact no correlation is found between TAD structure and gene expression. Genes at TAD boundaries are not expressed at different levels than genes within TADs [148]. Additionally, condensin I^{DC} binding to a gene is not necessary, nor sufficient, for transcriptional regulation. Although condensin I^{DC} binding correlates with RNA Pol II occupancy it does not predict dosage compensation status [76,96]. These results support the model that the DCC is not regulating expression on a gene-by-gene basis, but acting chromosome-wide to repress gene expression. Future studies of condensin's biochemical activities will reveal how condensin is able to achieve both mitotic chromosome compaction and gene repression.

Chromatin structure and gene expression

While condensin's effect on gene expression is not well understood, we know much more about how chromatin structure regulates gene expression. For a better understanding of how chromatin structure can regulate gene expression, I will first describe the key component of chromatin, the nucleosome, and how the nucleosome can be modified to alter chromatin structure. I will then focus my attention on one specific modification, histone acetylation, which is an essential part of gene regulation. Finally I will describe the unique roles of H4K16 acetylation and the MYST family HATs that acetylate this histone mark.

The nucleosome and histone modifications

Regulation of gene expression is essential to ensure normal cellular and biological functions. In eukaryotes, the modifications of chromatin structure provide unique transcription regulatory mechanisms. The compaction and organization of genomic DNA into chromatin not only packages DNA into higher-order structures, but also regulates key processes such as transcription, replication and DNA repair [151]. The nucleosome is composed of 147 bp of DNA wrapped around a protein core of basic histone proteins. The core is an octamer that is composed of two of each histone H2A, H2B, H3, and H4 [152]. The core histones H3, H2A and H2B can be replaced by histone variants that may differ from the core histones either by the variation of a few amino acids or by an additional protein domain [153]. Additionally, the eight histones have highly basic N-and/or C-terminal domains that protrude from the nucleosome core and can be posttranscriptionally modified by acetylation, methylation, phosphorylation, and ubiquitination [154,155]. These modifications are known to regulate chromatin as well as recruit proteins and complexes with specific enzymatic activities to rearrange nucleosomes.

The structure of the nucleosome affects higher-order folding of the chromatin fiber. Chromatin can form two structural states, an active state (euchromatin), in which the genomic regions are decondensed allowing factors to bind to DNA, and a repressive state (heterochromatin), in which the chromatin is densely packed [156]. High-resolution structure analysis of the nucleosome have shown that histone H4 tails are highly basic and are thought to bind to the acidic patch in the H2A-H2B dimer of the neighboring

nucleosome. The model suggests that continuous acetylation of H4 lysines, K5, K8, K12, and K16, would reduce the affinity of the bond formed by the H4 tail to the neighboring nucleosome [157]. Therefore modifying the H4 tail may have greater affects on the interactions between nucleosomes rather than the interactions with other histones with in the same nucleosome.

Role of histone acetylation

Histone acetylation is an essential part of gene regulation. It is the process through which an acetyl group from acetyl-coenzyme A is transferred to the ε-amino group of a lysine residue within the N-terminal tail protruding from the histone core [158]. This reaction is catalyzed by histone acetyltransferases (HATs). HATs categorized into three major families, the GNAT family, the MYST family, and the CBP/p300 family [159]. The reverse reaction in which an acetyl group is removed from a lysine residue is histone deacetylation. Histone deacetylation is achieved by histone deacetylases (HDACs), which fall into four classes (classes I, II, III, and IV) [160]. Histone acetylation has been closely correlated with increases in transcriptional activation, and changes in transcriptional activity [161,162]. Histones modified by acetyl groups add negative charges to the positive charges of lysine residues, thus, disrupting the electrostatic interaction existing between the positively charged histones and the negatively charged DNA [163,164]. As a consequence, histone acetylation contributes to the transformation from a densely packed heterochromatin state into a relaxed euchromatin state, allowing transcriptional machinery to come into contact with the DNA. In addition to gene transcription, histone acetylation provides a platform for protein

binding. Many HATs and chromatin-remodeling complexes have bromodomains, which allow them to interact with and bind to the acetylated histone tails [165]. Histone H4 acetylation, specifically H4K16ac, is important for transcription and the dosage compensation strategies in many species, therefore I will be describing the unique roles of H4K16 acetylation and the MYST family HATs that are known to acetylate this histone mark.

H4K16 acetylation

The H4 histone tail has been identified as an important factor for chromatin formation and stability. An *in vitro* chromatin formation study demonstrated that the histone H4 tail, specifically amino acids 14-19 is essential for chromatin-fiber compaction [166]. Histone H4 can be acetylated on lysines 5,8,12, and 16. H4K16ac is the only known modification in the 14-19 amino acid region, suggesting that it affects the higher order structure of chromatin. H4K16ac is a highly abundant modification in several organisms [167]. In yeast, over 80% of histone H4 molecules have an acetyl group on K16 [168]. Site-specific antibody studies have shown that this mark is usually present in the monoacetylated form [169,170]. In humans, mice, and yeast the order of the H4 tail acetylation is the same, from the N-terminus to the C-terminus, starting with the acetylation of K16, then K12, K8 and finally K5 [171,172]. This illustrates a conservation of the H4 acetylation mechanism.

A study using sedimentation assays to evaluate the degree of nucleosome array folding showed that H4K16ac is in fact the central switch for controlling higher order chromatin structure. This *in vitro* study showed that the acetylation of H4K16 alone

inhibited the formation of higher order 30-nm chromatin fibers and weakened the interactions between chromatin and non-histone proteins [135]. Nucleosome stacking is mediated by electrostatic interactions that are regulated by ion-ion associations and histone-tail bridging [173]. As stated earlier histone-tail bridging is formed when the highly charged region of the H4 tail, which includes K16, interacts with the acidic patch on the H2A-H2B dimer of an adjacent nucleosome [157,174]. H4K16ac alters these interactions thereby disrupting nucleosome array folding and stacking [173]. Substituting K16 with glutamine mimics acetylated lysine however does not cause decompaction of a nucleosome array, suggesting that K16 alone is critical for decompaction [175].

In addition to affecting nucleosome interactions, H4K16ac affects interactions of the nucleosome with chromatin associated proteins. Nucleosome and chromatin folding can be regulated by ATP dependent remodeling machinery; these remodeling complexes alter histone-DNA interactions within the nucleosome by utilizing the energy from ATP hydrolysis [176]. The ATPase ISWI is the catalytic core of several of these remodeling complexes and facilitates nucleosome sliding in cis along DNA [177]. The N-terminal tail of histone H4, specifically amino acids 17-19, is critical for ISWI binding and nucleosome remodeling by ISWI [178-180]. ISWI is unable to recognize its binding site when H4K12 or K16 are acetylated, therefore interfering with ISWI's function of compacting chromatin and sliding nucleosomes along DNA [135,179,180].

MYST Family Histone Acetyltransferases

H4K16ac is regulated by the catalytic activities of a MYST family HAT and a class III HDAC (Sir2 family) [181]. My work has identified a MYST family histone

acetyltransferase as an important player in X chromosome regulation in *C. elegans*, as described in Chapter 4. HATs have been classified into several families based on their structural homologies, the largest family of HATs being the MYST (MOZ, Ybf2/Sas3, Sas2, Tip60) family. MYST proteins are defined by their catalytic MYST domain, which contains an acetyl-coenzyme A binding domain and a C2HC-type zinc finger [182]. In mammals there are five MYST family HATs: MOZ, MORF, HBO1, MOF and Tip60. They are divided into three subgroups based on additional shared protein domains, MOZ and MORF, MOF and Tip60, and HBOI alone (Figure 1.8) [183,184]. MOZ and MORF are closely related, large multidomain proteins. MOZ and MORF have two PHD-type zinc fingers, a highly conserved MYST domain, an acidic region, and unique C-terminal ends consisting of a serine-rich and a methionine rich domain [183]. Although the binding characteristics of the PHD-type zinc fingers of MOZ and MORF have not been studied, PHD-type zinc fingers are found in several proteins that regulate chromatin structure and bind trimethylated H3K4 [185-187]. MOF and Tip60 are characterized by a conserved chromodomain and the MYST domain [183,184,188]. Many proteins involved in gene silencing possess a chromodomain. These domains are known to help direct the localization of different repressive chromatin complexes to specific histone methylation marks [189,190]. HBO1 is in a subgroup alone and does not have closely related homologues with the same domain structure. It has a MYST domain, a central C2HC zinc finger domain and an amino-terminal serine-rich domain [183]. MYST proteins are highly conserved and have a diverse variety of functions affecting several cellular processes, such as gene regulation, DNA replication, repair, and recombination,

cell division/differentiation and development [183]. I will focus on the unique protein complexes and the diverse biological functions of two specific MYST family HATs, MOF (Males absent on the first) and Tip60 (HIV Tat interacting protein of 60 kDa). Although MOF and Tip60 are closely related MYST histone acetyltransferases, the two proteins have different biological functions.

MOF containing complexes

In most species the major H4K16 histone acetyltransferase is MOF/KAT8/Sas2 [31,167,191,192]. MOF resides in multiprotein complexes. In flies, MOF is one of the key components of the dosage compensation complex, the male specific lethal (MSL) complex [28,29]. As discussed earlier the fly MSL complex is composed of five proteins, MSL1, MSL2, MSL3, MLE, and MOF, and two non-coding RNAs, roX1 and roX2 [31]. In addition to the MSL complex, MOF is also a component of several other complexes. Human MOF interacts with a histone methyltransferase, MLL1, in distinct complex, which methylates and acetylates histones [193]. The histone acetyltransferase activity of MOF and histone methyltransferase activity of MLL1 are required for transcriptional activation *in vitro* [193]. Other studies identified a number of unique MOF-associated proteins different from the subunits in the MSL complex and designated this complex as the NSL complex, found in both flies and human cells [194]. Both the MSL and the NSL complex can acetylate H4K16, however in addition to H4K16ac, the NSL complex can acetylate H4K5 and H4K8 [195]. Biochemical purifications have reveled that most of these MOF interacting proteins are conserved between *Drosophila* and mammals [31,193,194]. Lastly, in yeast the MOF homolog, Sas2, is the catalytic subunit of a yeast

HAT complex known as the SAS complex. The SAS complex is a small trimeric complex composed only Sas2, Sas4 and Sas5. It is required for most of the H4K16ac *in vivo* and exclusively acetylates H4K16ac *in vitro* [196].

MOF containing complexes have a diverse range of functions affecting several biological processes. In yeast the MOF homolog, Sas2, is the positive regulator of H4K16ac and maintains an open chromatin structure [191,192]. In mice, MOF activity also regulates H4K16ac, MOF mutants arrest in development at the blastocyst stage and lack H4K16ac, while the acetylation of other histone lysine residues are normal [197,198]. Mammalian MOF has a similar role to Sas2 and is required for the prevention of global chromatin condensation. MOF mutant embryos exhibit abnormal chromatin morphology prior to undergoing death by apoptosis [197]. MOF is also required for H4K16ac in human cells *in vitro* [167]. In addition to chromatin structure and morphology, MOF plays a role in gene regulation. The hyperacetylation and hypoacetylation of H4K16 regulated by Sas2 and Sir2 respectively at the euchromatin/ heterochromatin boundary maintains the regions between transcriptionally active and silent telomeric chromatin [100,166]. The MOF-NSL complex appears to be a global transcriptional regulator, it has been found to bind to a group of active promoters and regulate housekeeping genes in *Drosophila* [199-201]. In the presence of the MSL complex proteins MOF has a more specialized role in dosage compensation in flies and mammals. MOF functions to hyperacetylate H4K16 on the male X, thereby upregulating X-linked gene expression by two fold in male flies [28]. Recent microarray and RNA-seq analysis have provided evidence that mammals undergo X upregulation in both sexes to

balance X and autosomal expression [18,20,21,54]. Therefore in addition to its global functions, MOF-mediated H4K16ac is proposed to contribute to X upregulation in mammals [17]. In Chapter 4, I will show roles for H4K16ac in chromosome decondensation, gene regulation, and dosage compensation, however the *C. elegans* H4K16ac HAT, MYS-1, appears to be Tip60, rather than MOF (Figure 1.9).

Tip60 complex

Tip60 is a well-characterized MYST HAT and was first isolated in a screen for proteins interacting with the HIV tat gene product [202]. Tip60 is homologous to the yeast Esa1, the catalytic subunit of the nucleosome acetyltransferase of H4 (NuA4) complex [203] and the Piccolo NuA4 (picNuA4) subcomplex [204]. NuA4 is a large HAT complex, containing 12 subunits [205,206], while picNuA4 contains three subunits (Esa1, Yng2 and Epl1) and is responsible for the HAT activity of NuA4 [204]. NuA4 and picNuA4 are responsible for site specific and global acetylation of histone H4 and histone H2A, respectively [204]. Esa1 activity mediates site specific (targeted) and global (non-targeted) effects on acetylation [207,208]. *In vitro* and *in vivo* NuA4 can stimulate transcription when targeted to chromatin regions for H4 hyperacetylation by transcriptional activators [209]. Esa1 is generally recruited to ribosomal gene promoters and the loss of Esa1 function results in gene-specific decreases in transcription [207,210]. However it's global affects on acetylation is not required for transcription, as transcription is only modestly affected for a few genes [207,211]. In yeast the NuA4 complex shares subunits with the SWR1 complex [212]. The SWR1 complex uses ATP hydrolysis to replace canonical H2A-H2B with H2A.Z-H2B [213,214] *In vivo* the

acetylation of chromatin by NuA4 simulates SWR1 activity [215]. In higher eukaryotes NuA4 and SWR1 act together and is homologous to the TIP60/p400 complex, which has both histone aceyltransferase and histone exchange activities.

Tip60 can acetylate core histones H2A (K5), H4 (K5, K8, K12 and K16) *in vitro* [216-218]. The complex can also acetylate H3, but only on free histones [216]. In *Drosophila*, Tip60 can acetylate modified histone variant, such as phospho-H2Av [219]. Tip60 can also acetylate non-histone substrates, including the tumor suppressors Retinoblastoma (Rb) and Protein 53 (p53), and the oncogene c-Myc [220]. By acetylating these histone and non-histone proteins Tip60 performs a vast variety of biological processes.

Tip60 activity can play a role in transcriptional activation, as well as repress gene transcription. Tip60 is a key regulator in cell cycle progression and DNA damage response. It is known to acetylate and stabilize the transcription factor and oncogene c-Myc, which plays a direct role in G1/S progression by regulating genes required for growth, DNA replication or apoptosis. Additionally, Tip60 can be recruited to Myc-dependent promoters by c-Myc to contribute to histone acetylation [221,222]. Protein 53 (p53) is a transcription regulator that regulates G1/S arrest in response to DNA damage in human cells. Tip60 can act as a p53 coactivator and thus is responsible for either cell cycle arrest or apoptosis upon p53 activation, as well as p53-driven transcription [223,224]. Another way Tip60 regulates cell cycle progression is through E2F transcription. E2F proteins can activate or repress transcription. The activating E2F factors bind to promoters of their target genes and are required for the hyperacetylation

of target chromatin. In human cells ectopically expressed E2F1 recruits the Tip60 complex to target gene promoters, which leads to the H4 acetylation [225]. Tip60 mutations and deletions lead to different types of abnormalities in species. Tip60 mutant mouse embryos die before implantation, while the depletion of Tip60 in *Drosophila* leads to lethality before the pupa stage [226,227]. In *C. elegans* the depletion of the Tip60 homolog, MYS-1, results in premature cell cycle exit and differentiation, as well as eventual developmental arrest and lethality [228]. Interestingly in mouse ES cells, Tip60 is required for pluripotency. The depletion of Tip60 results in the upregulation of genes involved in differentiation and embryonic development and the downregulation of cell cycle regulators. However more genes are upregulated than downregulated, suggesting a role in transcriptional repression [229]. Overall, Tip60 is a protein that plays a role in several biological processes, by affecting the functions of different targets using its acetyltransferase activity as well as its protein-protein interactions.

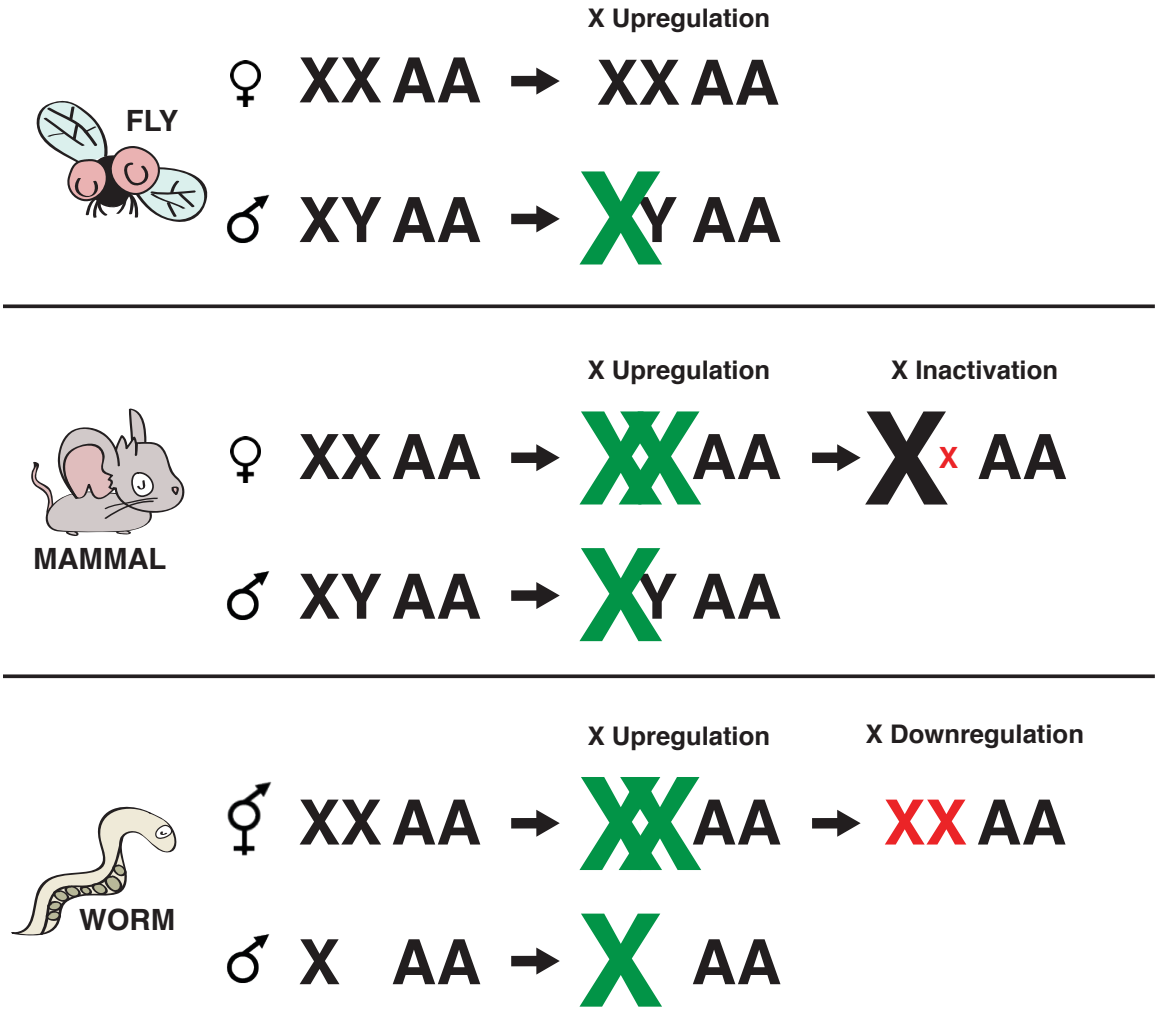

Figure 1.1 Different dosage compensation strategies. To equalize X-linked expression and balance X to autosomal expression between and within the sexes, flies upregulate the single male X, while evidence has shown that mammals and worms upregulate the X chromosomes in both sexes. In mammals one X is then inactivated in females and in worms both X chromosomes are downregulated in hermaphrodites.

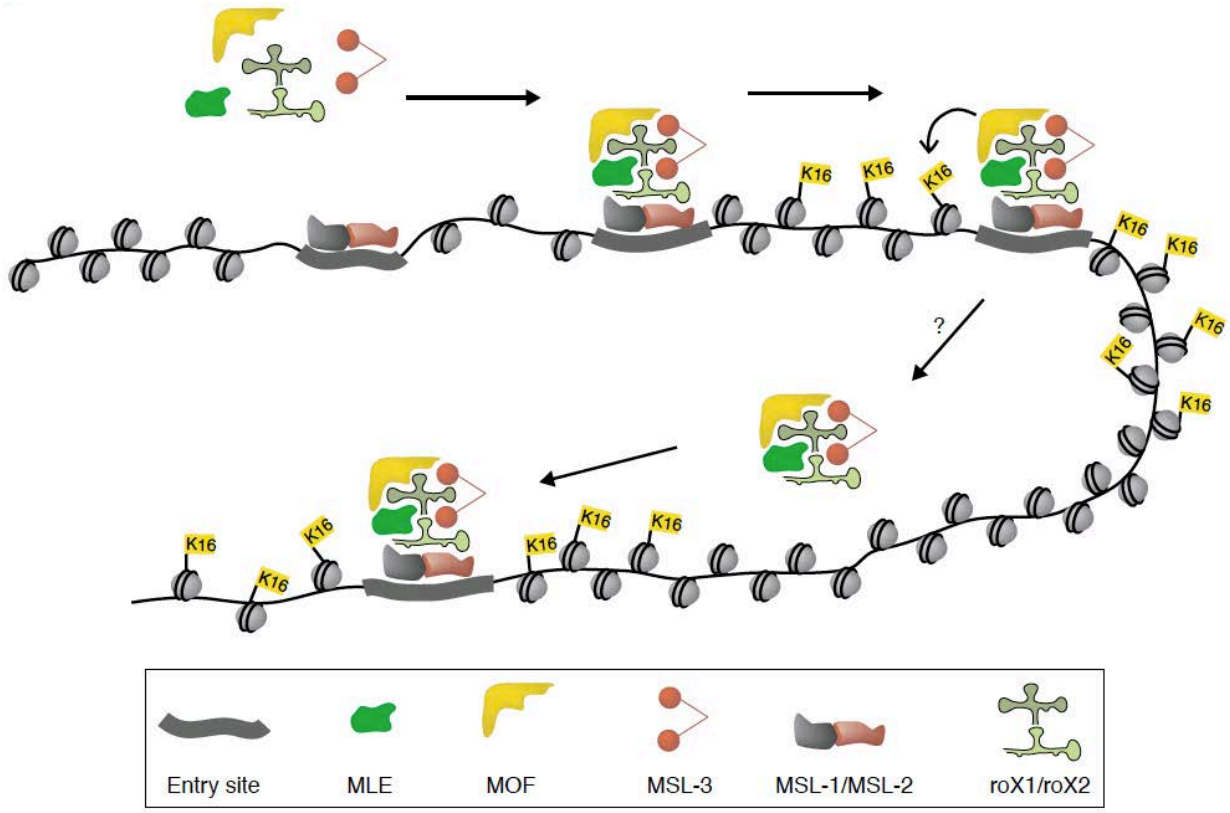

Figure 1.2 Dosage compensation in *Drosophila*. The MSL complex binds on distinct chromatin entry sites on the male X chromosome. The complex leads to hyperacetylation of the surrounding chromatin at H4K16, which is followed by the spreading of the complex along the X chromosome at additional sites. This leads to a two-fold enrichment of the male X chromosome. This figure is from Akhtar (2003).

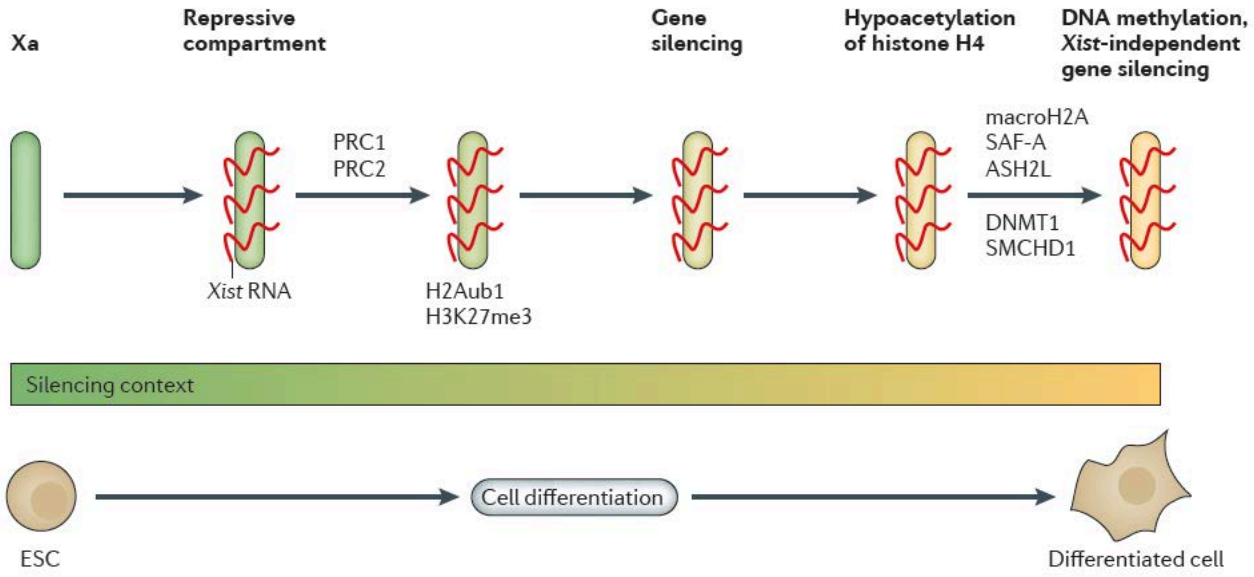

Figure 1.3 Stepwise model of mammalian X inactivation. Undifferentiated cells possess two active X chromosome and when the cells enter differentiation *Xist* expression triggers XCI. *Xist* RNA spreads along the Xi and recruits PRC1 and PRC2, which establishes H2Aub1 and H3K27me3. Genes begin to silence and more changes in histone modifications follow. Lastly, DNA methylation of gene promoters on the Xi ensures stable silencing. This figure is from Wutz (2011).

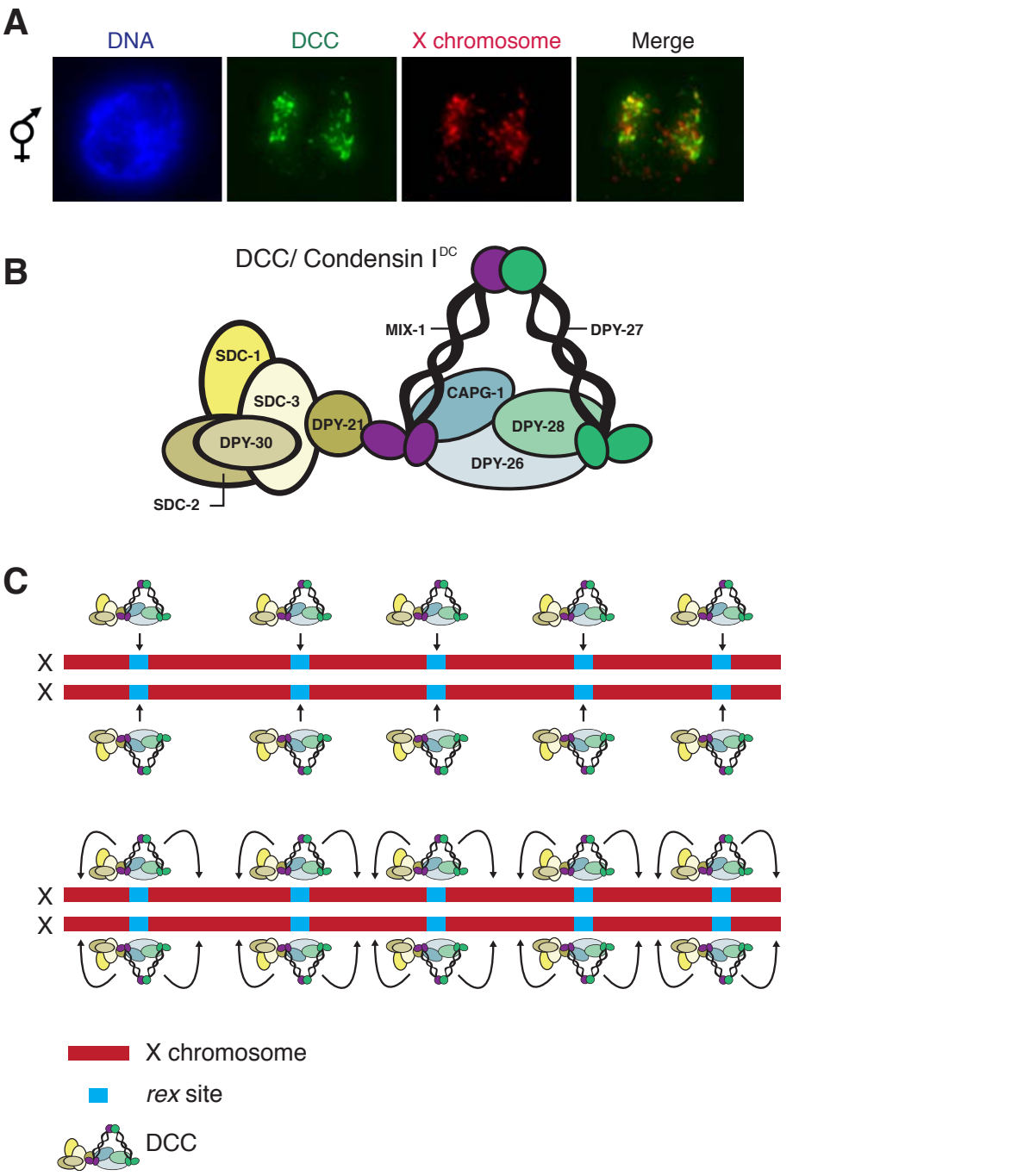

Figure 1.4 The dosage compensation complex (DCC) localizes to both X chromosomes in the hermaphrodite. (A) The DCC (green, IF) localizes to the X chromosomes (red, FISH) in hermaphrodite nuclei. (B) The DCC consists of a five subunit condensin complex, as well as at least five additional subunits. (C) The DCC is initially required to the X chromosome at a number of recruitment sites on the X (*rex*). After recruitment to the *rex* sites, the DCC spreads onto the X chromosome.

Human Condensin I	*C. elegans* Condensin I	*C. elegans* Condensin I^{DC}
SMC 2/hCAP-E	MIX-1	MIX-1
SMC 4/hCAP-C	SMC-4	DPY-27
hCAP-D2	DPY-28	DPY-28
hCAP-G	CAPG-1	CAPG-1
hCAP-H	DPY-26	DPY-26

Human Condensin II	*C. elegans* Condensin II
SMC 2/hCAP-E	MIX-1
SMC 4/hCAP-C	SMC-4
hCAP-D3	HCP-6
hCAP-G2	CAPG-2
hCAP-H2	KLE-2

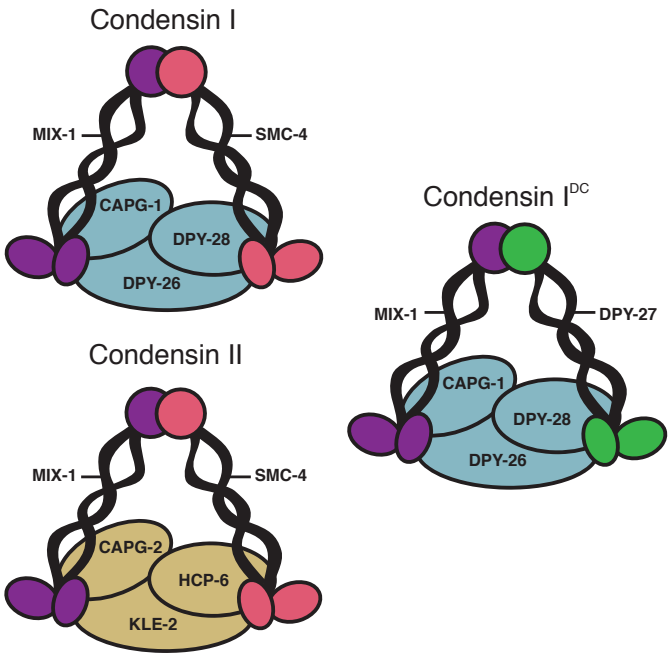

Figure 1.5 Three condensin complexes. *C. elegans* condensin subunits and their human homologs. Condensins I and II share the same pair of MIX-1 and SMC-4 subunits and have three unique CAP proteins. Condensin I contains DPY-28, CAPG-1, and DPY-26, while condensin II contains HCP-6, CAPG-2, and KLE-2. In addition, *C. elegans* has a condensin I-like complex (condensin I^{DC}) that functions in dosage compensation. Condensin I^{DC} differs from the canonical condensin I by only one subunit: DPY-27 replaces SMC-4.

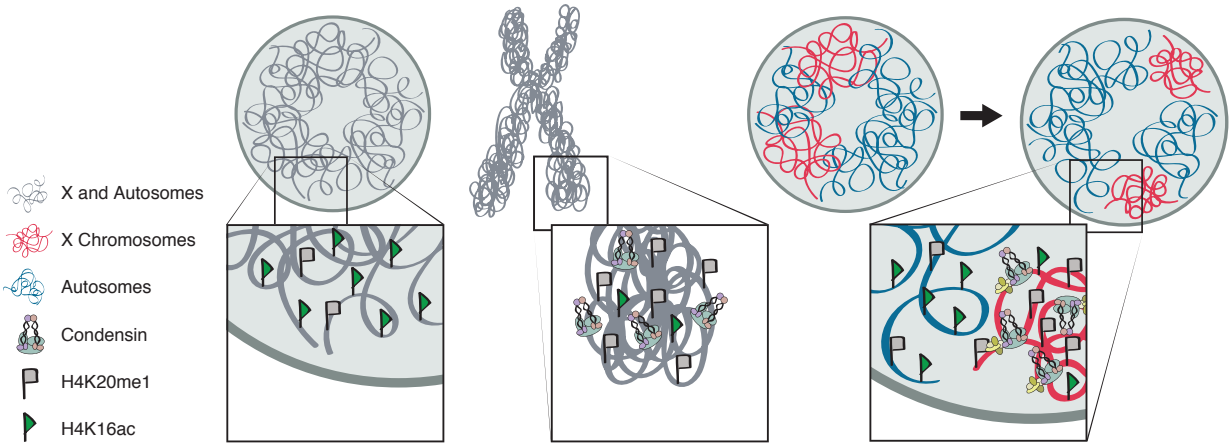

Figure 1.6 Condensin and chromatin mediated chromosome compaction. Similar distributions of histone modifications and condensin in condensed mitotic chromosomes and interphase dosage compensated X chromosomes. Compaction is accompanied by enrichment of H4K20me1 and depletion of H4K16ac in both mitotic chromosome condensation and interphase dosage compensated X chromosomes.

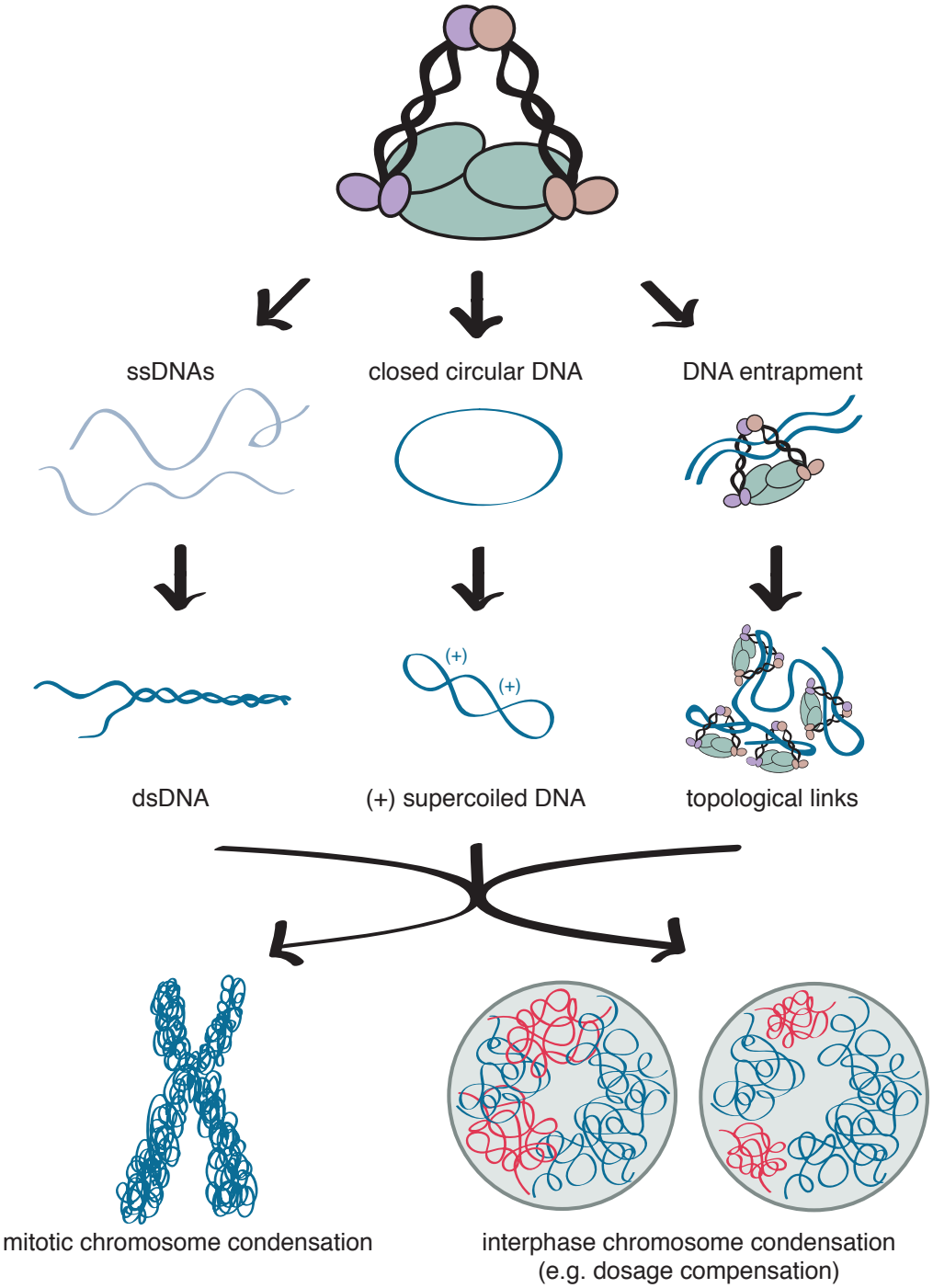

Figure 1.7 Molecular mechanisms of condensin activity. The proposed mechanisms by which condensin generates and maintains chromosome condensation in interphase and mitosis. Condensin's SMC proteins can reanneal complementary ssDNAs into dsDNAs, in preparation for subsequent coiling steps. Condensin can also introduce ATP-dependent positive supercoils into DNA *in vitro*. Alternatively, or in addition, condensin is proposed to entrap the chromatin fibers in its ring-like structure.

Figure 1.8 Schematic diagram comparing MYST family proteins and their protein domains. MYST family HATs aligned according to their conserved MYST HAT domain (dark blue). Based on their shared protein domains MYST proteins fall into three subfamilies. Domains are colored as indicated in the legend of the graph. The MYST proteins have a conserved acetyl-coenzyme A binding domain (dark gray) and a C2HC-type zinc finger (yellow). MOZ and MORF share two PHD fingers, a conserved N-terminal domain, and conserved C-terminal serine- and methionine-rich domains. MOF and Tip60 share a chromodomain. HBO1 contains an N-terminal serine-rich domain and an additional zinc finger domain. This schematic is an adaption from figures from Thomas et al., (2007) and Voss et al., (2009).

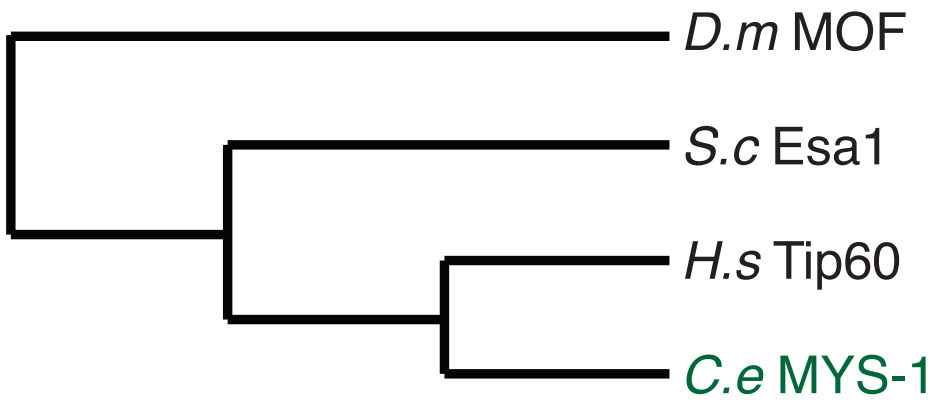

Figure 1.9 Phylogenetic tree of proteins closely related to MYS-1. The *C. elegans* H4K16ac HAT is MYS-1. MYS-1 is most homologous to human Tip60, rather than *Drosophila* MOF.

REFERENCES

1. Aristotle, and Peck, A.L. (1953). Generation of animals, (Cambridge, Mass., London,: Harvard university press; W. Heinemann ltd).
2. McClung, C.E. (1902). The accessory chromosome sex determinant? Biological Bulletin *3*, 43–84.
3. Stevens, N.M. (1905). Studies in spermatogenesis, (Washington, D. C.,: Carnegie institution of Washington).
4. Wilson, E.B. (1905). The Chromosomes in Relation to the Determination of Sex in Insects. Science *22*, 500-502.
5. Crews, D., Bergeron, J.M., Bull, J.J., Flores, D., Tousignant, A., Skipper, J.K., and Wibbels, T. (1994). Temperature-dependent sex determination in reptiles: proximate mechanisms, ultimate outcomes, and practical applications. Developmental genetics *15*, 297-312.
6. Graves, J.A. (2016). Evolution of vertebrate sex chromosomes and dosage compensation. Nature reviews. Genetics *17*, 33-46.
7. Disteche, C.M. (2016). Dosage compensation of the sex chromosomes and autosomes. Seminars in cell & developmental biology.
8. Mackensen, O. (1951). Viability and Sex Determination in the Honey Bee (Apis Mellifera L.). Genetics *36*, 500-509.
9. Sinclair, A.H., Berta, P., Palmer, M.S., Hawkins, J.R., Griffiths, B.L., Smith, M.J., Foster, J.W., Frischauf, A.M., Lovell-Badge, R., and Goodfellow, P.N. (1990). A gene from the human sex-determining region encodes a protein with homology to a conserved DNA-binding motif. Nature *346*, 240-244.
10. Smith, C.A., Roeszler, K.N., Ohnesorg, T., Cummins, D.M., Farlie, P.G., Doran, T.J., and Sinclair, A.H. (2009). The avian Z-linked gene DMRT1 is required for male sex determination in the chicken. Nature *461*, 267-271.
11. Madl, J.E., and Herman, R.K. (1979). Polyploids and sex determination in Caenorhabditis elegans. Genetics *93*, 393-402.
12. Parkhurst, S.M., Bopp, D., and Ish-Horowicz, D. (1990). X:A ratio, the primary sex-determining signal in Drosophila, is transduced by helix-loop-helix proteins. Cell *63*, 1179-1191.
13. Torres, E.M., Williams, B.R., and Amon, A. (2008). Aneuploidy: cells losing their balance. Genetics *179*, 737-746.
14. Ohno, S. (1967). Sex Chromosomes and Sex-Linked Genes. Berlin: Springer, 1-140.
15. Conrad, T., and Akhtar, A. (2011). Dosage compensation in Drosophila melanogaster: epigenetic fine-tuning of chromosome-wide transcription. Nature reviews. Genetics *13*, 123-134.
16. Ferrari, F., Alekseyenko, A.A., Park, P.J., and Kuroda, M.I. (2014). Transcriptional control of a whole chromosome: emerging models for dosage compensation. Nature structural & molecular biology *21*, 118-125.
17. Deng, X., Berletch, J.B., Ma, W., Nguyen, D.K., Hiatt, J.B., Noble, W.S., Shendure, J., and Disteche, C.M. (2013). Mammalian X upregulation is

associated with enhanced transcription initiation, RNA half-life, and MOF-mediated H4K16 acetylation. Developmental cell *25*, 55-68.
18. Deng, X., Hiatt, J.B., Nguyen, D.K., Ercan, S., Sturgill, D., Hillier, L.W., Schlesinger, F., Davis, C.A., Reinke, V.J., Gingeras, T.R., et al. (2011). Evidence for compensatory upregulation of expressed X-linked genes in mammals, Caenorhabditis elegans and Drosophila melanogaster. Nature genetics *43*, 1179-1185.
19. Gupta, V., Parisi, M., Sturgill, D., Nuttall, R., Doctolero, M., Dudko, O.K., Malley, J.D., Eastman, P.S., and Oliver, B. (2006). Global analysis of X-chromosome dosage compensation. Journal of biology *5*, 3.
20. Lin, H., Gupta, V., Vermilyea, M.D., Falciani, F., Lee, J.T., O'Neill, L.P., and Turner, B.M. (2007). Dosage compensation in the mouse balances up-regulation and silencing of X-linked genes. PLoS biology *5*, e326.
21. Lin, H., Halsall, J.A., Antczak, P., O'Neill, L.P., Falciani, F., and Turner, B.M. (2011). Relative overexpression of X-linked genes in mouse embryonic stem cells is consistent with Ohno's hypothesis. Nature genetics *43*, 1169-1170; author reply 1171-1162.
22. Yildirim, E., Sadreyev, R.I., Pinter, S.F., and Lee, J.T. (2012). X-chromosome hyperactivation in mammals via nonlinear relationships between chromatin states and transcription. Nature structural & molecular biology *19*, 56-61.
23. Barakat, T.S., and Gribnau, J. (2012). X chromosome inactivation in the cycle of life. Development *139*, 2085-2089.
24. Heard, E., and Disteche, C.M. (2006). Dosage compensation in mammals: fine-tuning the expression of the X chromosome. Genes & development *20*, 1848-1867.
25. Payer, B., and Lee, J.T. (2008). X chromosome dosage compensation: how mammals keep the balance. Annual review of genetics *42*, 733-772.
26. Csankovszki, G., Petty, E.L., and Collette, K.S. (2009). The worm solution: a chromosome-full of condensin helps gene expression go down. Chromosome research : an international journal on the molecular, supramolecular and evolutionary aspects of chromosome biology *17*, 621-635.
27. Meyer, B.J. (2010). Targeting X chromosomes for repression. Current opinion in genetics & development *20*, 179-189.
28. Akhtar, A., and Becker, P.B. (2000). Activation of transcription through histone H4 acetylation by MOF, an acetyltransferase essential for dosage compensation in Drosophila. Molecular cell *5*, 367-375.
29. Smith, E.R., Pannuti, A., Gu, W., Steurnagel, A., Cook, R.G., Allis, C.D., and Lucchesi, J.C. (2000). The drosophila MSL complex acetylates histone H4 at lysine 16, a chromatin modification linked to dosage compensation. Molecular and cellular biology *20*, 312-318.
30. Akhtar, A. (2003). Dosage compensation: an intertwined world of RNA and chromatin remodelling. Current opinion in genetics & development *13*, 161-169.
31. Smith, E.R., Cayrou, C., Huang, R., Lane, W.S., Cote, J., and Lucchesi, J.C. (2005). A human protein complex homologous to the Drosophila MSL complex is

responsible for the majority of histone H4 acetylation at lysine 16. Molecular and cellular biology *25*, 9175-9188.
32. Demakova, O.V., Kotlikova, I.V., Gordadze, P.R., Alekseyenko, A.A., Kuroda, M.I., and Zhimulev, I.F. (2003). The MSL complex levels are critical for its correct targeting to the chromosomes in Drosophila melanogaster. Chromosoma *112*, 103-115.
33. Gu, W., Wei, X., Pannuti, A., and Lucchesi, J.C. (2000). Targeting the chromatin-remodeling MSL complex of Drosophila to its sites of action on the X chromosome requires both acetyl transferase and ATPase activities. The EMBO journal *19*, 5202-5211.
34. Kelley, R.L., Wang, J., Bell, L., and Kuroda, M.I. (1997). Sex lethal controls dosage compensation in Drosophila by a non-splicing mechanism. Nature *387*, 195-199.
35. Lyman, L.M., Copps, K., Rastelli, L., Kelley, R.L., and Kuroda, M.I. (1997). Drosophila male-specific lethal-2 protein: structure/function analysis and dependence on MSL-1 for chromosome association. Genetics *147*, 1743-1753.
36. Palmer, M.J., Richman, R., Richter, L., and Kuroda, M.I. (1994). Sex-specific regulation of the male-specific lethal-1 dosage compensation gene in Drosophila. Genes & development *8*, 698-706.
37. Morales, V., Regnard, C., Izzo, A., Vetter, I., and Becker, P.B. (2005). The MRG domain mediates the functional integration of MSL3 into the dosage compensation complex. Molecular and cellular biology *25*, 5947-5954.
38. Morales, V., Straub, T., Neumann, M.F., Mengus, G., Akhtar, A., and Becker, P.B. (2004). Functional integration of the histone acetyltransferase MOF into the dosage compensation complex. The EMBO journal *23*, 2258-2268.
39. Richter, L., Bone, J.R., and Kuroda, M.I. (1996). RNA-dependent association of the Drosophila maleless protein with the male X chromosome. Genes to cells : devoted to molecular & cellular mechanisms *1*, 325-336.
40. Kelley, R.L., Meller, V.H., Gordadze, P.R., Roman, G., Davis, R.L., and Kuroda, M.I. (1999). Epigenetic spreading of the Drosophila dosage compensation complex from roX RNA genes into flanking chromatin. Cell *98*, 513-522.
41. Buscaino, A., Kocher, T., Kind, J.H., Holz, H., Taipale, M., Wagner, K., Wilm, M., and Akhtar, A. (2003). MOF-regulated acetylation of MSL-3 in the Drosophila dosage compensation complex. Molecular cell *11*, 1265-1277.
42. Hilfiker, A., Hilfiker-Kleiner, D., Pannuti, A., and Lucchesi, J.C. (1997). mof, a putative acetyl transferase gene related to the Tip60 and MOZ human genes and to the SAS genes of yeast, is required for dosage compensation in Drosophila. The EMBO journal *16*, 2054-2060.
43. Bone, J.R., Lavender, J., Richman, R., Palmer, M.J., Turner, B.M., and Kuroda, M.I. (1994). Acetylated histone H4 on the male X chromosome is associated with dosage compensation in Drosophila. Genes & development *8*, 96-104.
44. Alekseyenko, A.A., Larschan, E., Lai, W.R., Park, P.J., and Kuroda, M.I. (2006). High-resolution ChIP-chip analysis reveals that the Drosophila MSL complex

selectively identifies active genes on the male X chromosome. Genes & development *20*, 848-857.
45. Gilfillan, G.D., Straub, T., de Wit, E., Greil, F., Lamm, R., van Steensel, B., and Becker, P.B. (2006). Chromosome-wide gene-specific targeting of the Drosophila dosage compensation complex. Genes & development *20*, 858-870.
46. Kind, J., Vaquerizas, J.M., Gebhardt, P., Gentzel, M., Luscombe, N.M., Bertone, P., and Akhtar, A. (2008). Genome-wide analysis reveals MOF as a key regulator of dosage compensation and gene expression in Drosophila. Cell *133*, 813-828.
47. Smith, E.R., Allis, C.D., and Lucchesi, J.C. (2001). Linking global histone acetylation to the transcription enhancement of X-chromosomal genes in Drosophila males. The Journal of biological chemistry *276*, 31483-31486.
48. Kind, J., and Akhtar, A. (2007). Cotranscriptional recruitment of the dosage compensation complex to X-linked target genes. Genes & development *21*, 2030-2040.
49. Bell, O., Schwaiger, M., Oakeley, E.J., Lienert, F., Beisel, C., Stadler, M.B., and Schubeler, D. (2010). Accessibility of the Drosophila genome discriminates PcG repression, H4K16 acetylation and replication timing. Nature structural & molecular biology *17*, 894-900.
50. Zhang, Y., and Oliver, B. (2010). An evolutionary consequence of dosage compensation on Drosophila melanogaster female X-chromatin structure? BMC genomics *11*, 6.
51. Dunlap, D., Yokoyama, R., Ling, H., Sun, H.Y., McGill, K., Cugusi, S., and Lucchesi, J.C. (2012). Distinct contributions of MSL complex subunits to the transcriptional enhancement responsible for dosage compensation in Drosophila. Nucleic acids research *40*, 11281-11291.
52. Lyon, M.F. (1961). Gene action in the X-chromosome of the mouse (Mus musculus L.). Nature *190*, 372-373.
53. Adler, D.A., Rugarli, E.I., Lingenfelter, P.A., Tsuchiya, K., Poslinski, D., Liggitt, H.D., Chapman, V.M., Elliott, R.W., Ballabio, A., and Disteche, C.M. (1997). Evidence of evolutionary up-regulation of the single active X chromosome in mammals based on Clc4 expression levels in Mus spretus and Mus musculus. Proceedings of the National Academy of Sciences of the United States of America *94*, 9244-9248.
54. Nguyen, D.K., and Disteche, C.M. (2006). Dosage compensation of the active X chromosome in mammals. Nature genetics *38*, 47-53.
55. Lyon, M.F., Searle, A.G., Ford, C.E., and Ohno, S. (1964). A Mouse Translocation Suppressing Sex-Linked Variegation. Cytogenetics *3*, 306-323.
56. Borsani, G., Tonlorenzi, R., Simmler, M.C., Dandolo, L., Arnaud, D., Capra, V., Grompe, M., Pizzuti, A., Muzny, D., Lawrence, C., et al. (1991). Characterization of a murine gene expressed from the inactive X chromosome. Nature *351*, 325-329.
57. Brockdorff, N., Ashworth, A., Kay, G.F., Cooper, P., Smith, S., McCabe, V.M., Norris, D.P., Penny, G.D., Patel, D., and Rastan, S. (1991). Conservation of

position and exclusive expression of mouse Xist from the inactive X chromosome. Nature *351*, 329-331.
58. Lee, J.T., Davidow, L.S., and Warshawsky, D. (1999). Tsix, a gene antisense to Xist at the X-inactivation centre. Nature genetics *21*, 400-404.
59. Brown, C.J., Ballabio, A., Rupert, J.L., Lafreniere, R.G., Grompe, M., Tonlorenzi, R., and Willard, H.F. (1991). A gene from the region of the human X inactivation centre is expressed exclusively from the inactive X chromosome. Nature *349*, 38-44.
60. Brown, C.J., Hendrich, B.D., Rupert, J.L., Lafreniere, R.G., Xing, Y., Lawrence, J., and Willard, H.F. (1992). The human XIST gene: analysis of a 17 kb inactive X-specific RNA that contains conserved repeats and is highly localized within the nucleus. Cell *71*, 527-542.
61. Chaumeil, J., Le Baccon, P., Wutz, A., and Heard, E. (2006). A novel role for Xist RNA in the formation of a repressive nuclear compartment into which genes are recruited when silenced. Genes & development *20*, 2223-2237.
62. Zhao, J., Sun, B.K., Erwin, J.A., Song, J.J., and Lee, J.T. (2008). Polycomb proteins targeted by a short repeat RNA to the mouse X chromosome. Science *322*, 750-756.
63. Hernandez-Munoz, I., Lund, A.H., van der Stoop, P., Boutsma, E., Muijrers, I., Verhoeven, E., Nusinow, D.A., Panning, B., Marahrens, Y., and van Lohuizen, M. (2005). Stable X chromosome inactivation involves the PRC1 Polycomb complex and requires histone MACROH2A1 and the CULLIN3/SPOP ubiquitin E3 ligase. Proceedings of the National Academy of Sciences of the United States of America *102*, 7635-7640.
64. Wang, J., Mager, J., Chen, Y., Schneider, E., Cross, J.C., Nagy, A., and Magnuson, T. (2001). Imprinted X inactivation maintained by a mouse Polycomb group gene. Nature genetics *28*, 371-375.
65. Fang, J., Chen, T., Chadwick, B., Li, E., and Zhang, Y. (2004). Ring1b-mediated H2A ubiquitination associates with inactive X chromosomes and is involved in initiation of X inactivation. The Journal of biological chemistry *279*, 52812-52815.
66. Chadwick, B.P., and Willard, H.F. (2003). Chromatin of the Barr body: histone and non-histone proteins associated with or excluded from the inactive X chromosome. Human molecular genetics *12*, 2167-2178.
67. Jeppesen, P., and Turner, B.M. (1993). The inactive X chromosome in female mammals is distinguished by a lack of histone H4 acetylation, a cytogenetic marker for gene expression. Cell *74*, 281-289.
68. Costanzi, C., and Pehrson, J.R. (1998). Histone macroH2A1 is concentrated in the inactive X chromosome of female mammals. Nature *393*, 599-601.
69. Weber, M., Davies, J.J., Wittig, D., Oakeley, E.J., Haase, M., Lam, W.L., and Schubeler, D. (2005). Chromosome-wide and promoter-specific analyses identify sites of differential DNA methylation in normal and transformed human cells. Nature genetics *37*, 853-862.
70. Cotton, A.M., Lam, L., Affleck, J.G., Wilson, I.M., Penaherrera, M.S., McFadden, D.E., Kobor, M.S., Lam, W.L., Robinson, W.P., and Brown, C.J. (2011).

Chromosome-wide DNA methylation analysis predicts human tissue-specific X inactivation. Human genetics *130*, 187-201.
71. Wutz, A. (2011). Gene silencing in X-chromosome inactivation: advances in understanding facultative heterochromatin formation. Nature reviews. Genetics *12*, 542-553.
72. Rego, A., Sinclair, P.B., Tao, W., Kireev, I., and Belmont, A.S. (2008). The facultative heterochromatin of the inactive X chromosome has a distinctive condensed ultrastructure. Journal of cell science *121*, 1119-1127.
73. Eils, R., Dietzel, S., Bertin, E., Schrock, E., Speicher, M.R., Ried, T., Robert-Nicoud, M., Cremer, C., and Cremer, T. (1996). Three-dimensional reconstruction of painted human interphase chromosomes: active and inactive X chromosome territories have similar volumes but differ in shape and surface structure. The Journal of cell biology *135*, 1427-1440.
74. Engreitz, J.M., Pandya-Jones, A., McDonel, P., Shishkin, A., Sirokman, K., Surka, C., Kadri, S., Xing, J., Goren, A., Lander, E.S., et al. (2013). The Xist lncRNA exploits three-dimensional genome architecture to spread across the X chromosome. Science *341*, 1237973.
75. Albritton, S.E., Kranz, A.L., Rao, P., Kramer, M., Dieterich, C., and Ercan, S. (2014). Sex-biased gene expression and evolution of the x chromosome in nematodes. Genetics *197*, 865-883.
76. Kruesi, W.S., Core, L.J., Waters, C.T., Lis, J.T., and Meyer, B.J. (2013). Condensin controls recruitment of RNA polymerase II to achieve nematode X-chromosome dosage compensation. eLife *2*, e00808.
77. Sharma, R., Jost, D., Kind, J., Gomez-Saldivar, G., van Steensel, B., Askjaer, P., Vaillant, C., and Meister, P. (2014). Differential spatial and structural organization of the X chromosome underlies dosage compensation in C. elegans. Genes & development *28*, 2591-2596.
78. DeLong, L., Plenefisch, J.D., Klein, R.D., and Meyer, B.J. (1993). Feedback control of sex determination by dosage compensation revealed through Caenorhabditis elegans sdc-3 mutations. Genetics *133*, 875-896.
79. Hodgkin, J. (1983). X-Chromosome Dosage and Gene-Expression in Caenorhabditis-Elegans - 2 Unusual Dumpy Genes. Mol Gen Genet *192*, 452-458.
80. Hsu, D.R., and Meyer, B.J. (1994). The dpy-30 gene encodes an essential component of the Caenorhabditis elegans dosage compensation machinery. Genetics *137*, 999-1018.
81. Meyer, B.J., and Casson, L.P. (1986). Caenorhabditis Elegans Compensates for the Difference in X-Chromosome Dosage between the Sexes by Regulating Transcript Levels. Cell *47*, 871-881.
82. Nusbaum, C., and Meyer, B.J. (1989). The Caenorhabditis-Elegans Gene Sdc-2 Controls Sex Determination and Dosage Compensation in Xx Animals. Genetics *122*, 579-593.

83. Plenefisch, J.D., Delong, L., and Meyer, B.J. (1989). Genes That Implement the Hermaphrodite Mode of Dosage Compensation in Caenorhabditis-Elegans. Genetics *121*, 57-76.
84. Villeneuve, A.M., and Meyer, B.J. (1987). Sdc-1 - a Link between Sex Determination and Dosage Compensation in C-Elegans. Cell *48*, 25-37.
85. Csankovszki, G., Collette, K., Spahl, K., Carey, J., Snyder, M., Petty, E., Patel, U., Tabuchi, T., Liu, H., McLeod, I., et al. (2009). Three distinct condensin complexes control C. elegans chromosome dynamics. Current biology : CB *19*, 9-19.
86. Lieb, J.D., Albrecht, M.R., Chuang, P.T., and Meyer, B.J. (1998). MIX-1: an essential component of the C. elegans mitotic machinery executes X chromosome dosage compensation. Cell *92*, 265-277.
87. Hirano, T. (2012). Condensins: universal organizers of chromosomes with diverse functions. Genes & development *26*, 1659-1678.
88. Mets, D.G., and Meyer, B.J. (2009). Condensins regulate meiotic DNA break distribution, thus crossover frequency, by controlling chromosome structure. Cell *139*, 73-86.
89. Nishioka, K., Rice, J.C., Sarma, K., Erdjument-Bromage, H., Werner, J., Wang, Y., Chuikov, S., Valenzuela, P., Tempst, P., Steward, R., et al. (2002). PR-Set7 is a nucleosome-specific methyltransferase that modifies lysine 20 of histone H4 and is associated with silent chromatin. Molecular cell *9*, 1201-1213.
90. Dawes, H.E., Berlin, D.S., Lapidus, D.M., Nusbaum, C., Davis, T.L., and Meyer, B.J. (1999). Dosage compensation proteins targeted to X chromosomes by a determinant of hermaphrodite fate. Science *284*, 1800-1804.
91. Pferdehirt, R.R., Kruesi, W.S., and Meyer, B.J. (2011). An MLL/COMPASS subunit functions in the C. elegans dosage compensation complex to target X chromosomes for transcriptional regulation of gene expression. Genes & development *25*, 499-515.
92. Chuang, P.T., Lieb, J.D., and Meyer, B.J. (1996). Sex-specific assembly of a dosage compensation complex on the nematode X chromosome. Science *274*, 1736-1739.
93. Lieb, J.D., Capowski, E.E., Meneely, P., and Meyer, B.J. (1996). DPY-26, a link between dosage compensation and meiotic chromosome segregation in the nematode. Science *274*, 1732-1736.
94. Davis, T.L., and Meyer, B.J. (1997). SDC-3 coordinates the assembly of a dosage compensation complex on the nematode X chromosome. Development *124*, 1019-1031.
95. Hsu, D.R., Chuang, P.T., and Meyer, B.J. (1995). DPY-30, a nuclear protein essential early in embryogenesis for Caenorhabditis elegans dosage compensation. Development *121*, 3323-3334.
96. Jans, J., Gladden, J.M., Ralston, E.J., Pickle, C.S., Michel, A.H., Pferdehirt, R.R., Eisen, M.B., and Meyer, B.J. (2009). A condensin-like dosage compensation complex acts at a distance to control expression throughout the genome. Genes & development *23*, 602-618.

97. Ercan, S., Giresi, P.G., Whittle, C.M., Zhang, X., Green, R.D., and Lieb, J.D. (2007). X chromosome repression by localization of the C. elegans dosage compensation machinery to sites of transcription initiation. Nature genetics *39*, 403-408.
98. Petty, E.L., Collette, K.S., Cohen, A.J., Snyder, M.J., and Csankovszki, G. (2009). Restricting dosage compensation complex binding to the X chromosomes by H2A.Z/HTZ-1. PLoS genetics *5*, e1000699.
99. Pferdehirt, R.R., and Meyer, B.J. (2013). SUMOylation is essential for sex-specific assembly and function of the Caenorhabditis elegans dosage compensation complex on X chromosomes. Proceedings of the National Academy of Sciences of the United States of America *110*, E3810-3819.
100. Vielle, A., Lang, J., Dong, Y., Ercan, S., Kotwaliwale, C., Rechtsteiner, A., Appert, A., Chen, Q.B., Dose, A., Egelhofer, T., et al. (2012). H4K20me1 contributes to downregulation of X-linked genes for C. elegans dosage compensation. PLoS genetics *8*, e1002933.
101. Wells, M.B., Snyder, M.J., Custer, L.M., and Csankovszki, G. (2012). Caenorhabditis elegans dosage compensation regulates histone H4 chromatin state on X chromosomes. Molecular and cellular biology *32*, 1710-1719.
102. Hirota, T., Gerlich, D., Koch, B., Ellenberg, J., and Peters, J.M. (2004). Distinct functions of condensin I and II in mitotic chromosome assembly. Journal of cell science *117*, 6435-6445.
103. Ono, T., Fang, Y., Spector, D.L., and Hirano, T. (2004). Spatial and temporal regulation of Condensins I and II in mitotic chromosome assembly in human cells. Molecular biology of the cell *15*, 3296-3308.
104. Ono, T., Losada, A., Hirano, M., Myers, M.P., Neuwald, A.F., and Hirano, T. (2003). Differential contributions of condensin I and condensin II to mitotic chromosome architecture in vertebrate cells. Cell *115*, 109-121.
105. Chuang, P.T., Albertson, D.G., and Meyer, B.J. (1994). DPY-27:a chromosome condensation protein homolog that regulates C. elegans dosage compensation through association with the X chromosome. Cell *79*, 459-474.
106. Tsai, C.J., Mets, D.G., Albrecht, M.R., Nix, P., Chan, A., and Meyer, B.J. (2008). Meiotic crossover number and distribution are regulated by a dosage compensation protein that resembles a condensin subunit. Genes & development *22*, 194-211.
107. Collette, K.S., Petty, E.L., Golenberg, N., Bembenek, J.N., and Csankovszki, G. (2011). Different roles for Aurora B in condensin targeting during mitosis and meiosis. Journal of cell science *124*, 3684-3694.
108. Gerlich, D., Hirota, T., Koch, B., Peters, J.M., and Ellenberg, J. (2006). Condensin I stabilizes chromosomes mechanically through a dynamic interaction in live cells. Current biology : CB *16*, 333-344.
109. Hirano, T., and Mitchison, T.J. (1994). A heterodimeric coiled-coil protein required for mitotic chromosome condensation in vitro. Cell *79*, 449-458.
110. Shintomi, K., and Hirano, T. (2011). The relative ratio of condensin I to II determines chromosome shapes. Genes & development *25*, 1464-1469.

111. Fazzio, T.G., and Panning, B. (2010). Condensin complexes regulate mitotic progression and interphase chromatin structure in embryonic stem cells. The Journal of cell biology *188*, 491-503.
112. Lee, J., Ogushi, S., Saitou, M., and Hirano, T. (2011). Condensins I and II are essential for construction of bivalent chromosomes in mouse oocytes. Molecular biology of the cell *22*, 3465-3477.
113. Kim, J.H., Zhang, T., Wong, N.C., Davidson, N., Maksimovic, J., Oshlack, A., Earnshaw, W.C., Kalitsis, P., and Hudson, D.F. (2013). Condensin I associates with structural and gene regulatory regions in vertebrate chromosomes. Nature communications *4*, 2537.
114. Kranz, A.L., Jiao, C.Y., Winterkorn, L.H., Albritton, S.E., Kramer, M., and Ercan, S. (2013). Genome-wide analysis of condensin binding in Caenorhabditis elegans. Genome biology *14*, R112.
115. Van Bortle, K., Nichols, M.H., Li, L., Ong, C.T., Takenaka, N., Qin, Z.S., and Corces, V.G. (2014). Insulator function and topological domain border strength scale with architectural protein occupancy. Genome biology *15*, R82.
116. Green, L.C., Kalitsis, P., Chang, T.M., Cipetic, M., Kim, J.H., Marshall, O., Turnbull, L., Whitchurch, C.B., Vagnarelli, P., Samejima, K., et al. (2012). Contrasting roles of condensin I and condensin II in mitotic chromosome formation. Journal of cell science *125*, 1591-1604.
117. Freeman, L., Aragon-Alcaide, L., and Strunnikov, A. (2000). The condensin complex governs chromosome condensation and mitotic transmission of rDNA. The Journal of cell biology *149*, 811-824.
118. Hirano, T., Kobayashi, R., and Hirano, M. (1997). Condensins, chromosome condensation protein complexes containing XCAP-C, XCAP-E and a Xenopus homolog of the Drosophila Barren protein. Cell *89*, 511-521.
119. Sutani, T., Yuasa, T., Tomonaga, T., Dohmae, N., Takio, K., and Yanagida, M. (1999). Fission yeast condensin complex: essential roles of non-SMC subunits for condensation and Cdc2 phosphorylation of Cut3/SMC4. Genes & development *13*, 2271-2283.
120. Chan, R.C., Severson, A.F., and Meyer, B.J. (2004). Condensin restructures chromosomes in preparation for meiotic divisions. The Journal of cell biology *167*, 613-625.
121. Hagstrom, K.A., Holmes, V.F., Cozzarelli, N.R., and Meyer, B.J. (2002). C. elegans condensin promotes mitotic chromosome architecture, centromere organization, and sister chromatid segregation during mitosis and meiosis. Genes & development *16*, 729-742.
122. Hartl, T.A., Smith, H.F., and Bosco, G. (2008). Chromosome alignment and transvection are antagonized by condensin II. Science *322*, 1384-1387.
123. Hartl, T.A., Sweeney, S.J., Knepler, P.J., and Bosco, G. (2008). Condensin II resolves chromosomal associations to enable anaphase I segregation in Drosophila male meiosis. PLoS genetics *4*, e1000228.

124. Joyce, E.F., Williams, B.R., Xie, T., and Wu, C.T. (2012). Identification of genes that promote or antagonize somatic homolog pairing using a high-throughput FISH-based screen. PLoS genetics *8*, e1002667.
125. Buster, D.W., Daniel, S.G., Nguyen, H.Q., Windler, S.L., Skwarek, L.C., Peterson, M., Roberts, M., Meserve, J.H., Hartl, T., Klebba, J.E., et al. (2013). SCFSlimb ubiquitin ligase suppresses condensin II-mediated nuclear reorganization by degrading Cap-H2. The Journal of cell biology *201*, 49-63.
126. Bauer, C.R., Hartl, T.A., and Bosco, G. (2012). Condensin II promotes the formation of chromosome territories by inducing axial compaction of polyploid interphase chromosomes. PLoS genetics *8*, e1002873.
127. Rawlings, J.S., Gatzka, M., Thomas, P.G., and Ihle, J.N. (2011). Chromatin condensation via the condensin II complex is required for peripheral T-cell quiescence. The EMBO journal *30*, 263-276.
128. Xu, Y., Leung, C.G., Lee, D.C., Kennedy, B.K., and Crispino, J.D. (2006). MTB, the murine homolog of condensin II subunit CAP-G2, represses transcription and promotes erythroid cell differentiation. Leukemia *20*, 1261-1269.
129. Iwasaki, O., Tanaka, A., Tanizawa, H., Grewal, S.I., and Noma, K. (2010). Centromeric localization of dispersed Pol III genes in fission yeast. Molecular biology of the cell *21*, 254-265.
130. Haeusler, R.A., Pratt-Hyatt, M., Good, P.D., Gipson, T.A., and Engelke, D.R. (2008). Clustering of yeast tRNA genes is mediated by specific association of condensin with tRNA gene transcription complexes. Genes & development *22*, 2204-2214.
131. Lau, A.C., Nabeshima, K., and Csankovszki, G. (2014). The *C. elegans* dosage compensation complex mediates interphase X chromosome compaction. Epigenetics & chromatin *7*, 31.
132. Oda, H., Okamoto, I., Murphy, N., Chu, J., Price, S.M., Shen, M.M., Torres-Padilla, M.E., Heard, E., and Reinberg, D. (2009). Monomethylation of histone H4-lysine 20 is involved in chromosome structure and stability and is essential for mouse development. Molecular and cellular biology *29*, 2278-2295.
133. Rice, J.C., Nishioka, K., Sarma, K., Steward, R., Reinberg, D., and Allis, C.D. (2002). Mitotic-specific methylation of histone H4 Lys 20 follows increased PR-Set7 expression and its localization to mitotic chromosomes. Genes & development *16*, 2225-2230.
134. Wilkins, B.J., Rall, N.A., Ostwal, Y., Kruitwagen, T., Hiragami-Hamada, K., Winkler, M., Barral, Y., Fischle, W., and Neumann, H. (2014). A cascade of histone modifications induces chromatin condensation in mitosis. Science *343*, 77-80.
135. Shogren-Knaak, M., Ishii, H., Sun, J.M., Pazin, M.J., Davie, J.R., and Peterson, C.L. (2006). Histone H4-K16 acetylation controls chromatin structure and protein interactions. Science *311*, 844-847.
136. Liu, W., Tanasa, B., Tyurina, O.V., Zhou, T.Y., Gassmann, R., Liu, W.T., Ohgi, K.A., Benner, C., Garcia-Bassets, I., Aggarwal, A.K., et al. (2010). PHF8

mediates histone H4 lysine 20 demethylation events involved in cell cycle progression. Nature *466*, 508-512.
137. Kimura, K., and Hirano, T. (1997). ATP-dependent positive supercoiling of DNA by 13S condensin: a biochemical implication for chromosome condensation. Cell *90*, 625-634.
138. Sakai, A., Hizume, K., Sutani, T., Takeyasu, K., and Yanagida, M. (2003). Condensin but not cohesin SMC heterodimer induces DNA reannealing through protein-protein assembly. The EMBO journal *22*, 2764-2775.
139. Kimura, K., Cuvier, O., and Hirano, T. (2001). Chromosome condensation by a human condensin complex in Xenopus egg extracts. The Journal of biological chemistry *276*, 5417-5420.
140. Kimura, K., and Hirano, T. (2000). Dual roles of the 11S regulatory subcomplex in condensin functions. Proceedings of the National Academy of Sciences of the United States of America *97*, 11972-11977.
141. St-Pierre, J., Douziech, M., Bazile, F., Pascariu, M., Bonneil, E., Sauve, V., Ratsima, H., and D'Amours, D. (2009). Polo kinase regulates mitotic chromosome condensation by hyperactivation of condensin DNA supercoiling activity. Molecular cell *34*, 416-426.
142. Baxter, J., Sen, N., Martinez, V.L., De Carandini, M.E., Schvartzman, J.B., Diffley, J.F., and Aragon, L. (2011). Positive supercoiling of mitotic DNA drives decatenation by topoisomerase II in eukaryotes. Science *331*, 1328-1332.
143. Kimura, K., Rybenkov, V.V., Crisona, N.J., Hirano, T., and Cozzarelli, N.R. (1999). 13S condensin actively reconfigures DNA by introducing global positive writhe: implications for chromosome condensation. Cell *98*, 239-248.
144. Kimura, K., Hirano, M., Kobayashi, R., and Hirano, T. (1998). Phosphorylation and activation of 13S condensin by Cdc2 in vitro. Science *282*, 487-490.
145. Takemoto, A., Kimura, K., Yanagisawa, J., Yokoyama, S., and Hanaoka, F. (2006). Negative regulation of condensin I by CK2-mediated phosphorylation. The EMBO journal *25*, 5339-5348.
146. Cuylen, S., Metz, J., and Haering, C.H. (2011). Condensin structures chromosomal DNA through topological links. Nature structural & molecular biology *18*, 894-901.
147. Haering, C.H., Farcas, A.M., Arumugam, P., Metson, J., and Nasmyth, K. (2008). The cohesin ring concatenates sister DNA molecules. Nature *454*, 297-301.
148. Crane, E., Bian, Q., McCord, R.P., Lajoie, B.R., Wheeler, B.S., Ralston, E.J., Uzawa, S., Dekker, J., and Meyer, B.J. (2015). Condensin-driven remodelling of X chromosome topology during dosage compensation. Nature *523*, 240-244.
149. Dekker, J., and Mirny, L. (2013). Biological techniques: Chromosomes captured one by one. Nature *502*, 45-46.
150. Naumova, N., Imakaev, M., Fudenberg, G., Zhan, Y., Lajoie, B.R., Mirny, L.A., and Dekker, J. (2013). Organization of the mitotic chromosome. Science *342*, 948-953.

151. Luger, K., Dechassa, M.L., and Tremethick, D.J. (2012). New insights into nucleosome and chromatin structure: an ordered state or a disordered affair? Nat Rev Mol Cell Bio *13*, 436-447.
152. Clark, D.J. (2010). Nucleosome positioning, nucleosome spacing and the nucleosome code. Journal of biomolecular structure & dynamics *27*, 781-793.
153. Zink, L.M., and Hake, S.B. (2016). Histone variants: nuclear function and disease. Current opinion in genetics & development *37*, 82-89.
154. Bhaumik, S.R., Smith, E., and Shilatifard, A. (2007). Covalent modifications of histones during development and disease pathogenesis. Nature structural & molecular biology *14*, 1008-1016.
155. Kouzarides, T. (2007). Chromatin modifications and their function. Cell *128*, 693-705.
156. Campos, E.I., and Reinberg, D. (2009). Histones: annotating chromatin. Annual review of genetics *43*, 559-599.
157. Luger, K., Mader, A.W., Richmond, R.K., Sargent, D.F., and Richmond, T.J. (1997). Crystal structure of the nucleosome core particle at 2.8 A resolution. Nature *389*, 251-260.
158. Loidl, P. (1994). Histone Acetylation - Facts and Questions. Chromosoma *103*, 441-449.
159. Sterner, D.E., and Berger, S.L. (2000). Acetylation of histones and transcription-related factors. Microbiology and molecular biology reviews : MMBR *64*, 435-459.
160. Zhou, V.W., Goren, A., and Bernstein, B.E. (2011). Charting histone modifications and the functional organization of mammalian genomes. Nature reviews. Genetics *12*, 7-18.
161. Choudhary, C., Kumar, C., Gnad, F., Nielsen, M.L., Rehman, M., Walther, T.C., Olsen, J.V., and Mann, M. (2009). Lysine acetylation targets protein complexes and co-regulates major cellular functions. Science *325*, 834-840.
162. Jenuwein, T., and Allis, C.D. (2001). Translating the histone code. Science *293*, 1074-1080.
163. Hong, L., Schroth, G.P., Matthews, H.R., Yau, P., and Bradbury, E.M. (1993). Studies of the DNA binding properties of histone H4 amino terminus. Thermal denaturation studies reveal that acetylation markedly reduces the binding constant of the H4 "tail" to DNA. The Journal of biological chemistry *268*, 305-314.
164. Workman, J.L., and Kingston, R.E. (1998). Alteration of nucleosome structure as a mechanism of transcriptional regulation. Annu Rev Biochem *67*, 545-579.
165. Winston, F., and Allis, C.D. (1999). The bromodomain: a chromatin-targeting module? Nature structural biology *6*, 601-604.
166. Dorigo, B., Schalch, T., Bystricky, K., and Richmond, T.J. (2003). Chromatin fiber folding: requirement for the histone H4 N-terminal tail. Journal of molecular biology *327*, 85-96.
167. Taipale, M., Rea, S., Richter, K., Vilar, A., Lichter, P., Imhof, A., and Akhtar, A. (2005). hMOF histone acetyltransferase is required for histone H4 lysine 16 acetylation in mammalian cells. Molecular and cellular biology *25*, 6798-6810.

168. Smith, C.M., Gafken, P.R., Zhang, Z.L., Gottschling, D.E., Smith, J.B., and Smith, D.L. (2003). Mass spectrometric quantification of acetylation at specific lysines within the amino-terminal tail of histone H4. Anal Biochem *316*, 23-33.
169. Thorne, A.W., Kmiciek, D., Mitchelson, K., Sautiere, P., and Cranerobinson, C. (1990). Patterns of Histone Acetylation. Eur J Biochem *193*, 701-713.
170. Turner, B.M., Oneill, L.P., and Allan, I.M. (1989). Histone-H4 Acetylation in Human-Cells - Frequency of Acetylation at Different Sites Defined by Immunolabeling with Site-Specific Antibodies. FEBS letters *253*, 141-145.
171. Garcia, B.A., Hake, S.B., Diaz, R.L., Kauer, M., Morris, S.A., Recht, J., Shabanowitz, J., Mishra, N., Strahl, B.D., Allis, C.D., et al. (2007). Organismal differences in post-translational modifications in histones H3 and H4. Journal of Biological Chemistry *282*, 7641-7655.
172. Zhang, K.L., Williams, K.E., Huang, L., Yau, P., Siino, J.S., Bradbury, E.M., Jones, P.R., Minch, M.J., and Burlingame, A.L. (2002). Histone acetylation and deacetylation - Identification of acetylation and methylation sites of HeLa histone H4 by mass spectrometry. Mol Cell Proteomics *1*, 500-508.
173. Allahverdi, A., Yang, R.L., Korolev, N., Fan, Y.P., Davey, C.A., Liu, C.F., and Nordenskiold, L. (2011). The effects of histone H4 tail acetylations on cation-induced chromatin folding and self-association. Nucleic acids research *39*, 1680-1691.
174. Kalashnikova, A.A., Porter-Goff, M.E., Muthurajan, U.M., Luger, K., and Hansen, J.C. (2013). The role of the nucleosome acidic patch in modulating higher order chromatin structure. J R Soc Interface *10*.
175. Robinson, P.J., An, W., Routh, A., Martino, F., Chapman, L., Roeder, R.G., and Rhodes, D. (2008). 30 nm chromatin fibre decompaction requires both H4-K16 acetylation and linker histone eviction. Journal of molecular biology *381*, 816-825.
176. Vignali, M., Hassan, A.H., Neely, K.E., and Workman, J.L. (2000). ATP-dependent chromatin-remodeling complexes. Molecular and cellular biology *20*, 1899-1910.
177. Eberharter, A., Langst, G., and Becker, P.B. (2004). A nucleosome sliding assay for chromatin remodeling factors. Methods in enzymology *377*, 344-353.
178. Clapier, C.R., Langst, G., Corona, D.F., Becker, P.B., and Nightingale, K.P. (2001). Critical role for the histone H4 N terminus in nucleosome remodeling by ISWI. Molecular and cellular biology *21*, 875-883.
179. Clapier, C.R., Nightingale, K.P., and Becker, P.B. (2002). A critical epitope for substrate recognition by the nucleosome remodeling ATPase ISWI. Nucleic acids research *30*, 649-655.
180. Corona, D.F., Clapier, C.R., Becker, P.B., and Tamkun, J.W. (2002). Modulation of ISWI function by site-specific histone acetylation. EMBO reports *3*, 242-247.
181. Vaquero, A., Sternglanz, R., and Reinberg, D. (2007). NAD+-dependent deacetylation of H4 lysine 16 by class III HDACs. Oncogene *26*, 5505-5520.
182. Utley, R.T., and Cote, J. (2003). The MYST family of histone acetyltransferases. Current topics in microbiology and immunology *274*, 203-236.

183. Thomas, T., and Voss, A.K. (2007). The diverse biological roles of MYST histone acetyltransferase family proteins. Cell cycle *6*, 696-704.
184. Voss, A.K., and Thomas, T. (2009). MYST family histone acetyltransferases take center stage in stem cells and development. BioEssays : news and reviews in molecular, cellular and developmental biology *31*, 1050-1061.
185. Li, H., Ilin, S., Wang, W., Duncan, E.M., Wysocka, J., Allis, C.D., and Patel, D.J. (2006). Molecular basis for site-specific read-out of histone H3K4me3 by the BPTF PHD finger of NURF. Nature *442*, 91-95.
186. Shi, X., Hong, T., Walter, K.L., Ewalt, M., Michishita, E., Hung, T., Carney, D., Pena, P., Lan, F., Kaadige, M.R., et al. (2006). ING2 PHD domain links histone H3 lysine 4 methylation to active gene repression. Nature *442*, 96-99.
187. Wysocka, J., Swigut, T., Xiao, H., Milne, T.A., Kwon, S.Y., Landry, J., Kauer, M., Tackett, A.J., Chait, B.T., Badenhorst, P., et al. (2006). A PHD finger of NURF couples histone H3 lysine 4 trimethylation with chromatin remodelling. Nature *442*, 86-90.
188. Sanjuan, R., and Marin, I. (2001). Tracing the origin of the compensasome: evolutionary history of DEAH helicase and MYST acetyltransferase gene families. Molecular biology and evolution *18*, 330-343.
189. Fischle, W., Wang, Y., Jacobs, S.A., Kim, Y., Allis, C.D., and Khorasanizadeh, S. (2003). Molecular basis for the discrimination of repressive methyl-lysine marks in histone H3 by Polycomb and HP1 chromodomains. Genes & development *17*, 1870-1881.
190. Jacobs, S.A., Taverna, S.D., Zhang, Y., Briggs, S.D., Li, J., Eissenberg, J.C., Allis, C.D., and Khorasanizadeh, S. (2001). Specificity of the HP1 chromo domain for the methylated N-terminus of histone H3. The EMBO journal *20*, 5232-5241.
191. Kimura, A., Umehara, T., and Horikoshi, M. (2002). Chromosomal gradient of histone acetylation established by Sas2p and Sir2p functions as a shield against gene silencing. Nature genetics *32*, 370-377.
192. Suka, N., Luo, K., and Grunstein, M. (2002). Sir2p and Sas2p opposingly regulate acetylation of yeast histone H4 lysine16 and spreading of heterochromatin. Nature genetics *32*, 378-383.
193. Dou, Y., Milne, T.A., Tackett, A.J., Smith, E.R., Fukuda, A., Wysocka, J., Allis, C.D., Chait, B.T., Hess, J.L., and Roeder, R.G. (2005). Physical association and coordinate function of the H3 K4 methyltransferase MLL1 and the H4 K16 acetyltransferase MOF. Cell *121*, 873-885.
194. Mendjan, S., Taipale, M., Kind, J., Holz, H., Gebhardt, P., Schelder, M., Vermeulen, M., Buscaino, A., Duncan, K., Mueller, J., et al. (2006). Nuclear pore components are involved in the transcriptional regulation of dosage compensation in Drosophila. Molecular cell *21*, 811-823.
195. Cai, Y., Jin, J., Swanson, S.K., Cole, M.D., Choi, S.H., Florens, L., Washburn, M.P., Conaway, J.W., and Conaway, R.C. (2010). Subunit composition and substrate specificity of a MOF-containing histone acetyltransferase distinct from the male-specific lethal (MSL) complex. The Journal of biological chemistry *285*, 4268-4272.

196. Shia, W.J., Osada, S., Florens, L., Swanson, S.K., Washburn, M.P., and Workman, J.L. (2005). Characterization of the yeast trimeric-SAS acetyltransferase complex. The Journal of biological chemistry *280*, 11987-11994.
197. Thomas, T., Dixon, M.P., Kueh, A.J., and Voss, A.K. (2008). Mof (MYST1 or KAT8) is essential for progression of embryonic development past the blastocyst stage and required for normal chromatin architecture. Molecular and cellular biology *28*, 5093-5105.
198. Gupta, A., Guerin-Peyrou, T.G., Sharma, G.G., Park, C., Agarwal, M., Ganju, R.K., Pandita, S., Choi, K., Sukumar, S., Pandita, R.K., et al. (2008). The mammalian ortholog of Drosophila MOF that acetylates histone H4 lysine 16 is essential for embryogenesis and oncogenesis. Molecular and cellular biology *28*, 397-409.
199. Feller, C., Prestel, M., Hartmann, H., Straub, T., Soding, J., and Becker, P.B. (2012). The MOF-containing NSL complex associates globally with housekeeping genes, but activates only a defined subset. Nucleic acids research *40*, 1509-1522.
200. Lam, K.C., Muhlpfordt, F., Vaquerizas, J.M., Raja, S.J., Holz, H., Luscombe, N.M., Manke, T., and Akhtar, A. (2012). The NSL Complex Regulates Housekeeping Genes in Drosophila. PLoS genetics *8*.
201. Raja, S.J., Charapitsa, I., Conrad, T., Vaquerizas, J.M., Gebhardt, P., Holz, H., Kadlec, J., Fraterman, S., Luscombe, N.M., and Akhtar, A. (2010). The Nonspecific Lethal Complex Is a Transcriptional Regulator in Drosophila. Molecular cell *38*, 827-841.
202. Kamine, J., Elangovan, B., Subramanian, T., Coleman, D., and Chinnadurai, G. (1996). Identification of a cellular protein that specifically interacts with the essential cysteine region of the HIV-1 Tat transactivator. Virology *216*, 357-366.
203. Doyon, Y., Selleck, W., Lane, W.S., Tan, S., and Cote, J. (2004). Structural and functional conservation of the NuA4 histone acetyltransferase complex from yeast to humans. Molecular and cellular biology *24*, 1884-1896.
204. Boudreault, A.A., Cronier, D., Selleck, W., Lacoste, N., Utley, R.T., Allard, S., Savard, J., Lane, W.S., Tan, S., and Cote, J. (2003). Yeast enhancer of polycomb defines global Esa1-dependent acetylation of chromatin. Genes & development *17*, 1415-1428.
205. Allard, S., Utley, R.T., Savard, J., Clarke, A., Grant, P., Brandl, C.J., Pillus, L., Workman, J.L., and Cote, J. (1999). NuA4, an essential transcription adaptor/histone H4 acetyltransferase complex containing Esa1p and the ATM-related cofactor Tra1p. The EMBO journal *18*, 5108-5119.
206. Clarke, A.S., Lowell, J.E., Jacobson, S.J., and Pillus, L. (1999). Esa1p is an essential histone acetyltransferase required for cell cycle progression. Molecular and cellular biology *19*, 2515-2526.
207. Reid, J.L., Iyer, V.R., Brown, P.O., and Struhl, K. (2000). Coordinate regulation of yeast ribosomal protein genes is associated with targeted recruitment of Esa1 histone acetylase. Molecular cell *6*, 1297-1307.

208. Vogelauer, M., Wu, J., Suka, N., and Grunstein, M. (2000). Global histone acetylation and deacetylation in yeast. Nature *408*, 495-498.
209. Utley, R.T., Ikeda, K., Grant, P.A., Cote, J., Steger, D.J., Eberharter, A., John, S., and Workman, J.L. (1998). Transcriptional activators direct histone acetyltransferase complexes to nucleosomes. Nature *394*, 498-502.
210. Galarneau, L., Nourani, A., Boudreault, A.A., Zhang, Y., Heliot, L., Allard, S., Savard, J., Lane, W.S., Stillman, D.J., and Cote, J. (2000). Multiple links between the NuA4 histone acetyltransferase complex and epigenetic control of transcription. Molecular cell *5*, 927-937.
211. Reid, J.L., Moqtaderi, Z., and Struhl, K. (2004). Eaf3 regulates the global pattern of histone acetylation in Saccharomyces cerevisiae. Molecular and cellular biology *24*, 757-764.
212. Auger, A., Galarneau, L., Altaf, M., Nourani, A., Doyon, Y., Utley, R.T., Cronier, D., Allard, S., and Cote, J. (2008). Eaf1 is the platform for NuA4 molecular assembly that evolutionarily links chromatin acetylation to ATP-dependent exchange of histone H2A variants. Molecular and cellular biology *28*, 2257-2270.
213. Krogan, N.J., Keogh, M.C., Datta, N., Sawa, C., Ryan, O.W., Ding, H., Haw, R.A., Pootoolal, J., Tong, A., Canadien, V., et al. (2003). A Snf2 family ATPase complex required for recruitment of the histone H2A variant Htz1. Molecular cell *12*, 1565-1576.
214. Mizuguchi, G., Shen, X., Landry, J., Wu, W.H., Sen, S., and Wu, C. (2004). ATP-driven exchange of histone H2AZ variant catalyzed by SWR1 chromatin remodeling complex. Science *303*, 343-348.
215. Altaf, M., Auger, A., Monnet-Saksouk, J., Brodeur, J., Piquet, S., Cramet, M., Bouchard, N., Lacoste, N., Utley, R.T., Gaudreau, L., et al. (2010). NuA4-dependent acetylation of nucleosomal histones H4 and H2A directly stimulates incorporation of H2A.Z by the SWR1 complex. The Journal of biological chemistry *285*, 15966-15977.
216. Ikura, T., Ogryzko, V.V., Grigoriev, M., Groisman, R., Wang, J., Horikoshi, M., Scully, R., Qin, J., and Nakatani, Y. (2000). Involvement of the TIP60 histone acetylase complex in DNA repair and apoptosis. Cell *102*, 463-473.
217. Kimura, A., and Horikoshi, M. (1998). Tip60 acetylates six lysines of a specific class in core histones in vitro. Genes to cells : devoted to molecular & cellular mechanisms *3*, 789-800.
218. Smith, E.R., Eisen, A., Gu, W., Sattah, M., Pannuti, A., Zhou, J., Cook, R.G., Lucchesi, J.C., and Allis, C.D. (1998). ESA1 is a histone acetyltransferase that is essential for growth in yeast. Proceedings of the National Academy of Sciences of the United States of America *95*, 3561-3565.
219. Kusch, T., Florens, L., MacDonald, W.H., Swanson, S.K., Glaser, R.L., Yates, J.R., Abmayr, S.M., Washburn, M.P., and Workman, J.L. (2004). Acetylation by Tip60 is required for selective histone variant exchange at DNA lesions. Science *306*, 2084-2087.
220. Sapountzi, V., Logan, I.R., and Robson, C.N. (2006). Cellular functions of TIP60. The international journal of biochemistry & cell biology *38*, 1496-1509.

221. Frank, S.R., Parisi, T., Taubert, S., Fernandez, P., Fuchs, M., Chan, H.M., Livingston, D.M., and Amati, B. (2003). MYC recruits the TIP60 histone acetyltransferase complex to chromatin. EMBO reports *4*, 575-580.
222. Patel, J.H., Du, Y., Ard, P.G., Phillips, C., Carella, B., Chen, C.J., Rakowski, C., Chatterjee, C., Lieberman, P.M., Lane, W.S., et al. (2004). The c-MYC oncoprotein is a substrate of the acetyltransferases hGCN5/PCAF and TIP60. Molecular and cellular biology *24*, 10826-10834.
223. Sykes, S.M., Mellert, H.S., Holbert, M.A., Li, K., Marmorstein, R., Lane, W.S., and McMahon, S.B. (2006). Acetylation of the p53 DNA-binding domain regulates apoptosis induction. Molecular cell *24*, 841-851.
224. Tang, Y., Luo, J., Zhang, W., and Gu, W. (2006). Tip60-dependent acetylation of p53 modulates the decision between cell-cycle arrest and apoptosis. Molecular cell *24*, 827-839.
225. Taubert, S., Gorrini, C., Frank, S.R., Parisi, T., Fuchs, M., Chan, H.M., Livingston, D.M., and Amati, B. (2004). E2F-dependent histone acetylation and recruitment of the Tip60 acetyltransferase complex to chromatin in late G1. Molecular and cellular biology *24*, 4546-4556.
226. Gorrini, C., Squatrito, M., Luise, C., Syed, N., Perna, D., Wark, L., Martinato, F., Sardella, D., Verrecchia, A., Bennett, S., et al. (2007). Tip60 is a haplo-insufficient tumour suppressor required for an oncogene-induced DNA damage response. Nature *448*, 1063-U1012.
227. Zhu, X.M., Singh, N., Donnelly, C., Boimel, P., and Elefant, F. (2007). The cloning and characterization of the histone acetyltransferase human homolog Dmel\TIP60 in Drosophila melanogaster: Dmel\TIP60 is essential for multicellular development. Genetics *175*, 1229-1240.
228. Ceol, C.J., and Horvitz, H.R. (2004). A new class of C. elegans synMuv genes implicates a Tip60/NuA4-like HAT complex as a negative regulator of Ras signaling. Developmental cell *6*, 563-576.
229. Fazzio, T.G., Huff, J.T., and Panning, B. (2008). An RNAi screen of chromatin proteins identifies Tip60-p400 as a regulator of embryonic stem cell identity. Cell *134*, 162-174.

CHAPTER 2

The *C. elegans* dosage compensation complex mediates interphase X chromosome compaction

This chapter was published as Lau AC, Nabeshima K, Csankovszki G (2014) in Epigenetics & Chromatin as "The *C. elegans* dosage compensation complex mediates interphase X chromosome compaction." I conducted the experiments and image analysis for data shown in all figures.

ABSTRACT

Dosage compensation is a specialized gene regulatory mechanism which equalizes X-linked gene expression between sexes. In *Caenorhabditis elegans,* dosage compensation is achieved by the activity of the dosage compensation complex (DCC). The DCC localizes to both X chromosomes in hermaphrodites to downregulate gene expression by half. The DCC contains a subcomplex (condensin I^{DC}) similar to the evolutionarily conserved condensin complexes which play fundamental roles in chromosome dynamics during mitosis and meiosis. Therefore, mechanisms related to mitotic chromosome condensation have been long hypothesized to mediate dosage compensation. However experimental evidence was lacking.

Using 3D FISH microscopy to measure the volumes of X and chromosome I territories and to measure distances between individual loci, we show that hermaphrodite worms deficient in DCC proteins have enlarged interphase X chromosomes when compared to wild type. By contrast, chromosome I is unaffected. Interestingly, hermaphrodite worms depleted of condensin I or II show no phenotype. Therefore X chromosome compaction is specific to condensin I^{DC}. In addition, we show that SET-1, SET-4, and SIR-2.1, histone modifiers whose activity is regulated by the DCC, need to be present for the compaction of the X chromosome territory.

These results support the idea that condensin I^{DC}, and the histone modifications regulated by the DCC, mediate interphase X chromosome compaction. Our results link condensin-mediated chromosome compaction, an activity connected to mitotic chromosome condensation, to chromosome-wide repression of gene expression in interphase.

INTRODUCTION

In many species, such as humans, mice, flies, and worms, sex is determined by a chromosome-based method which entails a difference in sex chromosome number between heterogametic males (XY or XO) and homogametic females (XX). If left uncorrected this difference puts one sex at a disadvantage. Therefore, species have evolved a specialized gene regulatory mechanism to correct this imbalance, known as dosage compensation. Dosage compensation balances X and autosomal expression and equalizes gene expression between the sexes [1].

The molecular mechanisms of dosage compensation varies among species. Mammals, flies, and worms achieve dosage compensation using three distinct strategies. In the fly, *Drosophila melanogaster*, the male X is upregulated by two-fold, a mechanism that balances gene expression between the X and autosomes and equalizes male to female X-linked gene expression [2,3]. In mammals and the nematode *C. elegans*, it is hypothesized that an unknown mechanism upregulates X chromosome expression in both sexes [4-8]. Although X upregulation balances X and autosomal expression in males it also causes X overexpression in females/hermaphrodites. As a result, to prevent hyperexpression of the X chromosomes, mammalian XX females inactivate one X [9-11], while XX hermaphrodite *C. elegans* worms downregulate both X chromosomes two-fold [12,13]. Although dosage compensation mechanisms vary among species, all lead to the balance between X and autosomal expression and equalize gene expression between the sexes.

In *C. elegans*, dosage compensation is achieved by the dosage compensation complex (DCC) which binds to both X chromosomes to downregulate X-linked gene expression in hermaphrodites. Condensin I^{DC}, a subcomplex within the DCC, contains two SMC (structural maintenance of chromosome) proteins (DPY-27 and MIX-1) and three CAP (chromosome-associated polypeptide) proteins (DPY-26, DPY-28, and CAPG-1). In addition, the DCC contains five associated proteins (SDC-1, SDC-2, SDC-3, DPY-30, and DPY-21) [14-21]. Interestingly, condensin I^{DC} differs from the mitotic condensin I complex by only one subunit: DPY-27 replaces SMC-4 [15,21]. Condensins

are evolutionarily conserved complexes, which promote chromosome compaction, organization, and segregation during mitosis and meiosis [22]. Although condensin I^{DC} is homologous to condensin, the DCC appears to have no mitotic function, and it instead functions in the repression of gene expression. Because condensin complexes organize and compact chromosomes in preparation for mitosis, it has been long hypothesized that DCC activity also results in changes in X chromosome compaction [14]. However the direct experimental evidence supporting this hypothesis is lacking.

Condensins (I and II) are conserved protein complexes that organize chromatin structure and whose functions are best studied in mitosis and meiosis. Although structurally similar, the mitotic functions of condensins I and II differ. Condensin I laterally compacts mitotic chromosomes, whereas condensin II mediates axial compaction and rigidity [23-26]. During *C. elegans* meiosis, the depletion of condensin I or condensin II leads to an expansion of chromosome axial length [21]. In *Xenopus laevis* eggs, *S. pombe* and *S. cerevisiae,* condensin is required for mitotic chromosome condensation [27-30], while in other organisms, such as mammals and worms, condensin II is required for prophase condensation [15,24,31]. However, in many systems, including *Drosophila*, worms, mammals, and chicken DT40 cells, depletion of condensins I and II leads primarily to defects in anaphase chromosome segregation, such as lagging chromosomes and chromosome bridges, rather than defects in chromosome condensation [22]. Overall, in many organisms, mitotic chromosomes still compact when condensin is disrupted suggesting that condensin is not solely responsible for chromosome condensation.

Condensin activities are well studied in mitosis and meiosis, but the interphase functions of condensins are less understood. In higher eukaryotes condensin I is cytoplasmic in interphase and loads onto chromosomes after nuclear envelope breakdown, whereas condensin II is nuclear throughout the cell cycle [24,26,32-34]. Therefore, it is condensin II, rather than condensin I, that is thought to play an important role in the interphase nucleus in these organisms. In *Drosophila*, condensin II activity disrupts somatic homolog pairing and leads to interphase chromosome compaction [35-38]. In addition to compaction, condensin II is required for the proper formation of chromosome territories [39]. Evidence of condensin II-mediated interphase chromosome compaction has also been demonstrated during the development of quiescent naïve T-cells [40] and in mouse embryonic stem cells [41]. In both budding and fission yeast, condensin-dependent RNA polymerase III-transcribed gene clustering at or near the nucleolus contributes to the three-dimensional organization of the genome [42,43]. Although there is accumulating evidence demonstrating that condensin II, or the single yeast condensin, participates in interphase chromatin organization, whether the condensin I-like complex, condensin I^{DC}, organizes the interphase X chromosome in a similar manner is unclear.

Emerging evidence has uncovered that histone tail modifications also influence mitotic chromosome condensation. During cell cycle progression the acetylation of histone H4 lysine 16 (H4K16ac) increases during S phase and decreases during mitosis [44,45]. By contrast, histone H4 lysine 20 monomethylation (H4K20me1) levels are higher in mitosis [44,46]. Expression of the H4K20 methyltransferase, PR-SET7, is

coincident with the increase of H4K20me1 during mitosis [44,46]. The negative correlation between these two modifications during the cell cycle is consistent with previous findings that H4K20me1 antagonizes H4K16ac [47]. In yeast, the phosphorylation of histone H3 serine 10 recruits the Sir2 homolog Hst2 to promote deacetylation of H4K16ac. Together, this cascade of histone modifications was proposed to drive chromatin hypercondensation during mitosis, independently from condensin [45].

Interestingly, similar changes in histone modifications are observed on interphase dosage compensated X chromosomes in *C. elegans*. The DCC regulates SET-1 (PR-SET7 homolog) and SET-4 (SUV4-20 homolog), which together mediate the enrichment of H4K20me1 on the X chromosomes [48,49]. The DCC also regulates SIR-2.1 (Sir2 homolog), which mediates the depletion of H4K16ac on the X chromosomes [49]. These observations suggest that interphase dosage compensated X chromosomes possess some characteristics associated with condensed mitotic chromosome.

In this study, we present experimental evidence linking condensin-mediated chromosome compaction to chromosome-wide repression of gene expression during dosage compensation. We show that hermaphrodite worms deficient in DCC function, as well as male worms, exhibit enlarged X chromosomes when compared to wild type hermaphrodites. This result supports the idea that condensin I^{DC} mediates interphase X chromosome compaction. In addition, we show that DCC-regulated histone modifiers contribute to X chromosome compaction. Together these results give us more insight

into the functional link between mitotic chromosome condensation and epigenetic control of gene expression.

RESULTS

Dosage compensation mediates changes in X chromosome volumes

To look for changes in chromosome packaging in dosage compensation we utilized chromosome-paint 3D fluorescent *in situ* hybridization (FISH) to measure the volumes of chromosome X and I territories in wild type and DCC-depleted hermaphrodite and male nuclei. These chromosome-paints were generated from yeast artificial chromosome (YAC) DNA and cover approximately 90% of the X chromosome and 86% of chromosome I [50]. We analyzed intestinal nuclei, which are 32-ploid, making visualization and quantification easier [51]. Chromosome territories were defined by selecting intensity threshold based masks of both the chromosome paint signals and the whole nucleus. These defined mask selections allowed us to calculate the volume of the specific chromosome and the whole nucleus. We then quantified the volume of chromosome territories by calculating the percentage of nuclear volume occupied by the X or chromosome I paint in a single nucleus (see Materials and Methods) (Figure 2.1A). Normalization to total nuclear volumes was necessary to minimize the inherent sample-to-sample variation due to the harsh conditions of FISH. Based on DNA content and assuming equal packaging of all chromosomes, the expected percentages for the X and chromosome I are shown on Figure 2.1B [52]. If DCC activity results in chromosome compaction we expect to see a larger X chromosome territory in DCC-depleted nuclei compared to the wild type hermaphrodites. In addition, because males have one non-

dosage compensated X, we would expect the single male X territory to be about half as large as the two non-dosage compensated Xs in DCC-depleted hermaphrodites, but larger than half of the two dosage compensated Xs in wild type hermaphrodites.

We observed that the X chromosome territories in hermaphrodite nuclei depleted of the DCC subunit DPY-27 occupied a significantly larger percentage than in wild type hermaphrodite nuclei (Figure 2.1C and D). In wild type hermaphrodites the X chromosome territories were compact with a mean percent nuclear volume of 10.31 ± 1.98%. Depletion of the condensin I^{DC}-specific protein, DPY-27 [14], by feeding RNAi, led to enlarged X chromosomes compared to wild type, occupying 17.28 ± 3.16% of the nucleus (P = 8.49E-22). Interestingly, the volume of the X chromosomes in DPY-27-depleted hermaphrodite nuclei closely correlates with the X chromosome DNA content relative to the total genome size of *C. elegans,* 18%, see Figure 2.1B. The smaller percent nuclear volume in wild type hermaphrodites suggests that condensin I^{DC} activity results in X chromosomes that are more compact than genomic average.

We predicted that the percent nuclear volume of a single male X would be close to half of the volume of the two DPY-27-depleted hermaphrodite X chromosomes, about 9%, and close to the percent predicted by DNA content, about 10%, see Figure 2.1B. Surprisingly, we found that the single X chromosome territory in males was larger, occupying the mean percentage of 15.73 ± 2.63. It is possible that the DPY-27-depleted X chromosome territory is not fully decondensed because a small amount of DPY-27 remains after feeding RNAi. An alternate possibility is that chromosome decondensation might contribute to X upregulation in males. X upregulation has been hypothesized to

occur in both sexes in mammals and worms to balance the single male X to autosomes; however the mechanism in worms is unknown (see Discussion). We also analyzed males depleted of DPY-27 and found that the X chromosome remained unchanged compared to control males. Together these results support the idea that condensin I^{DC} mediates X chromosome compaction in hermaphrodites and suggest that chromosome decondensation may be involved in X upregulation in males.

We next asked whether the observed enlargement of chromosome territories was specific to the dosage compensated X chromosomes by analyzing the autosomal territory of chromosome I. The percentage occupied by chromosome I was consistent in wild type hermaphrodites (14.26 ± 2.57), males (14.24 ± 2.90), and *dpy-27(RNAi)* hermaphrodite worms (14.46 ± 2.50) (Figure 2.1E and F). Like the X chromosomes in DPY-27-depleted nuclei, the volume occupied by chromosome I closely correlates with the DNA content of chromosome I relative to the total genome size (Figure 2.1B). These data indicate that the chromosome territory enlargement in DPY-27-depleted nuclei is not occurring genome-wide but is unique to the dosage compensated X chromosomes.

Next, we wanted to test whether the loss of DCC subunits other than DPY-27 has similar effects on X chromosome volume. We performed the same analysis as described above in worms depleted of, or carrying mutations in the genes encoding, either DPY-30 or DPY-21. We chose these specific genes because dosage compensation function and DCC localization is disrupted when DPY-30 is depleted [53,54], whereas in DPY-21 depleted worms dosage compensation function is disrupted but the DCC still localizes to the X chromosome [20]. Similar to *dpy-27(RNAi)* worms,

dpy-30(RNAi) and *dpy-21(RNAi)* worms as well as *dpy-30(y228)* and *dpy-21(e428)* mutants had larger X chromosomes compared to control worms fed bacteria carrying an empty vector or wild type worms (Figure 2.2A-C and Figure 2.8). The mean percentages occupied by the X chromosomes in the DCC-depleted animals were 70% larger than the control. In addition, the size of chromosome I territory was unchanged, occupying a mean percentage of 14.5 in all backgrounds (Figure 2.2D and E, and Figure 2.8). Taken together, these results indicate that wild type and control intestinal nuclei have compact X chromosome territories and this organizational pattern is dependent upon dosage compensation.

Consistent with dosage compensation's role in reducing gene expression, our data show that relative size of X chromosomes is also reduced. We next wanted to determine if the two X chromosomes behave similarly and are compacted to similar extents. We performed this analysis in the 32-ploid intestinal nuclei. We measured individual chromosome volumes, arbitrarily designating the larger territory X_1 and the smaller territory X_2. Fifty-two percent of vector control worms, and 33% of *dpy-27(RNAi)* worms had two clear X chromosome territories. We observed that both chromosome territories X_1 and X_2 in hermaphrodite nuclei depleted of DPY-27 occupied a significantly larger percentage than in vector control nuclei (Figure 2.8). The caveat of this experiment is that the chromosomes are not individually marked and the X_1 territory in one genotype does not necessarily corresponds to X_1 in the other. However, together with the observation that both X chromosomes associate with the dosage compensation complex, we favor the interpretation that both Xs are affected to similar degrees.

Diploid DCC-depleted nuclei also have enlarged X chromosomes

Because intestinal nuclei are 32-ploid, the possibility remained that the enlarged X territories were a result of the dispersing of the multiple copies of the X chromosomes and not a result of perturbed compaction of individual chromosomes. To test this possibility, we examined the X chromosomes in the diploid tail tip hypodermal cells, hyp 8-11 [55]. We found similar results to that of intestinal nuclei in the diploid cells (Figure 2.3A and B). The X chromosome territories in vector control RNAi diploid cells were tightly compact occupying 9.94 ± 2.20%, whereas the X chromosome territories in *dpy-30*, *dpy-2*1, and *dpy-27* RNAi diploid cells were decondensed occupying 16.27 ± 2.62% (P = 6.70E-19), 16.09 ± 2.22% (P = 3.02E-20), and 16.17 ± 2.59% (P = 1.15E-18), respectively. Additionally, the percent volume occupied by chromosome I in diploid cells was not statistically different amongst the control and DCC-depleted animals, averaging 13.2% in all cases (Figure 2.3C and D). This suggests that the decondensed X chromatin structure in DCC-depleted worms is not solely a result of the dispersing of the multiple copies of the X chromosome in the 32-ploid intestinal nuclei, but it is a result of defective compaction. We did not look at separate X chromosome territories in diploid cells because due to their small size only a small percentage of nuclei had clearly distinguishable X chromosome territories. Only 35% of both vector and *dpy-27(RNAi)* diploid nuclei clearly exhibited two separate X chromosome territories.

X chromatin compaction is evident at all genomic distances examined

To further investigate the genomic scale at which condensin operates we performed 3D FISH with pairs of X chromosome YAC probes separated by genomic

distances ranging from 0.5 Mb to 7.2 Mb (Figure 2.4A and B). Such analysis has been previously used to demonstrate a role for polycomb repressive complexes in compacting chromatin in mouse embryonic stem cells, and a role for condensin II to promote compaction of chromosome territories in *Drosophila* [39,56]. Since this analysis is not possible in polyploidy intestinal nuclei we analyzed the pairs of probes in wild type and *dpy-21(e428)* mutant diploid tail tip cells. Eighty-three percent of wild type diploid cells and 79% of *dpy-21(e428)* diploid cells had two clear spots for each probe, while others had either no spots due to high background or had one spot (presumably due to the overlap of two closely spaced spots). Nuclei with 0 or one spot were excluded from our analysis. No nuclei had three or four spots. These observations indicate that these cells have an unreplicated diploid DNA content. At all four genomic distances we detected a significant increase in distances in *dpy-21(e428)* mutants compared to wild type (Figure 2.4C). This more dispersed distribution of the two loci found in *dpy-21(e428)* correlates with the larger X chromosome territories found in the dosage compensation mutants. These data suggest that dosage compensation can be linked to levels of higher-order X chromatin compaction, both at the level of whole chromosomes and at a genomic scale as small as 0.5 Mb and as large as 7.2 Mb.

X chromosome compaction is not regulated by condensin I or condensin II

Previous studies have found that condensin II promotes the formation of interphase chromosome territories in *Drosophila* [35,39]. Therefore, we next wanted to investigate whether the X chromosome compaction was specific to condensin I^{DC} or if condensin I or II are also contributing to this phenotype. To test this, we depleted SMC-

4, CAPG-2, or HCP-6. SMC-4 is a subunit of both condensins I and II, while CAPG-2 and HCP-6 are subunits specific to condensin II [15,21,31,57,58]. We performed a shorter, one generation RNAi feeding of SMC-4, CAPG-2, HCP-6, DPY-27, and empty vector, due to the lethality of SMC-4, CAPG-2, or HCP-6 depletion over two generations. One generation RNAi feeding depleted condensin subunits to below level of detection by western blotting (Figure 2.9). In addition the presence of chromatin bridges between many nuclei, a hallmark of chromosome segregation defects, in SMC-4, CAPG-2, and HCP-6-depleted worms, indicated successful depletion. Depleting SMC-4, CAPG-2, or HCP-6 did not change the level of compaction compared to control vector RNAi worms (Figure 2.5A and Figure 2.9). The mean volume occupied by the X chromosomes was consistently around 10.1%. However, even with the shorter one generation RNAi depletion, *dpy-27(RNAi)* X chromosome territories were large at 17.29 ± 2.45%. Similarly, there was no change in the volume of chromosome I when either SMC-4, CAPG-2, or HCP-6 were depleted compared to control animals (Figure 2.5B and Figure 2.9). Additionally, the same analysis was performed on the diploid tail tip hypodermal cells and similar results were found (Figure 2.10). Similar conclusions were reached when using 3D FISH with pairs of X chromosome YAC probes separated by the genomic distance of 1.2 Mb, the distance that showed the most significant difference between *dpy-21(e428)* mutants and wild type. 83% of *smc-4(RNAi)* diploid nuclei and 85% of *hcp-6(RNAi)* diploid nuclei had two clear spots for each probe, while no nuclei had three or four spots. At the genomic distance of 1.2 MB we did not detect a significant change in distances in *smc-4(RNAi)* or *hcp-6(RNAi)* worms compared to

vector control worms (Figure 2.5C). Therefore, we conclude that condensin I^{DC}, and not condensin I or condensin II, is primarily responsible for dosage compensation mediated X chromosome compaction. However we cannot rule out the possibility that condensin I or II are affecting interphase chromosome territories in *C. elegans* at levels undetectable by 3D FISH.

Changes in DCC-mediated histone modifiers effect X chromosome structure

We, and others, previously showed that DCC activity leads to the enrichment of H4K20me1 on the X chromosome by the methyltransferases SET-1 and SET-4 [48,49]. This activity then leads to the depletion of H4K16ac levels on X, via the deacetylase SIR-2.1 [49]. In order to determine whether these chromatin modifications contribute to compaction of the X, we examined *set-1(tm1821)*, *set-4(n4600)*, and *sir-2.1(ok434)* mutant worms. Mutations in *set-1*, *set-4,* or *sir-2.1* led to the loss of X chromosome compaction seen in wild type worms (Figure 2.6A and Figure 2.11). However, chromosome I showed no significant change in volume in these histone modifier mutants (Figure 2.6B and Figure 2.11). Interestingly, the DCC localizes normally to the X in *set-1(tm1821)*, *set-4(n4600)*, and *sir-2.1(ok434)* worms [48,49]. Therefore, DCC alone is not sufficient for the compaction of the X chromosome territory. We conclude that X chromosome compaction by the DCC requires the presence of these chromatin modifiers.

DISCUSSION

In this study, we sought to determine whether the condensin-like DCC compacts chromosomes for gene expression. We established that in wild type hermaphrodites,

the interphase X chromosomes are more compact than predicted based on DNA content. This compaction is dependent on the presence of the DCC as well as the DCC-regulated histone modifiers SET-1, SET-4, and SIR-2.1 (Figure 2.7). Together, our results suggest that mechanisms related to mitotic chromosome condensation mediate dosage compensation.

Previous gene expression studies in DCC mutants showed that X expression increases while autosomal expression decreases compared to wild type [59]. Assuming that these gene expression changes are reflected in chromosome volume changes, we would predict that an increase in the volume of the X is accompanied by a decrease in the volume of autosomes. If the X is occupying an extra 7% of the nucleus, the five pairs of autosomes together will occupy 7% less, approximately 1.4% less for each autosome. We did not detect any decrease in chromosome I volume, but our method may not be sensitive enough to detect such a small change.

Condensins and cell cycle regulation

Condensins are conserved complexes that play fundamental roles in chromosome dynamics throughout the cell cycle [22]. Similar to conserved condensin II activities, *C. elegans* condensin II is required for prophase chromosome condensation and anaphase segregation [31,58]. However, condensin I's role in *C. elegans* is less understood. It is believed that condensin I plays a less critical role in mitosis and development than condensin II, because condensin I depletions lead to less severe phenotypes [15]. Condensin's role in mitosis and meiosis has been widely studied, however recent evidence revealed that the condensin complexes also contribute to a

variety of interphase chromosome functions. A prominent example is the *C. elegans* condensin I-like complex, condensin I^{DC}, which does not function in mitosis or meiosis, but instead regulates chromosome- and sex-specific gene expression [12]. Interestingly, condensin I^{DC} differs from the condensin I complex by only one subunit. It is assumed that during evolution, the condensin I subunit SMC-4 duplicated and diverged giving rise to DPY-27. This resulted in the formation of condensin I^{DC} with the specialized function of dosage compensation. It is believed that the mechanism of dosage compensation is closely linked to condensin's role in regulating chromosome architecture.

In this study, we report that condensin I^{DC} is responsible for compacting interphase X chromosome territory, both at the level of whole chromosome territories, and by measuring 3D-distances between probe pairs separated by various genomic distances. Evidence of condensin-mediated interphase chromosome compaction has also been found in *Drosophila* and mice [35,39-41]. Condensin activity is required to unpair polytene chromosomes and disperse heterochromatin in *Drosophila* [39]. In mice, the condensin-mediated condensation is required for proper T-cell development and maintenance of the quiescent state [40]. Condensin has also been found to be required for chromatin compaction and viability in ES cell [41]. In these systems, condensin mediates chromosome changes genome-wide. By contrast, in *C. elegans*, condensin I^{DC} causes chromosome specific changes. It is also interesting to note that in flies and mice condensin II plays a role in interphase chromosome [35,39-41], while our data do not support a role for condensin II, only condensin I^{DC}. These differences between our findings and previous data may reflect a difference between the species or the type of

cells examined. Indeed, cell-type specific differences in condensin usage have been observed before, at least in the context of mitotic chromosome condensation [25].

It should be noted that our studies were performed on postmitotic cells. Whether there are differences in how condensin I^{DC} affects X chromosome compaction in G1, S, or G2 phase of cycling cells is unknown. However, a chromatin mark associated with dosage compensation, enrichment of H4K20me1, appears several cell cycles after the DCC assembles on the X chromosomes [48,60], suggesting that full compaction may require passage through mitosis.

Molecular mechanisms of condensin

Although some of the biological functions of condensins have been uncovered, our understanding of condensin's molecular mechanisms remains poor. Condensins contain two SMC (structural maintenance of chromosomes) proteins and three CAP (chromosome-associated polypeptide) proteins. The two SMC proteins are ATPases, and their ability to hydrolyze ATP is essential for condensin function [22]. One of the better-studied biochemical activities of condensin, found in many eukaryotic species, is its ability to supercoil DNA *in vitro*. This supercoiling requires its ATPase activity, as well as all five subunits [31,61-64]. The introduction of positive supercoiling is proposed to lead to the formation of chiral loops [22,65] and facilitate decatenation of sister chromatids by topoisomerase II [66]. This would further compact the chromatin fibers to form higher order assemblies. In addition to supercoiling, the SMC proteins of condensins have been found to play a role in reannealing complementary ssDNAs into dsDNAs [67]. Condensins' reannealing activity might help 'fix' ssDNA to prepare it for

the formation of mitotic chromosomes. Condensin is also believed to entrap the chromatin fiber by encircling two distinct segments of the chromatin fiber [68]. Together these ATP-dependent biochemical activities are thought to result in condensed mitotic chromosomes. In *C. elegans* specific point mutations of the ATP-binding motifs of DPY-27 and MIX-1 disrupt dosage compensation [14,16]. These results suggest another link between condensin's function in mitosis and dosage compensation.

Condensin and chromatin regulated chromosome compaction

In addition to condensin-mediated mitotic chromosome condensation, histone modifications have also been found to contribute to chromatin hypercondensation during mitosis [44-46]. Interestingly, similar histone modifications are present on interphase dosage compensated X chromosomes in *C. elegans*. The monomethylation of H4K20 is increased, whereas acetylation of H4K16 is decreased, both on mitotic chromosomes and on interphase dosage compensated X chromosomes [44-46,48,49]. This is consistent with the hypothesis that mechanisms related to mitotic chromosome condensation mediate dosage compensation. In mitosis, H4K16 deacetylation leads to a stronger interaction between H2A and H4 on adjacent nucleosomes, thus leading to the formation of higher order chromosomes packaging [45,69]. Our results suggest that DCC-mediated X chromosome compaction requires both the enrichment of H4K20me1 and the depletion of H4K16ac on the X chromosomes similar to the events occurring in mitosis. However, we cannot rule out the possibility that additional factors also contribute to the compaction of the X chromosome. In mitosis, it is believed that this cascade of histone modifications is acting independently of condensin to compact

chromosomes [45]. By contrast, X-enrichment of H4K20me1 and depletion of H4K16ac during dosage compensation is DCC- (therefore condensin-) dependent [49]. It will be interesting to determine the exact mechanistic contributions of these modifications both to mitotic chromosome condensation and dosage compensation.

Upregulation of the X chromosome

X upregulation balances the single male X to autosomes. In flies, X upregulation is male specific, but in mammals and worms it is hypothesized that upregulation occurs in both sexes. Male-specific upregulation of the X chromosome in *Drosophila* is mediated by the MSL (male-specific lethal) complex [70,71]. The MSL complex binds to the male X chromosome, concentrates MOF acetyltransferase activity, and leads to increased H4K16ac on the hyperactive X [72,73]. The MSL complex has been shown to mediate two chromatin alterations. First, the presence of the complex reduces the level of negative supercoiling [74]. Second, the acetylation of H4K16 alone weakens nucleosome packing in a chromatin fiber and causes chromatin decondensation on the male X chromosome [75]. Microarray and RNA-seq analysis have provided some evidence for X upregulation in mammals and worms [4-8]. In mammals it is believed that H4K16ac and enhanced transcription initiation contribute to X upregulation [4]. However, the mechanism in worms is unknown, but it may involve changes in chromatin structure. Our data show that in *C. elegans* the single male X chromosome territory is larger than expected. This result suggests that chromosome decondensation might contribute to the X upregulation mechanism. It will be of great interest to explore what is mediating chromosome decondensation in *C. elegans* males. Previous studies have

indicated that in the absence of DCC activity, H4K16ac is enriched on hermaphrodite X chromosomes, suggesting that this mark may be involved in the X upregulation process. However, males show no enrichment of H4K16ac by immunofluorescence microscopy [49]. In addition, there is no enrichment of H4K16ac on the X chromosomes in early hermaphrodite, male, or DCC-mutant embryos [60]. Therefore, further investigation is required to determine the mechanisms causing chromosome decondensation and X upregulation in males.

Conclusions

It has been long hypothesized that DCC activity results in interphase X chromosome compaction. However, the experimental evidence was lacking. Our results are consistent with this long standing hypothesis suggesting that dosage compensated X chromosomes maintain some characteristics associated with condensed mitotic chromosome. Our studies of *C. elegans* condensin I^{DC}-mediated compaction may shed further light on the mechanisms of chromatin organization and gene repression by condensin in other organisms. Future studies will examine the factors that directly contribute to X upregulation and possibly chromosome decondensation in males.

MATERIALS AND METHODS

Strains

All strains were maintained on NG agar plates with *E. coli* (OP50) as a food source, using standard methods [76]. Strains include: N2 Bristol strain (wild type); TY4403 *him-8(e1489)* IV; TY1936 *dpy-30(y228)* V/nT1 (*unc-?* (n754*) let-?*); TY3936 *dpy-21(e428)*; SS1075 *set-1(tm1821)* III/ hT2g; MT14911 *set-4(n4600)* II; VC199 *sir-*

2.1(ok434) IV. Males were obtained from *him-8(e1489)* hermaphrodites. Mutations in *him-8* cause X chromosome nondisjunction in meiosis and result in 38% of progeny being XO males.

RNA interference

E. coli HT115 bacteria expressing double stranded RNA for *dpy-30*, *dpy-21, dpy-27, smc-4, capg-2*, *hcp-6*, or vector control (polylinker), were used for feeding RNAi using the Ahringer laboratory RNAi feeding library [77]. One generation feeding RNAi (WT on *smc-4* RNAi, WT on *capg-2* RNAi, WT on *hcp-6* RNAi) was performed as follows: L1-stage larvae were placed on plates seeded with RNAi bacteria and grown to adulthood. Two generation feeding RNAi (all other analysis) was performed as follows; P_0 adults from one generation feeding RNAi were transferred to new RNAi plates to produce progeny for 24 h. These progeny (F_1 generation) were grown to adulthood and examined.

Fluorescent *in situ* hybridization (FISH)

FISH probe templates were generated by degenerate oligonucleotide primed PCR to amplify purified yeast artificial chromosome (YAC) DNA [50,78]. The labeled chromosome-paint probes were prepared as described previously [78]. To perform FISH, adult animals (24 h post-L4) with or without previous RNAi treatment were dissected and fixed in 2% PFA, 1× sperm salts, on a slide for 5 min at room temperature. The slide was covered with a coverslip and placed on a dry ice block for 10 min. The coverslip was quickly removed from the slide, and the slides were washed three times in PBST for 10 min each, dehydrated through an ethanol series (70%, 80%,

95%, 100% ethanol, 2 min each) and air dried. A total of 10 uL of probe was added to the slide. The samples were covered with a coverslip, placed on a 95°C heat block for 3 min, and slowly cooled to 37°C for an overnight incubation. The following washing regime was used at 37°C: three 5-min washes in 2× SSC with 50% formamide, then three 5-min washes in 2× SSC, and one 10-min wash in 1× SSC. Samples were incubated in PBST for 10 minutes with DAPI. Slides were mounted with Vectashield (Vector Laboratories) [78].

Microscopy and image analysis

Images were captured with a Hamamatsu Orca-Erga close-coupled-device (CCD) camera mounted on an Olympus BX61 motorized Z-drive microscope using a 60× APO oil immersion objective. 3D image stacks were collected for each nucleus at 0.2 micrometer Z-spacing. Projection images were generated from these optical sections.

For volume measurements, masks were set using the 'mask → segment' function. The mask is established by a user-defined intensity threshold value applied over an image in order to distinguish real signal from background signal and autofluorescence. The same standard of background signal exclusion was applied to all nuclei, based upon the levels of background signal and autofluorescence observed. This was done for each channel of an image. The total volume of the 'whole nucleus' mask was calculated from DAPI signal. DAPI signal was set as the primary mask and the three dimensional pixels (voxels) were measured through Slidebook (morphometry → volume). The volume of the X chromosome or chromosome I mask was calculated

from the paint signals. Chromosome-paint signals were set as the secondary mask and for each object in the primary mask. The number of overlapping voxels in the secondary mask was calculated by Slidebook (cross mask → mask overlaps). The percentage of nuclear volume occupied by either the X chromosome or chromosome I was obtained by dividing the volume of the specific chromosome over the volume of the whole nucleus. This percentage was calculated for each nucleus within an experimental set. The percentages where then averaged over all nuclei within an experimental set to calculate the final mean percentage of nuclear volume occupied by the X chromosome or chromosome I value shown on each graph. Descriptive statistics (standard deviation and sample size) were also calculated. Sample sizes are listed in each figure. Error bars shown are means +/- 1 standard deviation of the mean. Percent volume differences were evaluated by unpaired (two sample) Student's T-test.

To calculate the distance between two probes in three dimension, the xyz coordinate of the centroid of each YAC probe signals were determined and measured using Slidebook. The distance between the two probes was the distance between two separate spots closest to one another. The distances where then analyzed over all nuclei within an experimental set to calculate the final median and interquartile range of the data shown in boxplots. Descriptive statistics (minimum, maximum, and sample size) were also calculated. Sample sizes are listed in each figure. Whiskers shown indicate distribution from minimum to maximum. Probe distance differences were evaluated by unpaired (two sample) Student's T-test.

ACKNOWLEDGEMENTS

We thank members of the Csankovszki lab for helpful project discussions. This work was supported by National Science Foundation grant MCB 1021013 (to GC). Some nematode strains used in this work were provided by the *Caenorhabditis* Genetics Center, which is funded by the NIH National Center for Research Resources. The *set-1(tm1821)* allele was provided by the Mitani laboratory through the National Bioresource Project of the MEXT, Japan.

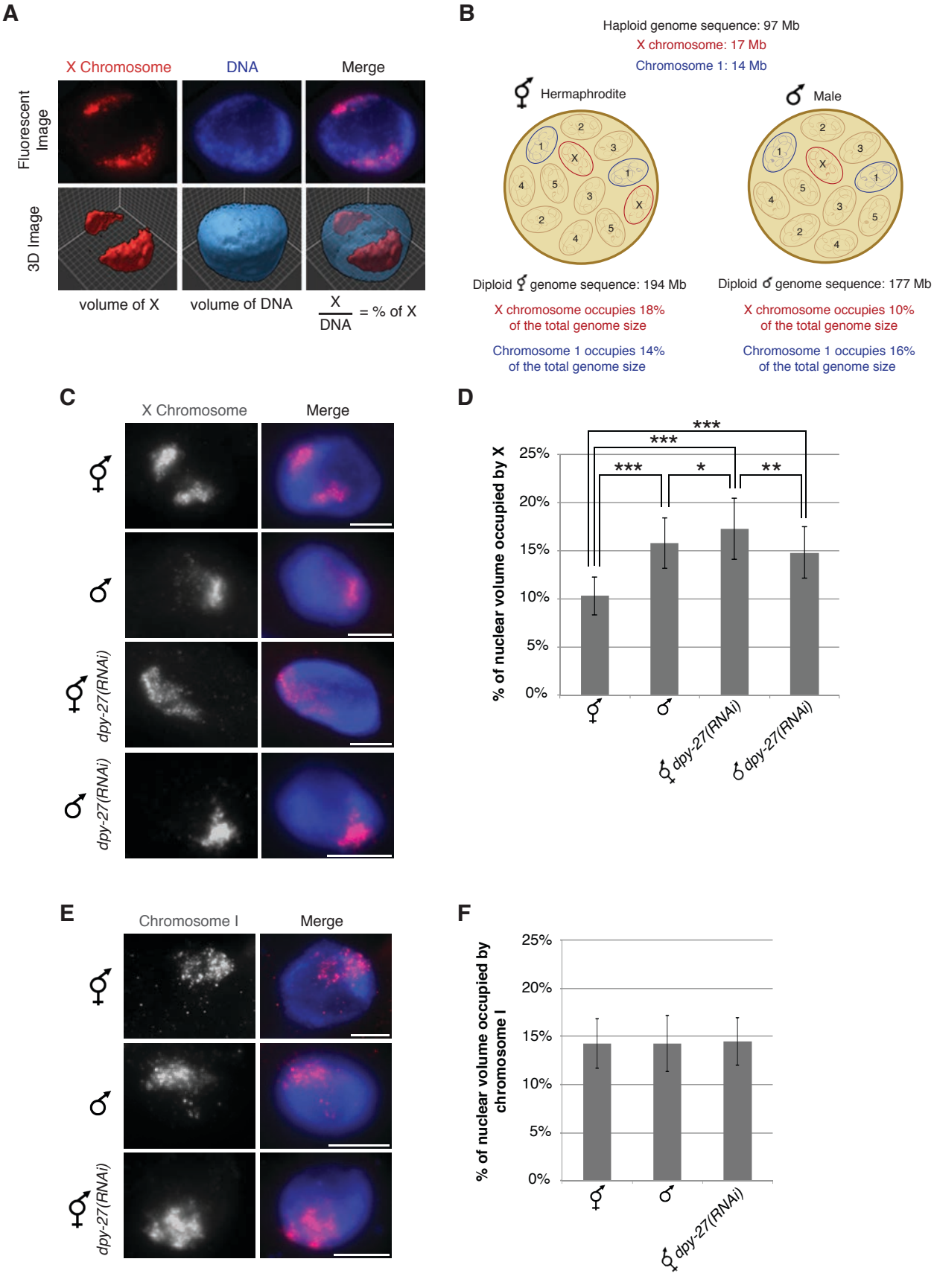
A
X Chromosome
DNA
Merge
Fluorescent Image
3D Image
volume of X
volume of DNA
X / DNA = % of X
B
Haploid genome sequence: 97 Mb
X chromosome: 17 Mb
Chromosome 1: 14 Mb
Hermaphrodite
Male
Diploid ♀ genome sequence: 194 Mb
Diploid ♂ genome sequence: 177 Mb
X chromosome occupies 18% of the total genome size
Chromosome 1 occupies 14% of the total genome size
X chromosome occupies 10% of the total genome size
Chromosome 1 occupies 16% of the total genome size
C
X Chromosome
Merge
dpy-27(RNAi)
dpy-27(RNAi)
D
% of nuclear volume occupied by X
25%
20%
15%
10%
5%
0%
***
***
***
*
**
dpy-27(RNAi)
dpy-27(RNAi)
E
Chromosome I
Merge
dpy-27(RNAi)
F
% of nuclear volume occupied by chromosome I
25%
20%
15%
10%
5%
0%
dpy-27(RNAi)

Figure 2.1 The absence of the DCC leads to enlarged X territories. (A) Chromosome-paint 3D FISH measures the volumes of chromosome X and I territories. Representation of how the percentage of nuclear volume occupied by the X or chromosome I paint were quantified in a single nucleus. (B) *C. elegans* has five pairs of autosomes and one pair of sex chromosomes. Hermaphrodites have 12 chromosomes with a total genome sequence of 194 Mb. The X chromosomes occupy 18% and chromosome I occupies 14% of the total hermaphrodite genome size. Males have 11 chromosomes with a total genome sequence of 177 Mb. The single X chromosome occupies 10% and chromosome I occupies 16% of the total male genome size. (C-D) Adult hermaphrodite and male intestinal nuclei stained with X-paint FISH (red) to label X chromosome territories and DAPI (blue) to label DNA. (C) Representative stained nuclei of wild type hermaphrodites, male *him-8(e1489)*, hermaphrodite and male *him-8(e1489) dpy-27* RNAi treated animals. Scale bars equal 5 µm. **(D)** Quantification of the percentage of nuclear volume occupied by X in wild type hermaphrodites (n = 40), male *him-8(e1489)* (n = 40), hermaphrodite *dpy-27(RNAi)* (n = 60), and male *him-8(e1489) dpy-27(RNAi)* (n = 22). Error bars indicate standard deviation. Asterisks indicate level of statistical significance by t-test analysis (one asterisk, $P < 0.05$; two asterisks, $P < 0.01$; three asterisks, $P < 0.001$). (E, F) Adult hermaphrodite and male intestinal nuclei stained with chromosome I paint FISH (red) to label chromosome I territories and DAPI (blue) to label DNA. (E) Representative stained nuclei of wild type hermaphrodites, male *him-8(e1489)* and hermaphrodite *dpy-27* RNAi treated animals. Scale bars equal 5 µm. (F) Quantification of the percentage of nuclear volume occupied by chromosome I in wild type hermaphrodites (n = 40), male *him-8(e1489)* (n = 40) and hermaphrodite *dpy-27(RNAi)* (n = 40). Error bars indicate standard deviation.

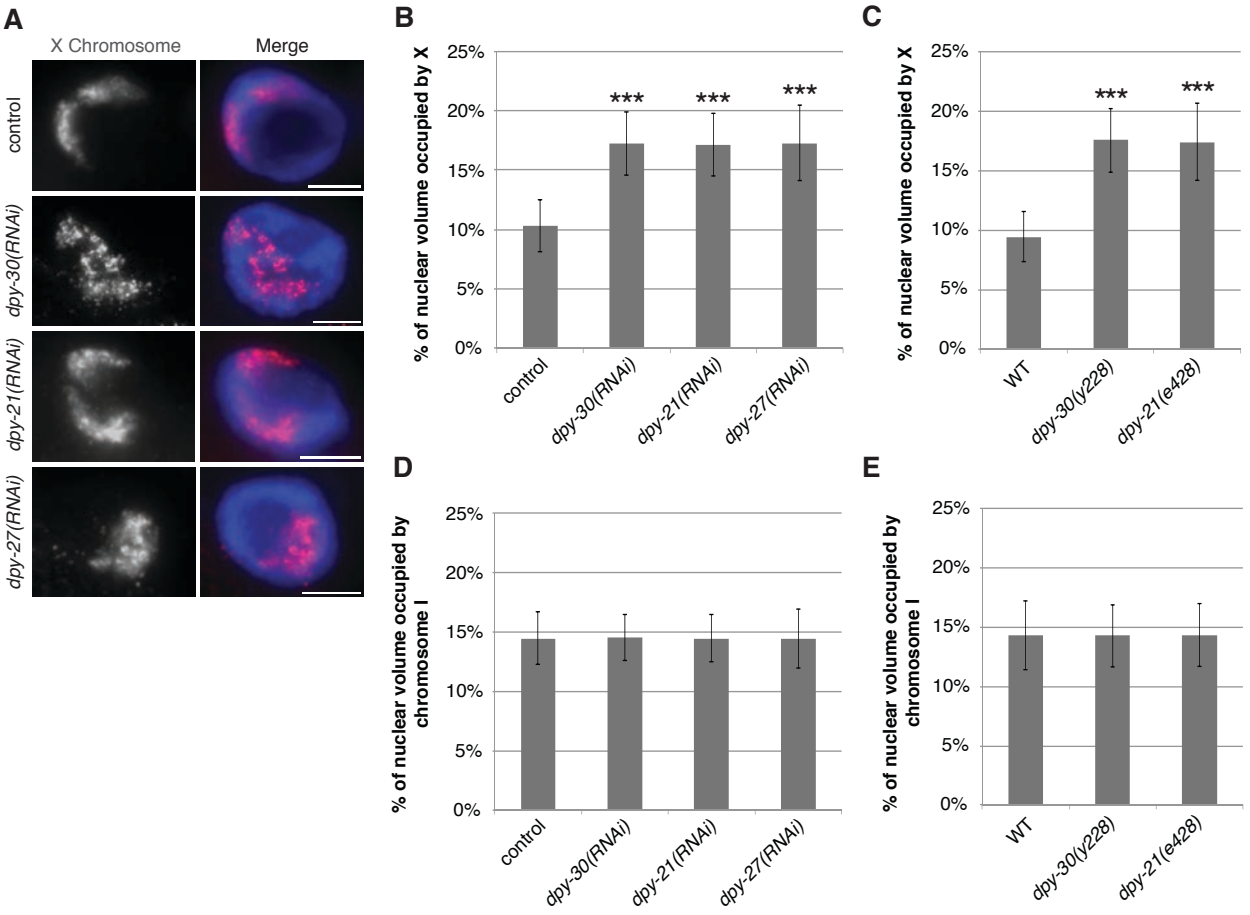

Figure 2.2 DCC depletion and mutations disrupt X chromosome compaction. (A, B) Adult RNAi treated hermaphrodite intestinal nuclei stained with X-paint FISH (red) to label X chromosome territories and DAPI (blue) to label DNA. (A) Representative stained nuclei after vector RNAi treatment, *dpy-30(RNAi)*, *dpy-21(RNAi)*, and *dpy-27(RNAi)*. Scale bars equal 5 µm. (B) Quantification of the percentage of nuclear volume occupied by X in vector RNAi (n = 60), *dpy-30(RNAi)* (n = 60), *dpy-21(RNAi)* (n = 60), and *dpy-27(RNAi)* (n = 60). Error bars indicate standard deviation. Asterisks indicate level of statistical significance by t-test analysis (three asterisks, $P < 0.001$). (C) Quantification of the percentage of nuclear volume occupied by X in wild type (n = 36), *dpy-30(y228)* (n = 24), and *dpy-21(e428)* (n = 21). Error bars indicate standard deviation. Asterisks indicate level of statistical significance by t-test analysis (three asterisks, $P < 0.001$). (D, E) Depletion or mutations of DCC leads to no difference in chromosome I size. (D) Quantification of the percentage of nuclear volume occupied by chromosome I in vector RNAi (n = 40), *dpy-30(RNAi)* (n = 40), *dpy-21(RNAi)* (n = 40), and *dpy-27(RNAi)* (n = 40). Error bars indicate standard deviation. (E) Quantification of the percentage of nuclear volume occupied by chromosome I in wild type (n = 25), *dpy-30(y228)* (n = 25), and *dpy-21(e428)* (n = 25). Error bars indicate standard deviation.

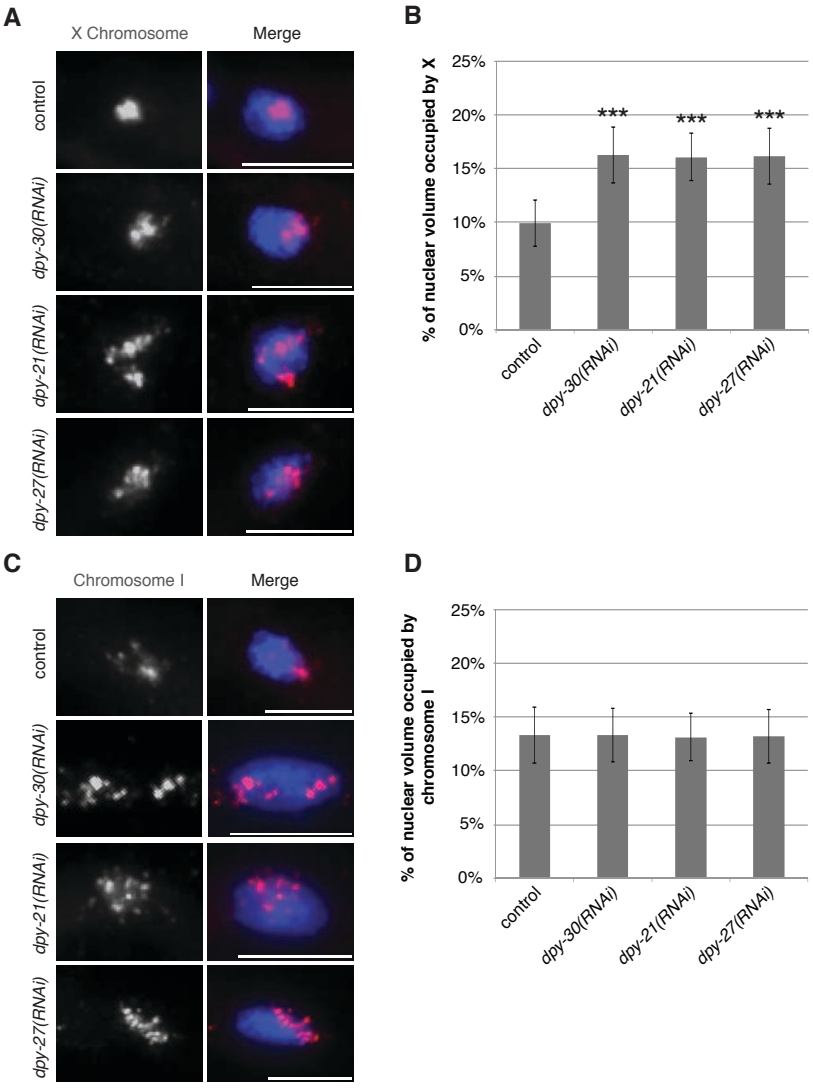

Figure 2.3 The decondensed X chromatin structure in DCC-depleted worms is a result of defective compaction. (A, B) Adult RNAi treated hermaphrodite diploid nuclei stained with X-paint FISH (red) to label X chromosome territories and DAPI (blue) to label DNA. (A) Representative stained nuclei after vector RNAi treatment, *dpy-30(RNAi)*, *dpy-21(RNAi)*, and *dpy-27(RNAi)*. Scale bars equal 5 µm. (B) Quantification of the percentage of nuclear volume occupied by X in vector RNAi (n = 40), *dpy-30(RNAi)* (n = 40), *dpy-21(RNAi)* (n = 40), and *dpy-27(RNAi)* (n = 40). Error bars indicate standard deviation. Asterisks indicate level of statistical significance by t-test analysis (three asterisks, $P < 0.001$). (C, D) Adult hermaphrodite diploid nuclei stained with chromosome I paint FISH (red) to label chromosome I territories and DAPI (blue) to label DNA after DCC depletion. (C) Representative stained nuclei after vector RNAi treatment, *dpy-30(RNAi)*, *dpy-21(RNAi)*, and *dpy-27(RNAi)*. Scale bars equal 5 µm. (D) Quantification of the percentage of nuclear volume occupied by chromosome I in vector RNAi (n = 40), *dpy-30(RNAi)* (n = 40), *dpy-21(RNAi)* (n= 40), and *dpy-27(RNAi)* (n = 40). Error bars indicate standard deviation.

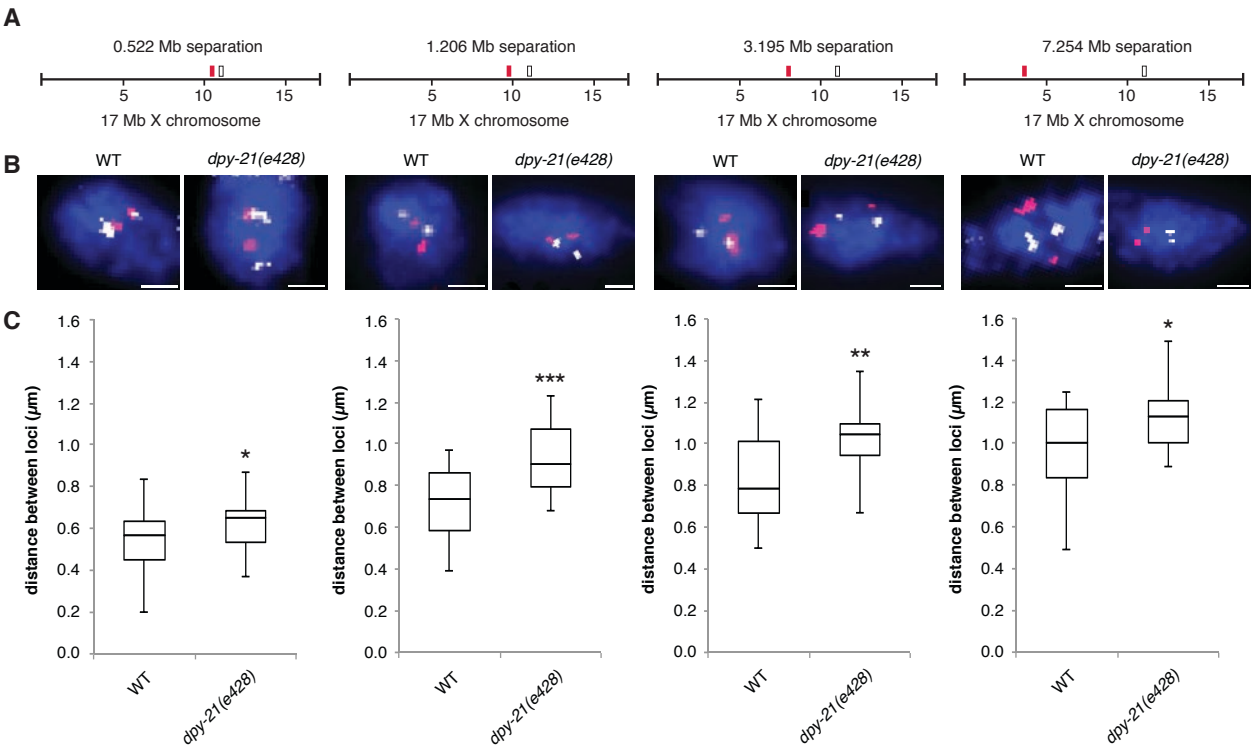

Figure 2.4 X chromatin compaction is evident at all genomic distances examined. (A) FISH probe pairs across the X chromosome. The position of YAC probes (red and white boxes) used in FISH is indicated. (B) 2D projections of 3D stacked images. Representative stained diploid nuclei of adult hermaphrodite wild type and *dpy-21(e428)* worms. Nuclei stained with probes pairs across the X chromosome (red and white) and counterstained with DAPI (blue) to label DNA. Scale bars equal 1 µm. (C) Boxplots indicating the distribution of 3D loci distances for wild type (n = 20) and *dpy-21(e428)* (n = 20) diploid nuclei. Boxes show the median and interquartile range of the data. Asterisks indicate level of statistical significance by t-test analysis (one asterisk, $P < 0.05$; two asterisks, $P < 0.01$; three asterisks, $P < 0.001$).

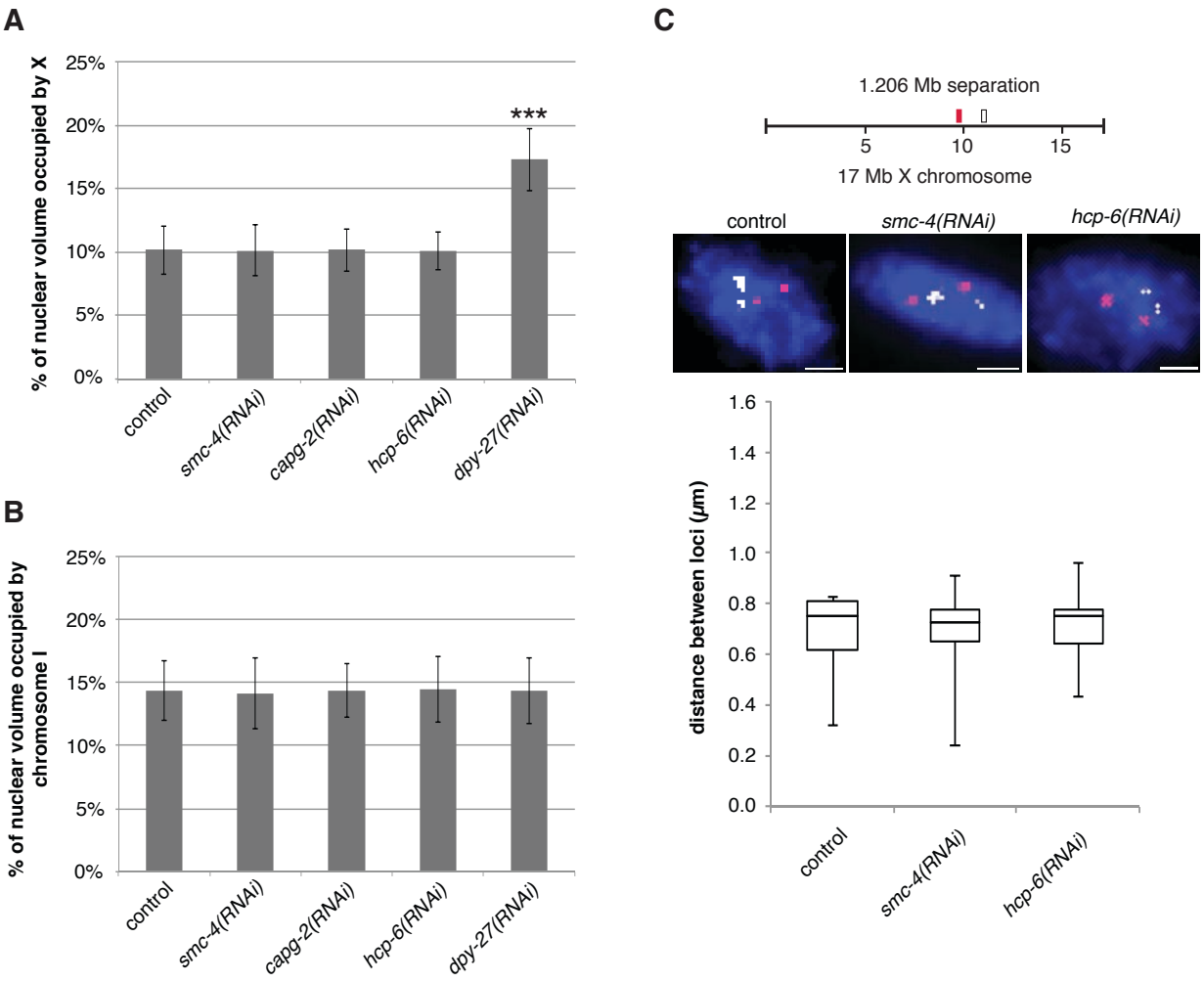

Figure 2.5 X chromosome compaction is not disrupted in condensin I or II depleted animals. (A) Quantification of the percentage of nuclear volume occupied by X in vector RNAi (n = 40), *smc-4(RNAi)* (n = 28), *capg-2(RNAi)* (n = 40), *hcp-6(RNAi)* (n = 40), and *dpy-27(RNAi)* (n = 34). Error bars indicate standard deviation. Asterisks indicate level of statistical significance by t-test analysis (three asterisks, $P < 0.001$). (B) Quantification of the percentage of nuclear volume occupied by chromosome I in vector RNAi (n = 40), *smc-4(RNAi)* (n = 29), *capg-2(RNAi)* (n = 40), *hcp-6(RNAi)* (n = 40), and *dpy-27(RNAi)* (n = 32). Error bars indicate standard deviation. (C) FISH probe pairs across the X chromosome. The position of YAC probes (red and white boxes) used in FISH is indicated. 2D projections of 3D stacked images. Representative stained diploid nuclei of vector RNAi, *smc-4(RNAi)* and *hcp-6(RNAi)* worms. Nuclei stained with probes pairs across the X chromosome (red and white) and counterstained with DAPI (blue) to label DNA. Scale bars equal 1 μm. Boxplots indicating the distribution of 3D loci distances for vector RNAi (n = 20) and *smc-4(RNAi)* (n = 20) and *hcp-6(RNAi)* (n = 20) diploid nuclei. Boxes show the median and interquartile range of the data.

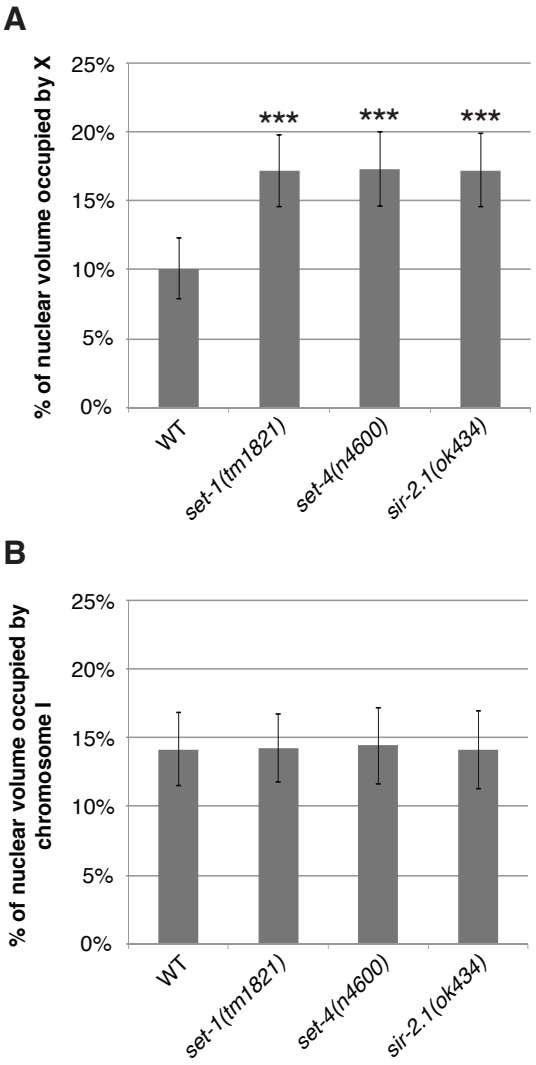

Figure 2.6 Depletion of the DCC-meditated histone modifiers leads to the loss of X chromosome compaction. (A) Quantification of the percentage of nuclear volume occupied by X in wild type (n = 40), *set-1(tm1821)* (n = 40), *set-4(n4600)* (n = 40) and *sir-2.1(ok434)* (n = 40). Error bars indicate standard deviation. Asterisks indicate level of statistical significance by t-test analysis (three asterisks, $P < 0.001$). (B) Quantification of the percentage of nuclear volume occupied by chromosome I in wild type (n = 40), *set-1(tm1821)* (n = 20), *set-4(n4600)* (n = 40), and *sir-2.1(ok434)* (n = 40). Error bars indicate standard deviation.

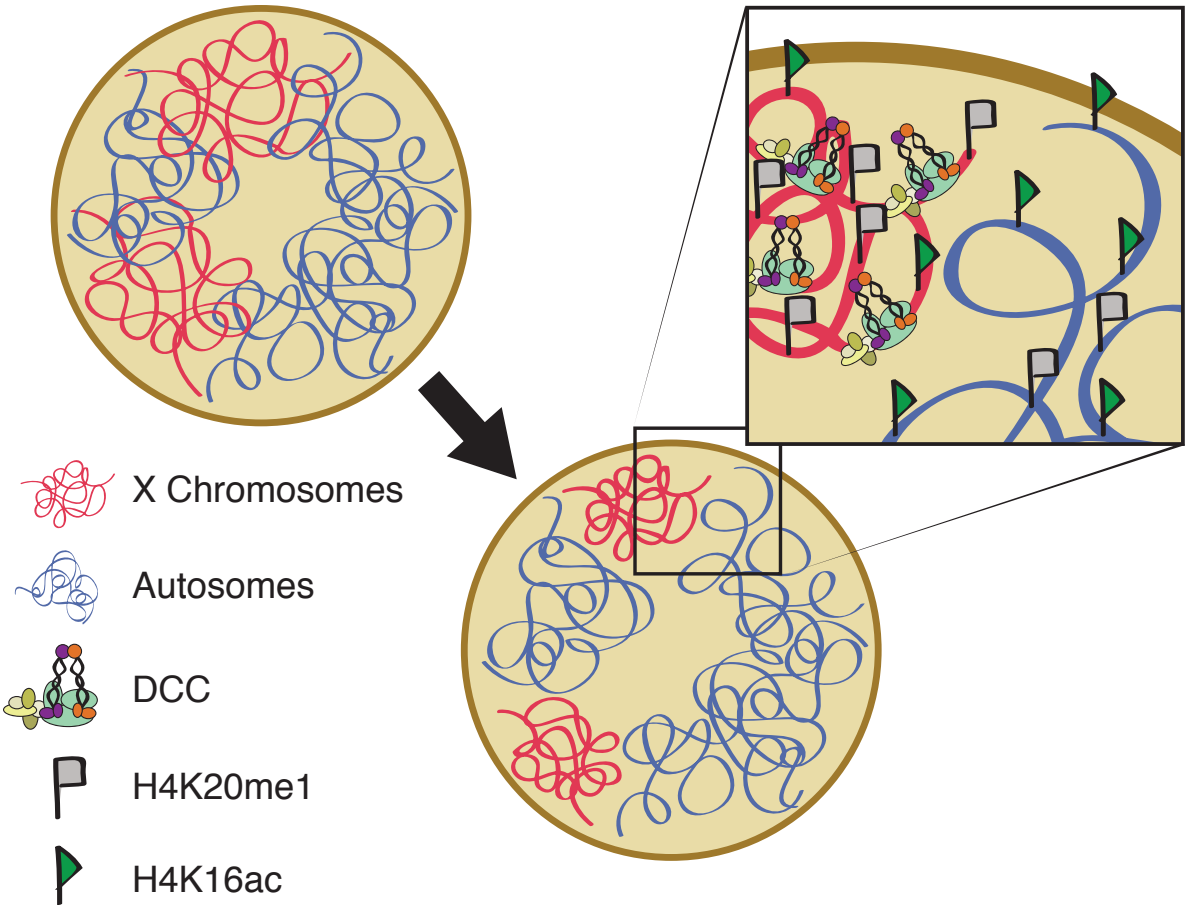

Figure 2.7 X chromosome compaction is dependent on the DCC and the DCC-mediated histone modifications. A graphical cartoon illustrates DCC and DCC-mediated histone modifications effects on hermaphrodite X chromosome structure. The DCC binds to both hermaphrodite X chromosomes and by regulating SET-1 and SET-4, mediates an enrichment of H4K20me on the X chromosome, which, in turn, through SIR-2.1 activity, depletes H4K16ac. These activities compact the X chromosome territories and downregulate X-linked gene expression by half.

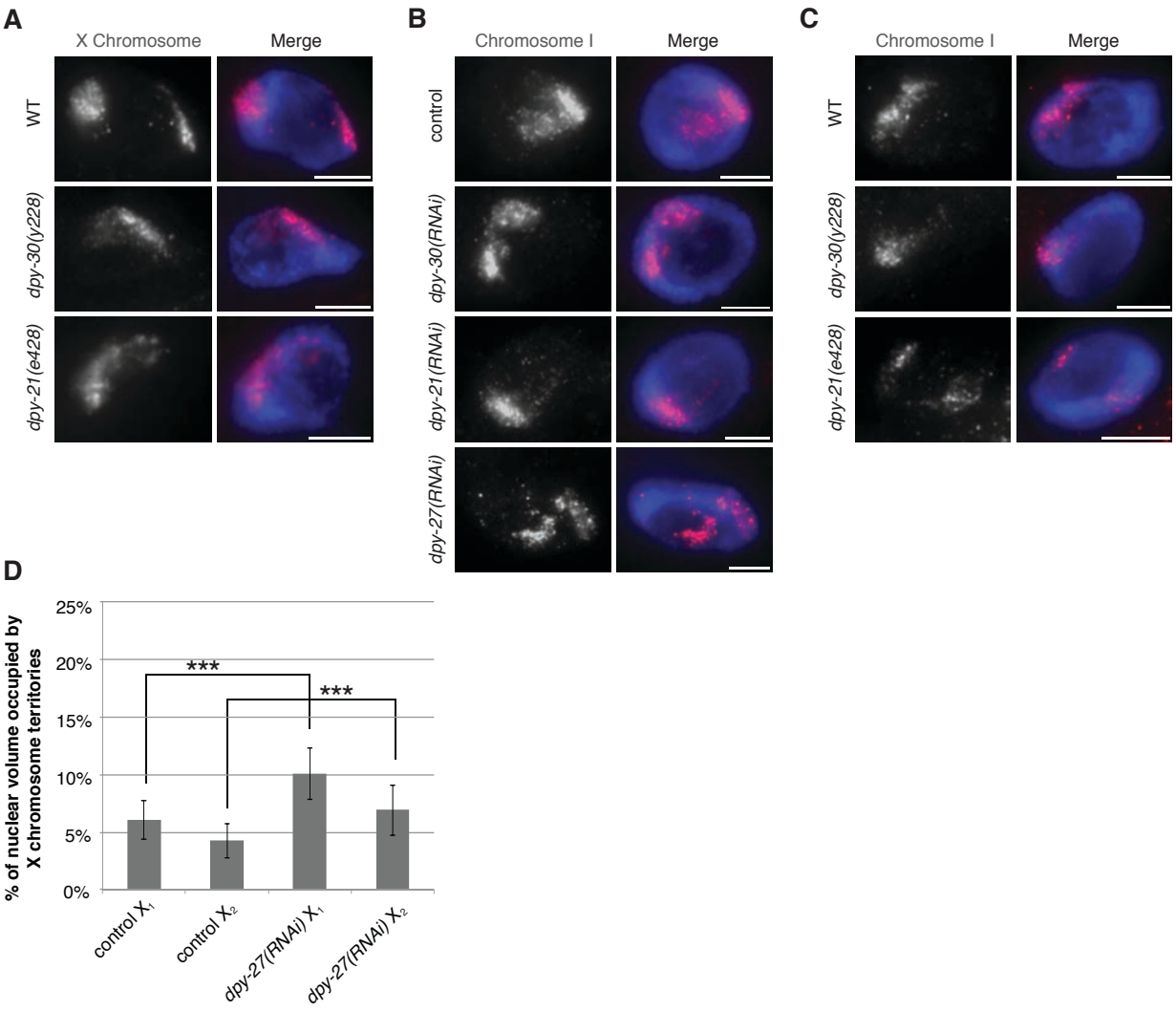

Figure 2.8 DCC depletion and mutants result in changes in the volume of the X chromosome. (A) Adult mutant hermaphrodite intestinal nuclei stained with X-paint FISH (red) to label X chromosome territories and DAPI (blue) to label DNA. Representative stained nuclei of wild type, *dpy-30(y228)*, and *dpy-21(e428)*. Scale bars equal 5 µm. (B) Adult RNAi treated hermaphrodite intestinal nuclei stained with chromosome I paint FISH (red) to label chromosome I territories and DAPI (blue) to label DNA after DCC depletion. Representative stained nuclei after vector RNAi treatment, *dpy-30(RNAi)*, *dpy-21(RNAi)*, and *dpy-27(RNAi)*. Scale bars equal 5 µm. (C) Adult mutant hermaphrodite intestinal nuclei stained with chromosome I paint FISH (red) to label chromosome I territories and DAPI (blue) to label DNA. Representative stained nuclei wild type, *dpy-30(y228)*, and *dpy-21(e428)*. Scale bars equal 5 µm. (D) Quantification of the percentage of nuclear volume occupied by individual X chromosome territories (larger territory arbitrarily designated as X_1 and the smaller territory as X_2) in control X_1 (n = 31), control X_2 (n = 31), *dpy-27(RNAi)* X_1 (n = 20), and *dpy-27(RNAi)* X_2 (n = 20). Error bars indicate standard deviation. Asterisks indicate level of statistical significance by t-test analysis (three asterisks, $P < 0.001$).

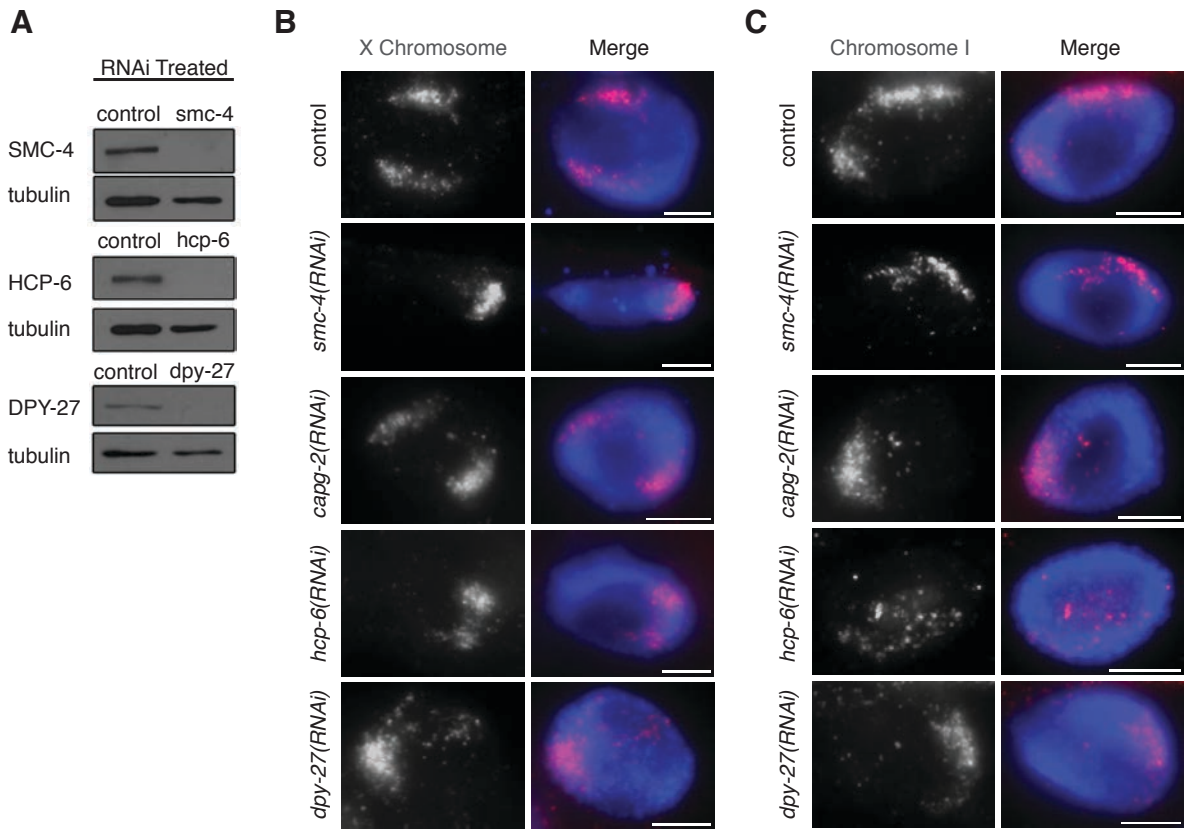

Figure 2.9 No changes in X or chromosome I size in condensin I or II depleted animals. (A) Western blot analysis of the depletion in adults after one-generation RNAi feeding (*smc-4*, *hcp-6*, *dpy-27*). Each subunit was successfully depleted. Tubulin is shown as a loading control. (B) Adult RNAi treated hermaphrodite intestinal nuclei stained with X-paint FISH (red) to label X chromosome territories and DAPI (blue) to label DNA. Representative stained nuclei after vector RNAi treatment, *smc-4(RNAi)*, *capg-2(RNAi)*, *hcp-6(RNAi)*, and *dpy-27(RNAi)*. Scale bars equal 5 µm. (C) Adult RNAi treated hermaphrodite intestinal nuclei stained with chromosome I paint FISH (red) to label chromosome I territories and DAPI (blue) to label DNA. Representative stained nuclei after vector RNAi treatment, *smc-4(RNAi)*, *capg-2(RNAi)*, *hcp-6(RNAi)*, and *dpy-27(RNAi)*. Scale bars equal 5 µm.

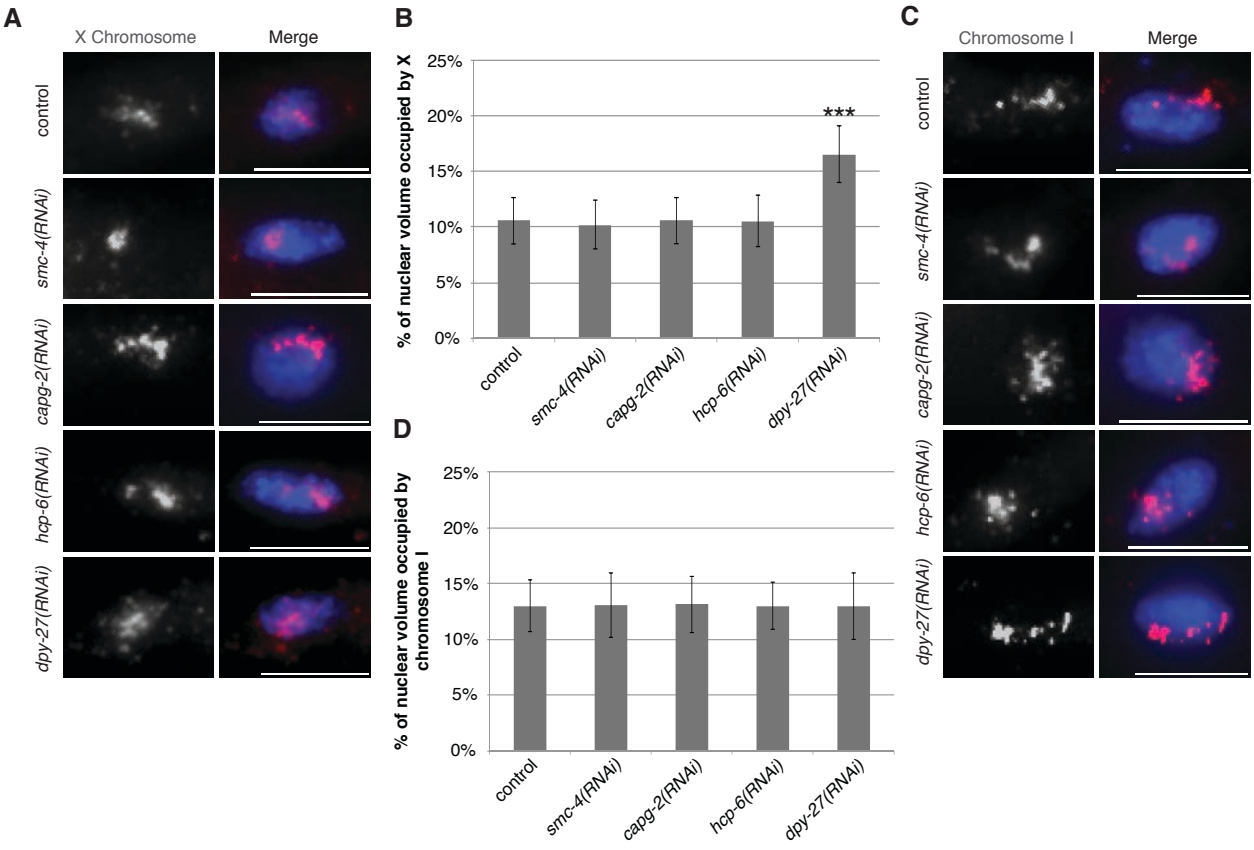

Figure 2.10 Diploid condensin I and II depleted nuclei show no change in chromosome volume. (A, B) Adult RNAi treated hermaphrodite diploid nuclei stained with X-paint FISH (red) to label X chromosome territories and DAPI (blue) to label DNA. (A) Representative stained nuclei after vector RNAi treatment, *smc-4(RNAi)*, *capg-2(RNAi)*, *hcp-6(RNAi)*, and *dpy-27(RNAi)*. Scale bars equal 5 µm. (B) Quantification of the percentage of nuclear volume occupied by X in vector RNAi (n = 40), *smc-4(RNAi)* (n = 25), *capg-2(RNAi)* (n = 40), *hcp-6(RNAi)* (n = 40), and *dpy-27(RNAi)* (n = 24). Error bars indicate standard deviation. Asterisks indicate level of statistical significance by t-test analysis (three asterisks, $P < 0.001$). (C, D) Adult RNAi treated hermaphrodite diploid nuclei stained with chromosome I paint FISH (red) to label chromosome I territories and DAPI (blue) to label DNA. (C) Representative stained nuclei after vector RNAi treatment, *smc-4(RNAi)*, *capg-2(RNAi)*, *hcp-6(RNAi)*, and *dpy-27(RNAi)*. Scale bars equal 5 µm. (D) Quantification of the percentage of nuclear volume occupied by chromosome I in vector RNAi (n = 30), *smc-4(RNAi)* (n = 25), *capg-2(RNAi)* (n = 40), *hcp-6(RNAi)* (n = 40), and *dpy-27(RNAi)* (n = 24). Error bars indicate standard deviation.

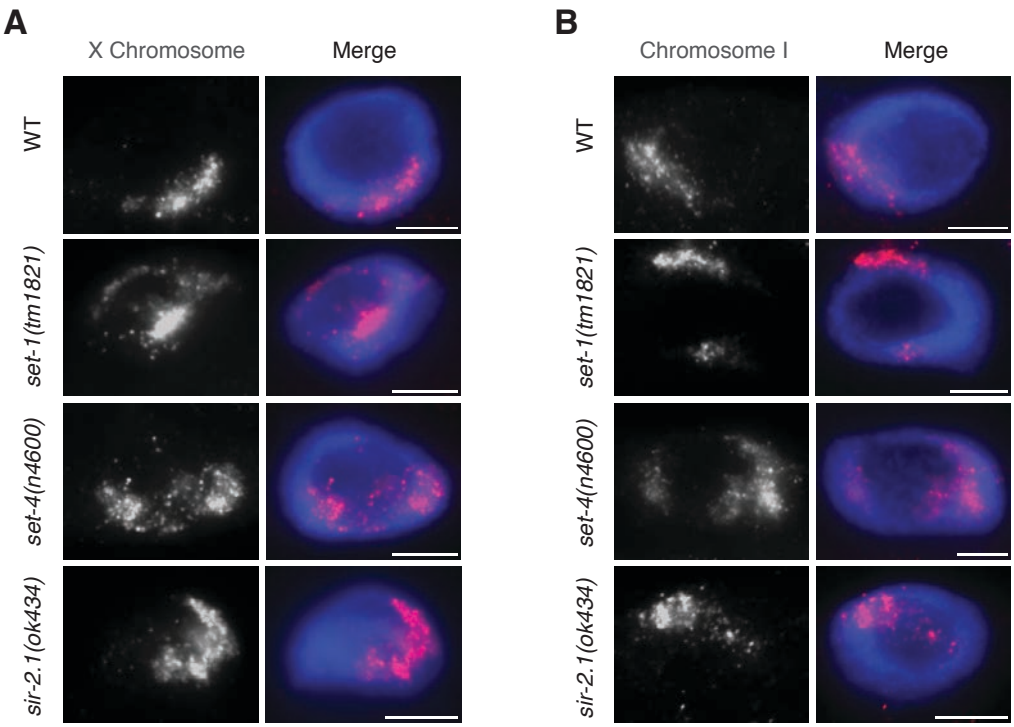

Figure 2.11 Changes in DCC mediated histone modifiers lead to disrupted X chromosomes but not chromosome I. (A) Adult mutant hermaphrodite intestinal nuclei stained with X paint FISH (red) to label X chromosome territories and DAPI (blue) to label DNA. Representative stained nuclei of wild type, *set-1(tm1821)*, *set-4(n4600)*, and *sir-2.1(ok434)*. Scale bars equal 5 µm. (B) Adult mutant hermaphrodite intestinal nuclei stained with chromosome I paint FISH (red) to label chromosome I territories and DAPI (blue) to label DNA. Representative stained nuclei of wild type, *set-1(tm1821)*, *set-4(n4600)*, and *sir-2.1(ok434)*. Scale bars equal 5 µm.

REFERENCES

1. Ohno, S. (1967). Sex Chromosomes and Sex-Linked Genes. Berlin: Springer, 1-140.
2. Conrad, T., and Akhtar, A. (2011). Dosage compensation in Drosophila melanogaster: epigenetic fine-tuning of chromosome-wide transcription. Nature reviews. Genetics *13*, 123-134.
3. Ferrari, F., Alekseyenko, A.A., Park, P.J., and Kuroda, M.I. (2014). Transcriptional control of a whole chromosome: emerging models for dosage compensation. Nature structural & molecular biology *21*, 118-125.
4. Deng, X., Berletch, J.B., Ma, W., Nguyen, D.K., Hiatt, J.B., Noble, W.S., Shendure, J., and Disteche, C.M. (2013). Mammalian X upregulation is associated with enhanced transcription initiation, RNA half-life, and MOF-mediated H4K16 acetylation. Developmental cell *25*, 55-68.
5. Deng, X., Hiatt, J.B., Nguyen, D.K., Ercan, S., Sturgill, D., Hillier, L.W., Schlesinger, F., Davis, C.A., Reinke, V.J., Gingeras, T.R., et al. (2011). Evidence for compensatory upregulation of expressed X-linked genes in mammals, Caenorhabditis elegans and Drosophila melanogaster. Nature genetics *43*, 1179-1185.
6. Gupta, V., Parisi, M., Sturgill, D., Nuttall, R., Doctolero, M., Dudko, O.K., Malley, J.D., Eastman, P.S., and Oliver, B. (2006). Global analysis of X-chromosome dosage compensation. Journal of biology *5*, 3.
7. Lin, H., Gupta, V., Vermilyea, M.D., Falciani, F., Lee, J.T., O'Neill, L.P., and Turner, B.M. (2007). Dosage compensation in the mouse balances up-regulation and silencing of X-linked genes. PLoS biology *5*, e326.
8. Lin, H., Halsall, J.A., Antczak, P., O'Neill, L.P., Falciani, F., and Turner, B.M. (2011). Relative overexpression of X-linked genes in mouse embryonic stem cells is consistent with Ohno's hypothesis. Nature genetics *43*, 1169-1170; author reply 1171-1162.
9. Barakat, T.S., and Gribnau, J. (2012). X chromosome inactivation in the cycle of life. Development *139*, 2085-2089.
10. Heard, E., and Disteche, C.M. (2006). Dosage compensation in mammals: fine-tuning the expression of the X chromosome. Genes & development *20*, 1848-1867.
11. Payer, B., and Lee, J.T. (2008). X chromosome dosage compensation: how mammals keep the balance. Annual review of genetics *42*, 733-772.
12. Csankovszki, G., Petty, E.L., and Collette, K.S. (2009). The worm solution: a chromosome-full of condensin helps gene expression go down. Chromosome research : an international journal on the molecular, supramolecular and evolutionary aspects of chromosome biology *17*, 621-635.
13. Meyer, B.J. (2010). Targeting X chromosomes for repression. Current opinion in genetics & development *20*, 179-189.

14. Chuang, P.T., Albertson, D.G., and Meyer, B.J. (1994). DPY-27:a chromosome condensation protein homolog that regulates C. elegans dosage compensation through association with the X chromosome. Cell *79*, 459-474.
15. Csankovszki, G., Collette, K., Spahl, K., Carey, J., Snyder, M., Petty, E., Patel, U., Tabuchi, T., Liu, H., McLeod, I., et al. (2009). Three distinct condensin complexes control C. elegans chromosome dynamics. Current biology : CB *19*, 9-19.
16. Lieb, J.D., Albrecht, M.R., Chuang, P.T., and Meyer, B.J. (1998). MIX-1: an essential component of the C. elegans mitotic machinery executes X chromosome dosage compensation. Cell *92*, 265-277.
17. Lieb, J.D., Capowski, E.E., Meneely, P., and Meyer, B.J. (1996). DPY-26, a link between dosage compensation and meiotic chromosome segregation in the nematode. Science *274*, 1732-1736.
18. Tsai, C.J., Mets, D.G., Albrecht, M.R., Nix, P., Chan, A., and Meyer, B.J. (2008). Meiotic crossover number and distribution are regulated by a dosage compensation protein that resembles a condensin subunit. Genes & development *22*, 194-211.
19. Hsu, D.R., and Meyer, B.J. (1994). The dpy-30 gene encodes an essential component of the Caenorhabditis elegans dosage compensation machinery. Genetics *137*, 999-1018.
20. Yonker, S.A., and Meyer, B.J. (2003). Recruitment of C. elegans dosage compensation proteins for gene-specific versus chromosome-wide repression. Development *130*, 6519-6532.
21. Mets, D.G., and Meyer, B.J. (2009). Condensins regulate meiotic DNA break distribution, thus crossover frequency, by controlling chromosome structure. Cell *139*, 73-86.
22. Hirano, T. (2012). Condensins: universal organizers of chromosomes with diverse functions. Genes & development *26*, 1659-1678.
23. Green, L.C., Kalitsis, P., Chang, T.M., Cipetic, M., Kim, J.H., Marshall, O., Turnbull, L., Whitchurch, C.B., Vagnarelli, P., Samejima, K., et al. (2012). Contrasting roles of condensin I and condensin II in mitotic chromosome formation. Journal of cell science *125*, 1591-1604.
24. Hirota, T., Gerlich, D., Koch, B., Ellenberg, J., and Peters, J.M. (2004). Distinct functions of condensin I and II in mitotic chromosome assembly. Journal of cell science *117*, 6435-6445.
25. Ono, T., Losada, A., Hirano, M., Myers, M.P., Neuwald, A.F., and Hirano, T. (2003). Differential contributions of condensin I and condensin II to mitotic chromosome architecture in vertebrate cells. Cell *115*, 109-121.
26. Shintomi, K., and Hirano, T. (2011). The relative ratio of condensin I to II determines chromosome shapes. Genes & development *25*, 1464-1469.
27. Freeman, L., Aragon-Alcaide, L., and Strunnikov, A. (2000). The condensin complex governs chromosome condensation and mitotic transmission of rDNA. The Journal of cell biology *149*, 811-824.

28. Hirano, T., Kobayashi, R., and Hirano, M. (1997). Condensins, chromosome condensation protein complexes containing XCAP-C, XCAP-E and a Xenopus homolog of the Drosophila Barren protein. Cell *89*, 511-521.
29. Hirano, T., and Mitchison, T.J. (1994). A heterodimeric coiled-coil protein required for mitotic chromosome condensation in vitro. Cell *79*, 449-458.
30. Sutani, T., Yuasa, T., Tomonaga, T., Dohmae, N., Takio, K., and Yanagida, M. (1999). Fission yeast condensin complex: essential roles of non-SMC subunits for condensation and Cdc2 phosphorylation of Cut3/SMC4. Genes & development *13*, 2271-2283.
31. Hagstrom, K.A., Holmes, V.F., Cozzarelli, N.R., and Meyer, B.J. (2002). C. elegans condensin promotes mitotic chromosome architecture, centromere organization, and sister chromatid segregation during mitosis and meiosis. Genes & development *16*, 729-742.
32. Collette, K.S., Petty, E.L., Golenberg, N., Bembenek, J.N., and Csankovszki, G. (2011). Different roles for Aurora B in condensin targeting during mitosis and meiosis. Journal of cell science *124*, 3684-3694.
33. Gerlich, D., Hirota, T., Koch, B., Peters, J.M., and Ellenberg, J. (2006). Condensin I stabilizes chromosomes mechanically through a dynamic interaction in live cells. Current biology : CB *16*, 333-344.
34. Ono, T., Fang, Y., Spector, D.L., and Hirano, T. (2004). Spatial and temporal regulation of Condensins I and II in mitotic chromosome assembly in human cells. Molecular biology of the cell *15*, 3296-3308.
35. Buster, D.W., Daniel, S.G., Nguyen, H.Q., Windler, S.L., Skwarek, L.C., Peterson, M., Roberts, M., Meserve, J.H., Hartl, T., Klebba, J.E., et al. (2013). SCFSlimb ubiquitin ligase suppresses condensin II-mediated nuclear reorganization by degrading Cap-H2. The Journal of cell biology *201*, 49-63.
36. Hartl, T.A., Smith, H.F., and Bosco, G. (2008). Chromosome alignment and transvection are antagonized by condensin II. Science *322*, 1384-1387.
37. Hartl, T.A., Sweeney, S.J., Knepler, P.J., and Bosco, G. (2008). Condensin II resolves chromosomal associations to enable anaphase I segregation in Drosophila male meiosis. PLoS genetics *4*, e1000228.
38. Joyce, E.F., Williams, B.R., Xie, T., and Wu, C.T. (2012). Identification of genes that promote or antagonize somatic homolog pairing using a high-throughput FISH-based screen. PLoS genetics *8*, e1002667.
39. Bauer, C.R., Hartl, T.A., and Bosco, G. (2012). Condensin II promotes the formation of chromosome territories by inducing axial compaction of polyploid interphase chromosomes. PLoS genetics *8*, e1002873.
40. Rawlings, J.S., Gatzka, M., Thomas, P.G., and Ihle, J.N. (2011). Chromatin condensation via the condensin II complex is required for peripheral T-cell quiescence. The EMBO journal *30*, 263-276.
41. Fazzio, T.G., and Panning, B. (2010). Condensin complexes regulate mitotic progression and interphase chromatin structure in embryonic stem cells. The Journal of cell biology *188*, 491-503.

42. Haeusler, R.A., Pratt-Hyatt, M., Good, P.D., Gipson, T.A., and Engelke, D.R. (2008). Clustering of yeast tRNA genes is mediated by specific association of condensin with tRNA gene transcription complexes. Genes & development *22*, 2204-2214.
43. Iwasaki, O., Tanaka, A., Tanizawa, H., Grewal, S.I., and Noma, K. (2010). Centromeric localization of dispersed Pol III genes in fission yeast. Molecular biology of the cell *21*, 254-265.
44. Rice, J.C., Nishioka, K., Sarma, K., Steward, R., Reinberg, D., and Allis, C.D. (2002). Mitotic-specific methylation of histone H4 Lys 20 follows increased PR-Set7 expression and its localization to mitotic chromosomes. Genes & development *16*, 2225-2230.
45. Wilkins, B.J., Rall, N.A., Ostwal, Y., Kruitwagen, T., Hiragami-Hamada, K., Winkler, M., Barral, Y., Fischle, W., and Neumann, H. (2014). A cascade of histone modifications induces chromatin condensation in mitosis. Science *343*, 77-80.
46. Oda, H., Okamoto, I., Murphy, N., Chu, J., Price, S.M., Shen, M.M., Torres-Padilla, M.E., Heard, E., and Reinberg, D. (2009). Monomethylation of histone H4-lysine 20 is involved in chromosome structure and stability and is essential for mouse development. Molecular and cellular biology *29*, 2278-2295.
47. Nishioka, K., Rice, J.C., Sarma, K., Erdjument-Bromage, H., Werner, J., Wang, Y., Chuikov, S., Valenzuela, P., Tempst, P., Steward, R., et al. (2002). PR-Set7 is a nucleosome-specific methyltransferase that modifies lysine 20 of histone H4 and is associated with silent chromatin. Molecular cell *9*, 1201-1213.
48. Vielle, A., Lang, J., Dong, Y., Ercan, S., Kotwaliwale, C., Rechtsteiner, A., Appert, A., Chen, Q.B., Dose, A., Egelhofer, T., et al. (2012). H4K20me1 contributes to downregulation of X-linked genes for C. elegans dosage compensation. PLoS genetics *8*, e1002933.
49. Wells, M.B., Snyder, M.J., Custer, L.M., and Csankovszki, G. (2012). Caenorhabditis elegans dosage compensation regulates histone H4 chromatin state on X chromosomes. Molecular and cellular biology *32*, 1710-1719.
50. Nabeshima, K., Mlynarczyk-Evans, S., and Villeneuve, A.M. (2011). Chromosome painting reveals asynaptic full alignment of homologs and HIM-8-dependent remodeling of X chromosome territories during Caenorhabditis elegans meiosis. PLoS genetics *7*, e1002231.
51. Hedgecock, E.M., and White, J.G. (1985). Polyploid tissues in the nematode Caenorhabditis elegans. Developmental biology *107*, 128-133.
52. Consortium, C.e.S. (1998). Genome sequence of the nematode C. elegans: a platform for investigating biology. Science *282*, 2012-2018.
53. Hsu, D.R., Chuang, P.T., and Meyer, B.J. (1995). DPY-30, a nuclear protein essential early in embryogenesis for Caenorhabditis elegans dosage compensation. Development *121*, 3323-3334.
54. Pferdehirt, R.R., Kruesi, W.S., and Meyer, B.J. (2011). An MLL/COMPASS subunit functions in the C. elegans dosage compensation complex to target X

chromosomes for transcriptional regulation of gene expression. Genes & development *25*, 499-515.
55. Sulston, J.E., Schierenberg, E., White, J.G., and Thomson, J.N. (1983). The embryonic cell lineage of the nematode Caenorhabditis elegans. Developmental biology *100*, 64-119.
56. Eskeland, R., Leeb, M., Grimes, G.R., Kress, C., Boyle, S., Sproul, D., Gilbert, N., Fan, Y., Skoultchi, A.I., Wutz, A., et al. (2010). Ring1B compacts chromatin structure and represses gene expression independent of histone ubiquitination. Molecular cell *38*, 452-464.
57. Stear, J.H., and Roth, M.B. (2002). Characterization of HCP-6, a C. elegans protein required to prevent chromosome twisting and merotelic attachment. Genes & development *16*, 1498-1508.
58. Chan, R.C., Severson, A.F., and Meyer, B.J. (2004). Condensin restructures chromosomes in preparation for meiotic divisions. The Journal of cell biology *167*, 613-625.
59. Jans, J., Gladden, J.M., Ralston, E.J., Pickle, C.S., Michel, A.H., Pferdehirt, R.R., Eisen, M.B., and Meyer, B.J. (2009). A condensin-like dosage compensation complex acts at a distance to control expression throughout the genome. Genes & development *23*, 602-618.
60. Custer, L.M., Snyder, M.J., Flegel, K., and Csankovszki, G. (2014). The onset of C. elegans dosage compensation is linked to the loss of developmental plasticity. Developmental biology *385*, 279-290.
61. Kimura, K., and Hirano, T. (2000). Dual roles of the 11S regulatory subcomplex in condensin functions. Proceedings of the National Academy of Sciences of the United States of America *97*, 11972-11977.
62. Kimura, K., Cuvier, O., and Hirano, T. (2001). Chromosome condensation by a human condensin complex in Xenopus egg extracts. The Journal of biological chemistry *276*, 5417-5420.
63. Kimura, K., and Hirano, T. (1997). ATP-dependent positive supercoiling of DNA by 13S condensin: a biochemical implication for chromosome condensation. Cell *90*, 625-634.
64. St-Pierre, J., Douziech, M., Bazile, F., Pascariu, M., Bonneil, E., Sauve, V., Ratsima, H., and D'Amours, D. (2009). Polo kinase regulates mitotic chromosome condensation by hyperactivation of condensin DNA supercoiling activity. Molecular cell *34*, 416-426.
65. Kimura, K., Rybenkov, V.V., Crisona, N.J., Hirano, T., and Cozzarelli, N.R. (1999). 13S condensin actively reconfigures DNA by introducing global positive writhe: implications for chromosome condensation. Cell *98*, 239-248.
66. Baxter, J., Sen, N., Martinez, V.L., De Carandini, M.E., Schvartzman, J.B., Diffley, J.F., and Aragon, L. (2011). Positive supercoiling of mitotic DNA drives decatenation by topoisomerase II in eukaryotes. Science *331*, 1328-1332.
67. Sakai, A., Hizume, K., Sutani, T., Takeyasu, K., and Yanagida, M. (2003). Condensin but not cohesin SMC heterodimer induces DNA reannealing through protein-protein assembly. The EMBO journal *22*, 2764-2775.

68. Cuylen, S., Metz, J., and Haering, C.H. (2011). Condensin structures chromosomal DNA through topological links. Nature structural & molecular biology *18*, 894-901.
69. Shogren-Knaak, M., Ishii, H., Sun, J.M., Pazin, M.J., Davie, J.R., and Peterson, C.L. (2006). Histone H4-K16 acetylation controls chromatin structure and protein interactions. Science *311*, 844-847.
70. Hamada, F.N., Park, P.J., Gordadze, P.R., and Kuroda, M.I. (2005). Global regulation of X chromosomal genes by the MSL complex in Drosophila melanogaster. Genes & development *19*, 2289-2294.
71. Straub, T., Gilfillan, G.D., Maier, V.K., and Becker, P.B. (2005). The Drosophila MSL complex activates the transcription of target genes. Genes & development *19*, 2284-2288.
72. Akhtar, A., and Becker, P.B. (2000). Activation of transcription through histone H4 acetylation by MOF, an acetyltransferase essential for dosage compensation in Drosophila. Molecular cell *5*, 367-375.
73. Smith, E.R., Pannuti, A., Gu, W., Steurnagel, A., Cook, R.G., Allis, C.D., and Lucchesi, J.C. (2000). The drosophila MSL complex acetylates histone H4 at lysine 16, a chromatin modification linked to dosage compensation. Molecular and cellular biology *20*, 312-318.
74. Dunlap, D., Yokoyama, R., Ling, H., Sun, H.Y., McGill, K., Cugusi, S., and Lucchesi, J.C. (2012). Distinct contributions of MSL complex subunits to the transcriptional enhancement responsible for dosage compensation in Drosophila. Nucleic acids research *40*, 11281-11291.
75. Corona, D.F., Clapier, C.R., Becker, P.B., and Tamkun, J.W. (2002). Modulation of ISWI function by site-specific histone acetylation. EMBO reports *3*, 242-247.
76. Brenner, S. (1974). The genetics of Caenorhabditis elegans. Genetics *77*, 71-94.
77. Kamath, R.S., and Ahringer, J. (2003). Genome-wide RNAi screening in Caenorhabditis elegans. Methods *30*, 313-321.
78. Csankovszki, G., McDonel, P., and Meyer, B.J. (2004). Recruitment and spreading of the C. elegans dosage compensation complex along X chromosomes. Science *303*, 1182-1185.

CHAPTER 3

Anchoring of heterochromatin to the nuclear lamina helps stabilize dosage compensation-mediated gene repression

This chapter has been submitted and pending revisions as Snyder M[1], Lau AC[1], Brouhard EA, Davis M, et al. (2016) in PLoS Genetics as "Anchoring of heterochromatin to the nuclear lamina helps stabilize dosage compensation-mediated gene repression" ([1]equal contribution). I conducted the image analysis for data shown in Figure 3.2, the RNA-sequencing analysis for data shown in Figure 3.9, 3.10, 3.16, and 3,17, the illustration for Figure 3.11, and assisted with worm counts in the RNAi screen for Figure 3.12. All other figures are the work of M. Snyder, E. Brouhard, M. Davis, J. Jiang, M. Sifuentes, and G. Csankovszki.

ABSTRACT

Higher order chromosome structure and nuclear architecture can have profound effects on regulation of gene expression. We analyzed how compartmentalizing the genome by tethering heterochromatic regions to the nuclear lamina can affect gene expression during *C. elegans* dosage compensation. In this organism, the dosage compensation complex (DCC) binds both X chromosomes of hermaphrodites to repress gene expression two-fold, thus balancing gene expression between XX hermaphrodites

and XO males. X chromosome structure is disrupted by mutations in DCC subunits. Using X chromosome paint fluorescence microscopy, we found that X chromosome structure and subnuclear localization are also disrupted when the mechanisms that anchor heterochromatin to the nuclear lamina are defective. Strikingly, the heterochromatic left end of the X chromosome is less affected than the gene-rich middle region, which lacks heterochromatic anchors. These changes in X chromosome structure and subnuclear localization are accompanied by small, but significant levels of derepression of X-linked genes as measured by RNA-seq, without any observable defects in DCC localization and DCC-mediated changes in histone modifications. Our results suggest a model where heterochromatin tethers on the left arm of the chromosome nucleate formation of a compact structure, which, by the action of the DCC, is propagated to the rest of the chromosome, contributing to gene repression.

AUTHOR SUMMARY

DNA isolated from the nucleus of a single human cell, if stretched out, would be 3 meters long. This amount of DNA must be packaged into a nucleus, which is orders of magnitude smaller. DNA of active genes tends to be loosely packed and localized internally within the nucleus, while DNA of inactive genes tends to be tightly packed and localized near the nuclear periphery. We studied the effects of DNA compaction and nuclear localization on gene expression levels using regulation of the X chromosomes in the nematode *Caenorhabditis elegans* as a model. In this organism, hermaphrodites have two X chromosome, and males have only one. Genes on the two X chromosomes in hermaphrodites are expressed at half the level compared to the male X, such that the

two Xs together express as much gene products as the single X in males. We found that silent regions at the left end of hermaphrodite X chromosomes are tethered to the nuclear periphery, and these tethers are used to build a compact chromosome structure. If this process is defective, gene expression levels are elevated, but less than two-fold. These results indicate that chromosome compaction and nuclear localization contribute to influencing gene expression levels, but other mechanisms must also contribute.

INTRODUCTION

Expression of genes must be tightly regulated both spatially and temporarily to ensure normal development. While our understanding of gene regulation at the level of transcription factor binding and modulation of chromatin structure is supported by an abundance of data, the contribution of the spatial organization of the nucleus to regulation of gene expression is not well understood. Regulation of sex chromosome-linked gene expression in the process of dosage compensation provides an excellent model to dissect the influence of different gene regulatory mechanisms on chromosome-wide modulation of gene activity. In the nematode *C. elegans*, dosage compensation downregulates expression of genes on the otherwise highly expressed X chromosomes of hermaphrodites, such that transcript levels from the two hermaphrodite X chromosomes are brought down to match transcript levels from the single X in males [1,2]. A complex of proteins called the dosage compensation complex (DCC) binds the length of both hermaphrodite X chromosomes to regulate transcription. The DCC contains a subcomplex, condensin I^{DC}, which is homologous to condensin complexes in

all eukaryotes responsible for compaction and segregation of chromosomes in mitosis and meiosis [3-5].

Although a number of studies in recent years uncovered molecular mechanisms of DCC action, how these alterations in X chromosome structure repress gene expression remains unknown. Consistent with a similarity to mitotic condensins, DCC binding leads to compaction of hermaphrodite X chromosomes in interphase [6,7]. The DCC also remodels the X chromosomes into topologically associating domains (TADs) with more regular spacing and stronger boundaries than those found on autosomes [8]. At the level of chromatin organization, posttranslational modifications of histones are also altered in a DCC-dependent manner: monomethylation of histone H4 lysine 20 (H4K20me1) becomes enriched, and acetylation of histone H4 lysine 16 (H4K16ac) becomes depleted on dosage compensated Xs as compared to autosomes [9,10]. Analysis of gene expression in H4K20 histone methyltransferase (HMT) mutants revealed that changes in H4K20me1 levels contribute to DCC-mediated repression, but are not fully responsible for the observed two-fold repression [11]. The relative contributions of chromosome condensation and partitioning of the chromosome into TADs are unclear. To date, no correlation has been found between genes being subjected to DCC-mediated repression and regions of the chromosome bound by the DCC [12,13], DCC induced changes in TADs [8] or posttranslational histone modifications [10]. These observations led to the suggestion that the DCC regulates gene expression not on a gene-by-gene basis, but rather chromosome-wide.

A model of DCC-mediated chromosome-wide repression mechanism is consistent with the idea of the formation of a repressive nuclear compartment. Organization of chromosomes within the nucleus is not random, but rather active and inactive portions of the genome are clustered together and separated into spatially distinct compartments [14-16]. One prominent feature of nuclear organization is positioning heterochromatic regions at the nuclear periphery or near the nucleolus [17-19]. An open question is to what extent this level of organization influences gene activity, rather than being a consequence of it. In this study we investigated the role of nuclear organization, particularly the tethering of heterochromatic regions to the nuclear lamina, in regulating genes on dosage compensated X chromosomes in *C. elegans*.

Genome-nuclear lamina interactions change dynamically during cellular differentiation and development and are known to influence gene activity. In *C. elegans*, tissue specific promoters are localized randomly in nuclei of undifferentiated cells, reflecting the pluripotent state of these cells. As cells commit to specific fates and differentiate, active promoters move toward the nuclear interior, while repressed promoters move toward the nuclear periphery [20]. Disruption of nuclear lamina anchoring by depletion of lamin (LMN-1) or lamin-interacting proteins leads to derepression of otherwise silent transgenes, demonstrating the relevance of the anchoring process to gene repression, at least in the context of transgenes [21]. Anchoring of these heterochromatic transgenic arrays to the nuclear lamina requires trimethylation of histone H3 lysine 9 (H3K9me3) by the HMTs MET-2 and SET-25, as well as the chromodomain protein CEC-4 [22,23]. The relevance of this process to the

regulation of endogenous gene expression is less clear. Gene expression does not change dramatically in the absence of H3K9me3 or CEC-4, but repression induced by heterochromatic anchoring does help restrict alternate cell fates in development [22,23]. These observations indicate that likely multiple mechanisms contribute to repression of genes not expressed in a given cell type, and the contribution of lamina anchoring to gene regulation may only become apparent in sensitized backgrounds. Similar results were obtained in other organisms. For example, in differentiating mouse embryonic stem cells, genome-nuclear lamina interactions are remodeled such that some, but not all, genes move away from the nuclear lamina when activated [24].

Consistent with a generally repressive environment, regions of the genome associated with the nuclear lamina (lamina associated domains, or LADs) are depleted of active chromatin marks and are enriched for repressive marks such as H3K9 and H3K27 methylation in a variety of organisms [24-27]. These silencing marks, and the enzymes that place them, are required for peripheral localization of heterochromatic transgenes and some developmentally regulated endogenous sequences [23,28-30]. Artificial tethering of genes to the nuclear lamina leads to repression of some, but not all, genes [31-34]. These observations are consistent with the idea that the vicinity of the nuclear lamina is a repressive environment, yet it is not incompatible with transcription. Therefore, subnuclear compartmentalization may not be a primary driver of gene expression levels, but rather serve as a mechanism to stabilize existing transcriptional programs [22].

Here we show that anchoring of heterochromatic regions to the nuclear lamina contributes to shaping the higher order structure and nuclear localization of dosage compensated X chromosomes. These X-chromosome-specific phenotypes were observed in multiple tissues, and thus appear to be inherent to the chromosome and not any cell-type specific differentiation program. We show that heterochromatin integrity and its nuclear lamina anchors are required for spatial organization of the nucleus and dosage compensation mediated condensation of the X chromosome. In mutant strains that lack these anchors, despite normal DCC localization to the X chromosome, we observe a small, but significant level of X derepression, consistent with the idea that anchoring contributes to stabilizing gene repression. Remarkably, tethering of heterochromatic regions of the X chromosome to the nuclear lamina affects the entire chromosome, not only the tethered domain. We propose a model in which the tethered domain nucleates formation of a compact structure, which facilitates the action of the DCC to compact the entire X chromosome.

RESULTS

In order to identify chromatin modifying genes that influence dosage compensation, we previously performed a targeted RNAi screen to analyze genes implicated in chromatin regulation, including histone variants, as well as genes containing chromo, bromo, or set domains [35]. The assay is based on rescue of males that inappropriately turn on dosage compensation. The DCC assembles on the X chromosome of *xol-1(y9) sex-1(y263)* males, leading to insufficient expression of genes from the single X chromosome and thus lethality. RNAi-mediated disruption of dosage

compensation can rescue a proportion of these males. Control vector RNAi leads to background level of rescue (about 1.5%), while RNAi of a component of the DCC rescues over 25% of males. We previously described the screen in detail, as well as the role of one of the hits from the screen, the histone H2A variant HTZ-1 [35]. In this study we characterize the remaining genes identified in this screen that led to low but reproducible levels of male rescue. These genes include the histone methyltransferases *met-2, set-32, set-20, set-6, set-25*, and the chromodomain protein *cec-4* (Figure 3.1). All of these histone methyltransferases are known (*met-2, set-25,* [23]) or predicted (*set-6, set-20, set-32* [36]) to modify histone H3K9. H3K9 methylation and the chromodomain protein CEC-4 were previously shown to work together in regulating nuclear organization and anchoring heterochromatic transgenic arrays to the nuclear lamina [21,22,37]. We therefore included in our analysis LEM-2 (hMAN1), a non-essential component of the nuclear lamina. RNAi of the single *C. elegans* lamin gene LMN-1 leads to embryonic lethality [38], precluding this type of analysis. However, RNAi-depletion of LEM-2 led to male rescue comparable to, or higher than, the rescue caused by depletion of the HMTs or CEC-4 (Figure 3.1). Chi square test of the data indicated that all genes rescued significantly more males than vector RNAi (Figure 3.1B). To ensure that the rescue is reproducible, we also performed the rescue assay with a subset of the identified genes in four independent biological replicates and analyzed the results using Student's t-test (Figure 3.12). With the exception of *set-6* and *set-20*, all genes identified in the screen rescued significantly more males than vector RNAi.

X chromosome decondensation in mutants

The finding of H3K9 methyltransferases, CEC-4, and LEM-2, in this screen suggested that nuclear organization, and specifically anchoring of chromosomal regions to the nuclear lamina (Figure 3.1C), might affect dosage compensation. To investigate X chromosome morphology and its location in the nucleus in the absence of these proteins, we performed X chromosome paint fluorescence *in situ* hybridization (FISH) in the various mutant backgrounds. First we investigated the 32-ploid nuclei of the intestine, because their large size facilitates visualization of chromosome territories. In wild type (N2) hermaphrodite worms, the X chromosome territories are kept compact by the action of the DCC [39] and the territory is found near the nuclear lamina (Figure 3.2A). Visual inspection of the X chromosome territories in *met-2(n4256), set-6(ok2195), set-20(ok2022), set-25(n5021), set-32(ok1457), cec-4(ok1324),* and *lem-2(ok1807)* hermaphrodites, revealed that the nuclear territory occupied by the X chromosomes became larger. As a control, we also analyzed the X chromosomes in *met-1(n4337)*, *hpl-1(tm1624)* and *hpl-2(tm1489)* mutants. MET-1 is an unrelated HMT, while HPL-1 and HPL-2 are homologs of the highly conserved heterochromatin protein and H3K9me3 binding protein HP-1 [40] (Figure 3.2A). To quantify X chromosome condensation, we measured the volumes of X chromosome territories, as in [39]. Briefly, we generated intensity threshold-based 3D masks for the X chromosome (X paint signal) and for the nucleus (DAPI signal). We then calculated the volume of the X chromosome and of the nucleus, and determined the portion of the nucleus occupied by the X chromosome. Normalization to total nuclear volume was necessary due to the

large variability in nuclear size after the harsh treatments involved in FISH. Quantification of the volume of the X chromosome territory showed that in the H3K9 HMT mutants, as well as in *cec-4* and *lem-2* mutants, the X chromosome occupied a much larger portion of the nucleus than in control wild type, or *met-1*, *hpl-1* or *hpl-2* mutant hermaphrodites. Lack of X chromosome condensation defects in *hpl-1* and *hpl-2* mutants are consistent with a previous study that reported no defects in nuclear lamina anchoring of heterochromatic transgenic arrays in *hpl-1* or *hpl-2* mutants [22]. In nuclei of wild type worms the X chromosome occupied about 10% of the nuclear volume, compared to an average of up to 20% percent in mutants ($p<0.001$, Student's t-test, for all comparisons between a mutant and wild type) (Figure 3.2B). In fact, the degree of decondensation in *set-25(n5021)* mutants is even larger than in DCC mutant or RNAi-depleted hermaphrodites (*dpy-21(e428)* and *dpy-27(RNAi)* [39] ($p=0.0251$ for comparison with *dpy-21*, and $p=0.00442$ for comparison with *dpy-27;* other differences were not statistically significant) (Figure 3.2). We conclude that the X chromosome is decondensed to a significant degree in worms carrying mutations in DCC subunits, as well as in H3K9 HMT, *cec-4* and *lem-2* mutants.

SET-25 and MET-2 are the only well characterized HMTs among the ones we identified. MET-2 introduces H3K9 mono- and dimethylation, while SET-25 introduces H3K9 trimethylation. Complete lack of H3K9 methylation, and loss of anchoring of heterochromatic arrays, are only observed in the *met-2 set-25* double mutants and not in *set-25* or *met-2* single mutants [23]. We therefore analyzed X chromosome structure in the *met-2(n4256) set-25(n5021)* double mutant strain and found that the X

chromosome morphology is comparable to single mutants without an obvious additive effect (p=0.56 for *met-2* compared to *met-2 set-25*; p=0.11 for *set-25* compared to *met-2 set-25*) (Figure 3.2A and B). For the rest of this study we concentrated on *lem-2, set-25 or met-2 set-25, and cec-4* mutants, and we will refer to them collectively as "tethering mutants".

One possible explanation for X decondensation phenotype is that the tethering defects diminish the ability of the DCC to condense the X chromosome. For example, the DCC may use these heterochromatic tethers as nucleation sites for a more compact chromosomal organization. An alternative possibility is that lack of tethering leads to chromosome decondensation independent of the DCC. We tested whether simultaneous disruptions of tethering and the DCC lead to increased levels of decondensation by measuring X chromosome volumes in *set-25* and *lem-2* mutants that were depleted of DPY-27 using RNAi (Figure 3.2B). X chromosomes of nuclei in *dpy-27(RNAi*) treated *lem-2* mutants were significantly different from wild type, but statistically indistinguishable from either *lem-2* mutants (p=0.77, Student's t-test) or *dpy-27(RNAi)* (p=0.26). Similarly, X chromosomes of nuclei in *dpy-27(RNAi)* treated *set-25* mutants were significantly different from wild type, but statistically indistinguishable from *set-25* mutants (p=0.052) and *dpy-27(RNAi)* (p=0.39). Therefore, at this resolution, we cannot detect any additional defects when tethering mutations are combined with DCC depletion, consistent with the hypothesis that the DCC and tethering genes work together, and are both required, to condense the X chromosomes.

To determine whether the phenotype is specific to the 32-ploid intestinal nuclei, we also examined diploid tail tip hypodermal cells hyp 8-11. Results were comparable to intestinal cells. In wild type cells, the X chromosome occupies about 10% of the nucleus, while it occupies a much larger portion of the nucleus in anchoring mutants ($p<0.001$ for all mutant comparisons to wild type) (Figure 3.13).

The dosage compensated X chromosome relocates to a more central position in tethering mutants

Previous studies showed that tethering mutants have a defect in anchoring heterochromatic transgenic arrays to the nuclear lamina [21-23]. Similarly, visual inspection of our images suggested that tethering mutants have a defect in subnuclear positioning of the X chromosome resulting in the X occupying a more central position (Figure 3.2). To quantify this defect, we performed an analysis similar to the three-zone assay used in [20]. We selected nuclei that we were spherical or ellipsoid shaped. From the Z-stacks generated during imaging, we selected the optical section toward the middle of the nucleus with the largest and brightest X-paint signal. This optical section was divided into three-zones of equal area, and the portion of the X signal located in each zone was quantified (Figure 3.3A). The percentage of nuclei in each genotype that can be quantified using this assay is shown in Figure 3.14. Representative irregularly shaped nuclei are also shown to illustrate that the X chromosome appeared qualitatively similar to X chromosome in round or ellipsoid shaped nuclei: compact and peripherally located in N2 hermaphrodites, and larger and more centrally located in tethering mutants. The three-zone assay showed that in wild type (N2) nuclei only about 20% of

the X chromosome signal was located in the central zone, while in tethering mutants over 40% of the X signal was located in this zone, suggesting that the X chromosome relocates to a more central position within the nucleus (Figure 3.3B). Comparisons of the portions of the X chromosome located in the central zone revealed statistically significant differences in all tethering mutants. As for volume measurement, the three-zone assay again failed to reveal additional defects in *met-2 set-25* double mutants compared to *set-25* single mutants. We then compared this effect to mutating or depleting a subunit of the DCC by RNAi. The three-zone assay showed less significant relocation of the X toward the center in *dpy-27* RNAi-treated hermaphrodites compared to tethering mutants. In *dpy-21* mutants, although the portion of the X in the central zone increased from 24% to 34%, the difference did not reach statistical significance (Figure 3.3B). One possible reason for the less significant relocation in dosage compensation mutants is the fact that *dpy-27(RNAi)* or a mutation in *dpy-21* does not completely disrupt dosage compensation function. Complete lack of DCC activity would be lethal to hermaphrodites, precluding this type of analysis (see analysis of the male X below).

H3K9me3 is generally found in heterochromatic regions of the genome. In *C. elegans,* several megabase regions at both ends of autosomes and the left end of the X chromosome are enriched for this mark [41]. These H3K9me3-enriched domains also coincide with nuclear lamina-associated domains, as assessed by ChIP [26] or DamID [23]. Together these results suggest a model in which both arms of autosomes and the left of arm of the X chromosome are tethered to the nuclear lamina [23,26,42-44]

(Figure 3.4A). Peripheral localization of heterochromatic chromosomal regions may be mediated by CEC-4, as is the case for heterochromatic transgenes [22].

To examine whether heterochromatic segments of the X chromosomes are affected differently than other chromosomal regions, we prepared probes to approximately 3-4 Mb regions of the chromosome. The X-left probe covers a region enriched for H3K9me3 and LEM-2, the X-mid probe covers a gene-rich portion of the chromosome with very little H3K9me3 and LEM-2, and the X-right probe covers a region with intermediate levels of H3K9me3 and LEM-2 (Figure 3.4A and B). We then assessed the level of decondensation of each of these regions by measuring the proportion of the nuclear volume occupied by this region of the X chromosome (Figure 3.4C). Surprisingly, the left end of the X chromosome was least affected and remained condensed both in tethering mutants and in DCC-depleted hermaphrodites. We only observed a mild level of decondensation in *set-25* mutants. By contrast, the gene-rich middle portion of the chromosome was most affected and was significantly decondensed in all tethering mutants. The right end of the chromosome, which contains some LEM-2 and H3K9me3 peaks, but fewer than the left end, exhibited an intermediate phenotype.

The gene-rich middle portion of the X chromosome was not only decondensed but also appeared to exhibit the greatest degree of central relocation. To quantify this effect, we again performed the three-zone assay and found that indeed the mid-X region was most affected (Figure 3.4D). While on average only 17% of the X-mid probe was located in the central zone in wild type nuclei, up to 50% of the same region was found

in this zone in tethering mutants. Relocation to a central position was less obvious for the left end of the chromosome and was not detectable for the right end. These results were at first unexpected. However, they are consistent with previous observations that have hinted at the existence of redundant tethering mechanisms in differentiated cells. The tethering mechanism mediated by heterochromatin is only essential for anchoring of heterochromatic arrays in embryonic cells, and the arrays remain anchored in differentiated tissues even in the absence of SET-25 and MET-2 [23]. Similarly, CEC-4 is required for anchoring in embryos, but other, yet unknown, mechanisms can compensate for the lack of CEC-4 protein in differentiated cells [22]. We note that all of our analysis was performed in terminally differentiated postmitotic cells of adult animals. Our results suggest that regions of the left end of the X chromosome are anchored to the nuclear periphery by an additional mechanism that is independent of SET-25, CEC-4, and LEM-2, and loss of H3K9me3-lamina mediated anchoring mechanism is not sufficient to significantly relocate this region. The lack of heterochromatic anchoring mechanism affects the middle of the chromosome disproportionately, even though this region is depleted of H3K9me3 and LEM-2 interactions. One possible interpretation of this result is that the few H3K9me3 sites and LEM-2-bound regions present in the middle of chromosome represent the only anchoring mechanism present in this region. In the absence of these tethers, the mid-X region is free to relocate more centrally, while redundant anchors maintain tethering to a greater degree at the two chromosome ends. The other interpretation, which is not mutually exclusive, is that heterochromatic anchors at the left end of the chromosome are used to nucleate a compact structure,

which is required to be able to pull the rest of the X chromosome toward the periphery and compact it efficiently (see Discussion).

Defects in DCC function had a somewhat different effect. The mid-X region was more decondensed after *dpy-27(RNAi)* than the right end, and the left end was unaffected, similar to the decondensation defects seen in tethering mutants. Less significant decompaction of the left end may be related to the somewhat lower levels of DCC binding in this region [41,45]. Alternatively, nuclear lamina tethers at the left end may be sufficient to compact this region even in the absence of the DCC. Although the portion of the mid-X region in the central domain increased in *dpy-27* RNAi, the difference did not reach statistical significance, suggesting again insufficient disruption of dosage compensation (Figure 3.4C and D).

Chromosomal phenotypes are dosage compensation dependent

To examine these X chromosomal phenotypes in the complete absence of DCC activity, we analyzed the X chromosome in males and in XO animals that develop as hermaphrodites due to a mutation in the *her-1* gene required for male development [46] (Figure 3.5). The XO hermaphrodites also carry a null mutation in the dosage compensation gene *sdc-2* to ensure that all XX progeny die due to dosage compensation defects and only XO animals survive [47]. The DCC is XX hermaphrodite-specific and does not bind to the male X or the X chromosome in XO hermaphrodites, therefore these backgrounds allow us to examine X chromosome structure in the complete absence of the DCC, but in the presence of heterochromatic anchors. In wild type males and in XO hermaphrodites, the single X occupied an large proportion of the

nucleus, about 16%, as we previously observed, which is significantly different from the 10% seen in wild types hermaphrodites [39] (Figure 3.5A and B). It is also different from what was seen in a different study analyzing nuclei of young embryos, possibly due to the differences in stage of development and differentiation status [7]. Note that the level of decondensation we observe is greater than what we see in tethering mutants, since 16% of the nucleus is occupied by a single X chromosome, compared to the two Xs in tethering mutant hermaphrodites. However, in *set-25* mutant males, the X did not decondense further compared to normal males (Figure 3.5A and B). In addition, the three-zone assay revealed that the X chromosome is located significantly more centrally in XO hermaphrodites and males, compared to wild type hermaphrodites (Figure 3.5C). Irregularly shaped nuclei that cannot be quantified using this assay also appeared to have large centrally located X chromosomes (Figure 3.14) While in *set-25* mutant males a slightly higher proportion of the X chromosome was located in the central zone, this difference was not statistically significant (Figure 3.5C). These results indicate that the activity of the DCC is required to condense and peripherally relocate the X chromosome, and that the lack of both DCC function and heterochromatic tethers (in *set-25* males) does not lead to additional defects.

We next analyzed the left, middle and right regions of the X chromosome in XO animals (Figure 3.5A, D, and E). All regions of the X chromosome were decondensed in XO animals, compared to hermaphrodites, but mutations in *set-25* did not lead to any further decondensation (Figure 3.5D). Furthermore, the mid-X region was more centrally located in XO animals than in hermaphrodites, but again mutations in *set-25* did not

lead to additional central relocation. While we cannot exclude the possibility that the X chromosome is affected in tethering mutant males, we conclude that hermaphrodite X chromosomes are more severely affected by these mutations than male X chromosomes.

Chromosomal phenotypes are X specific

To determine whether the chromosomal phenotypes are specific to the X chromosome, we analyzed the structure and localization of a similarly sized autosome, chromosome I (Figure 3.6A). Chromosome I occupies about 15% of the nucleus in wild type hermaphrodites, closely correlated with its genome content, indicating lack of condensation beyond genomic average [39]. As we found previously for dosage compensation mutants [39], the volume of chromosome I appeared unaffected in tethering mutants (Figure 3.6B). In addition, the three-zone assay revealed that a significant portion of chromosome I signal is located in the central zone in wild type hermaphrodites (39%) (Figure 3.6C). This value is significantly different from the value obtained for the X chromosome in wild type hermaphrodites (23%, Figure 3.3, $p=0.035$, Student's t-test), and more similar to the X chromosome in tethering mutants (ranging from 43% to 55%, Figure 3.3). In addition, mutations in tethering mutants did not lead to any further central relocation of chromosome I compared to the same chromosome in wild type hermaphrodites (Figure 3.6C). These results suggest that the X chromosome is more sensitive to the loss of heterochromatic tethers than the autosomes.

To confirm these results, we further examined different domains of chromosome I (Figure 3.6D). Chromosome I has two anchored heterochromatic domains, one at each

end (left and right), while the middle region lacks significant interactions with the nuclear lamina [23,26,41]. Our FISH analysis is consistent with these earlier observations. The left and right domains of the chromosome were located near the nuclear periphery, while the middle region was more centrally located. Neither volume measurements (Figure 3.6E), nor the three-zone analysis (Figure 3.6F) showed any significant differences between wild type (N2) and *set-25* mutant hermaphrodites. A significantly greater portion of the chromosome I middle domain was located in the central zone (36%) in wild type hermaphrodites compared to the X chromosome (17%, Figure 3.4, p=0.018, Student's t-test), and this value was more comparable to the centrally located portion of the mid-X region in tethering mutants (ranging from 37% to 51%, Figure 3.4). These results indicate that in wild type hermaphrodites, the two ends of chromosome I are peripherally located, while the middle domain is more centrally located. Furthermore, we conclude that this organization does not change significantly in the absence of heterochromatic tethers, and that the observed chromosomal phenotypes are specific to the dosage compensated X chromosome.

The distribution of H3K9me3 within the nucleus

Previous ChIP-chip analysis showed that H3K9me3 is enriched at both ends of autosomes and at the left end of the X chromosome, although peaks can be found elsewhere on the X as well [41]. To determine how this signal is distributed in the nucleus, we performed immunofluorescence microscopy (IF) with H3K9me3 specific antibodies in wild type cells and in tethering mutants (Figure 3.7). Antibodies specific to DCC subunit CAPG-1 were used as staining control and to mark the territories of the X

chromosomes. Figure 3.15 shows specificity of this newly developed antibody to CAPG-1. In wild type cells, the H3K9me3 signal was distributed all over the nucleus, with no obvious enrichment at the nuclear periphery, except for the presence of some peripherally located bright foci. Both the overall staining and the bright foci are H3K9me3-specific, as they were absent in *set-25* mutants. Sites of exceptionally high levels of H3K9me3 signal were not observed by ChIP [41]. Therefore, we interpret these bright foci as three-dimensional clustering of multiple H3K9me3 enriched loci. The X chromosome territory almost always contained, or was directly juxtaposed to one of these bright foci (Figure 3.7, top row). In rare cases, the X was not associated with the brightest foci, but foci of lesser intensity were still visible in the X territory (Figure 3.7, second row). H3K9me3 staining was comparable to wild type in *cec-4* and *lem-2* mutants, suggesting that the defects in tethering in these mutants are not related to lack of H3K9me3.

Notably, H3K9me3 was not absent in *met-2* mutants. In fact, *met-2* mutants were indistinguishable from wild type. This is in contrast to what was previously observed in *met-2* mutant embryos, where H3K9me3 levels were greatly reduced [23]. However, it is similar to what was observed in the germline, where *met-2* was reported to be dispensable for H3K9me3 [48], and similar to what we reported previously in intestinal nuclei of *met-2* mutants [49]. These results suggest tissue specific differences in the use of HMTs to deposit H3K9me3. Despite near-normal levels and distribution of H3K9me3 in *met-2* mutants, the X chromosomes were decondensed, suggesting that *met-2* contributes to the regulation of X chromosome structure in ways other than H3K9me3.

We also note that *set-32* mutants contained two types of nuclei. Some nuclei were indistinguishable from wild type (Figure 3.7, row 5) and some had reduced levels of H3K9me3 (Figure 3.7, row 6). The two *set-32* mutant nuclei depicted on Figure 3.7 come from the same worm, illustrating cell-to-cell variation within a single animal in this genetic background. These observations suggest that in contrast to what is seen in embryos [23], in differentiated cells, enzymes other than SET-25 contribute to the deposition of H3K9me3.

The DCC remains X-bound and the X chromosomes maintain enrichment for H4K20me1

A possible explanation for the dosage compensation defects in tethering mutants (Figure 3.1) is disruption of DCC localization. To test this possibility we stained worms with X-paint FISH probe followed by immunofluorescence using antibodies specific to the DCC subunit DPY-27. Despite changes in X chromosome morphology, we observed normal localization of the DCC to X chromosomes (Figure 3.8A). While we cannot exclude minor changes in DCC distribution along the X chromosome, we conclude that the DCC does associate with the X chromosomes in tethering mutants.

An alternative explanation for defects in dosage compensation in these mutants is that DCC function is disrupted. Previously characterized molecular functions of the DCC include condensation of the X chromosome [7,39], altering chromosome topology [8], and leading to a different distribution of posttranslational histone modifications, particularly H4K20me1 and H4K16ac [9,10]. To test whether mutations in tethering genes affect the ability of the DCC to lead to enrichment of H4K20me1 on the X, we co-

stained worms with antibodies specific to the DCC (to mark the location of the X) and antibodies specific to H4K20me1. Results showed that this chromatin mark continues to be enriched on the X chromosomes (Figure 3.8B). Therefore, at least some aspects of DCC function remain intact in tethering mutants. Although wild type level of enrichment of H4K20me1 on the X appears to be required for X chromosome condensation [39], our results indicate that it is not sufficient.

Derepression of X-linked genes in tethering mutants

To test how loss of heterochromatic anchoring affects gene expression, we performed mRNA-seq analysis (Figure 3.7). We performed this analysis in L1 stage larval hermaphrodites. By this stage, somatic cells are differentiated, dosage compensation-mediated chromatin marks are fully established [9,50], and gene expression differences resulting from DCC function are easily detectable using RNA-seq [11]. Based on the low level of male rescue observed upon RNAi-depletion of tethering genes (Figure 3.1), we did not expect major disruptions of regulation of X-linked genes. Therefore, to compare gene expression changes in tethering mutants to gene expression changes resulting from moderate changes in DCC function, we generated a data set using L1 hermaphrodite worms in which the DCC subunit DPY-27 was partially depleted by RNAi. Note that even though DPY-27 levels were significantly reduced in these worms (Figure 3.15C), there was very little lethality associated with the RNAi treatment, indicating that DCC function was only partially disrupted.

Under these mild *dpy-27(RNAi)* conditions, we observed a small increase in average X-linked gene expression compared to gene expression changes on

autosomes. These results are qualitatively similar to previously reported analysis of dosage compensation mediated gene expression changes [8,11,12], but the magnitude of change is smaller, indicating that this data is an appropriate representation of gene expression changes when DCC function is partially disrupted. The median $\log_2$ ratio of expression between *dpy-27(RNAi)* worms and control vector RNAi treated worms was significantly higher for expressed genes on the X (0.062) compared to expressed genes on the autosomes (-0.059) (Figure 3.9A, one-sided Wilcoxon rank-sum test $p = 3.09 \times 10^{-78}$), consistent with a small degree of X depression. When the X chromosome was compared to each autosome individually, again we observed a small, but statistically greater level of derepression on the X than any of the autosomes (Figure 3.9A, right). Strains carrying mutations in *cec-4(ok3124)* or *met-2(n4256) set-25(n5021)* showed similar X chromosome derepression compared to *dpy-27(RNAi)*. The median $\log_2$ ratio of expression between *cec-4(ok3124)*/control or *met-2(n4256) set-25(n5021)*/control was significantly higher on the X (0.095 and 0.057 respectively) compared to autosomes (-0.042 and -0.057 respectively) (Figure 3.9B and C, one sided Wilcoxon rank-sum test $p = 8.07 \times 10^{-42}$ and $p = 8.48 \times 10^{-18}$). Comparing the X to each autosome individually again revealed that in both backgrounds the X chromosome is more derepressed than any autosome (Figure 3.9B and C). These results suggest that lack of CEC-4, or MET-2 and SET-25, function leads to similar gene expression changes as a partial depletion of the DCC.

To examine whether the observed differences in gene expression might reflect random variations between average gene expression levels on chromosomes, we

examined the average gene expression change on each autosome compared to the rest of the genome (Figure 3.16). Small gene expression change differences were in fact observed between any autosome and the rest of the genome, and many of these differences were statistically significant (two-sided Wilcoxon rank sum test). However, for chromosomes I, II, III, and IV, the autosome was downregulated, not upregulated, compared to the rest of the genome (Figure 3.16). Chromosome V, the autosome with the most significant gene derepression when analyzed individually (Figure 3.9), was the only autosome that appeared upregulated compared to genomic average (Figure 3.16). However, the X chromosome is more derepressed than chromosome V (Figure 3.9). These analyses indicate that the greatest degree of derepression is seen on the X chromosome. Furthermore, the trends were the same in *dpy-27(RNAi)* and in *cec-4* and *met-2 set-25* mutants, again indicating that gene expression changes in tethering mutants are comparable to gene expression changes in partial DCC depletion conditions.

To complement our analysis of average gene expression, we also looked at genes whose expression changed significantly using DESeq2 analysis (Figure 3.17A). Consistent with previous gene expression studies [22], expression of very few genes changed significantly in *cec-4* mutants. However, the same was true for *dpy-27(RNAi).* In both cases, a slightly higher percentage of X-linked genes were upregulated than the percentage of upregulated autosomal genes, and a slightly higher percentage of X-linked genes were upregulated than downregulated. There were more significantly

derepressed genes in *met-2 set25* mutants, particularly on autosomes, consistent with a more significant silencing role for these genes [22].

To further determine whether there is a correlation between the degree of gene expression change in the tethering mutants and the degree of gene expression change in worms with a partial defect in DCC function, we plotted the $\log_2$ ratio of expression of the tethering mutants and control worms against the $\log_2$ ratio of expression of *dpy-27(RNAi)* and control vector worms (Figure 3.10A and B). With a $\log_2$ cutoff of 0.1 fold (10%) for upregulation, the largest percentage of X-linked genes fell in the quadrant of derepression in both *dpy-27(RNAi)* and tethering mutants (32-34% versus 3-19% on other quadrants), which was not true for autosomal genes. The regression analysis showed a moderate positive correlation between tethering mutants and *dpy-27(RNAi)* $\log_2$ ratios for both X and autosomal genes (R-squared values ranged from 0.36 and 0.49, Pearson correlation values between 0.6 and 0.7) (Figure 3.10D). Additionally, X-linked genes had slightly higher R-squared and Pearson correlation values compared to autosomal linked genes. Correlations of gene expression changes on the X indicate that the genes whose expression is most affected by depletion of the DCC are also the genes whose expression is most affected in tethering mutants. Correlations on autosomes may be explained by the observation that defects in DCC activity are proposed to affect not only X-linked gene expression, but indirectly also contribute to modulating autosomal gene expression [12]. There is a population of genes on autosomes whose expression is repressed by MET-2 and SET-25 independent of DCC-mediated changes (Figure 3.10B, red circle), consistent with a role for these genes in

general gene silencing [22]. A similar degree of correlation was observed when comparing *cec-4* to *met-2 set-25* (Figure 3.10C), and again the correlation was higher for X-linked genes than autosomal genes. A group of genes repressed by MET-2 and SET-25 but not affected by CEC-4 was again evident in this analysis (Figure 3.10C, red circle), as in a previous study [22].

To determine whether gene expression changes correlate with chromosomal changes, we compared $\log_2$ ratios of genes located at X chromosome left, middle, and right regions. Regions were designated based on LEM-2 ChIP-chip signals domains [26]. The region 0 Mb - 4 Mb was designated "left", 4 Mb - 15.75 Mb was designated "middle", and 15.75 Mb - 17 Mb was designated "right". Since the middle region of the X chromosome is subject to the greatest level of decondensation and relocation in tethering and DCC mutants (Figure 3.4), we hypothesized that genes in the middle of the X would be more derepressed compared to the right and left arms. However, when examining the distribution of $\log_2$ ratios in *dpy-27(RNAi)/*control, *cec-4(ok3124)/*control, and *met-2(n4256) set-25(n5021)/*control, the X chromosome regions did not show significant differences by two-sided Wilcoxon rank-sum test (Figure 3.17B, median $\log_2$ ratio between 0.047 and 0.099 and p-values ranged from 0.09 and 0.90). While surprising, these observations are consistent with the model that DCC induced changes in X chromosome structure modulate gene expression chromosome-wide rather than locally [8,11-13].

DISCUSSION

In a screen to identify genes with roles in regulating expression of X-linked genes subject to dosage compensation, we identified a group of genes with previously known roles in anchoring heterochromatic domains to the nuclear lamina. These genes include H3K9 HMTs, the chromodomain protein CEC-4 which binds H3K9 methylated chromatin, and the nuclear lamina protein LEM-2. Although H3K9me and nuclear lamina interactions are enriched at the left of the X chromosome, we find that these mutations disproportionately affect compaction and subnuclear localization of the gene-rich middle portion of the X chromosome. We propose the following model: (1) heterochromatic anchors at the left end of the X nucleate a compact chromatin structure, and (2) the activity of the DCC ensures that this structural organization encompasses the entire chromosome (Figure 3.11). Compartmentalization of the nucleus in this way may restrict availability of transcriptional activators for the X chromosomes, thus creating a repressive compartment to modulate X-linked gene expression.

Correlation between compaction, subnuclear localization and gene expression

Chromatin compaction and subnuclear localization are believed to be coordinated with gene expression levels to a certain degree [14-16]. We analyzed chromatin condensation, subnuclear localization, and gene expression changes in DCC-depleted animals and in tethering mutants. We observed elevated levels of X-linked gene expression (Figure 3.9), decreased compaction (Figure 3.2 and Figure 3.4), and relocation to a more central position (Figures 3.3-3.5), in both DCC mutants and tethering mutants, providing support for the hypothesis that these processes are

coordinated. However, the correlation is not perfect. The degree of gene expression change did not correlate well with the degree of decondensation and/or subnuclear relocation. At the whole chromosome level, the X chromosomes in tethering mutants decondensed to a degree comparable to DCC mutants (Figure 3.2). Similarly, the degree of relocation was greater in tethering mutants than in partial loss-of-function DCC mutant, and comparable to the XO animals that completely lack DCC function (Figure 3.3 and Figure 3.5). However, gene expression changes in tethering mutants are much less significant than in DCC mutants (Figure 3.9). Similar conclusions were reached when we analyzed different regions of the X chromosome: relocation and decondensation was most significant in the middle of the X chromosome in both DCC mutants and tethering mutants (Figure 3.4), but gene expression changes were comparable in all regions of the chromosome (Figure 3.17). A higher resolution study may reveal a stronger correlation, but at the level of whole chromosomes, or large chromosomal domains, the correlation between gene expression change, chromosome decondensation and subnuclear localization is limited. A recent study showed that chromatin decondensation, even in the absence of transcriptional activation, is sufficient to drive nuclear reorganization [51]. Similarly, in *cec-4* mutants, decondensation of transgenic arrays is coupled to their relocation within the nucleus, but it is accompanied by only minimal changes in gene expression [22]. This is reminiscent of our results, where chromatin decondensation and relocation in general correlate, but the degree of condensation does not reflect the degree of gene expression change.

We believe these results reflect the fact that repression by the DCC involves multiple mechanisms, and disruption of condensation and subnuclear localization is not sufficient to cause major changes in gene expression. Other DCC-mediated changes, for example enrichment of H4K20me1 on the X chromosome, are intact in tethering mutants (Figure 3.8), and are sufficient to maintain repression. However, it should be emphasized that loss of tethers (and/or the accompanying change in X chromosome packaging and nuclear organization) does result in gene expression changes that are biologically significant. While the gene expression change is modest (Figure 3.9), it is sufficient to rescue a significant proportion of males in our genetic assay (Figure 3.1 and Figure 3.12). Thus, chromatin condensation, subnuclear localization, and tethering to the nuclear periphery, may not be the primary determinants of gene expression change, or may act redundantly with other, yet unidentified, factors, but they do contribute to stabilizing gene expression programs in development [22] and during dosage compensation (this study).

Our results also reveal parallels with recent genome-wide chromosome conformation capture (Hi-C) analysis [8]. Dosage compensated X chromosomes are packaged into a structure with regularly spaced boundaries between topologically associated domains (TADs). In the absence of the DCC, boundaries become less well defined and TAD organization weakens, except at the left end of the X, which is the domain that is tethered to the nuclear lamina [8]. This parallels our observations that in DCC mutants the left end of the X chromosome remains less affected than the rest of the chromosome. Condensin has been implicated previously in chromosome territory

organization [39,52,53]. In condensin mutant fission yeast, disruption of condensin-dependent intrachromosomal interactions disturb chromosome territory organization [54]. Changes in condensin-mediated interactions and chromosome territory formation are also coordinated during different stages of the cell cycle [54]. It is likely that the observed changes in TAD formation [8] and chromosome compaction and subnuclear localization (Figures 3.2-3.5, [39]) in the absence of the condensin-like DCC similarly reflect the same underlying changes in chromosome structure analyzed at different resolutions and using different methods.

If TAD formation, chromatin condensation, and subnuclear localization indeed correlate, our results would predict that TADs at the left of the X chromosome would also be less disrupted in tethering mutants than along the rest of the X chromosome. These results and predictions would suggest that nuclear lamina anchors (both the anchors mediated by H3K9me3 and the yet uncharacterized anchors) are able to impose this level of organization (TAD formation) on the tethered portion of the chromosome. The DCC, in the presence of heterochromatic anchors, propagates this structure to the rest of the X chromosome (Figure 3.11). Autosomes in general lack regularly spaced TADs, except at the tethered ends of chromosome arms [8]. This observation is consistent with our observations of peripherally located chromosome I arms (Figure 3.6), and our suggestion that nuclear lamina anchors are sufficient to form regularly spaced TADs. However, since the DCC does not bind autosomes, TAD formation is not propagated to the rest of the chromosome.

Tethering to the nuclear lamina affects subnuclear localization, chromatin compaction and expression levels of endogenous genes chromosome-wide

Previous studies described the roles of lamin and lamin-associated proteins, MET-2, SET-25, and CEC-4 in anchoring heterochromatic transgene arrays to the nuclear lamina accompanied by various effects on silencing [21-23]. The loss of the sole lamin protein in *C. elegans*, LMN-1, or the combination of LEM-2 and emerin (*emr-1*) RNAi leads to transgenic array derepression and relocation [21]. MET-2 and SET-25 are redundantly required for both anchoring and transgene silencing, while CEC-4 is required for anchoring without an effect on silencing [22,23]. This same set of genes was identified in our study as influencing subnuclear localization, compaction, and gene expression of the X chromosome. There are some differences between how these genes affect silent transgene arrays compared to the X chromosome.

While MET-2 and SET-25 act redundantly on arrays, for the X chromosome their functions are not redundant. The effects on X compaction and subnuclear localization were indistinguishable in *met-2* or *set-25* single mutants, or *met-2 set-25* double mutants (Figure 3.2 and Figure 3.3). It was proposed that for transgenic array anchoring the residual amounts of H3K9me3 in *met-2* mutants and the normal levels H3K9me2 in *set-25* mutants are sufficient [23]. This is consistent with the observation that CEC-4 is able to bind all methylated forms of H3K9 [22]. These marks may be sufficient in the context of repetitive transgene arrays that accumulate a significantly higher density of H3K9 methylation than endogenous genomic regions, but may be insufficient for normal nuclear lamina association of the X chromosome.

CEC-4 activity is required for anchoring of transgenes to the nuclear lamina without an effect on silencing [22]. When examining effects on transcription of endogenous genes, minimal changes were observed in *cec-4* mutants, while a large number of genes were upregulated greater than four-fold in *met-2 set-25* [22]. This difference between *cec-4* and *met-2 set-25* is also apparent in our data sets (Figure 3.10). There is a group of genes repressed by MET-2 and SET-25, in a manner independent of DCC function. However, a similarly regulated group of genes was not apparent in *cec-4* mutants (Figure 3.10), consistent with CEC-4 having a less significant effect on gene silencing [22]. By contrast, the influence of CEC-4 on X-linked gene activity is comparable to the influence of MET-2 and SET-25 (Figure 3.10B and C). One possible interpretation of this result is that the changes in X-linked gene expression levels reflect the consequences of the similar chromosome-wide structural changes in the various mutants rather than direct repression by CEC-4 or H3K9 methylation.

Previous studies showed that mutations in tethering genes mainly affect the autosomes, leading to the loss of lamina association of chromosome arms, as assayed by LMN-1-DamID or LEM-2 ChIP. Changes on the X chromosome are less significant using these assays [22,23]. By contrast, our data argues that this loss of nuclear lamina interactions disproportionately leads to changes in compaction and subnuclear localization of the X chromosome (Figure 3.2 and Figure 3.3) compared to autosomes (Figure 3.6). It should be noted that the DamID and ChIP studies were performed in embryos, while our analysis was performed in fully differentiated cells of adults--a point in development where multiple, perhaps partially redundant, anchors may be present

[22,23]. It is also possible that the X chromosomes, which have fewer lamina interactions than the autosomes [26], are more sensitive to the loss of anchors. However, we favor the interpretation that heterochromatic tethers and the DCC cooperate to build the specialized structure of dosage compensated X chromosomes (Figure 3.11). While H3K9me3-mediated anchors are not required for maintaining anchoring of the left end of the X, these anchors may be required for the DCC to be able to propagate chromosome packaging to the rest of the chromosome. Since the DCC does not bind autosomes, their conformation is not sensitive to loss of this interaction between the anchors and the DCC. Although low resolution, our FISH analysis supports this hypothesis. The X chromosomes appear compact and in a well-defined peripheral territory only when tethered and DCC-bound. In both DCC and tethering mutants, the X paint signal becomes more diffuse with less well-defined borders (Figure 3.2, [39]). Chromosome I paint signals in wild type worms are more comparable to X paint signals in DCC mutants or tethering mutants than to X paint signals in wild type (Figure 3.6). Furthermore, the ends of chromosome I are anchored to the nuclear periphery, and remain anchored in tethering mutants, while the middle domain is more centrally located even in wild type worms, reminiscent of the organization of X chromosome in tethering mutants and in males (Figure 3.6, [39]). Overall, these observations suggest that the DCC and heterochromatic anchors work together to compact and peripherally relocate the middle domain of the X chromosomes not directly tethered to the nuclear periphery.

It is interesting to note that we observe significant chromosome decondensation despite normal DCC binding to the chromosome (Figure 3.8). Current models of DCC

binding to the X include a recruitment step to *rex* sites [12,55,56], which have very high levels of DCC binding [12,57], and tend to define TAD boundaries [8]. From these *rex* sites to DCC spreads to *dox* sites enriched at promoter regions [12,57]. From our low-resolution immunofluorescence analysis, DCC binding seems unaffected in tethering mutants. Yet, despite near normal levels of DCC, the X chromosome is not compacted, indicating that DCC function appears to be compromised.

Changes in nuclear organization during cellular differentiation and development

The mechanisms of anchoring appear to be different in embryonic cells compared to differentiated cells. Repetitive heterochromatic arrays require H3K9 methylation and CEC-4 for peripheral localization in embryonic cells but not in differentiated cells, suggesting that differentiated cells have other mechanisms in place for tethering genomic regions to the nuclear envelope [22,23]. Whether heterochromatin and CEC-4 mediated anchors continue to function in differentiated cells remained unclear [22], yet our results are consistent with this possibility. The left end of the X chromosome remains in the vicinity of the nuclear lamina in the absence of H3K9me3, LEM-2, or CEC-4 in fully differentiated cells, suggesting the existence of additional anchors (Figure 3.4). However, X chromosome morphology does change in the absence of these proteins, indicating that tethers mediated by them continue to influence chromosome structure in differentiated cells.

Our results are reminiscent of the findings in differentiating mouse cells [58]. In early development, lamin B receptor (*Lbr*) is the predominant mediator of interactions with the nuclear lamina. Later in development, lamin-A/C-dependent tethers appear,

sometimes accompanied by the loss of *Lbr*-mediated mechanisms. Loss of peripheral localization of heterochromatin is only observed when both types of tethers are absent [58]. It will be interesting to uncover the nature of the additional anchors in differentiated *C. elegans* tissues and how these anchors affect X chromosome morphology and dosage compensation. However, it is possible that the additional anchors will be cell-type specific, consistent with the observation in mammalian cells where various tissue-specific transmembrane proteins are used to anchor genomic regions to the nuclear lamina [59]. Tissue-specific differences between anchoring mechanisms are also consistent with observations that point mutations in lamin can exhibit tissue-specific defects in humans [60] as in *C. elegans* [21].

Summary

In a screen for genes that promote dosage compensation in *C. elegans*, we identified a group of genes implicated in anchoring heterochromatin to the nuclear lamina. When these genes are not functional, the X chromosome decondenses and moves away from the nuclear periphery. Decondensation and subnuclear relocation mostly affects the gene-rich middle portion of the X chromosome, while the tethered left end is less affected. We propose that the DCC uses these heterochromatic anchors to condense and position the X chromosome near the nuclear periphery. Moving the X chromosome into this peripheral compartment contributes to lowering X-linked gene expression levels. Establishment of this nuclear compartment as a way to regulate the X chromosome is consistent with previous observations [8, 12, 13] and our results (this

study), which found no correlation between DCC binding, DCC induced chromosomal changes, and repression of gene expression.

MATERIALS AND METHODS

C. elegans strains

Strains were maintained as described [61]. Strains include: N2 Bristol strain (wild type); MT16973 *met-1(n4337)* I; VC967 *set-32(ok1457)* I; VC1317 *lem-2(ok1807)* II; MT13293 *met-2(n4256)* III; PFR40 *hpl-2(tm1489)* III; MT17463 *set-25(n5021)* III; EKM104 *set-25(n5021)* III; *him-8(mn253)* IV; EKM99 *met-2(n4256) set-25(n5021)* III; RB2301 *cec-4(ok3124)* IV; TY4403 *him-8(e1489)* IV; *xol-1(y9) sex-1(y263)* X; TY1072 *her-1(e1520)* V; *sdc-2(y74*) X; EKM71 *dpy-21(e428)* V; RB1640 *set-20(ok2022)* X; VC2683 *set-6(ok2195)* X; PFR60 *hpl-1(tm1624)* X. Males were obtained from strains that carry a mutation in *him-8*, a gene required for the segregation of the X chromosome in meiosis, mutations in which lead to high incidence of males, but do not affect the soma. All strains were fed OP50 and grown at 15°C to avoid temperature sensitive sterility associated with some mutations in some the strains.

RNA Interference (RNAi)

E. coli HT115 bacteria cells carrying plasmids that express double stranded RNAi corresponding to the gene of interest, were grown from a single colony for 8-10 hours at 37°C and 125 mL were plated onto NGM plates supplemented with IPTG (02% w/v) and Ampicillin (1ug/ml) and allowed to dry overnight. For imaging experiments, worms were grown on RNAi plates for two generations at 15°C as follows: L1 worms were placed on a plate and allowed feed until they reached L4 stage whereby 2-3 L4 worms were

moved to a new plate and allowed to lay eggs for 24 hours. F1 worms were grown to 24 hours post L4 for fixation. The male rescue RNAi screen was described in detail in [35]. Briefly, *him-8(e1489)IV; xol-1(y9) sex-1(y263)X* worms were treated with RNAi as before. For results shown on Figure 3.1, L4 worms from the P0 generation were allowed to lay eggs for 24hr at 20°C, the parents were removed, and embryos were counted. For results shown on Figure 3.12, P0 worms were fed RNAi food for an additional day, until they reached young adult stage before egg collection began. Worms were grown at 20°C and males were counted and removed for 2-4 days after eggs were laid. Male rescue was calculated by dividing the number of observed males by the number of expected males. The *him-8(e1489)IV* strain consistently yields 38% male progeny so the expected number of males was assumed to be 38% of the embryos laid. Male rescue was calculated as: (Observed number of males)/(0.38 x number of eggs laid).

Antibodies

The following antibodies were used: rabbit anti-H3K9me3 (Active Motif #39766), rabbit anti-H4K20me1 (Abcam ab9051), rabbit anti-DPY-27 [4], rabbit anti-beta tubulin (Novus NB600-936). Anti-CAPG-1 antibodies were raised in goat using the same epitope as in [4]. Secondary anti-rabbit and anti-goat antibodies were purchased from Jackson Immunoresearch.

Immunofluorescence

Immunofluorescence experiments were performed as described [4]. Young adult worms were dissected in 1X sperm salts (50 mM Pipes pH 7, 25 mM KCl, 1 mM $MgSO_4$, 45 mM NaCl and 2 mM $CaCl_2$, supplemented with 1 mM levamisole), fixed in

2% paraformaldehyde in 1X sperm salts for 5 minutes and frozen on dry-ice for 10 minutes. For anti-H4K20me1 and anti-CAPG-1 staining, worms were in 1% PFA. After fixation, slides were frozen on a dry ice block for 20-30 minutes, washed three times in PBS with 0.1% Triton X-100 (PBST) before incubation with diluted primary antibodies in a humid chamber, overnight at room temperature. Slides were then washed three times with PBST, incubated for 4 hours with diluted secondary antibody at room temperature, washed again twice for 10 minutes each with PBST, and once for 10 minutes with PBST plus DAPI. Slides were mounted with Vectashield (Vector Labs). Antibodies were used at the following concentrations: CAPG-1, 1:1000; DPY-27, 1:100; H4K20me1, 1:200; H3K9me3, 1:500.

Fluorescence *In Situ* Hybridization (FISH)

Slides were prepared as for immunofluorescence through the PBST washes following fixation. Slides were then dehydrated with sequential 2 minute washes in 70%, 80%, 95% and 100% ethanol before being allowed to air dry for 5 minutes at room temperature. Full X-paint probe and chromosome I paint probe preparation was described in detail in [39, 62]. The X-left probe contained DNA amplified from the following YACs: Y35H6, Y47C4, Y51E2, Y02A12, Y105G12, Y97B8, Y76F7, Y40,H5, Y43D5, Y18F11, Y89H11 (covers the region from 0.1Mb to 4.2 Mb of the chromosome). The X-mid probe contained DNA amplified from the following YACs: Y18C11, Y50C2, Y70G9, Y44D2, Y102D2, Y97D4, Y97D9 (covers the region from 7.4Mb to 11.0 Mb). The X-right probe contained DNA amplified from the following YACs: Y31A8, Y52C11, Y42D5, Y53A6, Y7A5, Y46E1, Y50B3, Y25B5, Y43F3, Y52F1, Y68A3 (covers the

region from 14.0 Mb to 17.6 Mb of the chromosome). The Chromosome I left probe was made from the following YACs: Y73F10, Y50C1, Y65B4, Y18H1, Y73A3, Y34D9, Y48G8, Y52D1, Y71G12, Y102E12, Y71F9, Y115A10, Y44E3, Y74A12, Y74A11, Y39E12, Y40G6, Y110A7 (covers the region from the 0.2 - 4.6 Mb of the chromosome); chromosome I middle probe was made from the following YACs: Y70C6, Y46D1, Y54B12, Y101C10, Y39A9, Y53F1, Y97F9, Y97D1, Y97E2, Y43C3, Y43E2, Y49G9, Y102E5, Y106G6 (covering the region from 4.6 Mb - 10.1 Mb); the chromosome I right probe was made form the following YACs: Y71B8, Y19G12, Y37F4, Y95D11, Y53A2, Y47H9, Y47H10, Y45E10, Y91F4, Y50A7, Y43D10, Y40B1, Y63D3, Y112D2, Y54E5 (covering the region fro 10.1 - 15.07 Mb). 10 microliters of probe was added to each slide, covered with a coverslip and placed on a 95°C heat block for 5 minutes. The heat block was then cooled to 37°C slowly and the slides were moved to a 37°C incubator in a humid chamber and incubated overnight. Slides were washed as follows: 3 washes of 2X SSC/50% formamide for 5 minutes each; 3 washes of 2X SSC for 5 minutes each; 1 wash of 1X SSC for 10 minutes. All washes were performed in a 39°C water bath. Finally, the slides were washed once with PBST containing DAPI for 10 minutes at room temperature before mounting with Vectashield.

Quantification

Volume Quantification: Chromosome volumes were quantified as in [6]. Briefly, using the Mask: Segment function of Slidebook, a user-defined threshold is determined that separates signal from background and auto-fluorescence. The same level of background was used for all nuclei based on observed background. Masks were

calculated for each channel with DAPI being the primary mask and the X paint being the secondary mask. Nuclear volume was calculated by taking the number of voxels (volumetric pixels) for the DAPI channel to determine total DNA content (morphology: volume (voxels)). The overlapping voxels between the X and the DAPI was determined by using a cross mask of the DAPI and X paint signals (cross mask: mask overlaps) in Slidebook. The percent nuclear volume occupied by the X was determined by dividing the number of X voxels by the total number of DAPI voxels.

Three-zone assay quantification: Concentric ovals of equal area were drawn over one focal plane from the center of the Z stack that contained the largest amount of X FISH signal. Masks were made from each of these zones using the Advanced operations > Convert regions to mask objects function in Slidebook. A single plane from the X chromosome mask set for volume quantification was used here. The amount of X signal in each of the zones was calculated using the cross mask: mask overlap function in Slidebook where the zone mask was the primary mask and the X mask was the secondary mask. The total voxels for all three zones were summed and the voxels in each zone were divided by the total to determine what percentage of the X signal was located in each zone.

mRNA-seq

Worms were synchronized by bleaching gravid adults to isolate embryos and allowing worms to hatch overnight. Newly hatched L1 larval worms were plated and grown for 3 hours on NGM plates with OP50. To the worm pellet, ten volumes of Trizol were added and RNA was extracted and precipitated using the manufacturer's

instructions. Total RNA was cleaned using the Qiagen RNeasy kit. Non-stranded mRNA-seq libraries were prepared using TruSeq RNA Library Preparation Kit. Single-end 50-bp sequencing was performed using Illumina HiSeq-2000. Reads were trimmed for quality using the TrimGalore program from Babraham Bioinformatics (http://www.bioinformatics.babraham.ac.uk/projects/ trim_galore/) and aligned to the *C. elegans* genome version WS235 with Tophat v 2.0.13. Default parameters allow up to 20 hits for each read. Gene expression was quantified using Cufflinks v2.2.1 with use of "rescue method" for multi-reads and supplying gene annotation for WS235. Gene count estimation was performed using HTSeq-count tool v0.6.0 in the default "union" mode. Differential expression analysis was performed using DESeq2 v1.6.3 in R version 3.2.3. All analyses were performed which genes that had average expression level above 1 RPKM (fragments per kilobase per million, as calculated by Cufflinks).

Western blot

From the worm suspension collected for RNA-seq experiments, 50 mL of L1s were used for protein analysis. For CAPG-1 antibody validation, 50 mL of mixed stage worms were used. Equal volume of sample buffer was added (0.1 M Tris pH 6.8, 7.5 M urea, 2% SDS, 100mM b-ME, 0.05% bromophenol blue), the suspension was heated to 65°C for 10 minutes, sonicated for 30-seconds twice, heated to 65°C for 5 minutes, 95°C for 5 minutes, then kept at 37°C until loading onto SDS-PAGE gel. Proteins were transferred to nitrocellulose and probed with the appropriate antibodies.

ACKNOWLEDGEMENTS

We thank Nicholas Streicher and Stephanie Campbell who initiated analysis of histone methyltransferases and LEM-2 as part of their undergraduate research project. We also thank Jessica Trombley for assistance with worm counts in the RNAi screen.

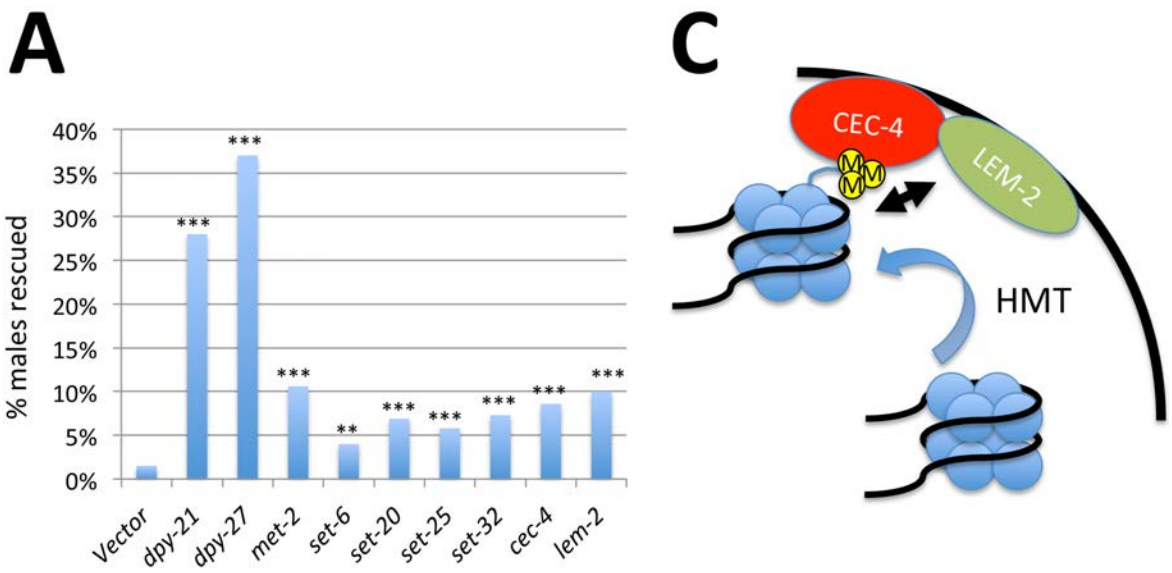

B

			OBSERVED		EXPECTED	
RNAi	n	total males	live males	dead	live males	dead
Vector	2165	822	12	810	12	810
dpy-21	503	191	54	137	3	188
dpy-27	1248	474	175	299	7	467
met-2	1657	629	67	562	9	620
set-32	1229	467	34	433	7	460
set-20	836	317	22	295	5	312
set-6	801	304	12	292	5	299
set-25	1575	599	35	564	9	590
cec-4	1814	689	59	630	10	679
lem-2	1072	407	41	366	6	401

Figure 3.1 RNAi screen to identify genes that promote dosage compensation. (A) Male rescue assay. RNAi-mediated depletion of the indicated genes in the *him-8 xol-1 sex-1* background led to rescue of the indicated percentage of males. Depleting DCC components DPY-21 and DPY-27 rescues a larger percentage of males than depletion of the other genes identified in this screen Asterisks indicate statistical significance based on Chi square test analysis of results, with expected rescue being equivalent to vector RNAi. * = $p<0.05$, ** = $p<0.01$, *** = $p<0.001$. (B) Raw data and expected table used in Chi square analysis. (C) Proposed mechanism of anchoring heterochromatic regions to the nuclear lamina. HMTs methylate H3K9. The chromodomain protein CEC-4 binds to this chromatin mark. Bound genomic regions are enriched for interaction with the nuclear lamina protein LEM-2.

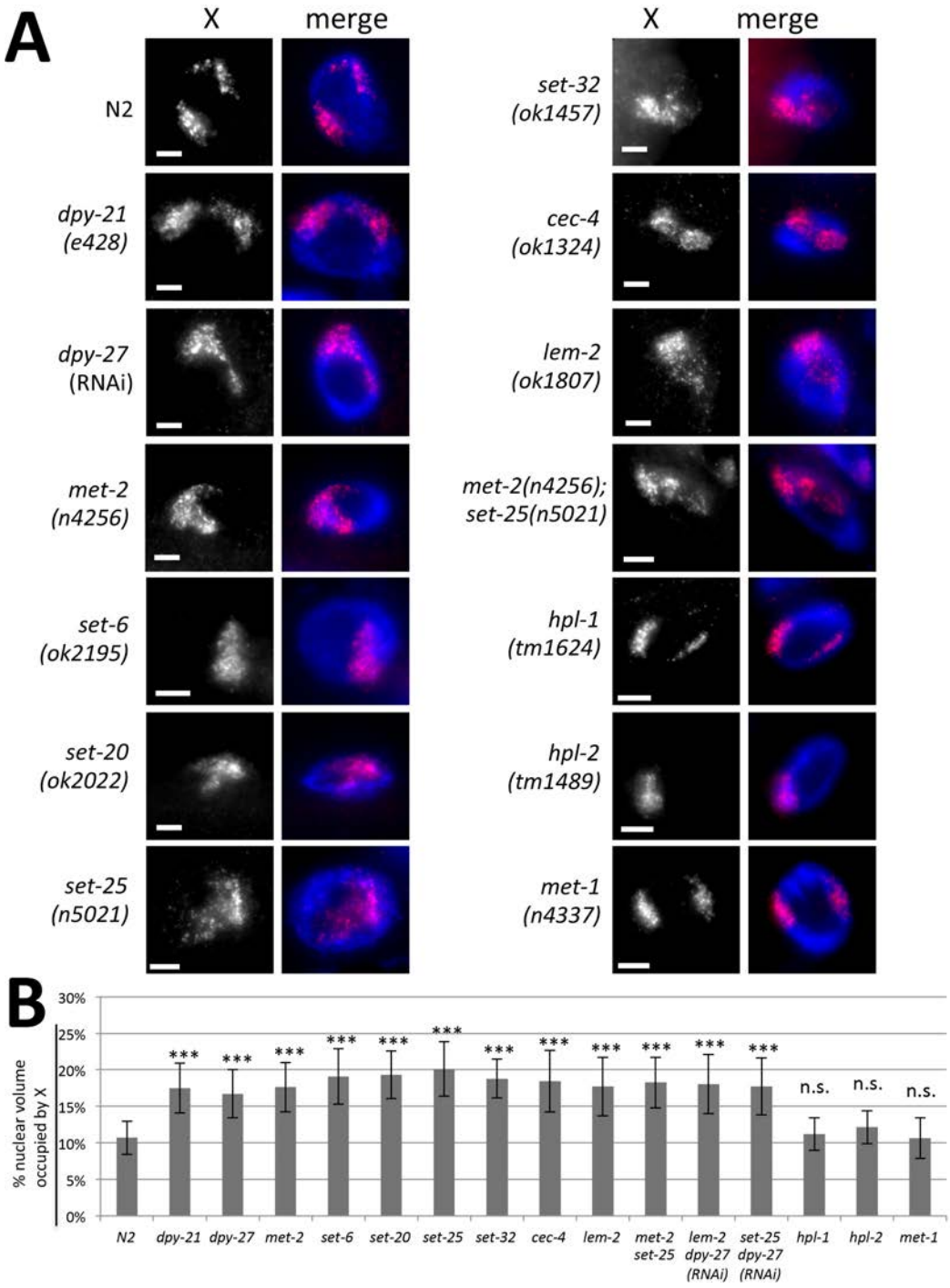

Figure 3.2 X chromosome decondensation in mutants. (A) X chromosome paint FISH (red) in representative images of intestinal nuclei (DAPI, blue) of hermaphrodite adult worms in each genotype. The X chromosomes are compact and peripherally localized in wild type (N2), *hpl-1*, *hpl-2* and *met-1* mutant hermaphrodites, but are decondensed and more centrally located in the other mutants. Scale bar, 5 mm. (B) Quantification of X chromosome volumes normalized to nuclear size (n=20 nuclei). Error bars indicate standard deviation. n.s. = $p>0.05$ not significant, *** = $p<0.001$ by Student's t-test (N2 compared to appropriate mutant).

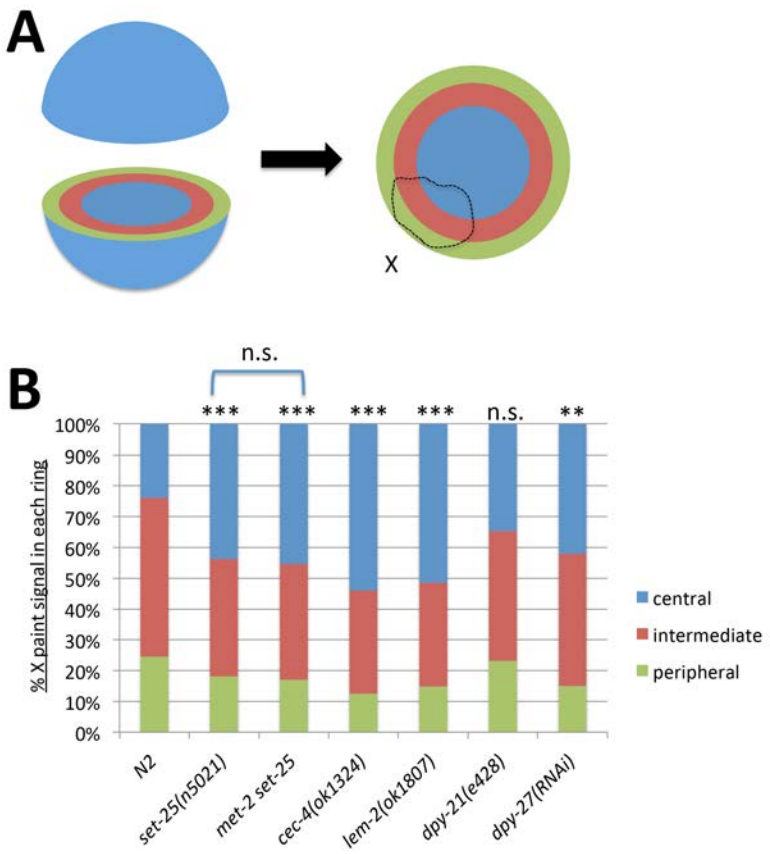

Figure 3.3 The X chromosome relocates centrally in the nucleus. (A) A diagram of the three-zone assay. An optical section from the middle of the nucleus was divided into three concentric rings of equal area. The proportion of the X chromosome paint signal in each zone (peripheral-intermediate-central) was quantified. (B) Results of quantification of the three-zone assay using whole X paint FISH probes in hermaphrodite intestinal nuclei (n=10). In tethering mutants, a larger portion of the X chromosome is located in the central zone compared to wild type hermaphrodites. Relocation to a central region is less significant in DCC mutants or DCC-depleted hermaphrodites. Asterisks indicate statistical analysis (Student's t-test) of the centrally located portion of the X chromosome (shown in blue). n.s. = $p>0.05$, * = $p<0.05$, ** = $p<0.01$, *** = $p<0.001$. See Table 3.1 for statistical data.

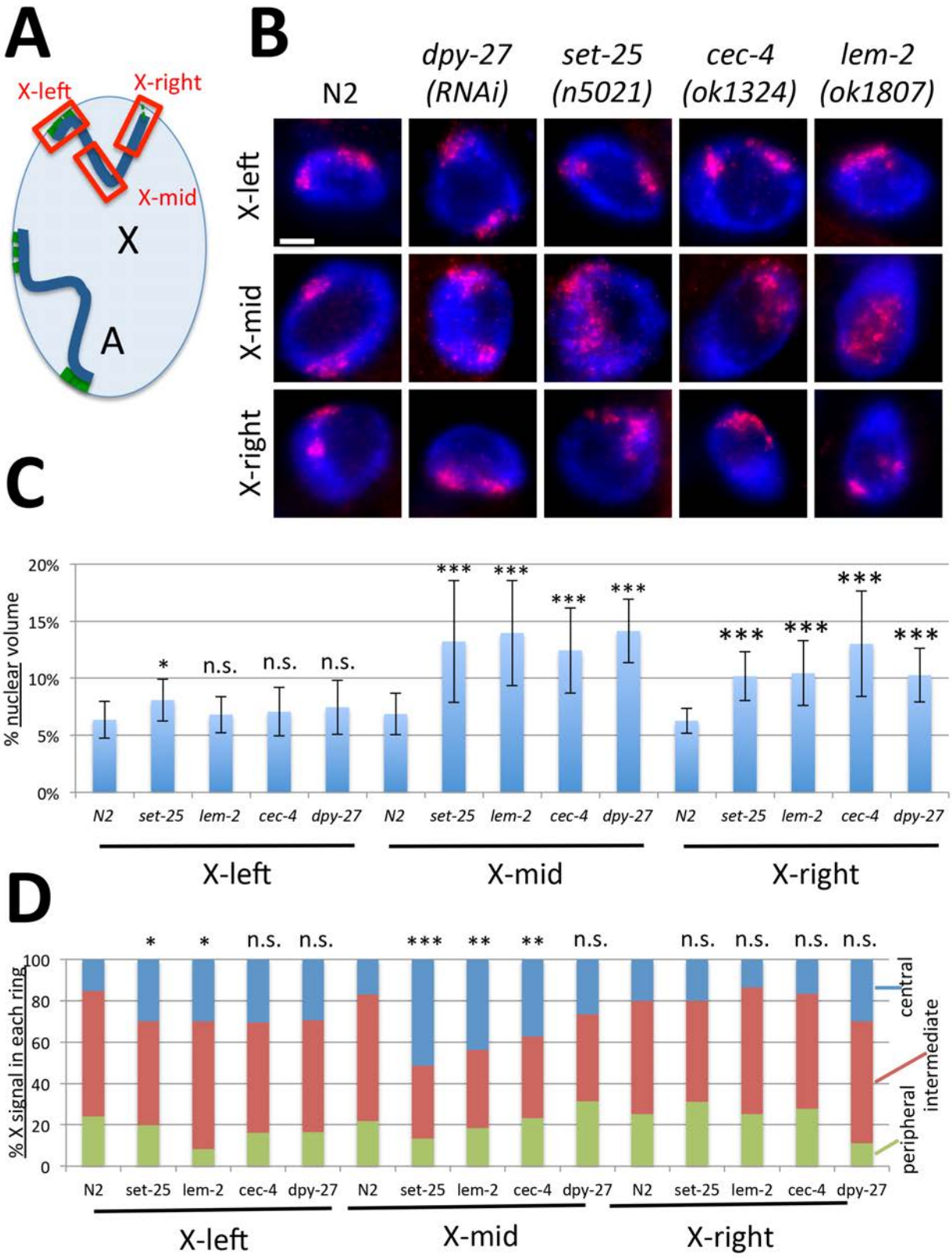
A
X-left
X-right
X-mid
X
A
B
N2
dpy-27 (RNAi)
set-25 (n5021)
cec-4 (ok1324)
lem-2 (ok1807)
X-left
X-mid
X-right
C
% nuclear volume
20%
15%
10%
5%
0%
*
n.s.
n.s.
n.s.
***
***
***
***
***
***
***
***
N2
set-25
lem-2
cec-4
dpy-27
X-left
X-mid
X-right
D
% X signal in each ring
100
80
60
40
20
0
*
*
n.s.
n.s.
***
**
**
n.s.
n.s.
n.s.
n.s.
n.s.
central
intermediate
peripheral
N2
set-25
lem-2
cec-4
dpy-27
X-left
X-mid
X-right

Figure 3.4 The middle region of the X chromosome is most affected in the absence of heterochromatic tethers. (A) Autosomes are anchored to the nuclear lamina at both chromosome arms (anchors shown in green), while the X chromosome only has a significant anchored domain at the left end. Probes used in FISH analysis are indicated in red. Each probe covered an approximately 3-4 Mb genomic region. (B) Representative images of X-left, X-mid, X-right FISH analysis in each genotype. The mid-X region appears most decondensed and most centrally located in mutants. Scale bar, 5 mm. (C) Quantification of volumes occupied by the indicated FISH probes, normalized to nuclear size (n=12 nuclei). Error bars indicate standard deviation. The greatest degree of decondensation in mutants is observed for the mid-X probe. (D) Three zone assay for each probe (n=12 nuclei). The greatest degree of central relocation is observed for the mid-X probe. Asterisks indicate statistical analysis of mutant to wild type comparisons of volumes in (C) and centrally located portion of the X in (D) using Student's t-test. n.s. = $p>0.05$, * = $p<0.05$, ** = $p<0.01$, *** = $p<0.001$. See Table 3.1 for statistical data.

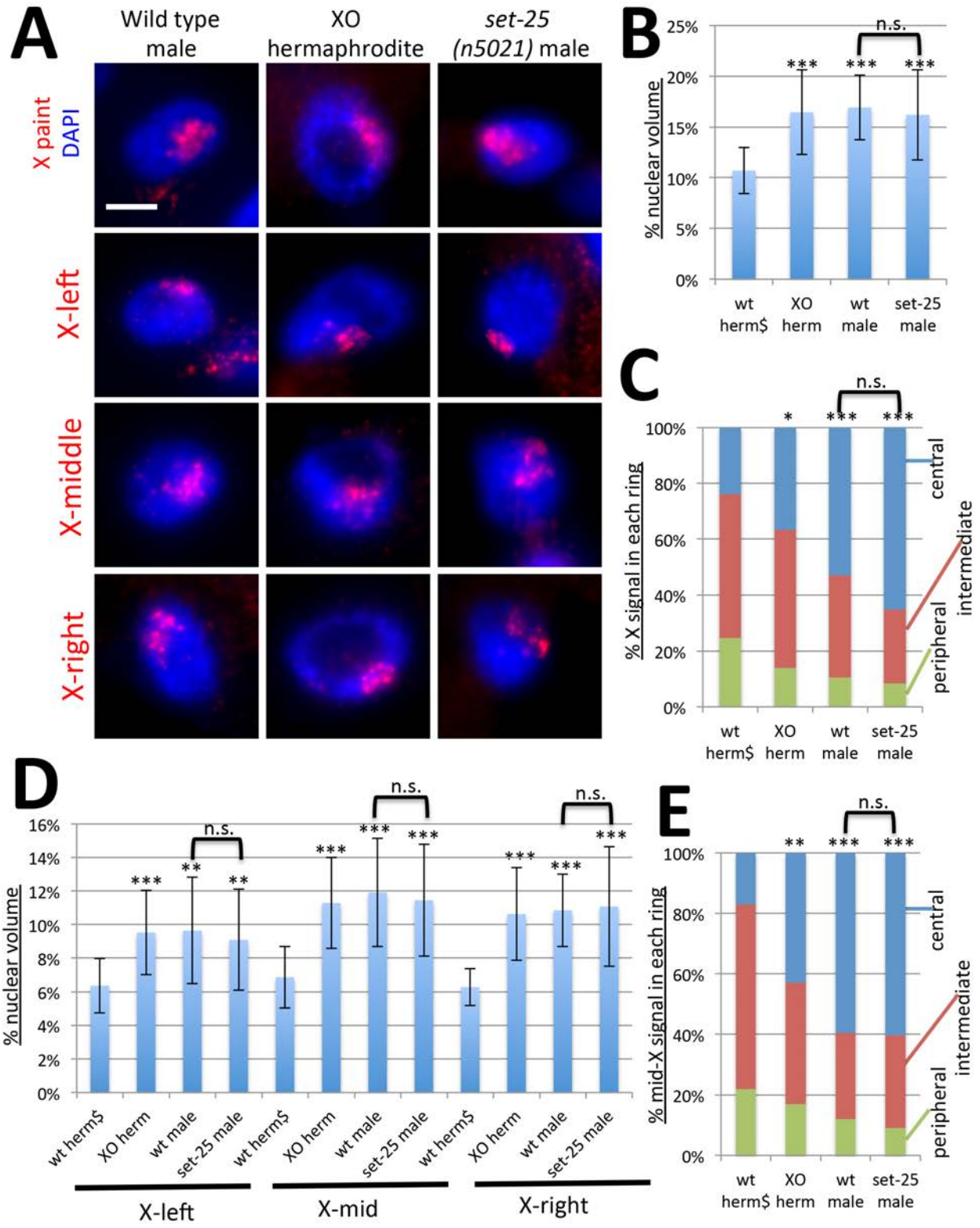
A
Wild type male
XO hermaphrodite
set-25 (n5021) male
X paint
DAPI
X-left
X-middle
X-right
B
% nuclear volume
25%
20%
15%
10%
5%
0%
n.s.
***
***
***
wt herm$
XO herm
wt male
set-25 male
C
% X signal in each ring
100%
80%
60%
40%
20%
0%
n.s.
*
***
***
central
intermediate
peripheral
wt herm$
XO herm
wt male
set-25 male
D
% nuclear volume
16%
14%
12%
10%
8%
6%
4%
2%
0%
n.s.
n.s.
***
**
**
***
***
***
***
***
***
wt herm$
XO herm
wt male
set-25 male
X-left
X-mid
X-right
E
% mid-X signal in each ring
100%
80%
60%
40%
20%
0%
n.s.
**
***
***
central
intermediate
peripheral
wt herm$
XO herm
wt male
set-25 male

Figure 3.5 The X chromosome is decondensed and centrally located in the absence of dosage compensation in XO animals. (A) Chromosome paint FISH (red) in intestinal nuclei (DAPI, blue) of male adult worms, XO hermaphrodites and *set-25* mutant males using whole X paint probe, and probes to the left, middle, and right domains of the X chromosome. The X chromosome, and the middle region of the X chromosome, appear large and diffuse and are located more toward the nuclear interior. *set-25* mutations do not have additional effects on X chromosome morphology in males. Scale bar, 5 mm. (B) Quantification of volumes occupied by the X paint probe (n=20 nuclei). The N2 hermaphrodite data point (wt herm) is repeated from Figure 3.2B and is marked by $ sign. (C) Three-zone assay for the whole chromosome X paint probe (n=10). Wt herm$ data point is repeated from Figure 3.3B. (D) Quantification of volumes occupied by the X-left, X-mid, and X-right probes normalized to nuclear size (n=20). Wt herm$ data points are repeated from Figure 3.4C. (E) Three zone assay for the mid-X probe (n=10). wt herm$ data point is repeated from Figure 3.4D. Error bars in (B) and (D) indicate standard deviation. Asterisks indicate statistical analysis compared to wild type hermaphrodites for volumes in (B) and (D) and centrally located portion of the X or mid-X (C) and (E), using Student's t-test. wt male and *set-25* male comparisons are also shown as indicated. n.s. = $p>0.05$, * = $p<0.05$, ** =$p<0.01$, *** = $p<0.001$. See Table 3.1 for statistical data.

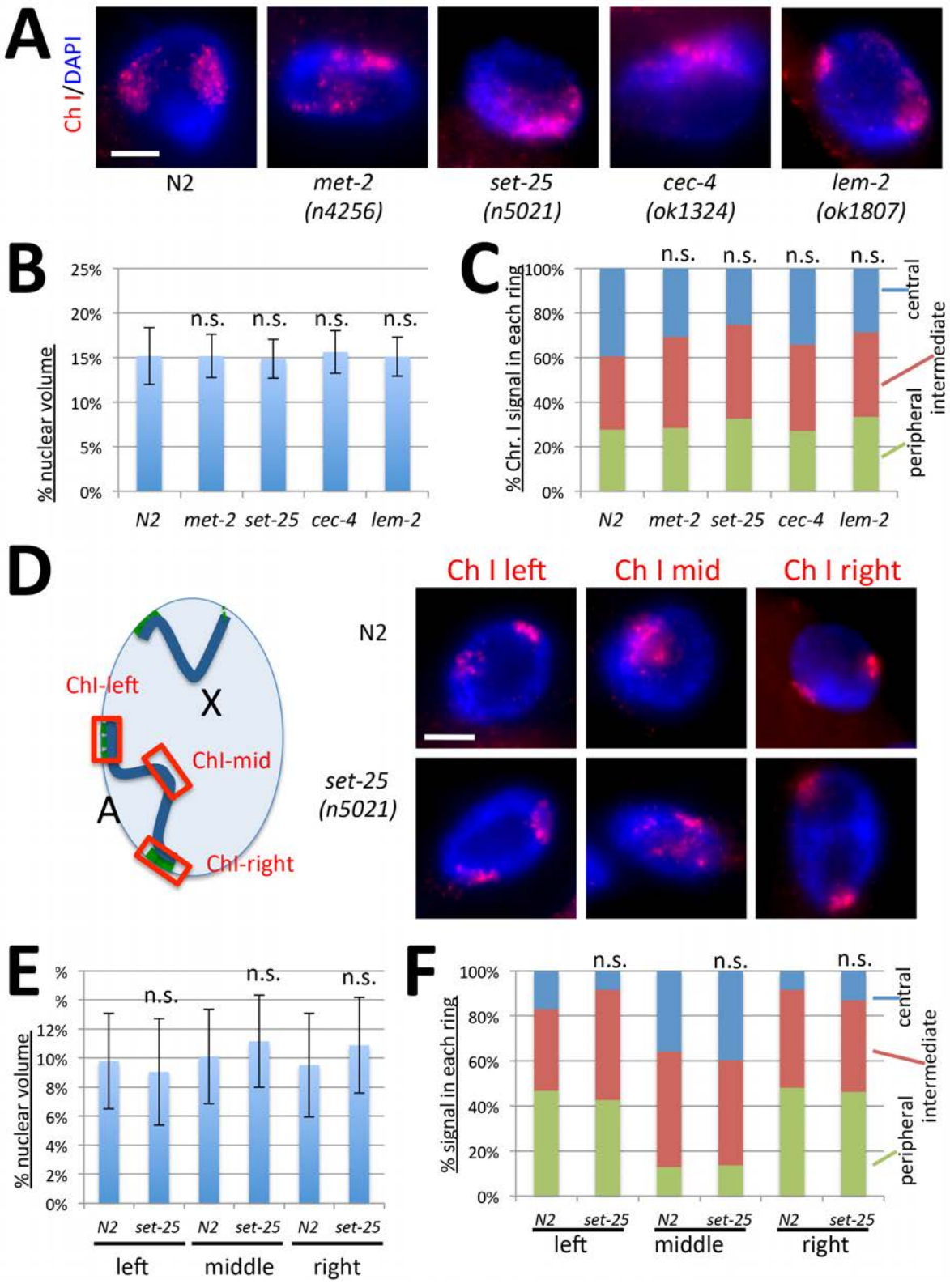
A
Ch I/DAPI
N2
met-2 (n4256)
set-25 (n5021)
cec-4 (ok1324)
lem-2 (ok1807)
B
% nuclear volume
25%
20%
15%
10%
5%
0%
n.s.
N2
met-2
set-25
cec-4
lem-2
C
% Chr. I signal in each ring
100%
80%
60%
40%
20%
0%
n.s.
central
intermediate
peripheral
D
Ch I left
Ch I mid
Ch I right
N2
set-25 (n5021)
ChI-left
ChI-mid
ChI-right
X
A
E
% nuclear volume
n.s.
left
middle
right
F
% signal in each ring
n.s.
central
intermediate
peripheral

Figure 3.6 Chromosome I structure and organization is not affected in tethering mutants. (A) Chromosome I paint FISH (red) in representative images of intestinal nuclei (DAPI, blue) of hermaphrodite adult worms. Chromosome I appears comparably sized in each background. Scale bar, 5 mm. (B) Quantification of chromosome I volumes normalized to nuclear size (n=12 nuclei). Error bars indicate standard deviation. (C) Three-zone assay for whole Chr I paint (n=10 nuclei). The chromosome did not relocate to a more central position in any of the mutants (D) FISH analysis of the left, middle and right regions of Chr I in wild type (N2) and *set-25(n5021)* mutant hermaphrodites. Diagram (left) indicates locations of probes, representative images are shown on the right. The left and right ends of the chromosome are peripherally located, but the middle appears more centrally located in both backgrounds. (E) Quantification of volumes occupied by Chr I domains (n=20 nuclei). Error bars indicate standard deviation (F) Three-zone assay for the left, middle and right domains of Chr I (n=10 nuclei). The middle domain is more centrally located than the left and right arms in both genotypes. Student's t-test did not reveal any statistically significant differences for volume measurements in (B) and (E), or for the portion of chromosome located in the central zone in (C) and (F), mutant compared to wild type. n.s. = $p > 0.05$. See Table 3.2 for statistical data.

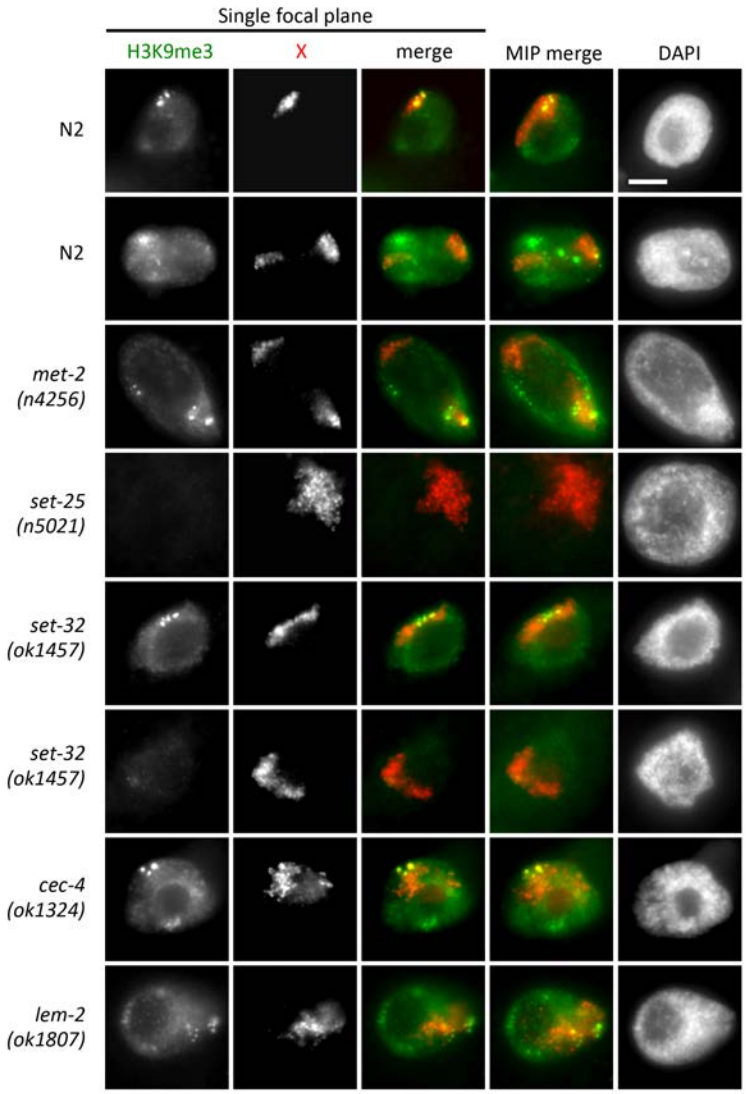

Figure 3.7 Analysis of H3K9me3 levels. Immunofluorescence analysis with antibodies specific to H3K9me3 (green), combined with antibodies specific to DCC subunit CAPG-1 (red) to mark the location of the X chromosomes. To illustrate the spatial proximity of the bright H3K9me3 foci to the X territory, single focal planes are shown. Maximum intensity projections of whole nuclei are shown for reference (right, MIP). The H3K9me3 signal is distributed diffusely in the nucleus with some peripherally localized bright foci. H3K9me3 signal intensity is only affected in *set-25* and *set-32* mutants. Scale bar, 5 µm.

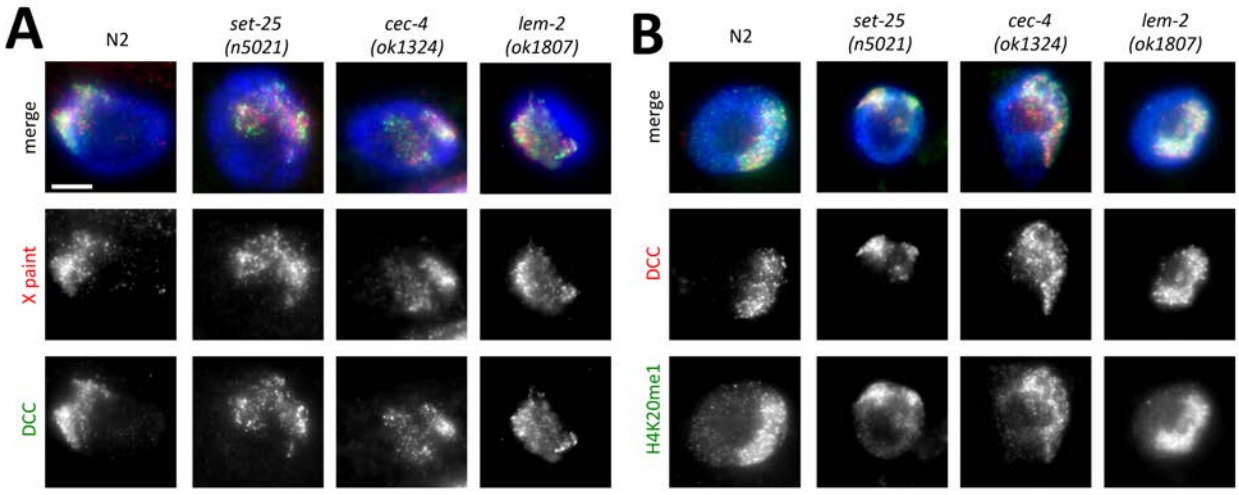

Figure 3.8 DCC localization and H4K20me1 enrichment in tethering mutants.
(A) Combined X paint fluorescence *in situ* hybridization (red) and immunofluorescence with antibodies specific to DCC component DPY-27 (green). The DCC remains localized on the decondensed X chromosomes of tethering mutants. (B) Immunofluorescence images with antibodies specific to H4K20me1 (green) and DCC component CAPG-1 (red) to mark the location of the X chromosome. H4K20me1 remains enriched on DCC-bound X chromosomes. Scale bar, 5 µm.

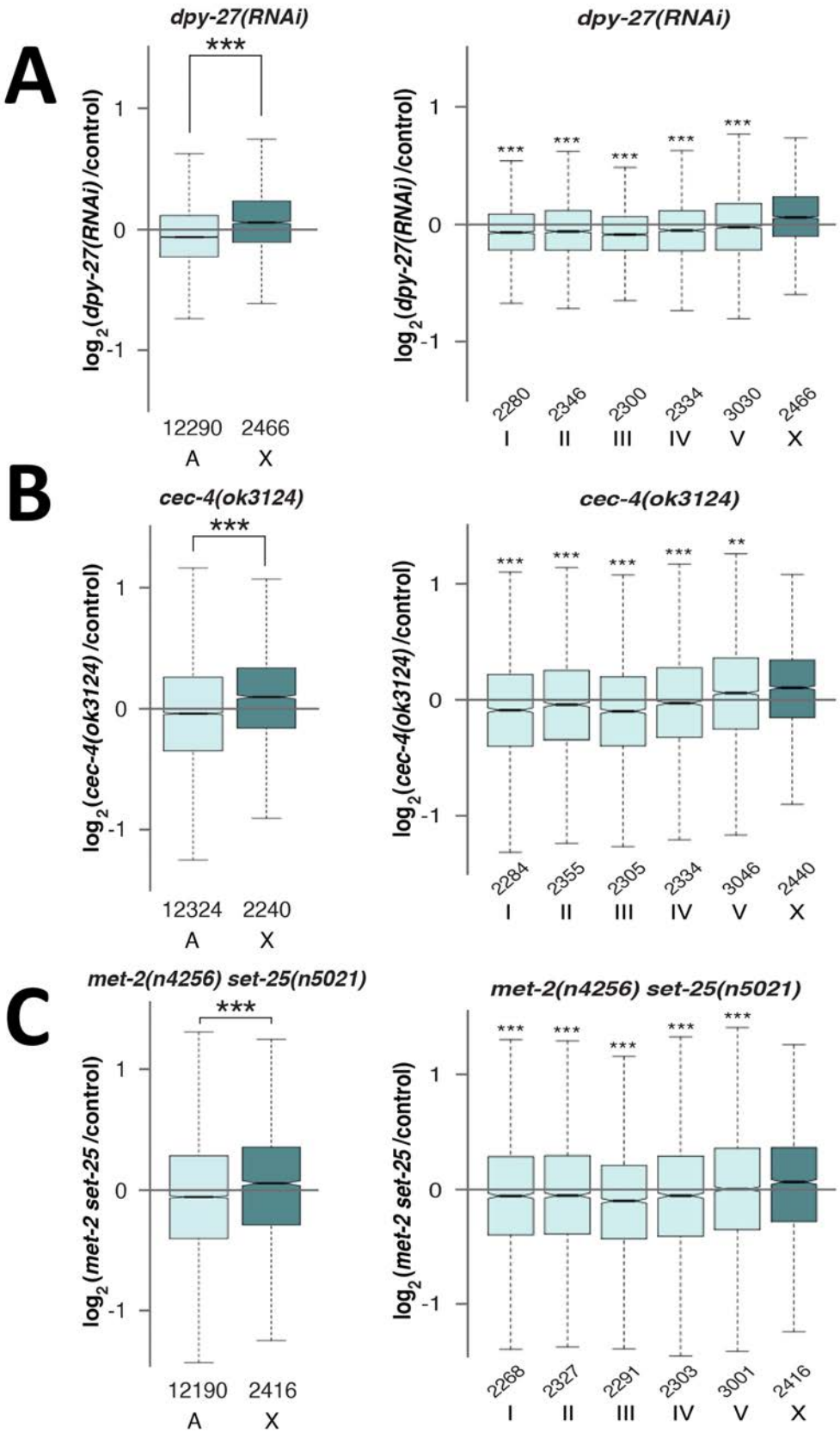
A
dpy-27(RNAi)
***
log2(dpy-27(RNAi)/control)
1
0
-1
12290
2466
A
X
dpy-27(RNAi)
***
***
***
***
***
***
2280
2346
2300
2334
3030
2466
I
II
III
IV
V
X
B
cec-4(ok3124)
***
log2(cec-4(ok3124)/control)
12324
2240
A
X
cec-4(ok3124)
***
***
***
***
**
2284
2355
2305
2334
3046
2440
I
II
III
IV
V
X
C
met-2(n4256) set-25(n5021)
***
log2(met-2 set-25/control)
12190
2416
A
X
met-2(n4256) set-25(n5021)
***
***
***
***
***
2268
2327
2291
2303
3001
2416
I
II
III
IV
V
X

Figure 3.9 RNA-seq analysis of gene expression changes in tethering mutants. (A-C) Boxplots show the distribution of $\log_2$ expression ratios on the X and autosome between *dpy-27(RNAi)* and control RNAi, *cec-4(ok3124)* mutant and control, and *met-2(n4256) set-25(n5021)* mutant and control. The X chromosome was significantly derepressed compared to autosomes (each autosome individually, or as a group) in *dpy-27(RNAi)* (A), *cec-4(ok3124)* mutants (B), and *met-2(n4256) set-25(n5021)* mutants (C). Increased expression from the X was tested between the X and all autosomes (left), or the X and individual autosomes (right) by one-sided Wilcoxon rank-sum test (** = $p < 0.01$, *** = $p < 0.001$).

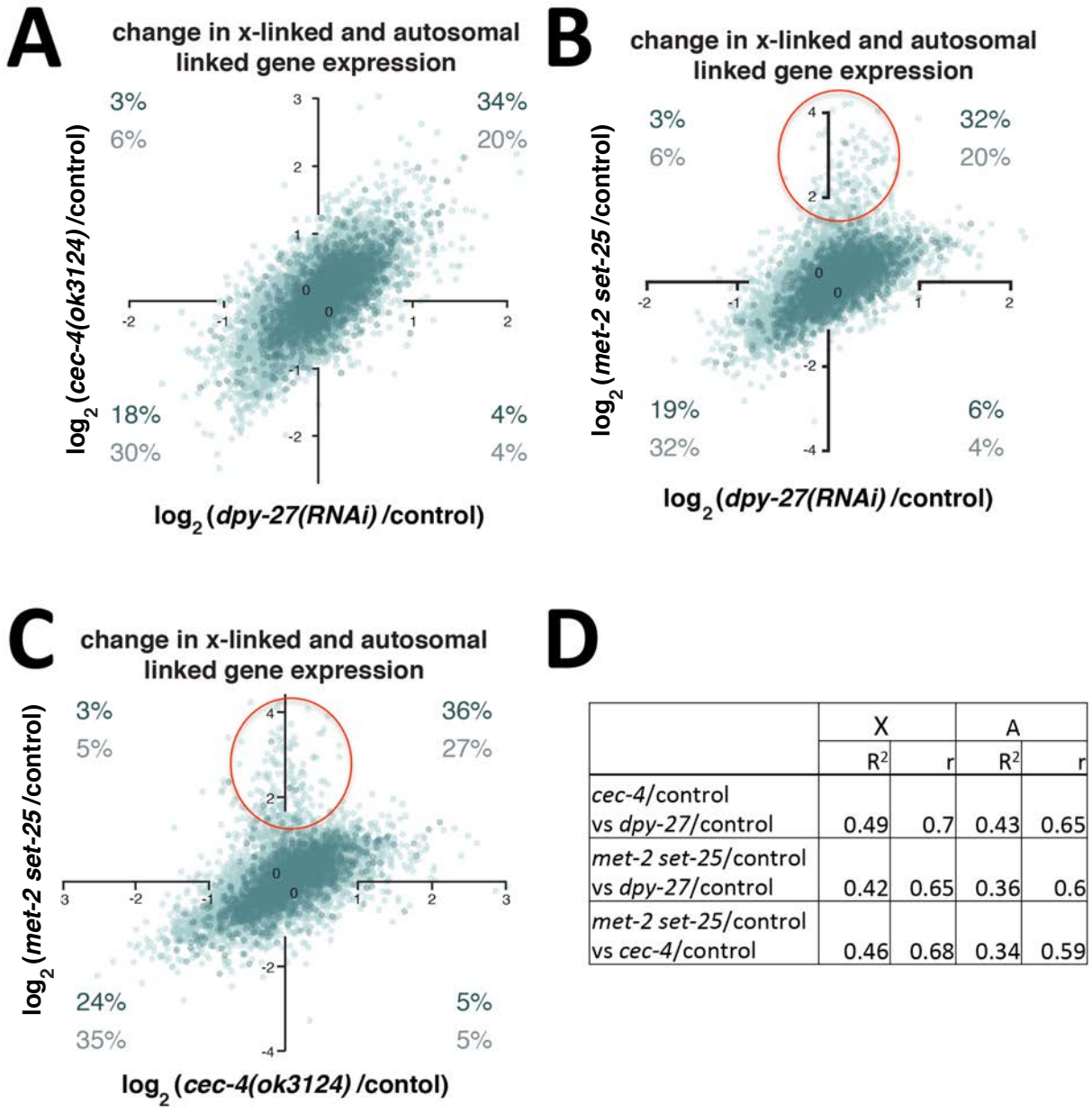

	X		A	
	R^2	r	R^2	r
cec-4/control vs *dpy-27*/control	0.49	0.7	0.43	0.65
met-2 set-25/control vs *dpy-27*/control	0.42	0.65	0.36	0.6
met-2 set-25/control vs *cec-4*/control	0.46	0.68	0.34	0.59

Figure 3.10 Comparison of gene expression changes in tethering mutants and partial DCC depletions. The magnitude of $\log_2$ expression ratios of X-linked (dark) and autosomal linked genes (light) between *cec-4(ok3124)* mutant and control plotted against *dpy-27(RNAi)* and control RNAi (A), *met-2(n4256) set-25(n5021)* mutant and control plotted against *dpy-27(RNAi)* and control RNAi (B), and *met-2(n4256) set-25(n5021)* mutant and control plotted against *cec-4(ok3124)* mutant and control (C). Red circles indicate a group of genes that are repressed by MET-2 and SET-25 independent of dosage compensation or *cec-4* function. Percent of X-linked (dark numbers) and autosomal genes (light numbers) with greater than 10% ($\log_2$ of 0.1) change in expression are indicated in each quadrant. (D) The R-squared of each regression and the Pearson correlation values are shown for X-linked (X) and autosomal genes (A) for each comparison.

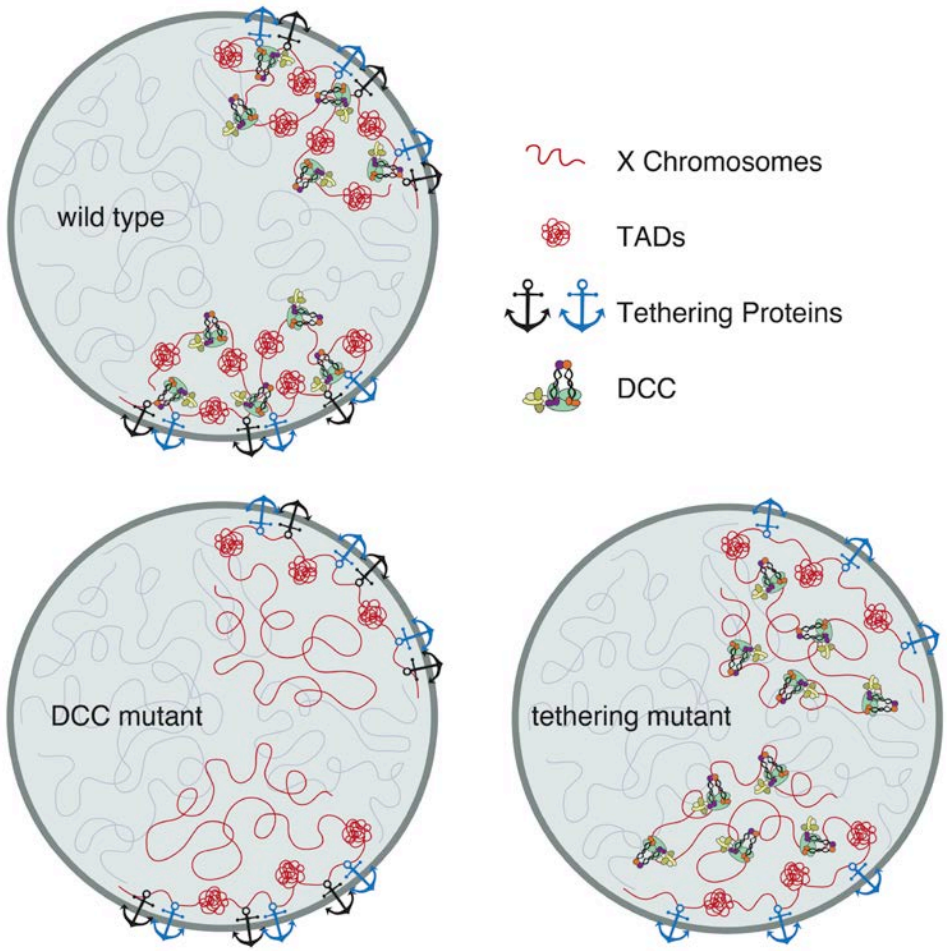

Figure 3.11 Model showing the effects of tethering and DCC function on X chromosome compaction and nuclear localization. In differentiated cells, multiple anchoring mechanisms tether the left end of the X chromosome to the nuclear lamina (black and blue anchors). In wild type cells, the DCC organizes the X chromatin into topologically associating domains (TADs) and uses heterochromatin anchors to compact the X chromosome and bring it to the nuclear periphery. In the absence of the DCC, the left end of the X remains peripheral and compact due to the action of the tethering proteins, and its TAD structure is maintained. The rest of the X chromosome loses its TAD organization, decondenses and moves more internally. When heterochromatic tethers (black anchors) are lost, redundant tethers (blue) keep the left end of the X near the nuclear lamina. Without the heterochromatic anchors, the DCC is unable to compact the rest of the chromosome and bring it near the periphery. Therefore, the rest of the X chromosome decondenses and relocates away from the nuclear lamina.

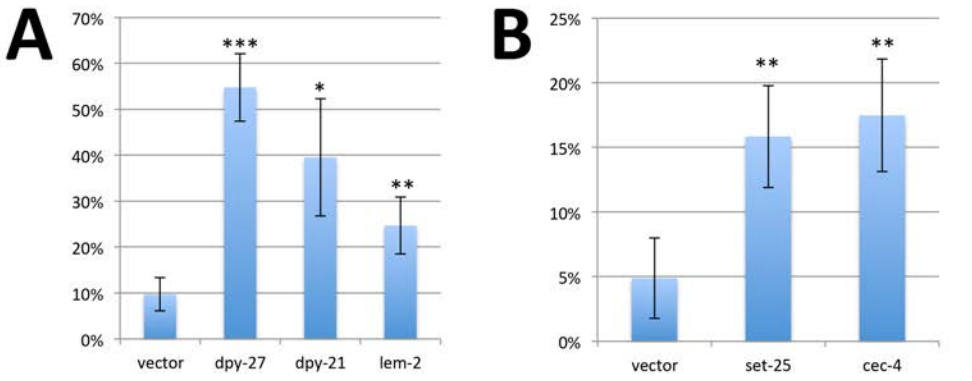

RNAi	n values in each replicate	t-test
vector	628, 660, 670, 511	
dpy-27	696, 658, 518, 756	0.000244383
dpy-21	596, 819, 548, 430	0.014998157
lem-2	654, 716, 743, 607	0.009565229

RNAi	n values in each replicate	t-test
vector	486, 399, 247, 592	
set-25	726, 436, 476, 512	0.005411048
cec-4	599, 458, 617, 552	0.004266121

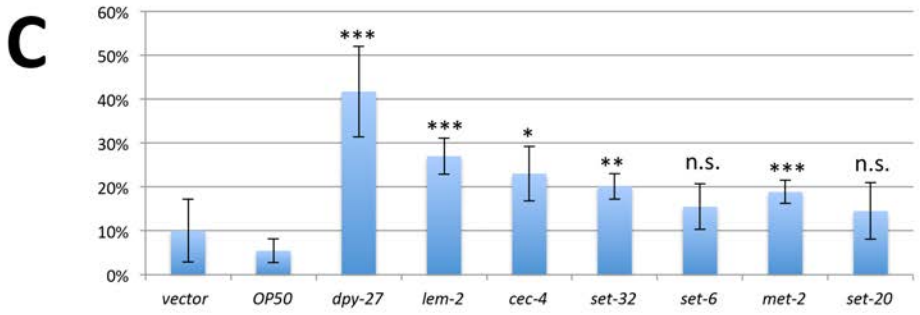

RNAi	n values in each replicate	t-test compared to vector
vector	524, 398, 717, 526, 689, 478, 338, 618	
OP50	438, 427, 610, 680	
dpy-27	232, 493, 356, 357, 449, 515, 488, 471	9.55966E-06
lem-2	469, 511, 504, 493	0.000454673
cec-4	496, 511, 504, 493	0.013910958
set-32	589, 544, 612, 494	0.006103465
set-6	267, 468, 339, 357	0.165680185
met-2	258, 418, 570, 214	0.000274968
set-20	663, 750, 643, 670	0.308095616

Figure 3.12 Additional male rescue analysis. A limited number of genes were analyzed in each experiment (A, B, and C), but using four independent biological replicates. Note that RNAi feeding of parents was extended by 24 hours compared to the experiment shown on Figure 3.1. This led to higher levels of male rescue overall, but the trend remained the same. OP50 is the normal bacterial food source, without any plasmid to produce RNA. With the exception of *set-6* and *set-20*, RNAi of all genes rescued significantly more males than control vector RNAi. It is important to point out that the few males rescued on vector RNAi plates were small and sickly, while the males rescued using RNAi of the other genes appeared more normal size and had better mobility. Error bars indicate standard deviation based on four replicates. Asterisks indicate statistical significance using Student t-test, n.s. = $p>0.05$, * = $p<0.05$, ** = $p<0.01$, *** = $p<0.001$. Numbers of embryos counted and p-values (compared to vector RNAi) are shown in the table below each graph.

.

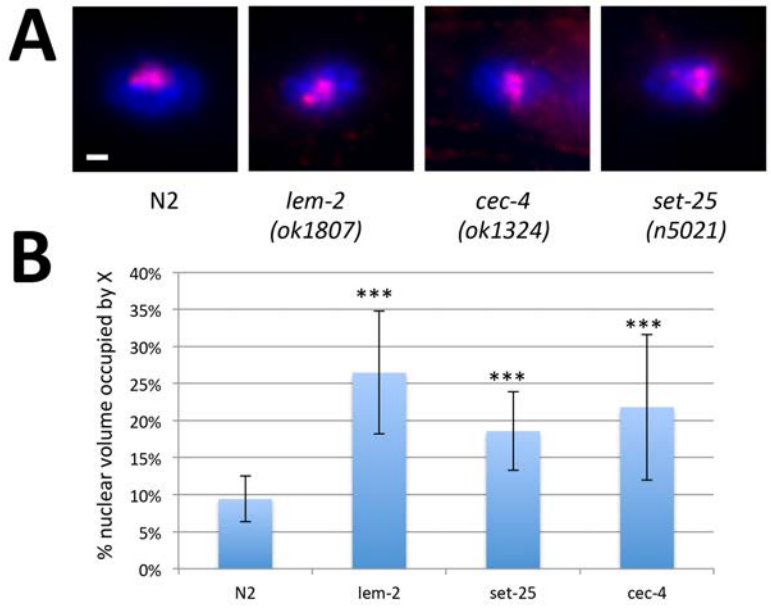

Figure 3.13 Chromosome volume measurements in hypodermal nuclei of hermaphrodites. (A) X chromosome paint FISH (red) in diploid tail tip hypodermal nuclei (DAPI, blue) of hermaphrodite adult worms. The X chromosomes are compact and peripherally localized in wild type (N2), but are decondensed and more centrally located in mutants. Scale bar, 1 mm. (B) Quantification of X chromosome volumes normalized to nuclear size (n=17-26 nuclei). Error bars indicate standard deviation. *** = $p<0.001$ by Student's t-test (N2 compared to appropriate mutant).

A

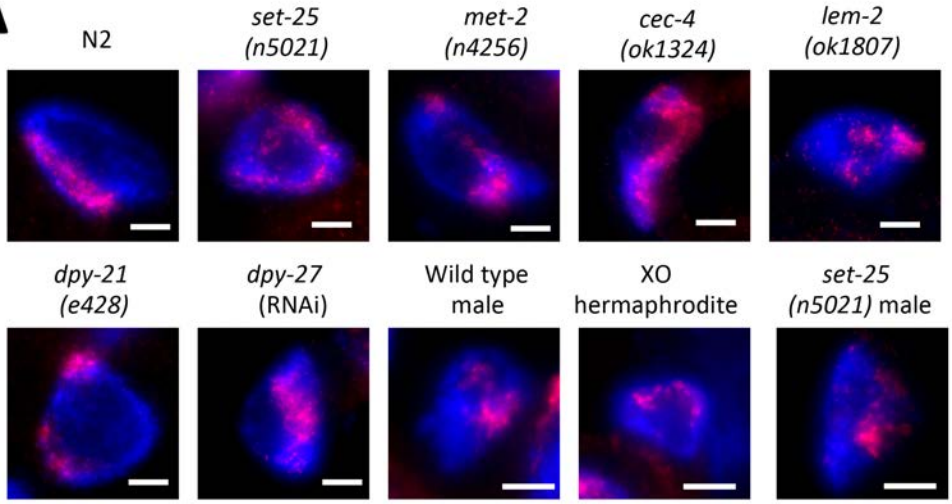

B

genotype	sex	n	% round or ellipsoid
n2	hermaphrodite	31	68%
set-25	hermaphrodite	23	70%
met-2	hermaphrodite	54	57%
cec-4	hermaphrodite	42	61%
lem-2	hermaphrodite	23	87%
dpy-21	hermaphrodite	54	48%
dpy-27(RNAi)	hermaphrodite	31	65%
him-8 (wild type)	male	107	80%
him8;set-25	male	77	86%
her-1; sdc-2, XO	hermaphrodite	109	74%

Figure 3.14 X paint FISH images in irregularly-shaped nuclei. (A) Representative irregularly shaped nuclei in the various backgrounds. The X is compact and peripherally located in N2 hermaphrodites and is decondensed and more centrally located in tethering mutants and in males. (B) Table indicating the percent of nuclei in each background that were suitable for analysis using the three-zone assay.

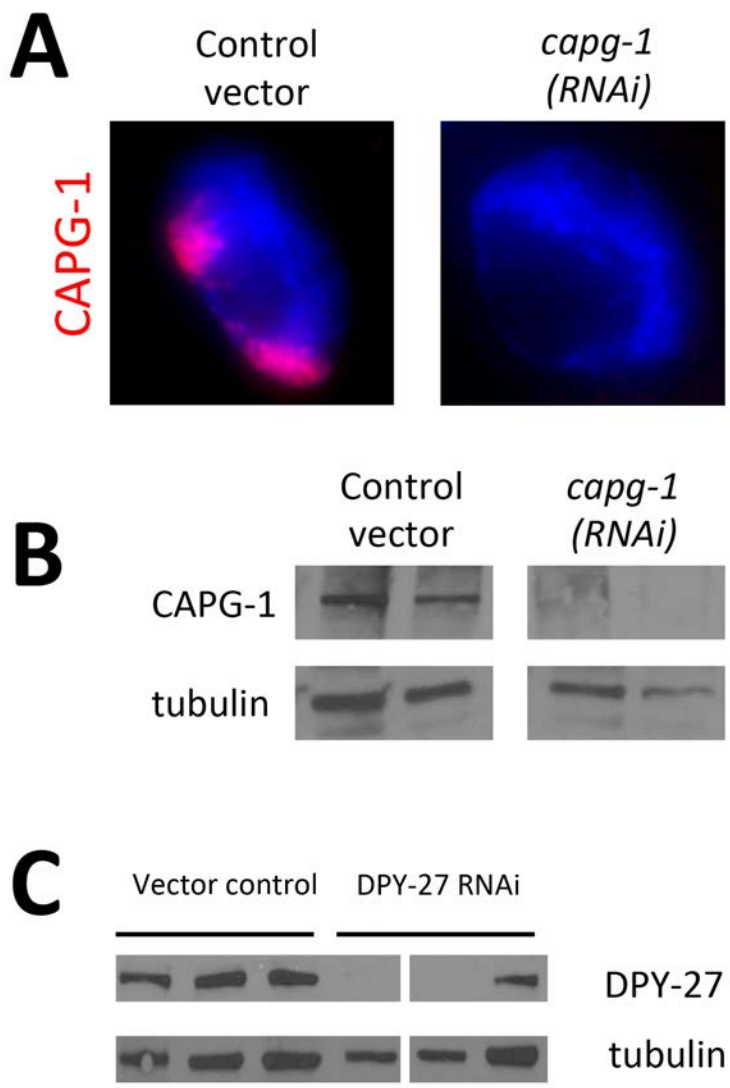

Figure 3.15 Antibody validation and RNAi-depletion control.
(A) Immunofluorescence analysis of the newly developed CAPG-1 antibody in nuclei of control vector RNAi-treated worms shows two territories corresponding to the X chromosomes. In *capg-1(RNAi)* nuclei, the signal is below level of detection, similar to what has been observed previously with other antibodies to DCC components. (B) On a western blot, the antibody recognizes a protein of the predicted size (131 kD) in control vector RNAi treated worms, but not in CAPG-1 RNAi treated worms. Tubulin was used as loading control. (C) Western blot analysis of three control and three *dpy-27(RNAi)* samples, indicating levels of DPY-27 depletion. Tubulin is shown as a loading control.

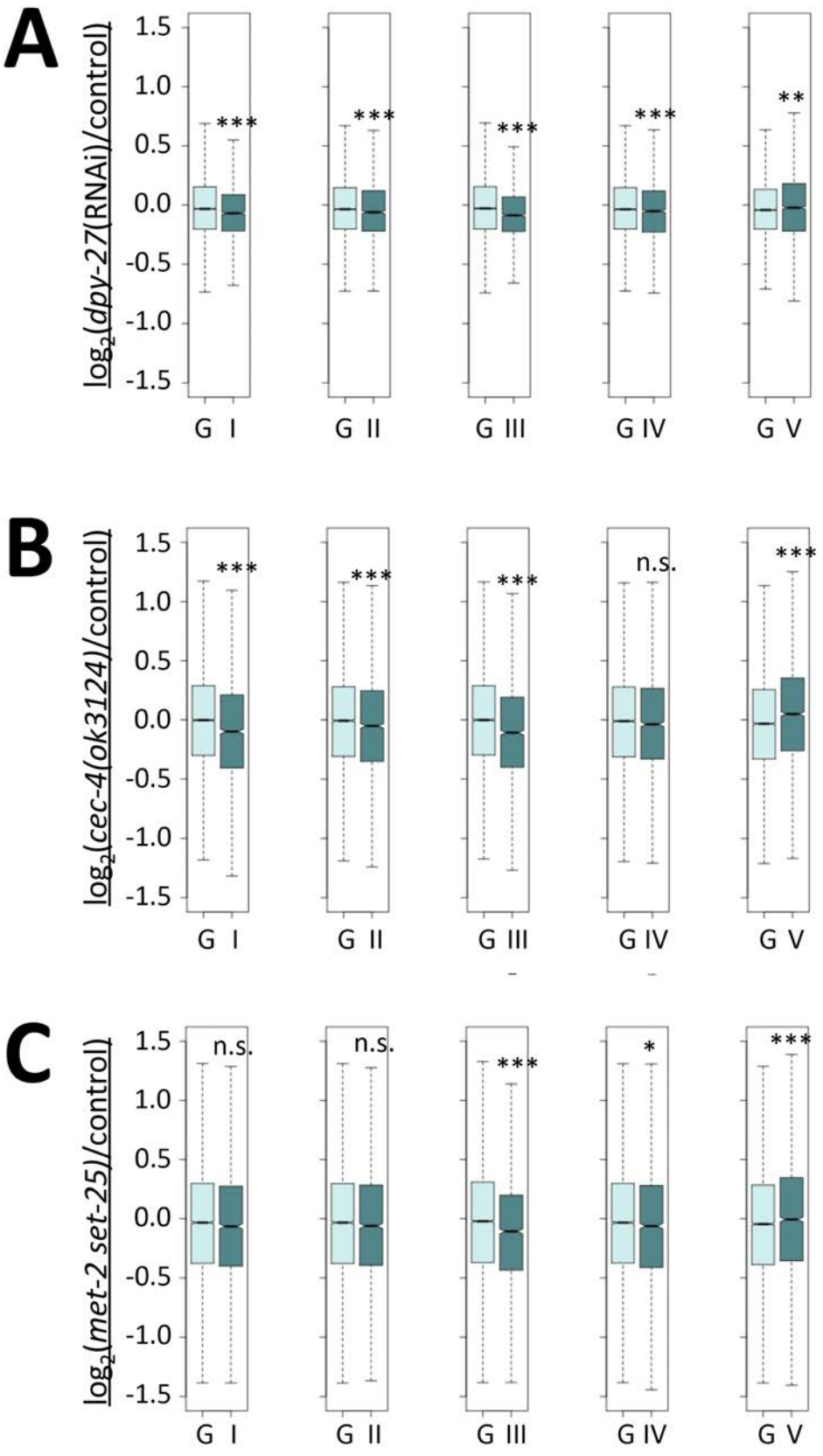
A
log2(dpy-27(RNAi)/control)
1.5
1.0
0.5
0.0
-0.5
-1.0
-1.5
***
***
***
***
**
G I
G II
G III
G IV
G V
B
log2(cec-4(ok3124)/control)
1.5
1.0
0.5
0.0
-0.5
-1.0
-1.5
***
***
***
n.s.
***
G I
G II
G III
G IV
G V
C
log2(met-2 set-25)/control)
1.5
1.0
0.5
0.0
-0.5
-1.0
-1.5
n.s.
n.s.
***
*
***
G I
G II
G III
G IV
G V

Figure 3.16 Additional comparison gene expression changes on individual chromosomes. (A-C) Boxplots show the distribution of $\log_2$ expression ratios on each autosomes (I, II, III, IV, and V) and the rest of the genome (labeled G) between *dpy-27(RNAi)* and control (A), *cec-4(ok3124)* mutant and control (B), and *met-2(n4256) set-25(n5021)* mutant and control. The only autosome that showed derepression compared to the rest of the genome is chromosome V. Differences in gene expression changes between the given chromosome and the rest of the genome were tested by two-sided Wilcoxon rank-sum test (n.s. = $p>0.05$, * = $p < 0.05$, ** = $p<0.01$, *** = $p < 0.001$).

A

		X total	X up	% up	X down	% down	A total	A up	% up	A down	% down
padj=.1	*dpy-27(RNAi)*	2466	54	2.19%	15	0.61%	12290	163	1.33%	183	1.49%
	cec-4	2240	80	3.57%	44	1.96%	12324	356	2.89%	972	7.89%
	met-2 set-25	2416	72	2.98%	101	4.18%	12190	507	4.16%	829	6.80%
padj=.05	*dpy-27(RNAi)*	2466	25	1.01%	3	0.12%	12290	90	0.73%	87	0.71%
	cec-4	2240	44	1.96%	28	1.25%	12324	205	1.66%	629	5.10%
	met-2 set-25	2416	39	1.61%	62	2.57%	12190	369	3.03%	450	3.69%

B

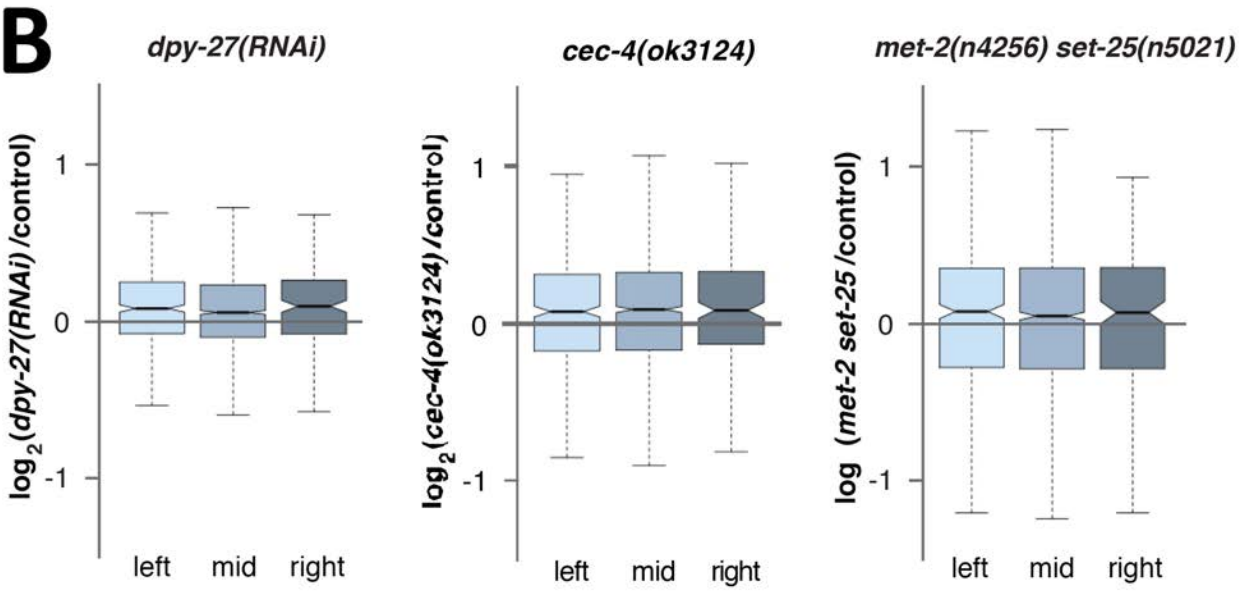

Figure 3.17 Additional analysis of gene expression changes. (A) Numbers and percentages of genes with significantly changed levels of gene expression (DESeq2, padj<0.1 and padj<0.05) on the X chromosome and the autosomes in each background. (B) Boxplots show the distribution of $\log_2$ expression ratios on X chromosome regions between *dpy-27* and control RNAi, *cec-4(ok3124)* mutant and control, and *met-2(n4256) set-25(n5021)* mutant and control. Expression differences between X regions were tested by two-sided Wilcoxon rank-sum test. No significant differences were found.

whole X paint

	N2	*set-25*	*met-2 set-25*	*cec-4*	*lem-2*	*dpy-21*	*dpy-27(RNAi*	XO herm	wt male	set-25 male
n	10	10	10	10	10	10	10	10	10	10
peripheral %	0.2460166	0.18108734	0.17100431	0.12483749	0.14885454	0.23171619	0.15055586	0.14006767	0.10578356	0.08473489
st dev	0.12317077	0.08394753	0.09806461	0.07869138	0.08338365	0.17584326	0.10072818	0.06415232	0.07645738	0.07217885
intermed %	0.51555485	0.38185777	0.37545447	0.33605121	0.33670623	0.42227491	0.42842662	0.49212446	0.36320889	0.26202141
st dev	0.11855283	0.05666637	0.08394526	0.08337165	0.06486988	0.12696711	0.09175781	0.09170447	0.08244027	0.12066364
central %	0.23842855	0.43705489	0.45354122	0.5391113	0.51443923	0.3460089	0.42101753	0.36780787	0.53100755	0.6532437
st dev	0.09564744	0.10651531	0.13278119	0.11776565	0.11001907	0.22261633	0.1343343	0.126949	0.13926637	0.17946691
t-test of central ring compared to N2 hermaphrodite										
		0.00085208	0.00070257	9.5192E-06	2.3491E-05	0.18809096	0.00320924	0.02177761	5.6208E-05	3.7175E-06
t-test of central ring compared to set-25 hermaphrodite								t-test compared to wt male		
			0.76784616							0.09960997

left X probe

	N2	set-25	lem-2	cec-4	dpy-27(RNAi)
n	12	12	12	12	12
peripheral %	0.24059006	0.19880636	0.08421264	0.16131613	0.16444175
st dev	0.12888683	0.16120025	0.08460705	0.13741298	0.17310133
intermed %	0.60562542	0.50227208	0.6161937	0.53208363	0.54276048
st dev	0.06694305	0.12348118	0.15840007	0.18913377	0.18914569
central %	0.15378454	0.29892157	0.29959368	0.30660023	0.29279777
st dev	0.13005938	0.14996516	0.20293387	0.25018588	0.24752464
t-test of central ring compared to N2 hermaphrodite					
		0.01895785	0.04995183	0.07821709	0.10355896

Middle X probe

	N2	set-25	lem-2	cec-4	dpy-27(RNAi	XO herm	wt male	set-25 male
n	12	12	12	12	12	10	10	10
peripheral %	0.219341	0.13426402	0.18524328	0.23265349	0.31545998	0.17023531	0.12021431	0.09025599
st dev	0.17906491	0.10996228	0.12817088	0.08833383	0.2030099	0.12669977	0.07361085	0.08042172
intermed %	0.61054607	0.35300007	0.37657471	0.39334755	0.41918957	0.40027687	0.28490383	0.30690104
st dev	0.16494192	0.08933676	0.14280516	0.08937391	0.09451049	0.18146025	0.17001368	0.16435189
central %	0.17011293	0.51273591	0.43818202	0.37399896	0.26535045	0.42948782	0.59488186	0.60284297
st dev	0.14102809	0.17738852	0.24039562	0.13893657	0.22160637	0.25248608	0.21750042	0.21740858
t-test of central ring compared to N2 hermaphrodite								
		4.3012E-05	0.0040592	0.00221382	0.23182446	0.00718188	9.0914E-05	7.4828E-05
							t-test with wt male	
								0.93565866

Right X probe

	N2	set-25	lem-2	cec-4	dpy-27(RNAi)
n	12	12	12	12	12
peripheral %	0.25088158	0.3116153	0.25253889	0.27816668	0.11216881
st dev	0.14277669	0.20004045	0.15345298	0.16198887	0.10510497
intermed %	0.54939892	0.48653712	0.61143382	0.55403456	0.58685975
st dev	0.09645279	0.14703048	0.0966098	0.15558981	0.20696769
central %	0.19971952	0.20184757	0.13602729	0.16779875	0.3009714
st dev	0.16839145	0.18234042	0.12730597	0.24469094	0.2564932
t-test of central ring compared to N2 hermaphrodite					
		0.97657508	0.30811983	0.71370518	0.26718607

Table 3.1 Statistical analysis of X chromosome FISH data using the three-zone assay. n indicates number of nuclei analyzed. Average % of paint signal in each ring and standard deviations are shown. Results of statistical analysis using Student's test on the portion of the signal in the central ring are below each data set.

Whole chr I paint					
	N2	*met-2*	*set-25*	*cec-4*	*lem-2*
n	10	10	10	10	10
peripheral %	0.27498174	0.28393391	0.32433095	0.27035885	0.33438014
st dev	0.15508742	0.1178846	0.15313704	0.12927037	0.08154668
intermed %	0.32962194	0.40729479	0.42261037	0.38715812	0.37789169
st dev	0.06548054	0.07281563	0.07054663	0.06638567	0.04499781
central %	0.39539632	0.3087713	0.25305867	0.34248303	0.28772817
st dev	0.19366442	0.12723365	0.16203304	0.17888866	0.09688504
t-test of central ring compared to N2 hermaphrodite					
		0.25490246	0.09205845	0.53367557	0.13946616
t-test of central ring compared to X chromosome paint central ring					
	0.03985768				

Left chr I paint		
	N2	*set-25*
n	10	10
peripheral %	0.46685393	0.42616007
st dev	0.17003909	0.15502068
intermed %	0.3625494	0.4885656
st dev	0.10119311	0.1273334
central %	0.17059667	0.08527433
st dev	0.10999698	0.08684983
t-test of central ring compared to N2		
		0.07102638

Middle chr I paint		
	N2	*set-25*
n	10	10
peripheral %	0.12857949	0.13774714
st dev	0.12385027	0.0527957
intermed %	0.51425098	0.46450183
st dev	0.14121135	0.13704882
central %	0.35716953	0.39775103
st dev	0.19140075	0.1152638
t-test of central ring compared to N2		
		0.57436305
t-test of central ring compared to X-mid central ring in N2		
	0.01802029	

Right chr I paint		
	N2	*set-25*
n	10	10
peripheral %	0.48173491	0.46238507
st dev	0.14179603	0.22371649
intermed %	0.4352292	0.40681055
st dev	0.08409888	0.12059219
central %	0.08303589	0.13080437
st dev	0.0771285	0.17828623
t-test of central ring compared to N2		
		0.45154159

Table 3.2 Statistical analysis of chromosome I FISH data using the three-zone assay. n indicates number of nuclei analyzed. Average % of paint signal in each ring and standard deviations are shown. Results of statistical analysis using Student's test on the portion of the signal in the central ring are below each data set.

REFERENCES

1. Lau, A.C., and Csankovszki, G. (2015). Balancing up and downregulation of the C. elegans X chromosomes. Current opinion in genetics & development *31*, 50-56.
2. Strome, S., Kelly, W.G., Ercan, S., and Lieb, J.D. (2014). Regulation of the X chromosomes in Caenorhabditis elegans. Cold Spring Harb Perspect Biol *6*.
3. Chuang, P.T., Albertson, D.G., and Meyer, B.J. (1994). DPY-27:a chromosome condensation protein homolog that regulates C. elegans dosage compensation through association with the X chromosome. Cell *79*, 459-474.
4. Csankovszki, G., Collette, K., Spahl, K., Carey, J., Snyder, M., Petty, E., Patel, U., Tabuchi, T., Liu, H., McLeod, I., et al. (2009). Three distinct condensin complexes control C. elegans chromosome dynamics. Current biology : CB *19*, 9-19.
5. Mets, D.G., and Meyer, B.J. (2009). Condensins regulate meiotic DNA break distribution, thus crossover frequency, by controlling chromosome structure. Cell *139*, 73-86.
6. Lau, A.C., and Csankovszki, G. (2014). Condensin-mediated chromosome organization and gene regulation. Frontiers in genetics *5*, 473.
7. Sharma, R., Jost, D., Kind, J., Gomez-Saldivar, G., van Steensel, B., Askjaer, P., Vaillant, C., and Meister, P. (2014). Differential spatial and structural organization of the X chromosome underlies dosage compensation in C. elegans. Genes & development *28*, 2591-2596.
8. Crane, E., Bian, Q., McCord, R.P., Lajoie, B.R., Wheeler, B.S., Ralston, E.J., Uzawa, S., Dekker, J., and Meyer, B.J. (2015). Condensin-driven remodelling of X chromosome topology during dosage compensation. Nature *523*, 240-244.
9. Vielle, A., Lang, J., Dong, Y., Ercan, S., Kotwaliwale, C., Rechtsteiner, A., Appert, A., Chen, Q.B., Dose, A., Egelhofer, T., et al. (2012). H4K20me1 contributes to downregulation of X-linked genes for C. elegans dosage compensation. PLoS genetics *8*, e1002933.
10. Wells, M.B., Snyder, M.J., Custer, L.M., and Csankovszki, G. (2012). Caenorhabditis elegans dosage compensation regulates histone H4 chromatin state on X chromosomes. Molecular and cellular biology *32*, 1710-1719.
11. Kramer, M., Kranz, A.L., Su, A., Winterkorn, L.H., Albritton, S.E., and Ercan, S. (2015). Developmental Dynamics of X-Chromosome Dosage Compensation by the DCC and H4K20me1 in C. elegans. PLoS genetics *11*, e1005698.
12. Jans, J., Gladden, J.M., Ralston, E.J., Pickle, C.S., Michel, A.H., Pferdehirt, R.R., Eisen, M.B., and Meyer, B.J. (2009). A condensin-like dosage compensation complex acts at a distance to control expression throughout the genome. Genes & development *23*, 602-618.
13. Kruesi, W.S., Core, L.J., Waters, C.T., Lis, J.T., and Meyer, B.J. (2013). Condensin controls recruitment of RNA polymerase II to achieve nematode X-chromosome dosage compensation. eLife *2*, e00808.

14. Bickmore, W.A., and van Steensel, B. (2013). Genome architecture: domain organization of interphase chromosomes. Cell *152*, 1270-1284.
15. Ciabrelli, F., and Cavalli, G. (2015). Chromatin-driven behavior of topologically associating domains. J Mol Biol *427*, 608-625.
16. Van Bortle, K., and Corces, V.G. (2012). Nuclear organization and genome function. Annu Rev Cell Dev Biol *28*, 163-187.
17. Akhtar, A., and Gasser, S.M. (2007). The nuclear envelope and transcriptional control. Nat Rev Genet *8*, 507-517.
18. Kind, J., and van Steensel, B. (2010). Genome-nuclear lamina interactions and gene regulation. Curr Opin Cell Biol *22*, 320-325.
19. Talamas, J.A., and Capelson, M. (2015). Nuclear envelope and genome interactions in cell fate. Frontiers in genetics *6*, 95.
20. Meister, P., Towbin, B.D., Pike, B.L., Ponti, A., and Gasser, S.M. (2010). The spatial dynamics of tissue-specific promoters during C. elegans development. Genes Dev *24*, 766-782.
21. Mattout, A., Pike, B.L., Towbin, B.D., Bank, E.M., Gonzalez-Sandoval, A., Stadler, M.B., Meister, P., Gruenbaum, Y., and Gasser, S.M. (2011). An EDMD mutation in C. elegans lamin blocks muscle-specific gene relocation and compromises muscle integrity. Curr Biol *21*, 1603-1614.
22. Gonzalez-Sandoval, A., Towbin, B.D., Kalck, V., Cabianca, D.S., Gaidatzis, D., Hauer, M.H., Geng, L., Wang, L., Yang, T., Wang, X., et al. (2015). Perinuclear Anchoring of H3K9-Methylated Chromatin Stabilizes Induced Cell Fate in C. elegans Embryos. Cell *163*, 1333-1347.
23. Towbin, B.D., Gonzalez-Aguilera, C., Sack, R., Gaidatzis, D., Kalck, V., Meister, P., Askjaer, P., and Gasser, S.M. (2012). Step-wise methylation of histone H3K9 positions heterochromatin at the nuclear periphery. Cell *150*, 934-947.
24. Peric-Hupkes, D., Meuleman, W., Pagie, L., Bruggeman, S.W., Solovei, I., Brugman, W., Graf, S., Flicek, P., Kerkhoven, R.M., van Lohuizen, M., et al. (2010). Molecular maps of the reorganization of genome-nuclear lamina interactions during differentiation. Mol Cell *38*, 603-613.
25. Guelen, L., Pagie, L., Brasset, E., Meuleman, W., Faza, M.B., Talhout, W., Eussen, B.H., de Klein, A., Wessels, L., de Laat, W., et al. (2008). Domain organization of human chromosomes revealed by mapping of nuclear lamina interactions. Nature *453*, 948-951.
26. Ikegami, K., Egelhofer, T.A., Strome, S., and Lieb, J.D. (2010). Caenorhabditis elegans chromosome arms are anchored to the nuclear membrane via discontinuous association with LEM-2. Genome Biol *11*, R120.
27. Pickersgill, H., Kalverda, B., de Wit, E., Talhout, W., Fornerod, M., and van Steensel, B. (2006). Characterization of the Drosophila melanogaster genome at the nuclear lamina. Nat Genet *38*, 1005-1014.
28. Bian, Q., Khanna, N., Alvikas, J., and Belmont, A.S. (2013). beta-Globin cis-elements determine differential nuclear targeting through epigenetic modifications. J Cell Biol *203*, 767-783.

29. Harr, J.C., Luperchio, T.R., Wong, X., Cohen, E., Wheelan, S.J., and Reddy, K.L. (2015). Directed targeting of chromatin to the nuclear lamina is mediated by chromatin state and A-type lamins. J Cell Biol *208*, 33-52.
30. Kind, J., Pagie, L., Ortabozkoyun, H., Boyle, S., de Vries, S.S., Janssen, H., Amendola, M., Nolen, L.D., Bickmore, W.A., and van Steensel, B. (2013). Single-cell dynamics of genome-nuclear lamina interactions. Cell *153*, 178-192.
31. Dialynas, G., Speese, S., Budnik, V., Geyer, P.K., and Wallrath, L.L. (2010). The role of Drosophila Lamin C in muscle function and gene expression. Development *137*, 3067-3077.
32. Finlan, L.E., Sproul, D., Thomson, I., Boyle, S., Kerr, E., Perry, P., Ylstra, B., Chubb, J.R., and Bickmore, W.A. (2008). Recruitment to the nuclear periphery can alter expression of genes in human cells. PLoS Genet *4*, e1000039.
33. Kumaran, R.I., and Spector, D.L. (2008). A genetic locus targeted to the nuclear periphery in living cells maintains its transcriptional competence. J Cell Biol *180*, 51-65.
34. Reddy, K.L., Zullo, J.M., Bertolino, E., and Singh, H. (2008). Transcriptional repression mediated by repositioning of genes to the nuclear lamina. Nature *452*, 243-247.
35. Petty, E.L., Collette, K.S., Cohen, A.J., Snyder, M.J., and Csankovszki, G. (2009). Restricting dosage compensation complex binding to the X chromosomes by H2A.Z/HTZ-1. PLoS genetics *5*, e1000699.
36. Andersen, E.C., and Horvitz, H.R. (2007). Two C. elegans histone methyltransferases repress lin-3 EGF transcription to inhibit vulval development. Development *134*, 2991-2999.
37. Towbin, B.D., Meister, P., Pike, B.L., and Gasser, S.M. (2010). Repetitive transgenes in C. elegans accumulate heterochromatic marks and are sequestered at the nuclear envelope in a copy-number- and lamin-dependent manner. Cold Spring Harb Symp Quant Biol *75*, 555-565.
38. Liu, J., Rolef Ben-Shahar, T., Riemer, D., Treinin, M., Spann, P., Weber, K., Fire, A., and Gruenbaum, Y. (2000). Essential roles for Caenorhabditis elegans lamin gene in nuclear organization, cell cycle progression, and spatial organization of nuclear pore complexes. Mol Biol Cell *11*, 3937-3947.
39. Lau, A.C., Nabeshima, K., and Csankovszki, G. (2014). The C. elegans dosage compensation complex mediates interphase X chromosome compaction. Epigenetics and Chromatin *7*.
40. Schott, S., Coustham, V., Simonet, T., Bedet, C., and Palladino, F. (2006). Unique and redundant functions of C. elegans HP1 proteins in post-embryonic development. Dev Biol *298*, 176-187.
41. Liu, T., Rechtsteiner, A., Egelhofer, T.A., Vielle, A., Latorre, I., Cheung, M.S., Ercan, S., Ikegami, K., Jensen, M., Kolasinska-Zwierz, P., et al. (2011). Broad chromosomal domains of histone modification patterns in C. elegans. Genome research *21*, 227-236.
42. Gonzalez-Sandoval, A., Towbin, B.D., and Gasser, S.M. (2013). The formation and sequestration of heterochromatin during development: delivered on 7

September 2012 at the 37th FEBS Congress in Sevilla, Spain. The FEBS journal *280*, 3212-3219.
43. Meister, P., and Taddei, A. (2013). Building silent compartments at the nuclear periphery: a recurrent theme. Curr Opin Genet Dev *23*, 96-103.
44. Towbin, B.D., Gonzalez-Sandoval, A., and Gasser, S.M. (2013). Mechanisms of heterochromatin subnuclear localization. Trends Biochem Sci *38*, 356-363.
45. Kranz, A.L., Jiao, C.Y., Winterkorn, L.H., Albritton, S.E., Kramer, M., and Ercan, S. (2013). Genome-wide analysis of condensin binding in Caenorhabditis elegans. Genome biology *14*, R112.
46. Hodgkin, J. (1980). More sex-determination mutants of Caenorhabditis elegans. Genetics *96*, 649-664.
47. Dawes, H.E., Berlin, D.S., Lapidus, D.M., Nusbaum, C., Davis, T.L., and Meyer, B.J. (1999). Dosage compensation proteins targeted to X chromosomes by a determinant of hermaphrodite fate. Science *284*, 1800-1804.
48. Bessler, J.B., Andersen, E.C., and Villeneuve, A.M. (2010). Differential localization and independent acquisition of the H3K9me2 and H3K9me3 chromatin modifications in the Caenorhabditis elegans adult germ line. PLoS Genet *6*, e1000830.
49. Jack, A.P., Bussemer, S., Hahn, M., Punzeler, S., Snyder, M., Wells, M., Csankovszki, G., Solovei, I., Schotta, G., and Hake, S.B. (2013). H3K56me3 is a novel, conserved heterochromatic mark that largely but not completely overlaps with H3K9me3 in both regulation and localization. PLoS One *8*, e51765.
50. Custer, L.M., Snyder, M.J., Flegel, K., and Csankovszki, G. (2014). The onset of C. elegans dosage compensation is linked to the loss of developmental plasticity. Developmental biology *385*, 279-290.
51. Therizols, P., Illingworth, R.S., Courilleau, C., Boyle, S., Wood, A.J., and Bickmore, W.A. (2014). Chromatin decondensation is sufficient to alter nuclear organization in embryonic stem cells. Science *346*, 1238-1242.
52. Bauer, C.R., Hartl, T.A., and Bosco, G. (2012). Condensin II promotes the formation of chromosome territories by inducing axial compaction of polyploid interphase chromosomes. PLoS genetics *8*, e1002873.
53. Buster, D.W., Daniel, S.G., Nguyen, H.Q., Windler, S.L., Skwarek, L.C., Peterson, M., Roberts, M., Meserve, J.H., Hartl, T., Klebba, J.E., et al. (2013). SCFSlimb ubiquitin ligase suppresses condensin II-mediated nuclear reorganization by degrading Cap-H2. The Journal of cell biology *201*, 49-63.
54. Iwasaki, O., Corcoran, C.J., and Noma, K.I. (2015). Involvement of condensin-directed gene associations in the organization and regulation of chromosome territories during the cell cycle. Nucleic Acids Res.
55. Csankovszki, G., McDonel, P., and Meyer, B.J. (2004). Recruitment and spreading of the C. elegans dosage compensation complex along X chromosomes. Science *303*, 1182-1185.
56. McDonel, P., Jans, J., Peterson, B.K., and Meyer, B.J. (2006). Clustered DNA motifs mark X chromosomes for repression by a dosage compensation complex. Nature *444*, 614-618.

57. Ercan, S., Giresi, P.G., Whittle, C.M., Zhang, X., Green, R.D., and Lieb, J.D. (2007). X chromosome repression by localization of the C. elegans dosage compensation machinery to sites of transcription initiation. Nature genetics *39*, 403-408.
58. Solovei, I., Wang, A.S., Thanisch, K., Schmidt, C.S., Krebs, S., Zwerger, M., Cohen, T.V., Devys, D., Foisner, R., Peichl, L., et al. (2013). LBR and lamin A/C sequentially tether peripheral heterochromatin and inversely regulate differentiation. Cell *152*, 584-598.
59. Zuleger, N., Boyle, S., Kelly, D.A., de las Heras, J.I., Lazou, V., Korfali, N., Batrakou, D.G., Randles, K.N., Morris, G.E., Harrison, D.J., et al. (2013). Specific nuclear envelope transmembrane proteins can promote the location of chromosomes to and from the nuclear periphery. Genome Biol *14*, R14.
60. Helbling-Leclerc, A., Bonne, G., and Schwartz, K. (2002). Emery-Dreifuss muscular dystrophy. Eur J Hum Genet *10*, 157-161.
61. Brenner, S. (1974). The genetics of Caenorhabditis elegans. Genetics *77*, 71-94.
62. Nabeshima, K., Mlynarczyk-Evans, S., and Villeneuve, A.M. (2011). Chromosome painting reveals asynaptic full alignment of homologs and HIM-8-dependent remodeling of X chromosome territories during Caenorhabditis elegans meiosis. PLoS genetics *7*, e1002231.

CHAPTER 4

An H4K16 histone acetyltransferase mediates decondensation of the X chromosome in *C. elegans* males

This chapter will be submitted soon with authors Lau AC, Zhu KP, Brouhard EA, and Csankovszki G as "An H4K16 histone acetyltransferase mediates decondensation of the X chromosome in *C. elegans* males." I conducted the experiments and analysis for all data shown aside from Figure 4.10.

ABSTRACT

In *C. elegans*, in order to equalize gene expression between the sexes and balance X and autosomal expression two steps are believed to be required. First, an unknown mechanism is hypothesized to upregulate the X chromosome in both sexes. This mechanism balances the X to autosomal expression in males, but creates X overexpression in hermaphrodites. Therefore, to restore the balance, hermaphrodites downregulate gene expression two-fold on both X chromosomes. While many studies have focused on X chromosome downregulation, the mechanism of X upregulation is not known. To gain more insight into X upregulation, we studied the effects of chromatin condensation and histone acetylation on gene expression levels in male *C. elegans*. We have uncovered that the H4K16 histone acetyltransferase MYS-1/Tip60 mediates

dramatic decondensation of the male X chromosome as measured by FISH. However, RNA-seq analysis revealed that MYS-1 contributes only slightly to upregulation of gene expression on the X chromosome. We find *in vivo* evidence decoupling H4K16 histone acetyltransferase mediated chromosome-wide decondensation from gene expression regulation. The X chromosome is more sensitive to MYS-1-mediated decondensation than the autosomes, despite similar levels of H4K16ac on all chromosomes, as measured by ChIP-seq. However, the distribution of H4K16ac is slightly different on the X compared to autosomes, and we find more peaks in intergenic regions, which may contribute to chromatin decondensation without affecting gene expression. These results indicate that H4K16ac and chromosome decondensation influence regulation of the male X chromosome, however other mechanisms must also play a role to achieve high levels of gene expression.

AUTHOR SUMMARY

Dosage compensation is a mechanism that occurs in organisms where females have two X chromosomes and males only have one. By altering gene expression levels on the X chromosomes, dosage compensation balances gene expression between the sexes. Disrupting dosage compensation leads to lethality in the affected sex. In the nematode *C. elegans*, dosage compensation is thought to be a two-step process. First, an unknown mechanism is hypothesized to upregulate X expression in both sexes, then a second, and better understood, mechanism downregulates gene expression by half on hermaphrodite X chromosomes. Chromosome condensation levels are generally believed to correlate with gene expression levels, with highly expressed chromosomal

regions being more decondensed than silent chromosomal regions. Here we analyze the role of chromosome condensation in X upregulation in males. Specifically, we show the chromatin modification involved in decondensing and upregulating the male X chromosomes in flies, also decondenses the X chromosome in male nematodes, but its influence on gene regulation is more modest. Therefore, we present evidence decoupling chromosome-wide decondensation from gene expression regulation. These data may shed further light on the relationship between chromosome condensation levels and gene expression regulation.

INTRODUCTION

In many organisms, sex is determined by a XY-based system, where females are homogametic (XX) and males are heterogametic (XY). The resulting difference in sex chromosome number is corrected by modulating gene expression levels chromosome-wide in a process called dosage compensation. According to Ohno's hypothesis, dosage compensation has to balances both X and autosomal (A) expression levels within one sex as well as gene expression between the sexes [1]. Dosage compensation strategies differ among species. *Drosophila* males upregulate their single X chromosome by a factor of two, leading to both an X:A gene expression balance in males and an equalization of X linked gene expression between the sexes [2,3]. Although controversial, some experimental evidence indicates that X upregulation also occurs in mammals and *C. elegans*; but in both sexes [4-9]. This upregulation balances X:A expression in males, however causes X overexpression in mammalian females and *C. elegans* hermaphrodites. To avoid X hyperexpression, mammalian females silence

one X chromosome by X inactivation [10-12], while hermaphrodite *C. elegans* worms repress both X chromosomes two-fold [13-15]. In *C. elegans* hermaphrodites, the dosage compensation complex (DCC) localizes to both X chromosomes to achieve the two-fold downregulation of X-linked gene expression. DCC localization leads to X chromosome compaction [16], as well as enrichment of H4K20me1 and the depletion of H4K16ac on the X chromosomes [17,18].

Although Ohno hypothesized the existence of an X-upregulation mechanism in 1967 [1], it was not until recently that evidence has emerged to support the idea in both mammals and *C. elegans*. Microarray analysis in mammalian tissues and *C. elegans* show that in both sexes X-linked genes are expressed at nearly the same levels as autosomal genes, rather than at half the average autosomal level supporting the idea of X-upregulation in both males and females/hermaphrodites [6,7,19]. Initial analysis of RNA-seq data did not find evidence for X-upregulation, showing that the average X-linked gene expression was roughly half that of the autosomal average [20]. However, more recent studies argued that the upregulation of X-linked genes is supported by RNA-seq data in mammals, *C. elegans* and *Drosophila* when considering the effects of the skewed gene content and regulation of the X chromosome [5,8]. RNA-seq in different nematode species found evidence both for and against X-upregulation. When excluding germline-repressed genes, all chromosomes showed equivalent levels of gene expression in both males and females/hermaphrodites, supporting the X-upregulation hypothesis. However, when comparing the expression of one-to-one orthologs located on the X in one species and the autosome in another, the autosomal

ortholog was more highly expressed, arguing against X-upregulation [21]. Furthermore, global run on sequencing analysis (GRO-seq) of active transcription in wild type *C. elegans* hermaphrodites showed that on average, X-linked genes have engaged RNA polymerase II levels comparable to autosomal genes. This implies that the DCC downregulates transcription on the X chromosomes to the level of the autosomes and not to half the level of autosomes. In hermaphrodites lacking dosage compensation, the X chromosomes have higher levels of engaged RNA Pol II compared to autosomes. Suggesting that in the absence of X chromosome downregulation, the X chromosomes are indeed highly expressed [22]. A recent study proposed that in *C. elegans* males, the single X chromosome interacts with nuclear pore proteins to achieve upregulation, though gene expression analysis was not performed [23]. Overall, evidence suggests that, in the absence of the DCC, on average, X-linked genes in *C. elegans* are expressed at a higher level than autosomal genes. However, whether this high level of gene expression is achieved by a chromosomal wide regulatory mechanism, or on a gene-by-gene basis, remains unknown.

In *Drosophila*, X-upregulation is male specific and is achieved by the male specific lethal (MSL) complex. The MSL complex binds to the male X chromosome, which leads to increased levels of H4K16ac by the MYST family histone acetyltransferase (HAT) MOF, as well as enhanced transcription [24,25]. H4K16ac decondenses the male X chromosome by weakening nucleosome packing in the chromatin fiber [26]. We recently showed that the male X chromosome is significantly decondensed in male *C. elegans* as well. Since X-repression in hermaphrodites is

accompanied by chromosome condensation [16], we hypothesized that X decondensation may accompany upregulation in males, as in flies. In this paper we report that the H4K16ac HAT, MYS-1, is also a key factor in regulating the architecture of the *C. elegans* male X chromosome. In contrast to the MYST protein MOF/KAT8/Sas2, the global H4K16 histone acetyltransferase in most organisms [27-30], we find that in *C. elegans* H4K16ac is mediated by the activity of a different MYST family histone acetyltransferase, the homolog of Tip60, MYS-1. Interestingly, while the lack of MYS-1 activity dramatically changes the compaction of the X chromosomes, these structural changes appear to be partially independent of transcription. In animals depleted of MYS-1, gene expression changes are biased toward the X chromosome, but are relatively modest. We propose that MYS-1/Tip60 mediated H4K16ac is a key factor in *C. elegans* male X decondensation and that it possible to decouple chromosome-wide decondensation from changes in transcription.

RESULTS

MYS-1 activity mediates X chromosome decondensation in males

We previously reported that the male X chromosome territory is significantly more decondensed in comparison to hermaphrodite Xs [16]. We used a 3D chromosome painting technique: fluorescence *in situ* hybridization (FISH), to visualize and measure the volumes of chromosome X and I territories, as described previously [16]. In hermaphrodites, X chromosome DNA takes up 18% of the genome, yet X chromosome territories are compact and occupy only 10% of the nuclear volume due to DCC-mediated compaction. By contrast, in males the single X represents 10% of the

genome, whereas it occupied a significantly larger percentage than the combined percent occupancy by both X chromosomes in hermaphrodite nuclei (Figure 4.1A and B, [16,31]). On the other hand, chromosome I volumes for both hermaphrodites and males are closely correlated to the DNA content of chromosome I (14-16%) (Figure 4.1D and E, [16]). These results indicate that the X chromosome in males is more decondensed than in hermaphrodites or what would be predicted based on DNA content.

To search for factors that might lead to decondensation of the male X chromosome, we tested the role of histone acetyltransferases (HATs). Acetylation of histones correlates with chromatin decondensation [32], and H4K16ac is known to be involved in X chromosome upregulation and decondensation in male *Drosophila* [24-26]. Therefore, we performed the same 3D chromosome FISH technique in male worms carrying mutations in or depleted of different histone acetyltransferases (HATs), MYS-1, MYS-2, MYS-4, and CBP-1. MYS-2 is the closest homolog of MOF [33], the fly HAT responsible for H4K16ac on the male X. MYS-1 and MYS-4 are other MYST family histone acetyltransferases [33], and CBP-1 is an unrelated HAT, the homolog of mammalian CBP/p300 [34]. The X chromosome territory in males carrying mutations in, or depleted for MYS-1 by RNAi, occupied a significantly smaller percentage than in control males or males depleted of the other HATs (Figure 4.1A-C). In control male worms, X chromosome territories were decondensed with a mean percent nuclear volume of 15.74±2.01%, while in *mys-1(n4075)* mutant males the X chromosome occupied 9.87±1.97% of the nucleus ($p = 5.76E-13$), close to the value predicted based

on DNA content [16,31] (Figure 4.1A and B). Similar results were seen in male worms depleted of MYS-1, with the X chromosome occupying 9.71±2.68% of the nucleus compared to the 14.85±2.79% in control males fed bacteria carrying an empty vector (p = 6.01E-14). The depletion of other HATs, MYS-2, MYS-4 and CBP-1, showed no significant change in X chromosome territories compared to control males, occupying 14.33±3.39%, 14.41±2.93%, and 14.64±3.01% respectively (Figure 4.1C and Figure 4.9). Additionally, chromosome I remained unaffected in *mys-1(n4075)* mutants and in males depleted MYS-1, MYS-2, MYS-4, and CBP-1, with a mean volume of consistently around 14% in all backgrounds (Figure 4.1D-F and Figure 4.9). These results suggest that MYS-1 activity is required for X chromosome decondensation in males and that this activity disproportionately affects the X chromosome compared to autosomes.

Putative worm Tip60/NuA4 complex members mediate male X chromosome decondensation.

MYS-1 is the *C. elegans* homolog of MYST family HAT Tip60, but also more distantly related to another MYST HAT, MOF, the HAT subunit of MSL and NSL complexes [33]. To determine whether MYS-1 acts in the context of a Tip60/NuA4-like complex, MOF-MSL-like complex, or MOF-NSL-like complex, we examined other putative members of these complexes. We found that only the depletion of Tip60/NuA4-like complex homologs altered X chromosome territories. Similar to *mys-1(RNAi)* males, males depleted of MRG-1 (homolog of MRG15) or SSL-1 (homolog of Domino) showed loss of X chromosome decompaction, with X chromosome territories occupying 11.08±2.86% (p = 3.28E-10), 10.40±2.67% (p = 2.17E-13), and 11.12±2.86% (p =

5.07E-10) respectively (Figure 4.1C and Figure 4.9). Similarly, in *ssl-1(n4077)* mutant males, the X chromosome territory occupied a mean percent nuclear volume of 9.83±2.38% (p = 6.72E-12) (Figure 4.1B). However, when depleting RHA-1 (homolog of MOF-MSL subunit MLE) (14.42±2.83%), or WRD-5.1 (homolog of WDS) (14.68±2.59%) and C16A11.4 (homolog of MBD-R2) (14.66±2.64%), we do not see a loss of decondensation compared to control males (14.85±2.79%) (Figure 4.1C and Figure 4.9). Chromosome I was unaffected in all backgrounds (Figure 4.1D-F and Figure 4.9). These results suggest that members of a putative Tip60/NuA4-like complex may work together to decondense the X chromosome in males.

The Tip60 complex in other organisms plays many roles, including cell cycle regulation and DNA repair [35]. Consistent with that, *mys-1* and *ssl-1* mutant males and hermaphrodites are sickly, and while maternal contribution of wild type protein and/or RNAi allows the hermaphrodites to survive to the adulthood, they do not produce viable progeny. In the case of *mys-1* and *ssl-1* mutant males, the maternal contribution of wild type protein and/or RNAi only allows them to survive to late larval/young adult stage and appear more sickly compared to hermaphrodites. This is consistent with MYS-1 playing general roles in both sexes but also having an additional function in males.

Distance measurements confirm Tip60 mediated decondensation of the male X

To confirm the X decondesation phenotype using a different assay, we performed 3D FISH with pairs of X chromosome YAC probes separated by a genomic distance of 1.2 Mb (Figure 4.2A), the genomic distance where we previously found the most significant differences in control and DCC mutant hermaphrodites [16]. We analyzed this

pair of probes in control male and *mys-1(RNAi)* male hypodermal nuclei, hyp7 cells. These hypodermal cells are tetraploid, therefore we expected to see two spots for each X-linked probe [36]. We detected a significant decrease in loci distance in *mys-1(RNAi)* males compared to control males, with the median distance of 1.06 μm between loci in the control males and a median distance of 0.67 μm in *mys-1(RNAi)* males (p = 1.51E-4) (Figure 4.2B and C). This less dispersed distribution of the two loci found in *mys-1(RNAi)* males correlates with the compact X chromosomes found in the males mutated or depleted of the putative worm Tip60/NuA4 complex members.

MYS-1 acetylates H4K16

Tip60 is known to acetylate H2AK5 and H4K5, K8, K12, and K16 *in vitro* [37-39]. To determine what histone marks depend on MYS-1 activity *in vivo* in *C. elegans*, we performed a combination of immunofluorescence microscopy (IF) and western blot analysis with antibodies specific for different histone marks in wild type and *mys-1(RNAi)* or *mys-1(n4075)* mutant worms. First, we tested H4K16ac because of its known role in X upregulation and decondensation in flies [24-26]. Indeed, mutations or depletion of MYS-1 led to greatly reduced levels of H4K16ac by IF and western blot analysis. Whereas other acetylation marks on H2A, H3, or H4 showed no reduction. We also found that mutations in *mys*-2, the closest homolog of the *Drosophila* H4K16ac HAT MOF, led to no reduction in H4K16ac compared to wild type (Figure 4.10). These results suggest that MYS-1 is the major H4K16 HAT in *C. elegans*. Interestingly, H3K14ac and H3K56ac levels increase in MYS-1 mutants compared to wild type, perhaps as part of a compensatory mechanism for the loss of H4K16ac. Overall, these

data suggest that similar to *Drosophila*, H4K16ac may be a key mediator in *C. elegans* X chromosome decondensation.

The X chromosome of XO hermaphrodites phenocopies the male X

To test whether it is the male (XO) karyotype or the male physiology that drives X decondensation, we examined a mutant strain, *her-1(e1520)*; *sdc-2(y74)*. This strain is karyotypically male (XO), but is transformed into a hermaphrodite by a genetic mutation in the male sex determination pathway [40]. Similar to males, MYS-1 mediated X chromosome decondensation is evident in XO hermaphrodites. X chromosome territories were decondensed in *her-1(e1520)*; *sdc-2(y74)* mutants occupying a mean percent of 15.42±2.49%, while X chromosome decondensation was lost in *her-1(e1520)*; *sdc-2(y74)* mutants depleted of MYS-1, with X chromosome territories occupying a mean percentage of 9.43±3.02% ($p = 3.89E-8$). This change in chromatin volumes was X-specific, with chromosome I occupying a mean percent of 14.65±2.42% and 14.11±2.57%, in *her-1(e1520)*; *sdc-2(y74)* mutants and *her-1(e1520)*; *sdc-2(y74)* mutants depleted of MYS-1 respectively (Figure 4.11). We demonstrate that *her-1(e1520)*; *sdc-2(y74)* hermaphrodites (hereinafter referred to as XO hermaphrodites) have the same X chromosome phenotypes as males. It is the male karyotype, not male physiology, that drives X decondensation. Since it is not possible to grow a large pure population of males, insead we used XO hermaphrodites in many subsequent experiments, because we are able to grow large pure populations of XO hermaphrodites.

X compaction and decondensation is initiated at the same time in development

We next wanted to determine the developmental timing of DCC-mediated X compaction in hermaphrodites and MYS-1-mediated X decondensation in males. We examined the X chromosomes in hermaphrodite and male embryos at different developmental stages. We found that in both hermaphrodite and male early stage embryos, the X chromosome volume was similar to what is expected based on DNA content. X chromosome compaction in hermaphrodites occurs gradually between the 20-75-cell embryo stage (Figure 4.3A and B). Nuclei in a 9-cell embryo have decondensed X chromosomes occupying 16.95±3.22% whereas nuclei in a 30-cell embryo have more condensed X chromosomes occupying 13.45±3.16%. At the 76-cell stage nuclei have compact X chromosomes occupying 11.42±2.34% consistent with X chromosome volume in adult wild type hermaphrodite intestinal nuclei or tail tip hypodermal cells [16]. In males we found the onset of X decondensation occurs more abruptly, but close to the time when X condensation begins in hermaphrodites, between the 25-40-cell stage (Figure 4.3A and C). Nuclei in a 25-cell male embryo have a compact X chromosome occupying 10.10±1.17%, while nuclei in a 40-cell or 56-cell embryo have a decondensed X chromosome occupying 13.74±2.69% and 14.49±2.52% respectively. These results indicate that X compaction in hermaphrodites and X decondensation in males occur around the same time in development. The fact that young male embryos have condensed X chromosomes may explain why X decondensation was not seen in males in a previous study [23]. Interestingly, the onset of X decondensation is in the same time window when zygotic transcription of a

significant number of X-linked genes is initiated [41]. The timing also coincides with DCC localization to the X in hermaphrodites, which begins at the 30-50-cell stage [42,43], and the stage when DCC-mediated repression becomes measurable by RNA-seq analysis [44]. These results suggests that changes in chromatin compaction may be related to changes in gene expression.

Transcription is not required for the initiation or maintenance of X decondensation

The observation that the timing of X decondensation coincides with the onset of X-linked gene transcription [41] (Figure 4.3) which suggests that transcription drives decondensation. Indeed, in mammals, inhibition of transcription did lead to increased compaction chromosome-wide, both for an autosome [45], or for the active X chromosome [46]. To test this hypothesis, we examined worms depleted of AMA-1, the large subunit in RNA polymerase II. Lack of zygotic transcription due to AMA-1 depletion causes embryonic lethality by 100-cell stage [47]. To test whether transcription is required for the initiation of X chromosome decondensation, we examined X chromosome territories in XO hermaphrodite embryos of different developmental stages, treated with control vector or *ama-1* RNAi. AMA-1 depletion was effective, as high embryonic lethality was evident. However, H4K16ac levels did not decrease (Figure 4.4A). The onset of X chromosome decondensation occurs between the 25-40-cell stage in XO hermaphrodites (Figure 4.4B), similar to that was observed in males (Figure 4.3). However, when transcription is severely reduced in XO hermaphrodites depleted of AMA-1, X decondensation still occurs between the 25- to 40-cell stage

(Figure 4.4B). These results suggest that the normal levels of transcription are not required for H4K16ac and for the initiation of X decondensation; therefore decondensation is not simply a consequence of high levels of transcriptional activity.

To test if continued transcription is needed to maintain decondensed X chromosome territories in adult worms, we fed L1 stage males AMA-1 RNAi and empty vector, and compared these worms once they reached young adulthood. AMA-1 depletion was effective, as the fed hermaphrodites lay dead embryos. The X chromosome territories in adult males depleted of AMA-1 showed no significant difference compared to the X chromosome territories in control males (Figure 4.4C). The X chromosome territory occupied a mean percent nuclear volume of 15.45±2.20% in control males and 15.05±3.11% in *ama-1(RNAi)* males. This finding suggests that the continued high levels of transcription are not required for the maintenance of male X chromosome decondensation.

H4K16ac is uniformly distributed in the nucleus

To examine whether the greater sensitivity of the male X to the loss of H4K16ac is reflected in higher levels of H4K16ac on the chromosome, we investigated the distribution of this mark genome-wide. We have previously shown by immunofluorescence that H4K16ac levels are depleted on the X chromosome in wild type XX animals due to dosage compensation, but not in XO males [18]. To further study H4K16ac binding at higher resolution, we performed ChIP-seq analysis of H4K16ac in wild type XX hermaphrodites and XO hermaphrodites. Using single-end sequencing we could uniquely align 78-92% of the 18-28 million reads to the genome,

for three replicates in each background. After normalization, the ratio of the fraction of reads that mapped to the X chromosome divided by the X chromosome genome fraction was 0.33 in XX hermaphrodites and 1.01 in XO hermaphrodites, mirroring previous immunofluorescence data [18]. To examine the peak distribution of H4K16ac, we plotted the chromosomal distributions of H4K16ac ChIP regions (Figure 4.5A). Consistent with what was previously seen by immunofluorescence, there were fewer H4K16ac peaks on the X compared to the autosomes, and the fraction of H4K16ac peaks on the X are significantly less than the fraction of the genome found on the X chromosome in XX hermaphrodites. In XO hermaphrodites, the distribution of H4K16ac on the X chromosome is almost equivalent to the genome fraction, consistent with lack of DCC-mediated reduction of H4K16ac in this background. However, H4K16ac does not appear to be more highly distributed on the X chromosome compared to the autosomes in XO hermaphrodites. Representative genome browser views of ChIP-seq scores for H4K16ac were used to visualize signal intensities of H4K16ac peaks (Figure 4.5B). H4K16ac binding across the X chromosome is underrepresented compared to autosomes in XX animals, whereas X and autosomal signal intensities are similar in XO hermaphrodites. Additionally, H4K16ac binding sites and intensities are similar across the autosomes in both XX and XO hermaphrodites. On the X chromosome, H4K16ac is enriched in XO hermaphrodites compared to XX hermaphrodites. These results suggests, that despite greater sensitivity to MYS-1 activity in terms of chromosome condensation, the X chromosome of XO animals overall does not have higher levels of H4K16ac.

Next, we examined H4K16ac levels around the annotated genes to determine whether differences can instead be seen in transcribed regions. It has been previously reported in mouse embryonic stem (ES) cells and human CD4+T cells that H4K16ac peaks are seen around the transcription start site (TSS) [48-50]. In flies, H4K16ac is found at the TSS and accumulates towards the 3' end of coding regions on the single male X, whereas on autosomes and in females H4K16ac is detected only at the promoters [51-54]. To examine the global profile of H4K16ac on transcribed regions, we created normalized z-scores for regions across gene bodies and extending 1 kb upstream of the TSS and 1 kb downstream of the transcription termination site (TTS). Metagene profiles derived from an average of all genes in the genome showed that H4K16ac levels on X and autosomal-linked genes peak near the TSS in both XX and XO hermaphrodites. In XX animals H4K16ac levels around transcribed regions are depleted on the X-linked genes compared to autosomal genes. Whereas in XO hermaphrodites H4K16ac levels on the X chromosome are almost equivalent to the average autosomal levels around transcribed regions (Figure 4.5C). When examining chromosomes separately, X-linked genes on average have lower levels of H4K16ac compared to all autosomes in XX animals (Figure 4.5D). In XO hermaphrodites, H4K16ac levels are enriched on the X compared to chromosome V however in comparison to the other autosomes, the levels of H4K16ac on the X are nearly equivalent (Figure 4.5E). These results suggest that H4K16ac is not enriched on X-linked genes compared to the autosomal genes in XO hermaphrodites, and differences

in H4K16ac levels in genic regions is not the cause of the observed X-specific decondensation.

To get an overview of the fraction of X and autosomal binding across the genomic regions, we characterized H4K16ac binding regions into four categories: promoter, exon, intron and intergenic. Relative to autosomes, the X chromosome has a higher fraction of H4K16ac peaks located in the intergenic regions in both XX animals and XO hermaphrodites (Figure 4.5F). In XX hermaphrodites the DCC initially binds to both X chromosomes via sequence-specific recruitment on X (*rex*) sites. These sites are often found in intergenic regions and many coincide with boundaries between topologically associating domain (TAD) boundaries. Long-range interactions between rex sites are proposed to reshape X chromatin structure [55]. This led us to investigate H4K16ac binding surrounding *rex* sites in XX and XO hermaphrodites. We examined *rex* sites at TAD boundaries that have the strongest *rex-rex* interactions as categorized by [55]. Genome browser views of ChIP-seq scores for H4K16ac revealed that in XX hermaphrodites, H4K16ac is absent in the region surrounding *rex* sites, while in XO hermaphrodites H4K16ac is often, but not present near *rex* sites (Figure 4.12). Although highly speculative, these observations suggest that the differences in H4K16ac binding patterns between the X and autosomes, perhaps at *rex* sites and at other intergenic sites, may contribute to the X specific decondensation.

MYS-1 activity is biased toward upregulation of X-linked genes

To analyze how gene expression levels are regulated on the X chromosome, we first performed mRNA-seq analysis and compared average gene expression levels of all

X and autosomal-linked genes in XX and XO hermaphrodites. In *C. elegans*, it is difficult to compare X and autosomal expression levels in whole adult worms due to X chromosome silencing in germ cells by a process unrelated to dosage compensation [56]. Our data comes from L3 animals, which have approximately 100 germ cells and 700 somatic cells [57]. Therefore RNA levels should be dominated by somatic gene expression. Consistent with previous data, we observed a median X:A expression ratio of 0.88 in wild type XX animals and 0.86 in XO hermaphrodites (Figure 4.6A) [5,20]. These values are significantly higher than 0.5, which would be expected if the X chromosomes are expressed at the same level as autosomes in XO hermaphrodites, and are subjected to DCC-mediated repression in XX hermaphrodites. To exclude the small contribution of germline-expressed genes, we followed previous methods of limiting analysis to only highly expressed genes [21]. Overall gene expression levels of highly expressed genes are similar between X and autosomes with the median X:A ratio of 1.01 and 1.00 for XX and XO hermaphrodites respectively (Figure 4.6A). This data is consistent with previous observations [5,6,21] that X-linked genes, on average, are more highly expressed than autosomal genes in XO animals.

In order to study effects of MYS-1 on X chromosome expression, we analyzed gene expression changes in L3 stage MYS-1 depleted XO hermaphrodites by RNA-seq analysis. X-linked genes that are upregulated in XO animals should be the same genes that are repressed by the DCC in XX animals. Therefore, to be able to compare the genes affected by MYS-1 in XO worms to the genes affected by DCC-mediated repression in XX animals, we also analyzed *dpy-21(e428)* mutant XX hermaphrodites.

DPY-21 is a non-condensin protein member of the DCC. These null mutants (*e428*) are viable, however dosage compensation function is disrupted [58]. At the L3 stage, *dpy-21(e428)* mutation caused X chromosome derepression, and we observed an increase in average X-linked gene expression compared to gene expression changes on autosomes. The median $\log_2$ ratio of expression between *dpy-21(e428)* worms and wild type XX hermaphrodites was significantly higher on the X (0.447) compared to autosomes (-0.080) and compared to each chromosome (Figure 4.7B, one-sided Wilcoxon rank-sum test $p < .001$). These results are similar to previously reported data of dosage compensation mediated gene expression changes [44,55,59]. To test how MYS-1 effects gene expression in XO hermaphrodites, we depleted MYS-1 by RNAi (Figure 4.13). Contrary to the X chromosome derepression found in *dpy-21(e428)* hermaphrodites, but consistent with role for MYS-1 in X upregulation, depleting MYS-1 in XO hermaphrodites caused a small decrease in the average expression levels of X-linked genes. We detected a very small decrease in average X-linked gene expression relative to gene expression changes on autosomes. The median $\log_2$ ratio of expression between *mys-1(RNAi)* XO hermaphrodites and control XO hermaphrodites was significantly lower on the X (-0.021) compared to autosomes (-0.008) and compared to each chromosome (Figure 4.6B, one-sided Wilcoxon rank-sum test $p < .05$). Thus, MYS-1 contributes to the observed higher level of gene expression on the X chromosome in XO hermaphrodites, but the effects are minor. To determine whether MYS-1 contributes to upregulation of the same set of genes as are repressed by the DCC, we plotted the $\log_2$ ratio of expression of *mys-1(RNAi)* XO hermaphrodites and

control XO hermaphrodites against the $\log_2$ ratio of expression of *dpy-21(e428)* mutants and wild type XX hermaphrodites. A larger subset of X-linked genes (24% verses 2-12% for genes in other quadrants) were both derepressed in *dpy-21(e428)* mutants and had reduced expression in *mys-1(RNAi)* XO hermaphrodites, whereas autosomal genes did not show such an effect (Figure 4.6C). Additionally, the X-linked genes that are most affected by the DCC in hermaphrodites are also more highly upregulated in XO hermaphrodites by MYS-1. The top 5%, top 10%, and top 15% of highly differentially expressed X-linked genes identified in *dpy-21(e428)* mutants are also more highly differentially expressed in *mys-1(RNAi)* XO hermaphrodites (Figure 4.6D). We conclude that MYS-1 activity causes a mild upregulation of X-linked genes and that the genes most affected by lose of dosage compensation in *dpy-21(e428)* mutants are also the genes whose expression is most upregulated by MYS-1 in XO hermaphrodites. However, MYS-1 activity alone does not explain the significantly higher level of gene expression on the X chromosome of XO animals. These findings also indicate the effects of MYS-1 on chromosome condensation and on gene expression regulation can largely be decoupled.

Similar correlations of H4K16ac and gene expression on the X and autosomes

We next wanted to compare the relationship between H4K16ac binding and gene expression on the X to the relationship on autosomes. We generated H4K16ac profiles for gene bodies for X and autosomal-linked genes subdivided by quartiles of expression. In both XX and XO hermaphrodites, regardless of whether they were X-linked genes or autosomal genes, H4K16ac positively correlated with gene expression (Figure 4.7A),

consistent with the patterns of H4K16ac previously reported in mouse ES cells and human CD4+T cells, and with the involvement of H4K16ac in transcriptional activation [48-50]. We note, however, that the top two quartiles had essentially identical levels of H4K16ac on the X chromosome, suggesting that the most highly expressed genes on the X do not have exceptionally high levels of H4K16ac. We then plotted the average ChIP score within 500 bp upstream of the TSS against the RNA levels of X and autosomal genes for pairwise comparisons between H4K16ac binding and gene expression (Figure 4.7B and C). We found slight dependencies between H4K16ac and gene expression, consistent with an overall correlation between the two. However, overall X and autosomal genes have similar relationships between H4K16ac and transcription.

Lastly, to determine whether the genes whose expression is most affected by loss of MYS-1 activity have higher levels of H4K16ac, we examined the top 15% downregulated X-linked genes in *mys-1(RNAi)* XO hermaphrodites and X-linked genes that were not differentially expressed. We found that the levels of H4K16ac were similar in these two groups, suggesting there is no correlation between regulation by MYS-1 and H4K16ac levels (Figure 4.7D). This observation is consistent with the interpretation that MYS-1 has large effects on chromosome condensation levels, but only small effects on gene expression.

DISCUSSION

In this study, we sought to investigate the relationship between X chromosome specific higher order structural changes and gene expression levels on the highly

expressed male X chromosome in *C. elegans*. According to Ohno's hypothesis, dosage compensation in *C. elegans* is achieved in two steps, X-upregulation in both sexes followed by the DCC-mediated repression of the X in hermaphrodites. While many studies have focused on X chromosome downregulation, it is currently unknown how high levels of gene expression on the male X chromosome are achieved. We established that male X chromosomes are significantly decondensed, relative to what would be predicted based on DNA content. This observation, and the generally held belief that chromatin decondensation and transcriptional activation correlate [60], raised the possibility that MYS-1 mediated X decondensation may be a key event in the X upregulation process. X chromosome decondensation requires the activity of members of a Tip60-like complex, including the histone acetyltransferase, MYS-1, the major H4K16 HAT in nematodes (Figure 4.8). Interestingly, H4K16ac levels are nearly equivalent on the X and autosomes in XO hermaphrodites; however they are more highly distributed in intergenic regions on the X, potentially contributing to the decondensation phenotype. When MYS-1 is depleted in XO hermaphrodites, gene expression on the X chromosome is repressed to a slightly greater degree than on autosomes. Together, our results suggest that MYS-1 mediated H4K16ac is a key factor in X decondensation and plays a modest role in X-upregulation in male *C. elegans*. Additionally, our data decouples H4K16 HAT-mediated decondensation from gene expression regulation *in vivo* on an endogenous chromosome.

MYS-1 is a MYST family histone acetyltransferase with specificity for H4K16

In most species, the major H4K16 histone acetyltransferase is MOF/KAT8/Sas2 [27-30]. However we find that MYS-1, homolog of histone acetyltransferase Tip60, is responsible for acetylating H4K16 in *C. elegans*. Both MOF and Tip60 are MYST family histone acetyltransferases. MYST proteins are defined by their catalytic MYST domain, which contains an acetyl-coenzyme A binding domain and a C2HC-type zinc finger. Additionally, MOF and Tip60 fall under the same subfamily of MYST proteins, sharing a similar chromodomain in addition to the MYST domain [33,35,61]. Although structurally similar, MOF and Tip60 have different biological functions. In yeast, mice and flies, the acetylation of H4K16ac mediated by MOF homologs is required for maintaining open chromatin structure [27,29,62,63]. Mammalian MOF mutant embryos have cells with abnormal chromatin morphology prior to undergoing death by apoptosis [62]. In flies, MOF can reduce negative supercoiling and weaken nucleosome packing, which causes chromatin decondensation [63-65]. In conjunction with regulating chromatin structure and morphology, MOF plays a role in gene regulation. The yeast MOF homolog Sas2 mediates H4K16ac and regulates the boundary between transcriptionally active and silent telomeric chromatin [17,66]. In *Drosophila*, MOF appears to be a global transcriptional regulator when acting in the NSL complex, which can acetylate H4K5, H4K8 and H4K16ac [67]. The MOF-NSL complex binds to a subset of active promoters and regulates housekeeping genes genome wide [68-70]. In addition to global transcription, MOF plays a specialized role in dosage compensation in flies and mammals. MOF hyperacetylates H4K16ac on the male X in flies [24] and MOF may

play a role in X uprgulation in mammals as well [5,7,8,19]. We show that in *C. elegans* H4K16ac plays a similar role in X chromosome decondensation, and gene regulation, although effects on gene regulation are minor. However, the H4K16ac HAT appears to be Tip60, rather than MOF. *C. elegans* homologs of the MOF-MSL complex members (other than RHA-1, distantly related to MLE) are lacking or have not been uncovered. MRG-1, the chromodomain protein related to MSL subunit MSL3, is more closely related to MRG15 (Tip60 complex subunit) than to MSL3 [71]. Therefore, *C. elegans* may not have a MOF-MSL-like complex, and instead uses a Tip60-like complex to acetylate H4K16.

In vitro, Tip60 can acetylate H2A (K5), H3 (K14), H4 (K5, K8, K12 and K16), as well as histone variants and non-histone proteins [38,72]. We found that MYS-1 is responsible for H4K16ac *in vivo*. Tip60 activity can also play a role in gene regulation; however, it contributes to both transcriptional activation and transcriptional repression [35]. Tip60, like MOF, binds to promoters of many genes in mammals, often with other HATs [49,73-75], consistent with a role in regulating transcription. However, Tip60 is better known for its global role in different cellular activities. It is a key regulator in cell cycle progression and DNA damage response, and has the ability to acetylate key transcription factors involved in cell growth, DNA damage and apoptosis, such as c-Myc and p53 [76,77]. In addition to acetylating these transcription factors, Tip60 can be recruited by these transcription factors to acetylate histones [78,79]. MYS-1, the *C. elegans* homolog of Tip60 has also been implicated in cell cycle regulation [80] and cell fate maintenance [81]. Overall, Tip60 is a protein that plays a role in several biological

processes by affecting the functions of different targets using its acetyltransferase activity as well as its protein-protein interactions. We find that the *C. elegans* homolog of Tip60, MYS-1, also functions in similar roles as the MYST HAT MOF. We postulate that in *C. elegans,* the MYS-1 complex may perform the function of both the Tip60 complex and the MOF complex, as has been suggested previously in fission yeast [82].

Chromosome decondensation, histone acetylation and gene expression

Chromatin decondensation and acetylation are thought to correlate with transcriptional activation [60]. An early study found that inhibiting transcription of the Balbani ring genes in polytene chromosome of dipteran insects caused the chromatin fibers to thicken and form condensed chromatin, illustrating a direct correlation between chromosome decondensation and transcription and suggests transcription precedes chromosome conformation [83]. In mouse ES cells, the induction of *HoxB* gene cluster expression was accompanied by an increase in active histone modifications and visible decondensation of the chromatin [84]. Studies of the β-globin loci have also provided evidence for the correlations between transcription and nucleosome modifications. In mice, humans and chickens, active β-globin loci are enriched in hyperacetylated H3 and H4, and H3K4me2, while the silent domain neighboring the chicken β-globin locus has hypoacetylated histones and H3K9me2 [85-87]. Additionally, *in vitro* studies have provided extensive evidence showing H4K16ac inhibits chromatin fiber compaction by weakening nucleosome-nucleosome interactions, which is thought to create a more permissive state for transcription [32,66,88,89]. A more global example of chromosome decondensation and gene expression regulation is evident in fly dosage compensation.

MOF-mediated acetylation decondenses the X chromosome which hyperactivates the single male X [24,25].

To further understand the relationships between histone acetylation and chromosome decondensation, we analyzed how H4K16ac affects X chromosome structure and X-linked gene expression. We observed that in mutant or MYS-1-depleted XO worms, the absence of MYS-1 activity compacts the single X chromosome and leads to decreased levels of X-linked gene expression. Although H4K16ac is uniformly distributed on the X and autosomes in XO animals, the loss of H4K16ac results in no detectable change in autosomal compaction. Therefore, H4K16ac and chromosome decondensation correlate on the X chromosome but not on the autosomes. Similar to what we see in autosomes, a recent study in mouse ES cells found that broad domains of histone acetylation are lost during ES cell differentiation, but result in no change in compaction [48]. We find increased levels of H3K14ac and H3K56ac in MYS-1 mutants compared to wild type worms. It is possible that the lack of condensation defects on the autosomes is due to these marks compensating for the loss of H4K16ac. This suggests that H4K16ac and chromatin compaction are not always correlated.

Interestingly, the X chromosome is more sensitive to MYS-1-mediated decondensation than autosomes (Figure 4.1), despite near equal levels of H4K16ac levels (Figure 4.5). We do find that H4K16ac is more concentrated on intergenic regions on the X compared to autosomes. Some intergenic regions, including *rex* sites at TAD boundaries, are known to influence X chromosome structure and their acetylation may contribute to decondensation of the X chromosome. Alternatively, the X chromosome

may be more sensitive to histone acetylation mediated changes in compaction due to its unique properties. For example, MNase-seq analysis in *C. elegans* has found that on average X-linked gene promoters have higher nucleosome occupancy compared to autosomal promoters [90]. In addition, the autosomes have two large heterochromatic regions associated with the nuclear lamina at their ends, while the X chromosome only has one such region [91]. Due to these and other differences, the X may respond differently to changes in acetylation levels than the autosomes.

In addition, our results largely decouple chromatin decondensation from changes in transcription. We find a greater degree of X chromosome compaction compared to change in X-linked gene expression in MYS-1 depleted XO worms, suggesting that chromatin compaction and gene expression do not necessarily correlate. Other studies have also shown that chromatin decondensation, histone acetylation and transcriptional activation are not always perfectly correlated. In the absence of transcriptional activation, chromatin decondensation is sufficient to alter nuclear organization in mouse ES cells [92], indicating that transcriptional activation and chromatin decondensation can act separately in mouse ES cells. Additionally, some mutant versions of acidic activator domains can induce chromatin decondensation without activating transcription, and they are thought to do so by recruiting HATs and chromatin modifying proteins [93]. Suggesting again that gene expression and decondensation can be decoupled. The increase in other acetylation marks may also be enough to compensate for the loss of H4K6ac to minimize gene expression changes.

Whether histone acetylation and chromatin decompaction are the cause or consequence of transcriptional activity is also debated. We find the male X chromosome decondenses at the same time as the onset of X-linked gene transcription, signifying that transcription may drive chromatin decondensation. However, when we deplete AMA-1, the large subunit of RNA Pol II, histone acetylation levels did not change, and decondensation was not disrupted. Therefore, MYS-1 is able to mediate male X chromosome decondensation even when transcription is severely reduced. These results are different from prior studies in which inhibition of transcription led to condensation of chromosome territories [45,46]. Overall, our results suggest that increased transcription and chromatin decondensation may create a permissive chromatin state, but they are not sufficient to cause transcriptional activation. Furthermore, high levels of transcription are not necessary for large-scale changes in chromatin compaction.

X-upregulation

Ohno hypothesized that X chromosome gene expression between the sexes must be balanced, as well as X to autosomal expression within a sex [1]. X upregulation is the mechanism that balances the X to autosomal gene expression in males. In *Drosophila*, X upregulation occurs in only males, whereas in mammals and *C. elegans* X upregulation is hypothesized to occur in both sexes. Whether this is accomplished by a chromosome-wide upregulatory mechanisms or instead by a gene-by-gene basis, remains unclear. Our study adds to the body of evidence concerning the regulation of the X chromosome, and uncovers both similarities and differences between nematodes

and other organisms. Our data shows that the *C. elegans* H4K16 HAT, MYS-1, is decondensing the male X chromosome (Figure 4.1), similar to what is observed on the fly male X [63]. *Mof* mutant mice [62] and ES cells [94] also exhibit abnormal chromatin condensation, although more globally, and not just limited to the X chromosome. It should be noted however; that in all cases, including our data, it is unclear whether the condensation defects are due to the lack of H4K16ac, or some other activity attributable to the HAT. Therefore, the H4K16 HAT appears to have major effects on chromatin condensation in many organisms. However, the H4K16 HAT in *C. elegans* appears to act in a Tip60-like complex, rather than a MOF-MSL-like complex.

In nematodes, MYS-1 contributes only slightly to the observed high levels of gene expression on the X chromosome in XO hermaphrodites. The effects of gene expression in *mys-1* depleted worms are minor, although they appear to be biased toward the X chromosomes (Figure 4.6). This result is very different from flies, where a mutation in *mof* causes a two-fold effect on gene expression on the X chromosome [24], but is comparable to the magnitude of the effect of *mof* depletion in mouse ES cells [4]. Again, compensation by other acetylation marks may contribute to the minimal effects on gene expression.

Because H4K16ac binding patterns and levels are similar on the X and the autosomes, we believe the MYS-1 activity affecting X-linked gene expression is also acting genome wide in *C. elegans*. When examining the relationship between H4K16ac and gene expression, we observe correlations similar to those found in CD4+T cells, undifferentiated ES cells, and early *C. elegans* embryos [48,50,95], with higher levels of

H4K16ac at the promoter and transcribed regions of highly transcribed genes. The correlations are similar on the X and autosomes, although the levels of H4K16ac are almost the same in the top two quartiles of expressed X-linked genes. Dependencies between H4K16ac and gene expression levels appear to be similar on the X and autosomes, but genes with similar expression levels can have widely different levels of H4K16ac.

Overall, although MYS-1 appears to be a key factor in *C. elegans* X chromosome regulation (at least at the level of chromosome condensation), there must be additional X-specific factors that affect gene regulation. In flies, it is believed that the active regions in the *Drosophila* genome associates with nuclear pore factors and are targeted to a special compartment [96]. A recent study in *C. elegans* males proposed that X upregulation is achieved through the interaction between the male X and nuclear pore proteins [23]. These, and other, X-specific factors may act along with MYS-1 activity to result in high levels of gene expression on the single male X.

Conclusions

Although the hypothesis of X upregulation has been around for several decades, it is not until recently that evidence emerged showing that the X chromosomes are in fact highly expressed in mice and worms. Our gene expression analysis is consistent with the highly debated hypothesis that X upregulation occurs in *C. elegans* males, as we see an X:A expression ratio much higher than 0.5. We show that a TIP60-like complex acetylates H4K16 and decondenses the X in *C. elegans* males, and we suggest that this decondensation contributes in part to the upregulation of gene

expression on the chromosome. H4K16ac is a key factor in male-specific X upregulation in *Drosophila* [24,25] and has been implicated in the same process in mammals [4], suggesting conservation of mechanisms. While the high degree of X compaction in MYS-1 mutants does not always lead to low gene expression, we do observe a decrease in X-linked expression. Thus, we also present the first endogenous chromosome-wide data decoupling the degree of decondensation from the level of gene expression change. Future studies will examine the additional factors that directly contribute to regulation of X-linked gene expression in males.

MATERIALS AND METHODS

Strains

All strains were maintained on NGM agar plates with *E. coli* (OP50) as a food source, using standard methods [97]. Strain include: N2 Bristol strain (wild type); TY4403 *him-8(e1489)* IV; MT13172 *mys-1(n4075)* V/nT1 [qIs51]; MT12963 *ssl-1(n4077)* III/eT1; VC1931 mys-2(ok2429)/hln1 [unc-101(sy241)] I; TY1072 *her-1(e1520)* V; *sdc-2(y74)* X; and EKM71 *dpy-21(e428)*.

RNA Interference

E. coli HT115 bacteria expressing double stranded RNA for *mys-1*, *mys-1, mys-4, cbp-1, mrg-1*, *ssl-1*, *pbrm*-1, *rha-1*, *wdr-5.1*, *c16A11.4*, *ama-1* or vector control (polylinker), were used for feeding RNAi using the Ahringer laboratory RNAi feeding library [98]. To obtain AMA-1 depleted adults, one generation feeding RNAi was performed as follows: L1-stage *him-8(e1489)* larvae were placed on plates seeded with *ama-1* or control RNAi bacteria and were grown to adulthood and examined. To obtain

AMA-1-depleted embryos, *her-1(e1520)* V; *sdc-2(y74)* X L3 stage larvae were placed on plates seeded with *ama-1* or control RNAi bacteria and grown to adulthood. The progeny (F_1 generation) embryos were examined. Two generation feeding RNAi (all other analysis) was performed as follows; P_0 adults from one generation feeding RNAi were transferred to new RNAi plates to produce progeny for 24 hours. These progeny (F_1 generation) were grown to adulthood and examined.

Fluorescence *in situ* hybridization (FISH)

To generate FISH probe templates, purified yeast artificial chromosome (YAC) DNA were amplified by degenerate oligonucleotide primed PCR [99,100]. The labeled chromosome-paint probes were prepared and FISH was preformed as previously described [16,100].

Microscopy and Image Analysis

Detailed description of image analysis was previously described [16]. To summarize: masks (intensity threshold value) were applied over an image to distinguish real signal from background for all nuclei for each channel. DAPI mask was used as the total volume of the nucleus. The percent nuclear volume was obtained by dividing the volume of the specific chromosome over the volume of the whole nucleus. The percentages were averaged over all nuclei within an experimental set to calculate the final mean percentages. Descriptive statistics (standard deviation and sample size) were also calculated. Sample sizes are listed in each figure. Error bars shown are means +/- 1 standard deviation of the mean. Percent volume differences were evaluated by unpaired (two sample) Student's T-test.

Distance measurements between two probes were described previously [16]. In brief the distance between the two probes (containing DNA amplified from YACs: either Y44D2 or Y108G6) was the distance between two separate spots closest to one another. The final median and interquartile range of the data is shown in boxplots. Sample sizes are listed in each figure. Whiskers shown indicate distribution from minimum to maximum. Probe distance differences were evaluated by unpaired (two sample) Student's T-test.

Immunofluorescence

Immunofluorescence experiments were performed as described [101]. Young adult worms were dissected in 1X sperm salts (50 mM Pipes pH 7, 25 mM KCl, 1 mM $MgSO_4$, 45 mM NaCl and 2 mM $CaCl_2$, supplemented with 1 mM levamisole), fixed in 4% paraformaldehyde in 1X sperm salts for 5 minutes and frozen on dry-ice for 10 minutes. Slides washed three times in PBST before incubation with diluted primary antibodies in a humid chamber, overnight at room temperature. Slides were then washed three times for 10 minutes with PBST, incubated for 1 hour with diluted secondary antibody at 37°C, washed twice for 10 minutes with PBST, and once for 10 minutes with PBST plus DAPI. Slides were mounted with Vectashield (Vector Labs). Antibodies were used at the following concentrations: H4K16ac (Millipore 07-329) at1:500 and H2A5ac (Abcam ab1764) at 1:100.

Western blot analysis

Adult mutant or RNAi-treated worms were collected. Equal volume of sample buffer (0.1 M Tris pH 6.8, 7.5 M urea, 2% SDS, 100mM β-ME, 0.05% bromophenol

blue) was added to worms. Lysates were prepared by heating worms to 65°C for 10 minutes, sonicating for two 30 second bursts, heating to 65°C for 5 minutes, heating to 95°C for 5 minutes, then kept at 37°C until loading onto SDS-PAGE gel. Proteins were transferred to nitrocellulose and blotted with the following antibodies: H4K16ac (Millipore 07-329) at 1:250, H3K9ac (Abcam ab4441) at 1:1000, H3K14ac (Abcam ab5946) at 1:500, H3K56ac (Millipore 07-677) at 1:4000, H4K5ac (Upstate 07-327) at 1:500, H4K8ac (Abcam ab5823) at 1:2000, β tubulin (Novus NB600-936) at 1:1000 and Anti-MYS-1 antibodies were raised in rabbit against the N-terminal 28 amino acids (TEPKKEIIEDENHGISKKIPTDPRQYEK) at 1:500.

Worm growth and collection

Strains were maintained at 20°C on NGM agar plates. Worm populations were synchronized by bleaching gravid adults and allowing the embryos to hatch overnight. Larval (L1s) worms were plated and grown for 24 hours at 20°C on NGM plates for L3 collection. For MYS-1 RNAi, synchronized L1s were placed on seeded RNAi plates and grown to gravid adults. Embryos were collected by bleaching and hatched overnight. Larval (L1s) worms were plated and grown for 24 hours at 20°C on RNAi plates for L3 collection.

Chromatin Immunoprecipitation (ChIP)

ChIP preparation is a variation of two previous described methods [102,103]. Frozen synchronized L3 worm pellets were crushed (pulverized by grinding in liquid nitrogen with a mortar and pestle) and crosslinked in ten volumes of 1.1% formaldehyde in PBS plus protease and phosphatase inhibitors. The lysate was rotated at room

temperature for 20 minutes. 2.5 M glycine was added to a final concentration of 125 mM and rocked gently for 5 minutes at room temperature to quench formaldehyde. Lysate was centrifuged at 4000 x g for 3 minutes and the supernatant was removed. The pellet was resuspended in 10 ml of cold PBS plus protease and phosphatase inhibitors and pelleted by spinning at 4000 x g for 3 minutes. The pellet was resuspended in one volume of FA buffer (50 mM HEPES/KOH pH 7.5, 1 mM EDTA, 1% Triton X-100, 0.1% sodium deoxycholate; 150 mM NaCl) plus protease and phosphatase inhibitors. To obtain chromatin fragments lysate was sonicated on high, for 30 seconds on 30 seconds off, two times for 10 minutes and one time for 15 minutes. 50 ul of the lystate was used to make ChIP input library. 3 ug of anti-H4K16ac (Millipore 07-329) was added to 400 ul of lysate (containing approximately 50 ug DNA). The ChIP mix was rotated overnight at 4°C. 50 ul of protein G Dynabeads (Invitrogen) was added and rotated for 2 hours. The beads were washed two times in FA buffer for 5 minutes. Then washed for 5 minutes in FA-1 M NaCl buffer (50 mM HEPES/KOH pH 7.5, 1 mM EDTA, 1% Triton X-100, 0.1% sodium deoxycholate; 1 M NaCl) and 10 minutes in FA-500 mM NaCl buffer (50 mM HEPES/KOH pH 7.5, 1 mM EDTA, 1% Triton X-100, 0.1% sodium deoxycholate; 500 mM NaCl). The beads were then washed for 10 minutes in TEL buffer (0.25 M LiCL, 1% NP-40, 1% sodium deoxycholate, 1 mM EDTA, 10 mM Tris-HCL pH 8.0) and then two times in TE (10 mM Tris-HCL pH 8.0, 1 mM EDTA) for 5 minutes. To elute the immunoprecipitation product and reverse crosslink, beads were incubated with 400 ul of ChIP Elution Buffer (1% SDS, 250 mM NaCl, 10 mM Tris pH 8.0, 1 mM EDTA) at 65°C for 2 hours with agitation ever 30 minutes (IP input lysate was

treated similarly to reverse crosslink). DNA was purified using Qiagen PCR purification kit.

ChIP-seq

Raw data files, wiggle tracks of ChIP enrichment per base pair, and peak bed files are provided at Gene Expression Omnibus database (http://www.ncbi.nlm.nih.gov/geo/) under accession number [GSE84307]. ChIP DNA were ligated to Illumina adaptors and amplified by PCR. Library DNA was between 200-550 bp in size. Single-end 50 bp sequencing was performed using Illumina HiSeq-2500 High-Output. Reads were trimmed for quality using the Trim Galore! v0.3.7 program from Babraham Bioinformatics (http://www.bioinformatics.babraham.ac.uk/projects/trim_galore/) and aligned to the *C. elegans* genome version WS235 with Bowtie 1.1.1 [104]. We allowed up to two mismatches, returned only the best alignment, and restricted a read to map to at most four locations in the genome. MACS2 version 2.1.0 [105] was first used to filter duplicates reads and to correct for bias downsampling was performed in either the input or the ChIP. Multiple replicates (input and ChIP) were input into MACS2 callpeak with options --broad and p-value (-p 1E-5) for peak calling and genome-wide coverage. MACS2 coverage reads were normalized to the genome-wide median coverage, excluding the mitochondrial chromosome, and final ChIP enrichment scores per base were obtained by subtracting the input coverage. For XO hermaphrodites, X and autosomes were normalized separately, due to having half the amount of X reads compared to autosomes. MACS2 coverage reads on the autosomes were normalized to

the genome-wide median coverage, whereas MACS2 coverage reads on X chromosome were normalized to half the genome-wide median coverage and final ChIP enrichment scores were combined after normalization. Lastly, datasets were standardized by z-score transformation of the ChIP enrichment values based on the presumed background. Annotation of ChIP binding sites was done using the *cis*-regulatory element annotation system (CEAS) [106] with default settings. The ChIP-seq data was visualized by IGV browser [107].

mRNA-seq

Raw data files, RNA-seq RPKM values, and differential expression analysis values are provided at Gene Expression Omnibus database (http://www.ncbi.nlm.nih.gov/geo/) under accession number [GSE84307]. For RNA preparation, ten volumes of Trizol was added. Samples were vortexed 30''/ice 30'' for 5 minutes total. RNA was extracted and precipitated using the manufacturer's instructions. The Qiagen RNeasy kit was used to clean total RNA. The TruSeq RNA Library Preparation Kit was used to prepare non-stranded mRNA-seq libraries. Single-end 50-bp sequencing was performed using Illumina HiSeq-2000. Reads were trimmed for quality using Trim Galore! and aligned to the *C. elegans* genome version WS235 with Tophat v2.0.13 [108] using default parameters, allowing up to 20 hits for each read. Gene expression was quantified using Cufflinks v2.2.1 [109] with use of "rescue method" for multi-reads and supplying gene annotation for WS235. Gene count estimation was performed using HTSeq-count tool v0.6.0 in the default "union" mode [110]. Differential expression analysis was performed using DESeq2 v1.6.3 [111] in R

version 3.2.3. All analyses were performed with genes that had average expression level above 1 RPKM (reads per kilobase per million, as calculated by Cufflinks).

ACKNOWLEDGEMENTS

We thank members of the Csankovszki lab for helpful project discussions and Jianhao Jiang for critical reading of the manuscript. We also thank the *Caenorhabditis* Genetics Center, which is funded by the NIH National Center for Research Resources, for some nematode strains used in this work. The work was supported by NIH grant R01 GM079533 to G.C.

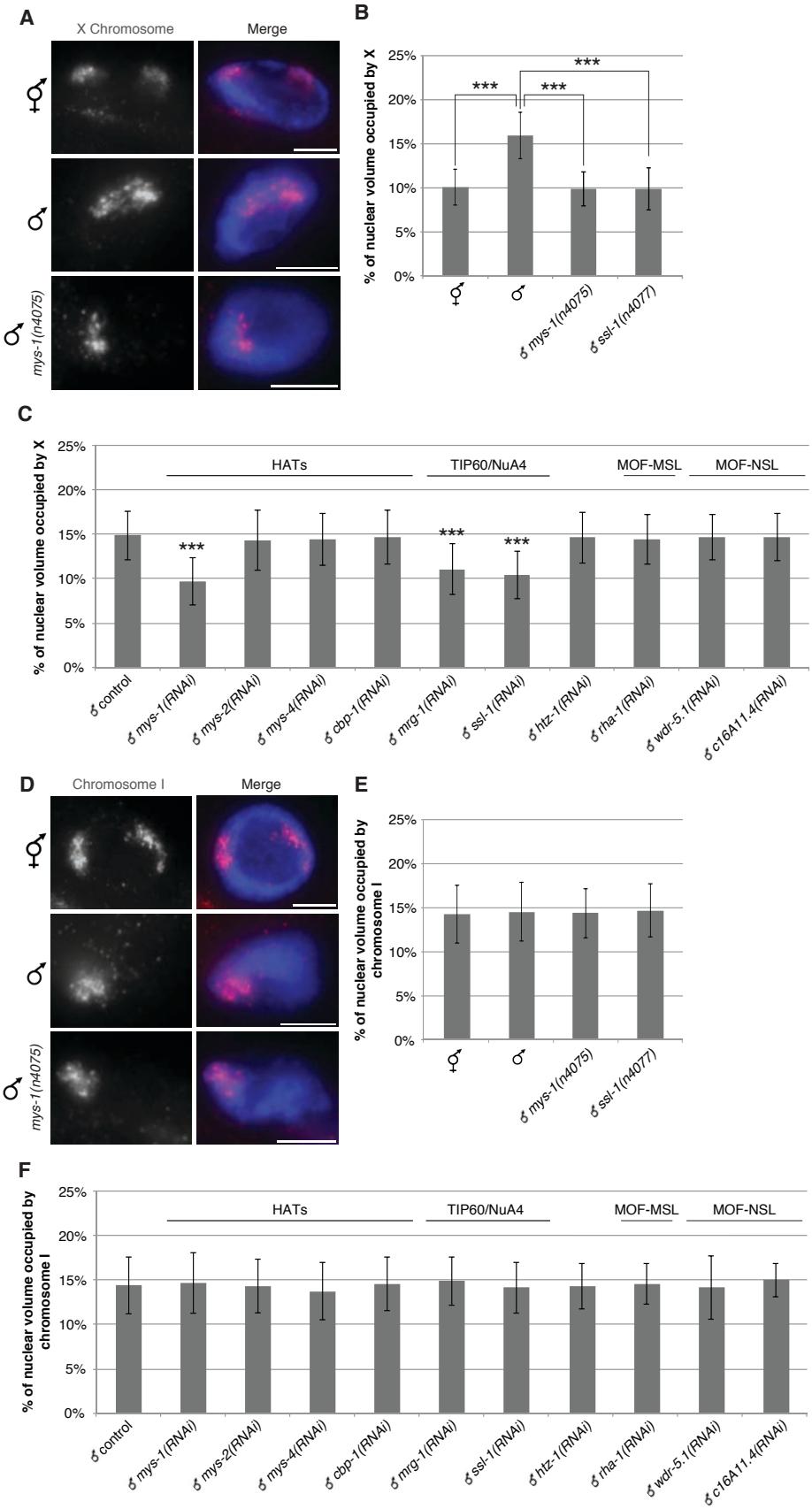
A
X Chromosome
Merge
♀
♂
♂ mys-1(n4075)
B
% of nuclear volume occupied by X
25%
20%
15%
10%
5%
0%
***
***
***
♀
♂
♂ mys-1(n4075)
♂ ssl-1(n4077)
C
% of nuclear volume occupied by X
HATs
TIP60/NuA4
MOF-MSL
MOF-NSL
***
***
***
♂ control
♂ mys-1(RNAi)
♂ mys-2(RNAi)
♂ mys-4(RNAi)
♂ cbp-1(RNAi)
♂ mrg-1(RNAi)
♂ ssl-1(RNAi)
♂ htz-1(RNAi)
♂ rha-1(RNAi)
♂ wdr-5.1(RNAi)
♂ c16A11.4(RNAi)
D
Chromosome I
Merge
♀
♂
♂ mys-1(n4075)
E
% of nuclear volume occupied by chromosome I
♀
♂
♂ mys-1(n4075)
♂ ssl-1(n4077)
F
% of nuclear volume occupied by chromosome I
HATs
TIP60/NuA4
MOF-MSL
MOF-NSL
♂ control
♂ mys-1(RNAi)
♂ mys-2(RNAi)
♂ mys-4(RNAi)
♂ cbp-1(RNAi)
♂ mrg-1(RNAi)
♂ ssl-1(RNAi)
♂ htz-1(RNAi)
♂ rha-1(RNAi)
♂ wdr-5.1(RNAi)
♂ c16A11.4(RNAi)

Figure 4.1 MYS-1 and putative worm Tip60/NuA4-like complex members mediate X chromosome decondensation. (A-C) Adult mutant and RNAi treated male intestinal nuclei stained with X-paint FISH (red) to label X chromosome territories and DAPI (blue) to label DNA. (A) Representative stained nuclei of wild type hermaphrodite, wild type males, and *mys-1(n4075)* males. Scale bars equal 5 μm. (B) Quantification of the percentage of nuclear volume occupied by X in wild type hermaphrodites (n = 27), wild type males (n = 27), *mys-1(n4075)* males (n = 20), and *ssl-1(n4077)* males (n = 20). Error bars indicate standard deviation. Asterisks indicate level of statistical significance by t-test analysis (***, $P < .001$). (C) Quantification of the percentage of nuclear volume occupied by X in vector RNAi (n = 77), histone acetyltransferases (HATs), and histone acetyltransferases complex member (Tip60/NuA4, MOF-MSL, MOF-NSL) RNAi treated males. *mys-1(RNAi)* (n = 30), *mys-2(RNAi)* (n = 24), *mys-4(RNAi)* (n = 27), *cbp-1(RNAi)* (n = 26), *mrg-1(RNAi)* (n = 40), *ssl-1(RNAi)* (n = 40), *pbrm-1(RNAi)* (n = 40), *rha-1(RNAi)* (n = 40), *wrd-5.1(RNAi)* (n=40), and *c16A11.4(RNAi)* (n = 40). Error bars indicate standard deviation. Asterisks indicate level of statistical significance by t-test analysis (***, $P < .001$). (D-F) Adult mutant and RNAi treated male intestinal nuclei stained with chromosome I paint FISH (red) to label chromosome I territories and DAPI (blue) to label DNA. (D) Representative stained nuclei of wild type hermaphrodite, wild type males, and *mys-1(n4075)* males. Scale bars equal 5 μm. (E) Quantification of the percentage of nuclear volume occupied by chromosome I in wild type hermaphrodites (n = 20), wild type males (n = 17), *mys-1(n4075)* males (n = 18), and *ssl-1(n4077)* males (n = 16). Error bars indicate standard deviation. (F) Quantification of the percentage of nuclear volume occupied by chromosome I in vector RNAi (n = 43), histone acetyltransferases (HATs), and histone acetyltransferases complex member (Tip60/NuA4, MOF-MSL, MOF-NSL) RNAi treated males. *mys-1(RNAi)* (n = 21), *mys-2(RNAi)* (n = 23), *mys-4(RNAi)* (n = 17), *cbp-1(RNAi)* (n = 28), *mrg-1(RNAi)* (n = 17), *ssl-1(RNAi)* (n = 17), *pbrm-1(RNAi)* (n = 20), *rha-1(RNAi)* (n = 20), *wrd-5.1(RNAi)* (n=17), and *c16A11.4(RNAi)* (n = 20). Error bars indicate standard deviation.

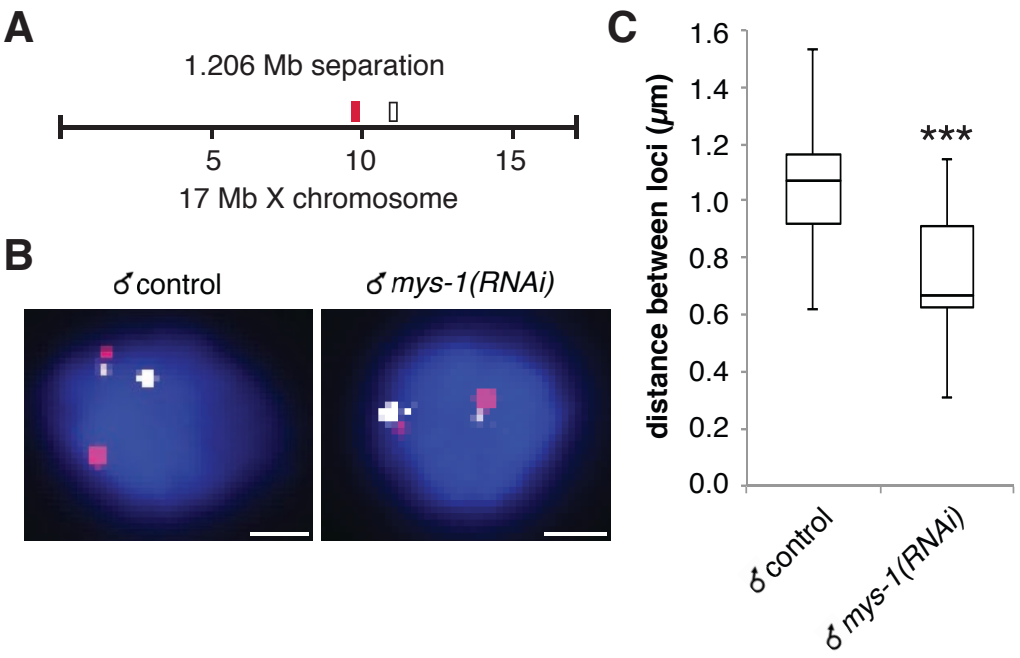

Figure 4.2 Male X chromatin decondensation is evident at the genomic scale of 1.2 Mb. (A) FISH probe pairs across the X chromosome. The position of YAC probes (red and white boxes) used in FISH is indicated. (B) 2D projections of 3D stacked images. Representative stained tetraploid nuclei of adult males fed vector RNAi and *mys-1(RNAi)*. Nuclei stained with probes pairs across the X chromosome (red and white) and counterstained with DAPI (blue) to label DNA. Scale bars equal 1 μm. (C) Boxplots indicating the distribution of 3D loci distances of male vector RNAi and *mys-1(RNAi)* diploid nuclei. Boxes show the median and interquartile range of the data. Asterisks indicate level of statistical significance by t-test analysis (***, P < .001).

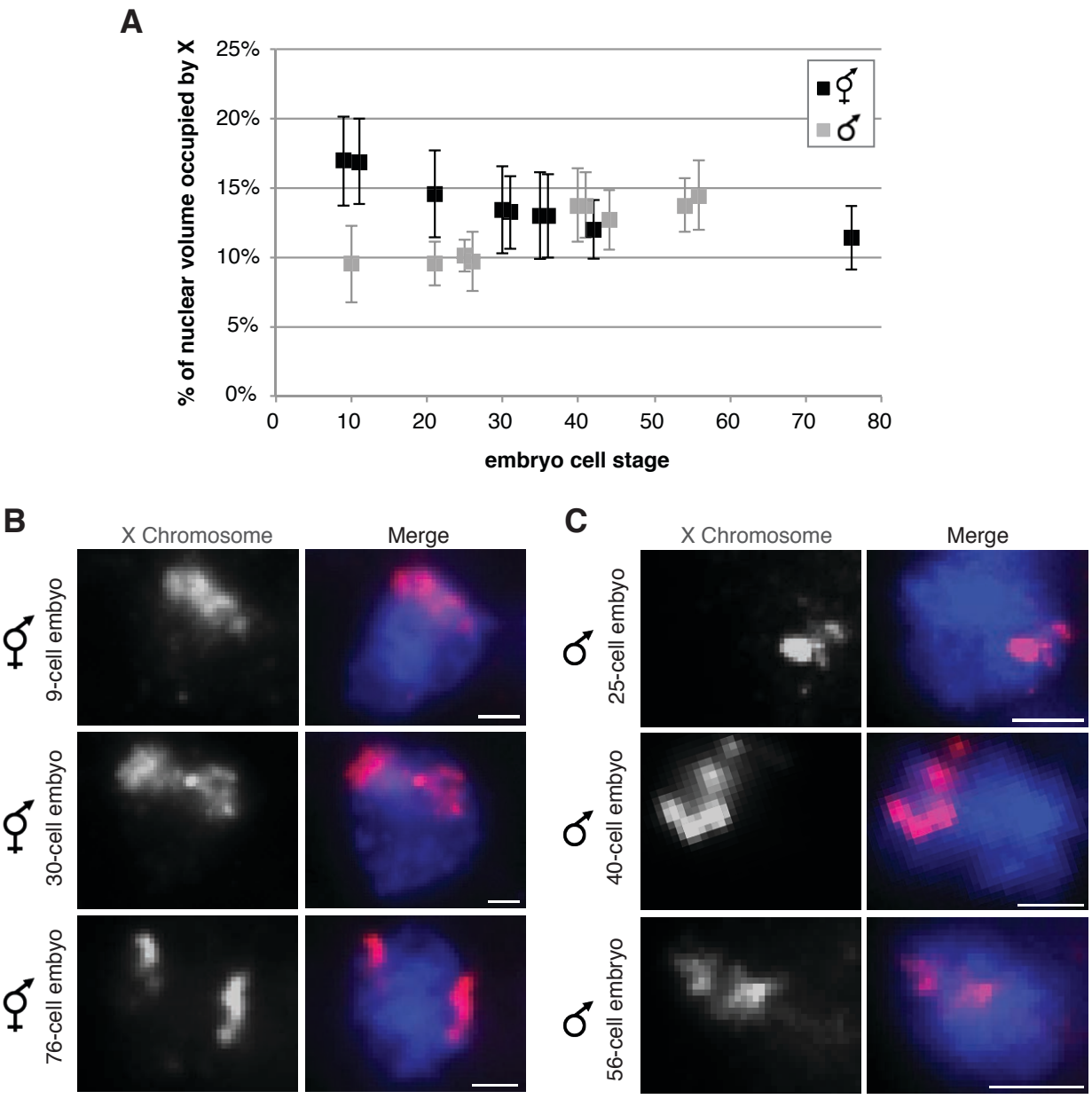

Figure 4.3 Hermaphrodite X chromosome compaction and male X chromosome decondensation occur simultaneously in development. Hermaphrodite and male embryos stained X-paint FISH (red) to label X chromosome territories and DAPI (blue) to label DNA. (A) Plot of quantified percentages of nuclear volume occupied by X in wild type hermaphrodite embryos (black) and male embryos (gray). Each point represents one embryo (n = 10 nuclei per embryo). Error bars indicate standard deviation. (B) Representative stained nuclei of wild type hermaphrodites at various developmental stages (9-cell, 30-cell, 76-cell). Scale bars equal 5 μm. (C) Representative stained nuclei of male *him-8(e1489)* animals at various developmental stages (25-cell, 40-cell, 56-cell). Scale bars equal 1 μm.

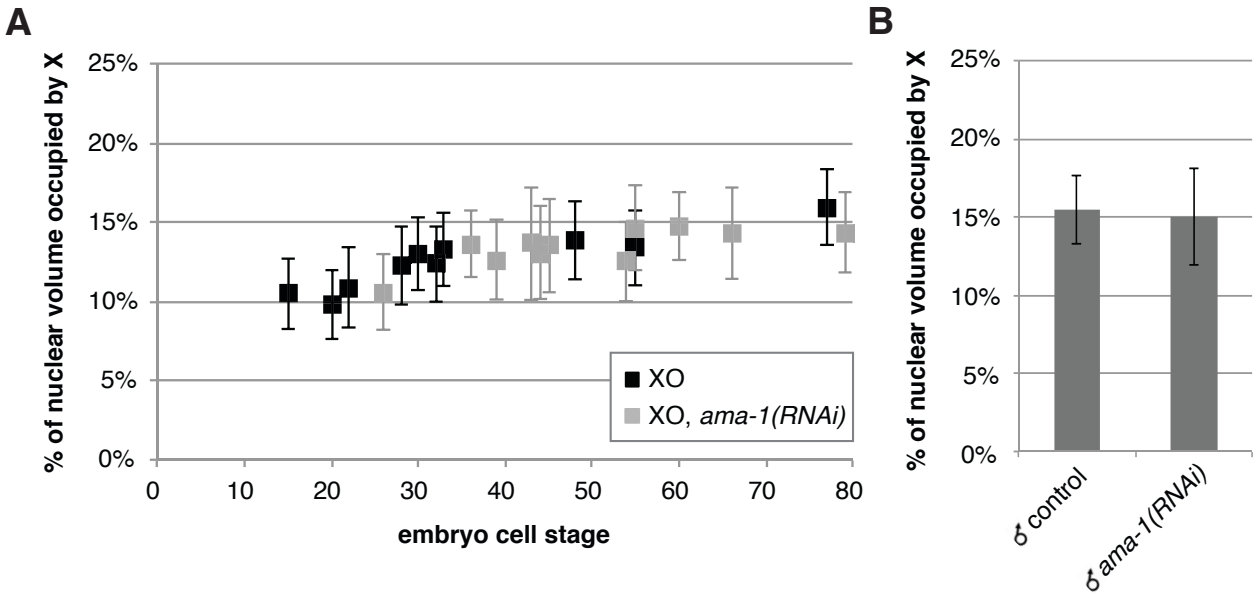

Figure 4.4 Transcription is not required for the initiation or maintenance of X decondensation. (A) H4K16ac immunofluorescence stained nuclei of XO embryos and XO embryos fed *ama-1(RNAi)*. H4K16ac levels did not decrease in XO embryos fed *ama-1(RNAi)*. (B) Plot of quantified percentages of nuclear volume occupied by X in XO embryos fed vector RNAi (black) and XO embryos fed *ama-1(RNAi)* (gray). Each point represents one embryo (n = 10 nuclei per embryo). Error bars indicate standard deviation. (C) Quantification of the percentage of nuclear volume occupied by adult males fed vector RNAi (n = 20) and *ama-1(RNAi)* (large subunit of RNA polymerase II) (n = 20). Error bars indicate standard deviation.

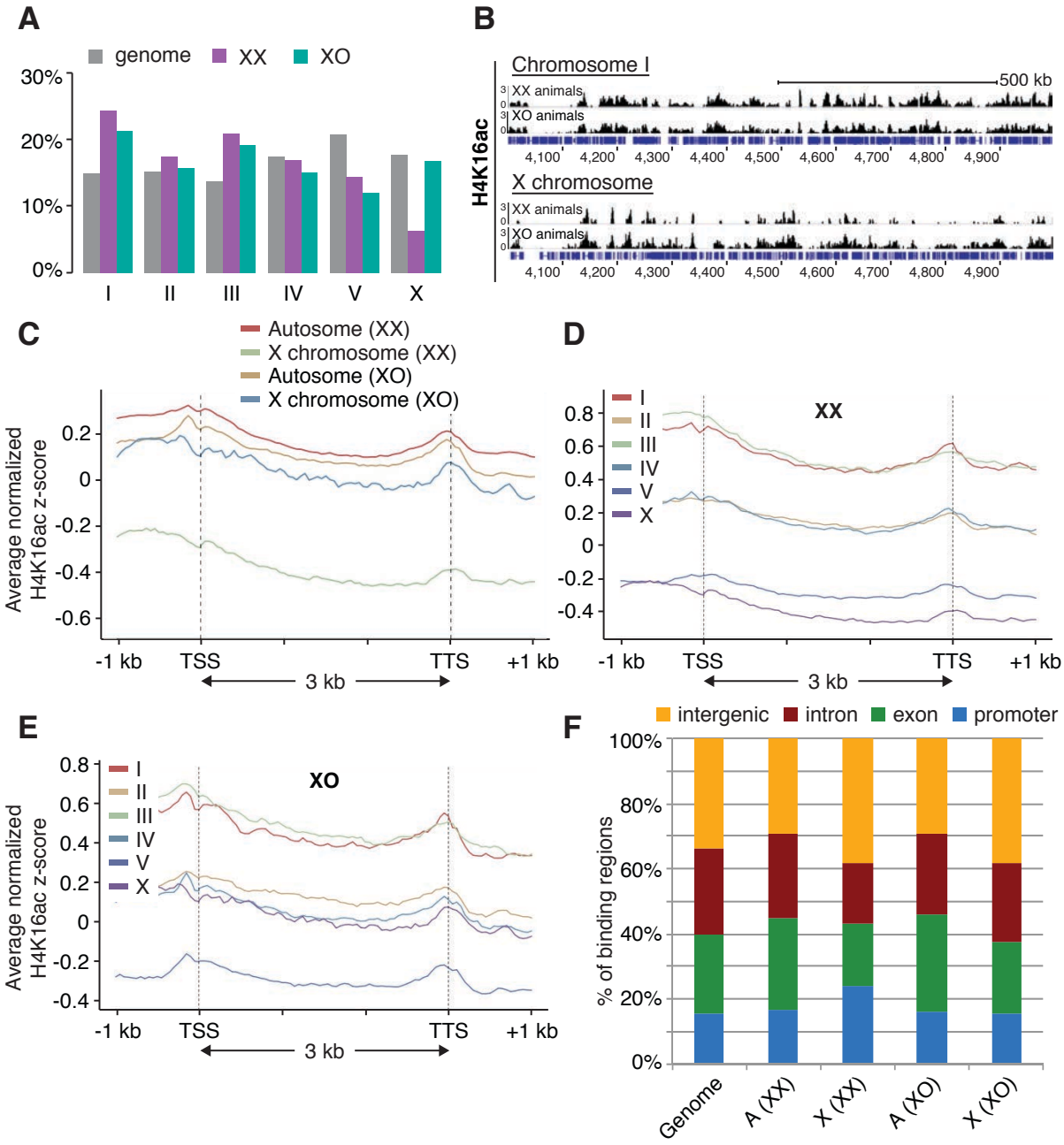
A
genome
XX
XO
30%
20%
10%
0%
I
II
III
IV
V
X
B
Chromosome I
500 kb
XX animals
XO animals
H4K16ac
4,100
4,200
4,300
4,400
4,500
4,600
4,700
4,800
4,900
X chromosome
C
Autosome (XX)
X chromosome (XX)
Autosome (XO)
X chromosome (XO)
Average normalized H4K16ac z-score
0.2
0
-0.2
-0.4
-0.6
-1 kb
TSS
TTS
+1 kb
3 kb
D
XX
0.8
0.6
0.4
0.2
0
-0.2
-0.4
E
XO
F
intergenic
intron
exon
promoter
% of binding regions
100%
80%
60%
40%
20%
0%
Genome
A (XX)
X (XX)
A (XO)
X (XO)

Figure 4.5 Profile of H4K16ac in XX and XO animals. H4K16ac ChIP-seq in XX and XO hermaphrodites. (A) Chromosomal distributions of H4K16ac ChIP regions compared to the fraction of the genome found on each chromosome. (B) Representative IGV genome browser views of ChIP-seq scores for H4K16ac. (C) Average normalized H4K16ac ChIP-seq enrichment scores plotted for X and autosomes across the gene body. (D-E) Average normalized H4K16ac ChIP-seq enrichment scores plotted for each chromosome across the gene body in (D) XX hermaphrodites and (E) XO hermaphrodites. (F) Percentage of H4K16ac peak found across each category of genomic sequence on the X and autosomes in XX and XO hermaphrodites compared to the fraction the genome found in each genomic category.
each category of genomic sequence on the X and autosomes in XX and XO hermaphrodites compared to the fraction the genome found in each genomic category.

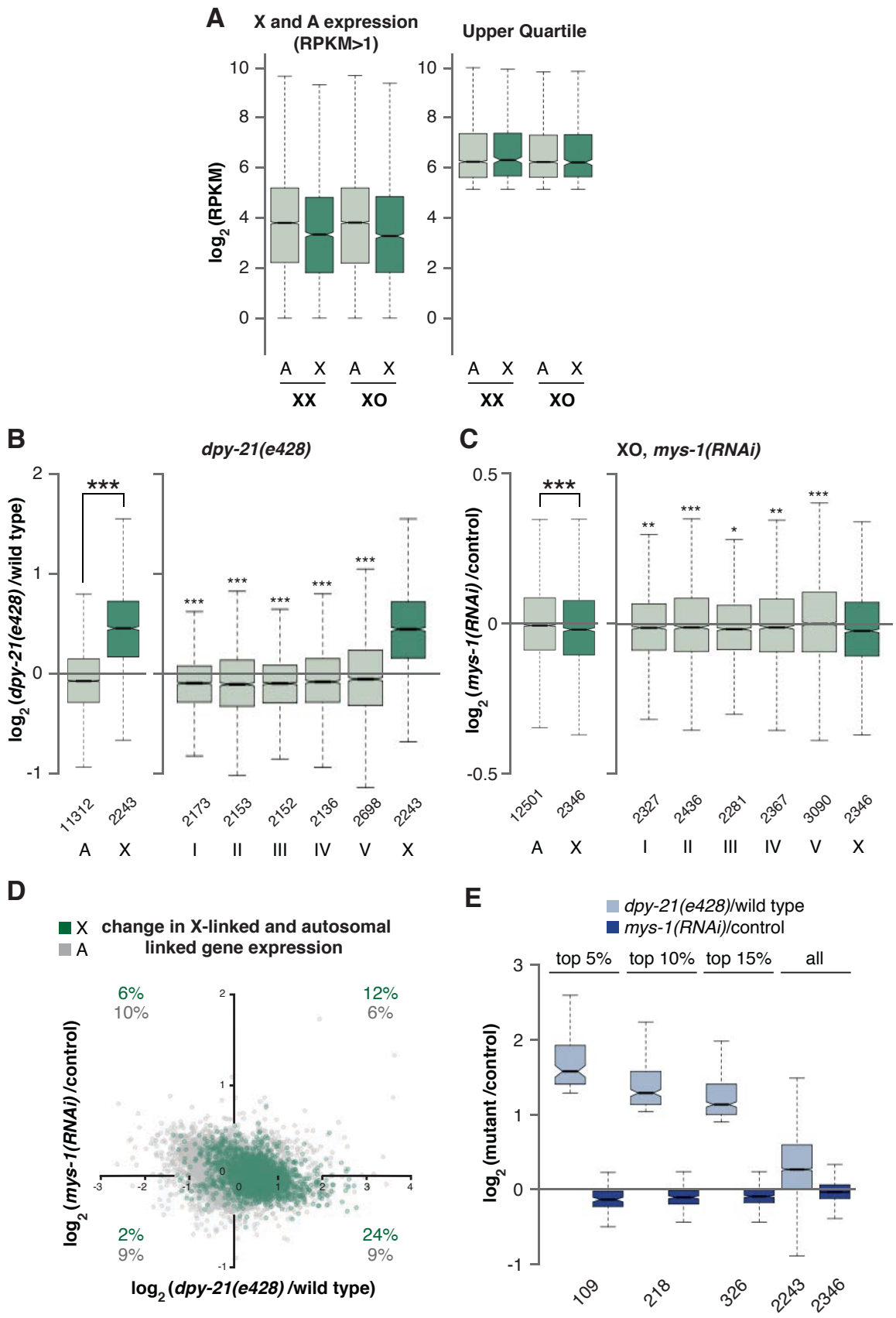
A
X and A expression (RPKM>1)
Upper Quartile
log2 (RPKM)
A X A X
XX XO
B
dpy-21(e428)
log2 (dpy-21(e428) /wild type)
11312 2243 2173 2153 2152 2136 2698 2243
A X I II III IV V X
C
XO, mys-1(RNAi)
log2 (mys-1(RNAi) /control)
12501 2346 2327 2436 2281 2367 3090 2346
A X I II III IV V X
D
X change in X-linked and autosomal
A linked gene expression
6% 10% 12% 6%
2% 9% 24% 9%
log2 (mys-1(RNAi) /control)
log2 (dpy-21(e428) /wild type)
E
dpy-21(e428)/wild type
mys-1(RNAi)/control
top 5% top 10% top 15% all
log2 (mutant /control)
109 218 326 2243 2346

Figure 4.6 RNA-seq analysis of gene expression changes in MYS-1 depleted XO worms. (A) X and autosome expression levels of genes with RPKM>1 and genes whose expression is in the upper quartile in XX and XO hermaphrodites. (***, P < .001 by two-sided Wilcoxon rank-sum test). (B) Boxplot shows the distribution of $\log_2$ expression ratios on the X, autosomes and on all separate chromosomes between *dpy-21(e428)* mutant XX hermaphrodites and wild type XX hermaphrodites. X chromosome was significantly derepressed compared to the autosomal average and all other chromosomes. Increased expression from the X was tested between X and autosome by one-sided Wilcoxon rank-sum test (***, P < .001). (C) Boxplot shows the distribution of $\log_2$ expression ratios on the X, autosomes and on all separate chromosomes between XO hermaphrodites fed *mys-1(RNAi)* and XO hermaphrodites fed vector RNAi. X chromosome was statistically significantly repressed compared to the autosomal average and all other chromosomes, although the degree of repression was minor. Decreased expression from the X was tested between X and autosomes by one-sided Wilcoxon rank-sum test (*, P < .05; **, P < .01; ***, P < .001). (D) The magnitude of $\log_2$ expression ratios of X-linked (green) and autosomal genes (gray) between XO hermaphrodites fed *mys-1(RNAi)* and control XO plotted against *dpy-21(e428)* mutants and wild type animals. The percentages of X-linked and autosomal genes with >10% change in expression (±0.1 in $\log_2$) in both knockdown and mutant compared to control worms are indicated in each quadrant. (E) Boxplots show the distribution of $\log_2$ ratios on the X between *dpy-21(e428)* mutants and wild type animals, and *mys-1(RNAi)* XO hermaphrodites and control XO hermaphrodites. The first 3 sets of boxplots show the distribution of $\log_2$ ratios of the top 5%, top 10%, and top 15% of highly differentially expressed X-linked genes in *dpy-21(e428)* mutants. The last set shows the distribution of all X-linked genes.

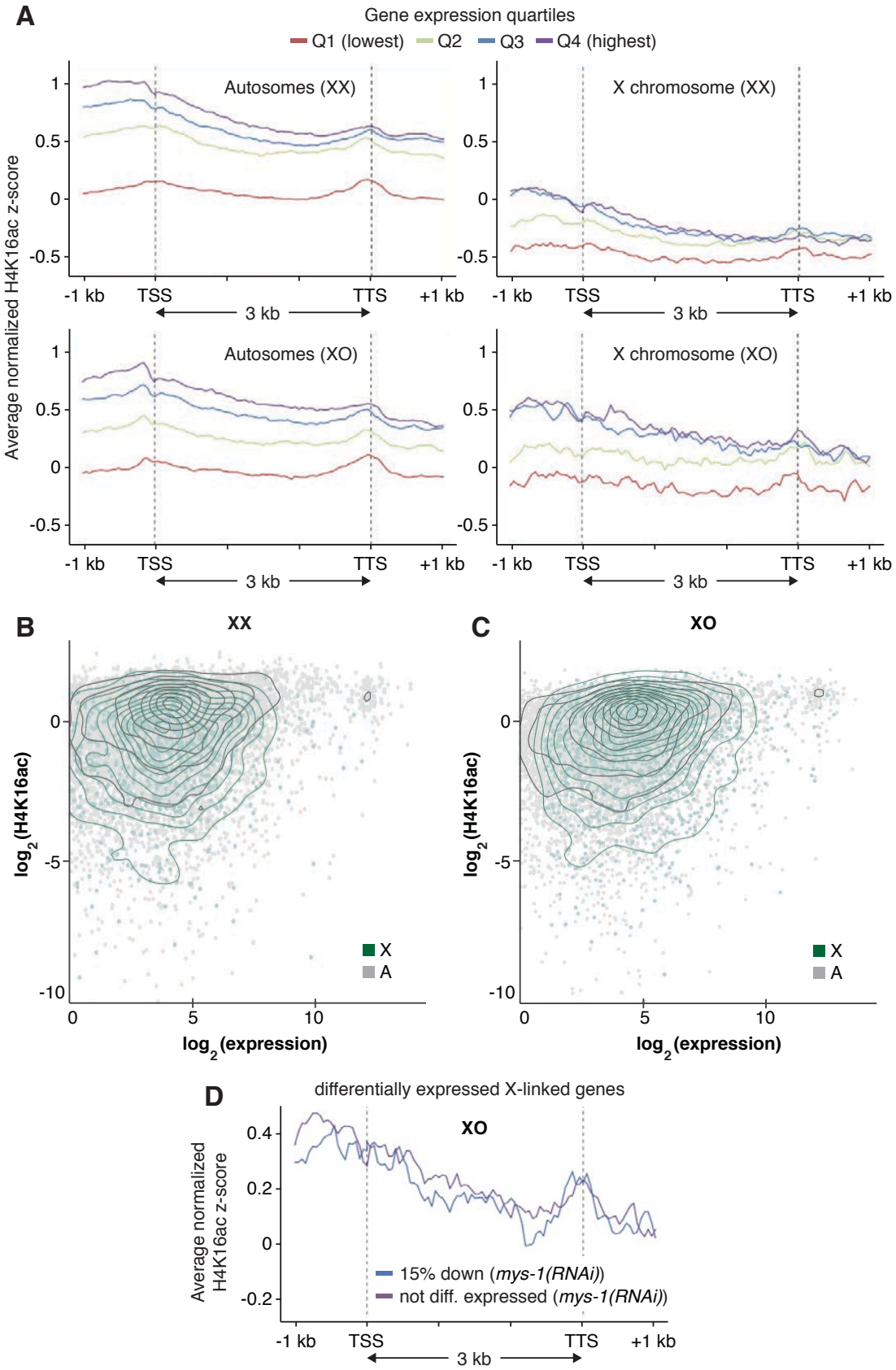
A
Gene expression quartiles
Q1 (lowest)
Q2
Q3
Q4 (highest)
Average normalized H4K16ac z-score
Autosomes (XX)
X chromosome (XX)
Autosomes (XO)
X chromosome (XO)
-1 kb
TSS
TTS
+1 kb
3 kb
B
XX
C
XO
log2(H4K16ac)
log2(expression)
X
A
D
differentially expressed X-linked genes
XO
Average normalized H4K16ac z-score
15% down (mys-1(RNAi))
not diff. expressed (mys-1(RNAi))

Figure 4.7 Relationships between levels of H4K16ac and gene expression. (A) Average normalized H4K16ac ChIP-seq enrichment scores separated into quartiles according to expression plotted for X and autosomes in XX and XO hermaphrodites. (B-C) Average H4K16ac ChIP score within 500 bp upstream of the TSS plotted against the RNA level of each gene for (B) XX and (C) XO hermaphrodites. Expressed autosomal genes (RPKM>1) are represented as gray points, with point density shown by black line contour. Expressed X-linked (RPKM>1) are represented by green dots, and green line contour. (D) Average normalized H4K16ac ChIP-seq enrichment scores in XO hermaphrodites separated by the top 15% downregulated X-linked genes in *mys-1(RNAi)* XO hermaphrodites and X-linked genes that were not differentially expressed.

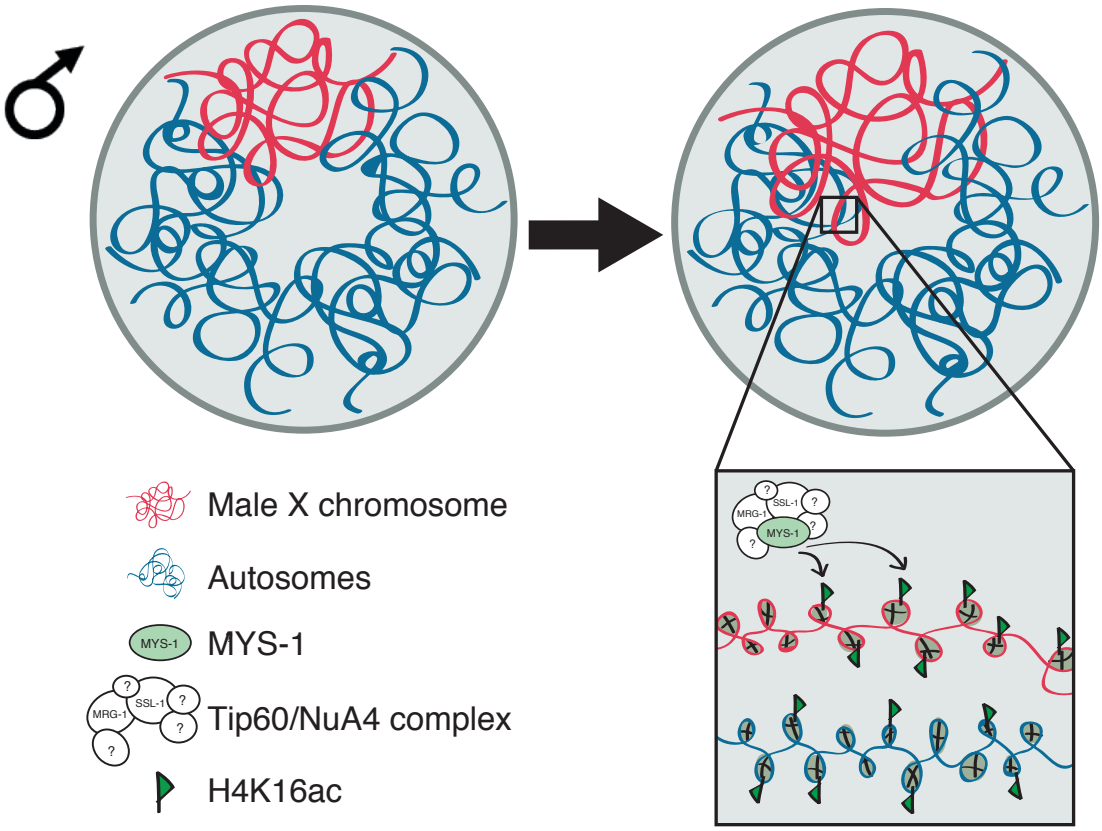

Figure 4.8 X chromosome decondensation in males is dependent on the activity of a putative Tip60/NuA4-like complex. A graphical cartoon illustrates MYS-1 and H4K16ac effects on male X chromosome structure. The HAT MYS-1, which is a member of a putative worm Tip60/NuA4-like complex, mediates the binding of H4K16ac on X and autosomes, however more highly distributed in intergenic regions of the X. This activity decondenses the X chromosome territories and makes small contribution to X-linked gene upregulation in males.

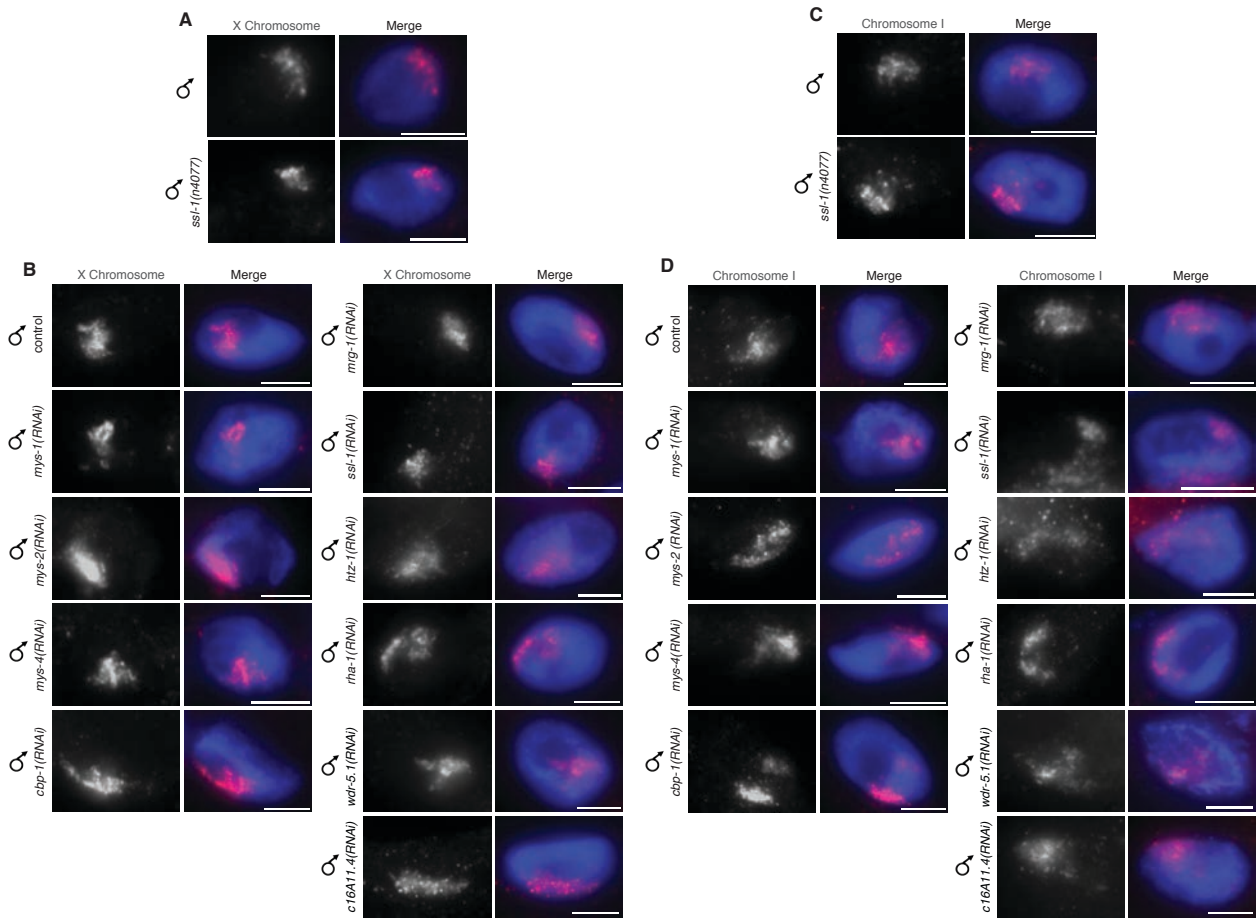

Figure 4.9 Tip60/NuA4-like complex members mediate X chromosome decondensation. (A) Representative images of X-paint FISH stained nuclei of wild type males, and *ssl-1(n4077)* males, and (B) in males depleted of HATs and Tip60/NuA4, MOF-MSL, MOF-NSL complex members. (C) Representative images of chromosome I-paint FISH of wild type and *ssl-1(n4077)* males and (D) males depleted of HATs and Tip60/NuA4, MOF-MSL, MOF-NSL complex members Scale bars equal 5 μm.

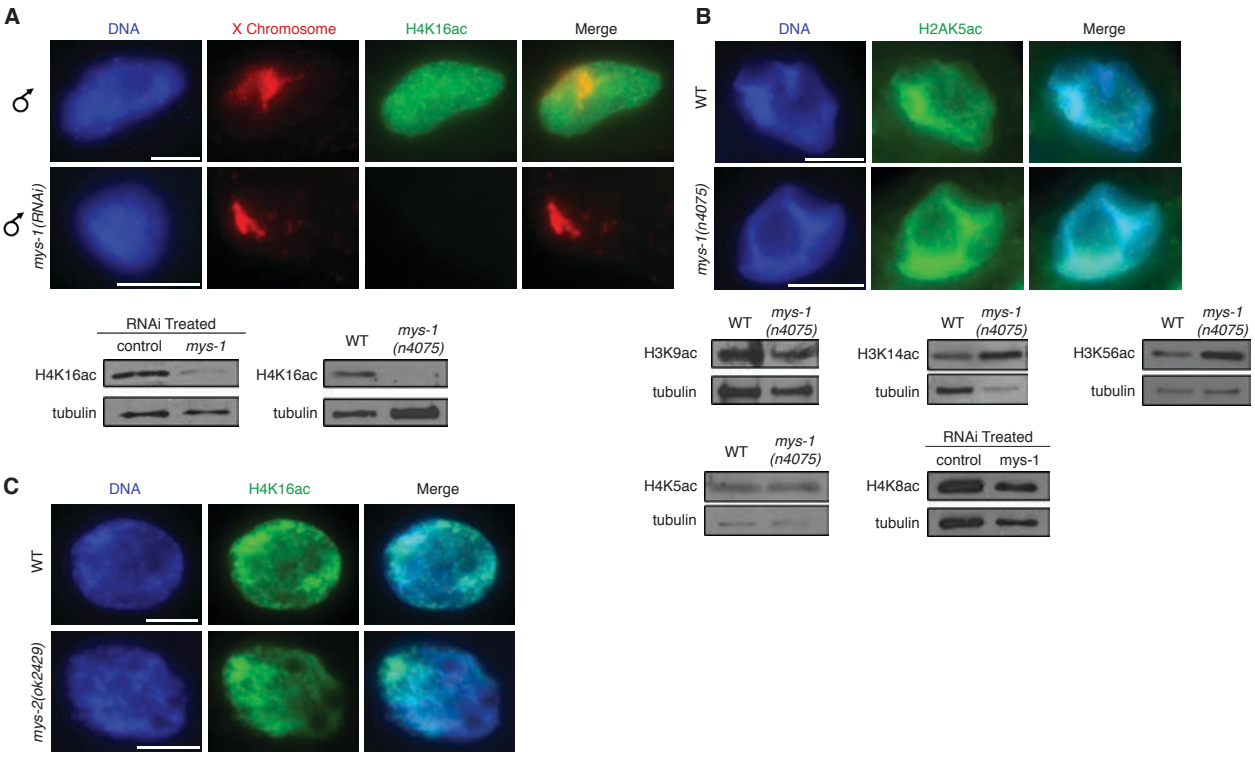

Figure 4.10 MYS-1 acetylates H4K16. (A) H4K16ac immunofluorescence and western blot analysis of adult MYS-1 mutant and RNAi treated worms. H4K16ac levels are depleted in *mys-1(RNAi)* and *mys-1(n4075)* mutant males compared to control males, both by immunofluorescence and western blot analysis. Scale bars equal 5 μm. Tubulin is shown as a loading control. (B) Immunofluorescence and western blot analysis of adult MYS-1 mutant and RNAi treated worms probed for additional histone acetylation marks. H2AK5ac, H3K9ac, H3K14ac, H3K56ac, H4K5ac, and H4K8ac are not depleted in *mys-1(n4075)* mutants or in *mys-1(RNAi)* worms. Scale bars equal 5 μm. Tubulin is shown as a loading control. (C) H4K16ac immunofluorescence of adult MYS-2 mutants. H4K16ac levels are not depleted in *mys-2(ok2429)* mutants compared to wild type.

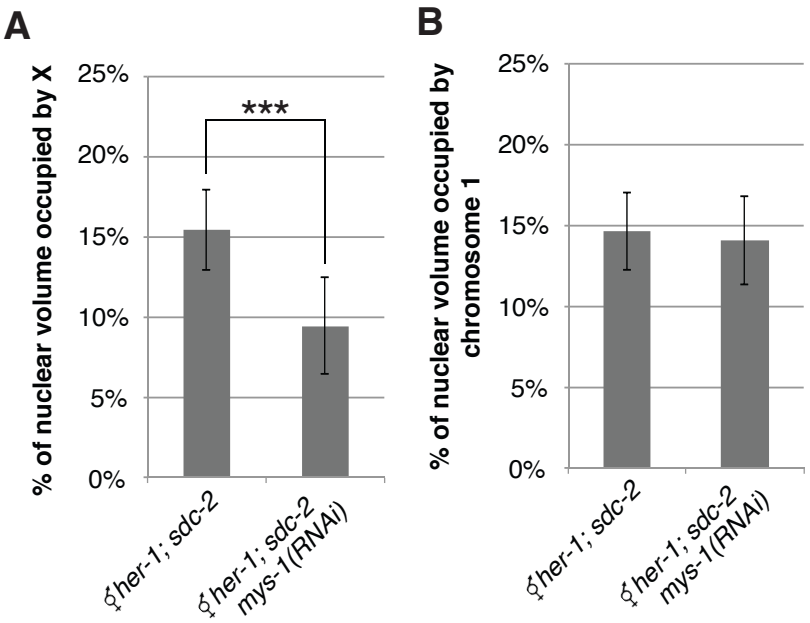

Figure 4.11 MYS-1 mediated X chromosome decondensation is evident in XO hermaphrodites. (A) Quantification of the percentage of nuclear volume occupied by X in adult XO hermaphrodites; *her-1(e1520)* V; *sdc-2(y74)* X (n = 20) and *her-1(e1520)* V; *sdc-2(y74)* X fed *mys-1(RNAi)* (n = 20). Error bars indicate standard deviation. Asterisks indicate level of statistical significance by t-test analysis (***, P < .001). (B) Quantification of the percentage of nuclear volume occupied by chromosome I in XO hermaphrodites; *her-1(e1520)* V; *sdc-2(y74)* X (n = 20), *her-1(e1520)* V and *sdc-2(y74)* X fed *mys-1(RNAi)* (n = 16). Error bars indicate standard deviation.

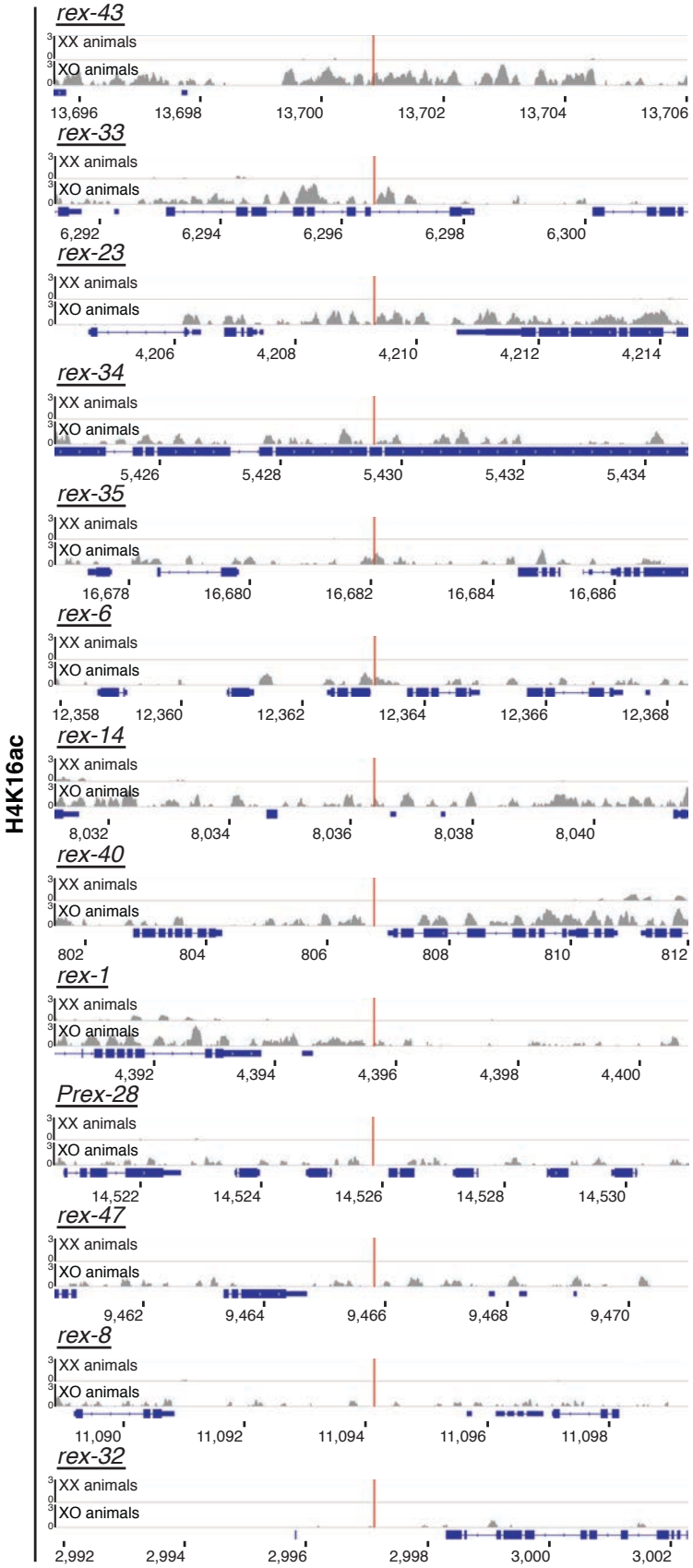
H4K16ac
rex-43
XX animals
XO animals
13,696
13,698
13,700
13,702
13,704
13,706
rex-33
6,292
6,294
6,296
6,298
6,300
rex-23
4,206
4,208
4,210
4,212
4,214
rex-34
5,426
5,428
5,430
5,432
5,434
rex-35
16,678
16,680
16,682
16,684
16,686
rex-6
12,358
12,360
12,362
12,364
12,366
12,368
rex-14
8,032
8,034
8,036
8,038
8,040
rex-40
802
804
806
808
810
812
rex-1
4,392
4,394
4,396
4,398
4,400
Prex-28
14,522
14,524
14,526
14,528
14,530
rex-47
9,462
9,464
9,466
9,468
9,470
rex-8
11,090
11,092
11,094
11,096
11,098
rex-32
2,992
2,994
2,996
2,998
3,000
3,002

Figure 4.12 Profile of H4K16ac at *rex* sites in XX and XO animals. Representative IGV genome browser views of ChIP-seq scores for H4K16ac at *rex* sites (red line) at TAD boundaries that have the strongest *rex-rex* interactions in XX and XO hermaphrodites.

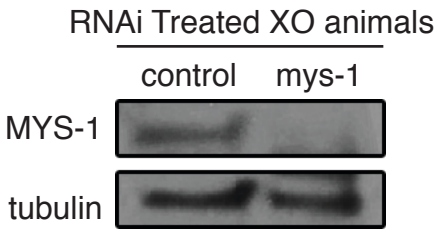

Figure 4.13 MYS-1 is depleted for RNA-seq. Western blot analysis of the depletion in L3 worms after MYS-1 RNAi feeding for RNA-seq samples. MYS-1 was successfully depleted. Tubulin is shown as a loading control.

REFERENCES

1. Ohno, S. (1967). Sex Chromosomes and Sex-Linked Genes. Berlin: Springer, 1-140.
2. Conrad, T., and Akhtar, A. (2011). Dosage compensation in Drosophila melanogaster: epigenetic fine-tuning of chromosome-wide transcription. Nature reviews. Genetics *13*, 123-134.
3. Ferrari, F., Alekseyenko, A.A., Park, P.J., and Kuroda, M.I. (2014). Transcriptional control of a whole chromosome: emerging models for dosage compensation. Nature structural & molecular biology *21*, 118-125.
4. Deng, X., Berletch, J.B., Ma, W., Nguyen, D.K., Hiatt, J.B., Noble, W.S., Shendure, J., and Disteche, C.M. (2013). Mammalian X upregulation is associated with enhanced transcription initiation, RNA half-life, and MOF-mediated H4K16 acetylation. Developmental cell *25*, 55-68.
5. Deng, X., Hiatt, J.B., Nguyen, D.K., Ercan, S., Sturgill, D., Hillier, L.W., Schlesinger, F., Davis, C.A., Reinke, V.J., Gingeras, T.R., et al. (2011). Evidence for compensatory upregulation of expressed X-linked genes in mammals, Caenorhabditis elegans and Drosophila melanogaster. Nature genetics *43*, 1179-1185.
6. Gupta, V., Parisi, M., Sturgill, D., Nuttall, R., Doctolero, M., Dudko, O.K., Malley, J.D., Eastman, P.S., and Oliver, B. (2006). Global analysis of X-chromosome dosage compensation. Journal of biology *5*, 3.
7. Lin, H., Gupta, V., Vermilyea, M.D., Falciani, F., Lee, J.T., O'Neill, L.P., and Turner, B.M. (2007). Dosage compensation in the mouse balances up-regulation and silencing of X-linked genes. PLoS biology *5*, e326.
8. Lin, H., Halsall, J.A., Antczak, P., O'Neill, L.P., Falciani, F., and Turner, B.M. (2011). Relative overexpression of X-linked genes in mouse embryonic stem cells is consistent with Ohno's hypothesis. Nature genetics *43*, 1169-1170; author reply 1171-1162.
9. Yildirim, E., Sadreyev, R.I., Pinter, S.F., and Lee, J.T. (2012). X-chromosome hyperactivation in mammals via nonlinear relationships between chromatin states and transcription. Nature structural & molecular biology *19*, 56-61.
10. Barakat, T.S., and Gribnau, J. (2012). X chromosome inactivation in the cycle of life. Development *139*, 2085-2089.
11. Heard, E., and Disteche, C.M. (2006). Dosage compensation in mammals: fine-tuning the expression of the X chromosome. Genes & development *20*, 1848-1867.
12. Payer, B., and Lee, J.T. (2008). X chromosome dosage compensation: how mammals keep the balance. Annual review of genetics *42*, 733-772.
13. Lau, A.C., and Csankovszki, G. (2014). Condensin-mediated chromosome organization and gene regulation. Frontiers in genetics *5*, 473.
14. Lau, A.C., and Csankovszki, G. (2015). Balancing up and downregulation of the C. elegans X chromosomes. Current opinion in genetics & development *31*, 50-56.

15. Meyer, B.J. (2010). Targeting X chromosomes for repression. Current opinion in genetics & development *20*, 179-189.
16. Lau, A.C., Nabeshima, K., and Csankovszki, G. (2014). The *C. elegans* dosage compensation complex mediates interphase X chromosome compaction. Epigenetics & chromatin *7*, 31.
17. Vielle, A., Lang, J., Dong, Y., Ercan, S., Kotwaliwale, C., Rechtsteiner, A., Appert, A., Chen, Q.B., Dose, A., Egelhofer, T., et al. (2012). H4K20me1 contributes to downregulation of X-linked genes for C. elegans dosage compensation. PLoS genetics *8*, e1002933.
18. Wells, M.B., Snyder, M.J., Custer, L.M., and Csankovszki, G. (2012). Caenorhabditis elegans dosage compensation regulates histone H4 chromatin state on X chromosomes. Molecular and cellular biology *32*, 1710-1719.
19. Nguyen, D.K., and Disteche, C.M. (2006). Dosage compensation of the active X chromosome in mammals. Nature genetics *38*, 47-53.
20. Xiong, Y., Chen, X., Chen, Z., Wang, X., Shi, S., Wang, X., Zhang, J., and He, X. (2010). RNA sequencing shows no dosage compensation of the active X-chromosome. Nature genetics *42*, 1043-1047.
21. Albritton, S.E., Kranz, A.L., Rao, P., Kramer, M., Dieterich, C., and Ercan, S. (2014). Sex-biased gene expression and evolution of the x chromosome in nematodes. Genetics *197*, 865-883.
22. Kruesi, W.S., Core, L.J., Waters, C.T., Lis, J.T., and Meyer, B.J. (2013). Condensin controls recruitment of RNA polymerase II to achieve nematode X-chromosome dosage compensation. eLife *2*, e00808.
23. Sharma, R., Jost, D., Kind, J., Gomez-Saldivar, G., van Steensel, B., Askjaer, P., Vaillant, C., and Meister, P. (2014). Differential spatial and structural organization of the X chromosome underlies dosage compensation in C. elegans. Genes & development *28*, 2591-2596.
24. Akhtar, A., and Becker, P.B. (2000). Activation of transcription through histone H4 acetylation by MOF, an acetyltransferase essential for dosage compensation in Drosophila. Molecular cell *5*, 367-375.
25. Smith, E.R., Pannuti, A., Gu, W., Steurnagel, A., Cook, R.G., Allis, C.D., and Lucchesi, J.C. (2000). The drosophila MSL complex acetylates histone H4 at lysine 16, a chromatin modification linked to dosage compensation. Molecular and cellular biology *20*, 312-318.
26. Corona, D.F., Clapier, C.R., Becker, P.B., and Tamkun, J.W. (2002). Modulation of ISWI function by site-specific histone acetylation. EMBO reports *3*, 242-247.
27. Kimura, A., Umehara, T., and Horikoshi, M. (2002). Chromosomal gradient of histone acetylation established by Sas2p and Sir2p functions as a shield against gene silencing. Nature genetics *32*, 370-377.
28. Smith, E.R., Cayrou, C., Huang, R., Lane, W.S., Cote, J., and Lucchesi, J.C. (2005). A human protein complex homologous to the Drosophila MSL complex is responsible for the majority of histone H4 acetylation at lysine 16. Molecular and cellular biology *25*, 9175-9188.

29. Suka, N., Luo, K., and Grunstein, M. (2002). Sir2p and Sas2p opposingly regulate acetylation of yeast histone H4 lysine16 and spreading of heterochromatin. Nature genetics *32*, 378-383.
30. Taipale, M., Rea, S., Richter, K., Vilar, A., Lichter, P., Imhof, A., and Akhtar, A. (2005). hMOF histone acetyltransferase is required for histone H4 lysine 16 acetylation in mammalian cells. Molecular and cellular biology *25*, 6798-6810.
31. Consortium, C.e.S. (1998). Genome sequence of the nematode C. elegans: a platform for investigating biology. Science *282*, 2012-2018.
32. Shogren-Knaak, M., Ishii, H., Sun, J.M., Pazin, M.J., Davie, J.R., and Peterson, C.L. (2006). Histone H4-K16 acetylation controls chromatin structure and protein interactions. Science *311*, 844-847.
33. Sanjuan, R., and Marin, I. (2001). Tracing the origin of the compensasome: evolutionary history of DEAH helicase and MYST acetyltransferase gene families. Molecular biology and evolution *18*, 330-343.
34. Shi, Y., and Mello, C. (1998). A CBP/p300 homolog specifies multiple differentiation pathways in Caenorhabditis elegans. Genes & development *12*, 943-955.
35. Thomas, T., and Voss, A.K. (2007). The diverse biological roles of MYST histone acetyltransferase family proteins. Cell cycle *6*, 696-704.
36. Hedgecock, E.M., and White, J.G. (1985). Polyploid tissues in the nematode Caenorhabditis elegans. Developmental biology *107*, 128-133.
37. Ikura, T., Ogryzko, V.V., Grigoriev, M., Groisman, R., Wang, J., Horikoshi, M., Scully, R., Qin, J., and Nakatani, Y. (2000). Involvement of the TIP60 histone acetylase complex in DNA repair and apoptosis. Cell *102*, 463-473.
38. Kimura, A., and Horikoshi, M. (1998). Tip60 acetylates six lysines of a specific class in core histones in vitro. Genes to cells : devoted to molecular & cellular mechanisms *3*, 789-800.
39. Smith, E.R., Eisen, A., Gu, W., Sattah, M., Pannuti, A., Zhou, J., Cook, R.G., Lucchesi, J.C., and Allis, C.D. (1998). ESA1 is a histone acetyltransferase that is essential for growth in yeast. Proceedings of the National Academy of Sciences of the United States of America *95*, 3561-3565.
40. Davis, T.L., and Meyer, B.J. (1997). SDC-3 coordinates the assembly of a dosage compensation complex on the nematode X chromosome. Development *124*, 1019-1031.
41. Baugh, L.R., Hill, A.A., Slonim, D.K., Brown, E.L., and Hunter, C.P. (2003). Composition and dynamics of the Caenorhabditis elegans early embryonic transcriptome. Development *130*, 889-900.
42. Dawes, H.E., Berlin, D.S., Lapidus, D.M., Nusbaum, C., Davis, T.L., and Meyer, B.J. (1999). Dosage compensation proteins targeted to X chromosomes by a determinant of hermaphrodite fate. Science *284*, 1800-1804.
43. Chuang, P.T., Lieb, J.D., and Meyer, B.J. (1996). Sex-specific assembly of a dosage compensation complex on the nematode X chromosome. Science *274*, 1736-1739.

44. Kramer, M., Kranz, A.L., Su, A., Winterkorn, L.H., Albritton, S.E., and Ercan, S. (2015). Developmental Dynamics of X-Chromosome Dosage Compensation by the DCC and H4K20me1 in C. elegans. PLoS genetics *11*, e1005698.
45. Croft, J.A., Bridger, J.M., Boyle, S., Perry, P., Teague, P., and Bickmore, W.A. (1999). Differences in the localization and morphology of chromosomes in the human nucleus. The Journal of cell biology *145*, 1119-1131.
46. Naughton, C., Sproul, D., Hamilton, C., and Gilbert, N. (2010). Analysis of active and inactive X chromosome architecture reveals the independent organization of 30 nm and large-scale chromatin structures. Molecular cell *40*, 397-409.
47. Powell-Coffman, J.A., Knight, J., and Wood, W.B. (1996). Onset of C. elegans gastrulation is blocked by inhibition of embryonic transcription with an RNA polymerase antisense RNA. Developmental biology *178*, 472-483.
48. Taylor, G.C., Eskeland, R., Hekimoglu-Balkan, B., Pradeepa, M.M., and Bickmore, W.A. (2013). H4K16 acetylation marks active genes and enhancers of embryonic stem cells, but does not alter chromatin compaction. Genome research *23*, 2053-2065.
49. Wang, Z., Zang, C., Cui, K., Schones, D.E., Barski, A., Peng, W., and Zhao, K. (2009). Genome-wide mapping of HATs and HDACs reveals distinct functions in active and inactive genes. Cell *138*, 1019-1031.
50. Wang, Z., Zang, C., Rosenfeld, J.A., Schones, D.E., Barski, A., Cuddapah, S., Cui, K., Roh, T.Y., Peng, W., Zhang, M.Q., et al. (2008). Combinatorial patterns of histone acetylations and methylations in the human genome. Nature genetics *40*, 897-903.
51. Alekseyenko, A.A., Larschan, E., Lai, W.R., Park, P.J., and Kuroda, M.I. (2006). High-resolution ChIP-chip analysis reveals that the Drosophila MSL complex selectively identifies active genes on the male X chromosome. Genes & development *20*, 848-857.
52. Gilfillan, G.D., Straub, T., de Wit, E., Greil, F., Lamm, R., van Steensel, B., and Becker, P.B. (2006). Chromosome-wide gene-specific targeting of the Drosophila dosage compensation complex. Genes & development *20*, 858-870.
53. Kind, J., Vaquerizas, J.M., Gebhardt, P., Gentzel, M., Luscombe, N.M., Bertone, P., and Akhtar, A. (2008). Genome-wide analysis reveals MOF as a key regulator of dosage compensation and gene expression in Drosophila. Cell *133*, 813-828.
54. Smith, E.R., Allis, C.D., and Lucchesi, J.C. (2001). Linking global histone acetylation to the transcription enhancement of X-chromosomal genes in Drosophila males. The Journal of biological chemistry *276*, 31483-31486.
55. Crane, E., Bian, Q., McCord, R.P., Lajoie, B.R., Wheeler, B.S., Ralston, E.J., Uzawa, S., Dekker, J., and Meyer, B.J. (2015). Condensin-driven remodelling of X chromosome topology during dosage compensation. Nature *523*, 240-244.
56. Kelly, W.G., Schaner, C.E., Dernburg, A.F., Lee, M.H., Kim, S.K., Villeneuve, A.M., and Reinke, V. (2002). X-chromosome silencing in the germline of C. elegans. Development *129*, 479-492.

57. Crittenden, S.L., Leonhard, K.A., Byrd, D.T., and Kimble, J. (2006). Cellular analyses of the mitotic region in the Caenorhabditis elegans adult germ line. Molecular biology of the cell *17*, 3051-3061.
58. Yonker, S.A., and Meyer, B.J. (2003). Recruitment of C. elegans dosage compensation proteins for gene-specific versus chromosome-wide repression. Development *130*, 6519-6532.
59. Jans, J., Gladden, J.M., Ralston, E.J., Pickle, C.S., Michel, A.H., Pferdehirt, R.R., Eisen, M.B., and Meyer, B.J. (2009). A condensin-like dosage compensation complex acts at a distance to control expression throughout the genome. Genes & development *23*, 602-618.
60. Wegel, E., and Shaw, P. (2005). Gene activation and deactivation related changes in the three-dimensional structure of chromatin. Chromosoma *114*, 331-337.
61. Voss, A.K., and Thomas, T. (2009). MYST family histone acetyltransferases take center stage in stem cells and development. BioEssays : news and reviews in molecular, cellular and developmental biology *31*, 1050-1061.
62. Thomas, T., Dixon, M.P., Kueh, A.J., and Voss, A.K. (2008). Mof (MYST1 or KAT8) is essential for progression of embryonic development past the blastocyst stage and required for normal chromatin architecture. Molecular and cellular biology *28*, 5093-5105.
63. Dunlap, D., Yokoyama, R., Ling, H., Sun, H.Y., McGill, K., Cugusi, S., and Lucchesi, J.C. (2012). Distinct contributions of MSL complex subunits to the transcriptional enhancement responsible for dosage compensation in Drosophila. Nucleic acids research *40*, 11281-11291.
64. Bell, O., Schwaiger, M., Oakeley, E.J., Lienert, F., Beisel, C., Stadler, M.B., and Schubeler, D. (2010). Accessibility of the Drosophila genome discriminates PcG repression, H4K16 acetylation and replication timing. Nature structural & molecular biology *17*, 894-900.
65. Zhang, Y., and Oliver, B. (2010). An evolutionary consequence of dosage compensation on Drosophila melanogaster female X-chromatin structure? BMC genomics *11*, 6.
66. Dorigo, B., Schalch, T., Bystricky, K., and Richmond, T.J. (2003). Chromatin fiber folding: requirement for the histone H4 N-terminal tail. Journal of molecular biology *327*, 85-96.
67. Cai, Y., Jin, J., Swanson, S.K., Cole, M.D., Choi, S.H., Florens, L., Washburn, M.P., Conaway, J.W., and Conaway, R.C. (2010). Subunit composition and substrate specificity of a MOF-containing histone acetyltransferase distinct from the male-specific lethal (MSL) complex. The Journal of biological chemistry *285*, 4268-4272.
68. Feller, C., Prestel, M., Hartmann, H., Straub, T., Soding, J., and Becker, P.B. (2012). The MOF-containing NSL complex associates globally with housekeeping genes, but activates only a defined subset. Nucleic acids research *40*, 1509-1522.

69. Lam, K.C., Muhlpfordt, F., Vaquerizas, J.M., Raja, S.J., Holz, H., Luscombe, N.M., Manke, T., and Akhtar, A. (2012). The NSL Complex Regulates Housekeeping Genes in Drosophila. PLoS genetics *8*.
70. Raja, S.J., Charapitsa, I., Conrad, T., Vaquerizas, J.M., Gebhardt, P., Holz, H., Kadlec, J., Fraterman, S., Luscombe, N.M., and Akhtar, A. (2010). The Nonspecific Lethal Complex Is a Transcriptional Regulator in Drosophila. Molecular cell *38*, 827-841.
71. Marin, I., and Baker, B.S. (2000). Origin and evolution of the regulatory gene male-specific lethal-3. Molecular biology and evolution *17*, 1240-1250.
72. Kusch, T., Florens, L., MacDonald, W.H., Swanson, S.K., Glaser, R.L., Yates, J.R., Abmayr, S.M., Washburn, M.P., and Workman, J.L. (2004). Acetylation by Tip60 is required for selective histone variant exchange at DNA lesions. Science *306*, 2084-2087.
73. Chen, P.B., Hung, J.H., Hickman, T.L., Coles, A.H., Carey, J.F., Weng, Z., Chu, F., and Fazzio, T.G. (2013). Hdac6 regulates Tip60-p400 function in stem cells. eLife *2*, e01557.
74. Fazzio, T.G., Huff, J.T., and Panning, B. (2008). An RNAi screen of chromatin proteins identifies Tip60-p400 as a regulator of embryonic stem cell identity. Cell *134*, 162-174.
75. Ravens, S., Yu, C., Ye, T., Stierle, M., and Tora, L. (2015). Tip60 complex binds to active Pol II promoters and a subset of enhancers and co-regulates the c-Myc network in mouse embryonic stem cells. Epigenetics & chromatin *8*, 45.
76. Patel, J.H., Du, Y., Ard, P.G., Phillips, C., Carella, B., Chen, C.J., Rakowski, C., Chatterjee, C., Lieberman, P.M., Lane, W.S., et al. (2004). The c-MYC oncoprotein is a substrate of the acetyltransferases hGCN5/PCAF and TIP60. Molecular and cellular biology *24*, 10826-10834.
77. Sykes, S.M., Mellert, H.S., Holbert, M.A., Li, K., Marmorstein, R., Lane, W.S., and McMahon, S.B. (2006). Acetylation of the p53 DNA-binding domain regulates apoptosis induction. Molecular cell *24*, 841-851.
78. Frank, S.R., Parisi, T., Taubert, S., Fernandez, P., Fuchs, M., Chan, H.M., Livingston, D.M., and Amati, B. (2003). MYC recruits the TIP60 histone acetyltransferase complex to chromatin. EMBO reports *4*, 575-580.
79. Taubert, S., Gorrini, C., Frank, S.R., Parisi, T., Fuchs, M., Chan, H.M., Livingston, D.M., and Amati, B. (2004). E2F-dependent histone acetylation and recruitment of the Tip60 acetyltransferase complex to chromatin in late G1. Molecular and cellular biology *24*, 4546-4556.
80. Ceol, C.J., and Horvitz, H.R. (2004). A new class of C. elegans synMuv genes implicates a Tip60/NuA4-like HAT complex as a negative regulator of Ras signaling. Developmental cell *6*, 563-576.
81. Shibata, Y., Sawa, H., and Nishiwaki, K. (2014). HTZ-1/H2A.z and MYS-1/MYST HAT act redundantly to maintain cell fates in somatic gonadal cells through repression of ceh-22 in C. elegans. Development *141*, 209-218.

82. Wang, J., Tadeo, X., Hou, H., Tu, P.G., Thompson, J., Yates, J.R., 3rd, and Jia, S. (2013). Epe1 recruits BET family bromodomain protein Bdf2 to establish heterochromatin boundaries. Genes & development *27*, 1886-1902.
83. Andersson, K., Bjorkroth, B., and Daneholt, B. (1984). Packing of a specific gene into higher order structures following repression of RNA synthesis. The Journal of cell biology *98*, 1296-1303.
84. Chambeyron, S., and Bickmore, W.A. (2004). Chromatin decondensation and nuclear reorganization of the HoxB locus upon induction of transcription. Genes & development *18*, 1119-1130.
85. Bulger, M., Schubeler, D., Bender, M.A., Hamilton, J., Farrell, C.M., Hardison, R.C., and Groudine, M. (2003). A complex chromatin landscape revealed by patterns of nuclease sensitivity and histone modification within the mouse beta-globin locus. Molecular and cellular biology *23*, 5234-5244.
86. Kim, A., and Dean, A. (2003). A human globin enhancer causes both discrete and widespread alterations in chromatin structure. Molecular and cellular biology *23*, 8099-8109.
87. Litt, M.D., Simpson, M., Gaszner, M., Allis, C.D., and Felsenfeld, G. (2001). Correlation between histone lysine methylation and developmental changes at the chicken beta-globin locus. Science *293*, 2453-2455.
88. Allahverdi, A., Yang, R.L., Korolev, N., Fan, Y.P., Davey, C.A., Liu, C.F., and Nordenskiold, L. (2011). The effects of histone H4 tail acetylations on cation-induced chromatin folding and self-association. Nucleic acids research *39*, 1680-1691.
89. Robinson, P.J., An, W., Routh, A., Martino, F., Chapman, L., Roeder, R.G., and Rhodes, D. (2008). 30 nm chromatin fibre decompaction requires both H4-K16 acetylation and linker histone eviction. Journal of molecular biology *381*, 816-825.
90. Ercan, S., Lubling, Y., Segal, E., and Lieb, J.D. (2011). High nucleosome occupancy is encoded at X-linked gene promoters in C. elegans. Genome research *21*, 237-244.
91. Ikegami, K., Egelhofer, T.A., Strome, S., and Lieb, J.D. (2010). Caenorhabditis elegans chromosome arms are anchored to the nuclear membrane via discontinuous association with LEM-2. Genome biology *11*, R120.
92. Therizols, P., Illingworth, R.S., Courilleau, C., Boyle, S., Wood, A.J., and Bickmore, W.A. (2014). Chromatin decondensation is sufficient to alter nuclear organization in embryonic stem cells. Science *346*, 1238-1242.
93. Carpenter, A.E., Memedula, S., Plutz, M.J., and Belmont, A.S. (2005). Common effects of acidic activators on large-scale chromatin structure and transcription. Molecular and cellular biology *25*, 958-968.
94. Li, X., Li, L., Pandey, R., Byun, J.S., Gardner, K., Qin, Z., and Dou, Y. (2012). The histone acetyltransferase MOF is a key regulator of the embryonic stem cell core transcriptional network. Cell stem cell *11*, 163-178.
95. Liu, T., Rechtsteiner, A., Egelhofer, T.A., Vielle, A., Latorre, I., Cheung, M.S., Ercan, S., Ikegami, K., Jensen, M., Kolasinska-Zwierz, P., et al. (2011). Broad

chromosomal domains of histone modification patterns in C. elegans. Genome research *21*, 227-236.
96. Mendjan, S., Taipale, M., Kind, J., Holz, H., Gebhardt, P., Schelder, M., Vermeulen, M., Buscaino, A., Duncan, K., Mueller, J., et al. (2006). Nuclear pore components are involved in the transcriptional regulation of dosage compensation in Drosophila. Molecular cell *21*, 811-823.
97. Brenner, S. (1974). The genetics of Caenorhabditis elegans. Genetics *77*, 71-94.
98. Kamath, R.S., and Ahringer, J. (2003). Genome-wide RNAi screening in Caenorhabditis elegans. Methods *30*, 313-321.
99. Nabeshima, K., Mlynarczyk-Evans, S., and Villeneuve, A.M. (2011). Chromosome painting reveals asynaptic full alignment of homologs and HIM-8-dependent remodeling of X chromosome territories during Caenorhabditis elegans meiosis. PLoS genetics *7*, e1002231.
100. Csankovszki, G., McDonel, P., and Meyer, B.J. (2004). Recruitment and spreading of the C. elegans dosage compensation complex along X chromosomes. Science *303*, 1182-1185.
101. Csankovszki, G., Collette, K., Spahl, K., Carey, J., Snyder, M., Petty, E., Patel, U., Tabuchi, T., Liu, H., McLeod, I., et al. (2009). Three distinct condensin complexes control C. elegans chromosome dynamics. Current biology : CB *19*, 9-19.
102. Kranz, A.L., Jiao, C.Y., Winterkorn, L.H., Albritton, S.E., Kramer, M., and Ercan, S. (2013). Genome-wide analysis of condensin binding in Caenorhabditis elegans. Genome biology *14*, R112.
103. Ni, J.Z., Chen, E., and Gu, S.G. (2014). Complex coding of endogenous siRNA, transcriptional silencing and H3K9 methylation on native targets of germline nuclear RNAi in C. elegans. BMC genomics *15*, 1157.
104. Langmead, B. (2010). Aligning short sequencing reads with Bowtie. Current protocols in bioinformatics / editoral board, Andreas D. Baxevanis ... [et al.] *Chapter 11*, Unit 11 17.
105. Zhang, Y., Liu, T., Meyer, C.A., Eeckhoute, J., Johnson, D.S., Bernstein, B.E., Nusbaum, C., Myers, R.M., Brown, M., Li, W., et al. (2008). Model-based analysis of ChIP-Seq (MACS). Genome biology *9*, R137.
106. Shin, H., Liu, T., Manrai, A.K., and Liu, X.S. (2009). CEAS: cis-regulatory element annotation system. Bioinformatics *25*, 2605-2606.
107. Thorvaldsdottir, H., Robinson, J.T., and Mesirov, J.P. (2013). Integrative Genomics Viewer (IGV): high-performance genomics data visualization and exploration. Briefings in bioinformatics *14*, 178-192.
108. Trapnell, C., Pachter, L., and Salzberg, S.L. (2009). TopHat: discovering splice junctions with RNA-Seq. Bioinformatics *25*, 1105-1111.
109. Trapnell, C., Roberts, A., Goff, L., Pertea, G., Kim, D., Kelley, D.R., Pimentel, H., Salzberg, S.L., Rinn, J.L., and Pachter, L. (2012). Differential gene and transcript expression analysis of RNA-seq experiments with TopHat and Cufflinks. Nature protocols *7*, 562-578.

110. Anders, S., Pyl, P.T., and Huber, W. (2015). HTSeq--a Python framework to work with high-throughput sequencing data. Bioinformatics *31*, 166-169.
111. Anders, S., and Huber, W. (2010). Differential expression analysis for sequence count data. Genome biology *11*, R106.

CHAPTER 5

A role for histone acetyltransferase activity in targeting the *C. elegans* dosage compensation complex to the X chromosomes

ABSTRACT

Dosage compensation is the gene regulatory mechanism that equalizes X-linked gene expression between the sexes. Worm dosage compensation is achieved by the activity of the dosage compensation complex (DCC). The DCC binds specifically to the X chromosome in hermaphrodites to downregulate transcription by two fold. How the DCC is able to distinguish the X from the autosomes is also not fully understood, although an X-enriched sequence motif is known to be involved. In this study we demonstrated that chromatin structure modulation by histone acetyltransferases (HATs) plays a role in DCC targeting. HATs are responsible for acetylating the histones within the nucleosome. Using FISH microscopy we noticed that hermaphrodite worms depleted of the HATs MYS-1, MYS-4 or CBP-1 exhibit a dispersed X chromosome structure when normally the X chromosome territory is compact. By contrast chromosome I remains unchanged. This contradicts the belief that histone acetylation influences a less compact chromatin configuration. In addition, using immunofluorescence and FISH microscopy, we find that DCC localization is disrupted in HAT depletions. We see mislocalization of the DCC away from the X chromosomes and

onto autosomes, suggesting that HATs play a role in targeting the DCC to the X chromosomes, which in turn is responsible for maintaining a compact X chromosome structure. Therefore, chromatin organization likely plays an important, and as yet incompletely understood, role in *C. elegans* dosage compensation.

INTRODUCTION

Dosage compensation is a mechanism that equalizes X linked gene expression between the sexes and balances X to autosomes within the sexes. Although dosage compensation mechanisms vary among species [1-4], all require chromosome-specific-targeting of molecular complexes, which in turn regulates transcription over large domains [5,6]. The study of dosage compensation allows for a better understanding of the mechanisms by which domain-specific regulatory complexes are recruited to specific regions and function over large distances. Ultimately, this will further our knowledge of how gene regulation is achieved.

Chromatin changes play a large role in dosage compensation. Fly dosage compensation involves the two-fold upregulation of the single male X chromosome, which is achieved by the MSL complex-mediated H6K16ac hyperacetylation [7-9]. In mammals the non-coding RNA *Xist* [10,11] along with the recruitment of the repressive complexes PRC1 and PRC2 transcriptionally inactivates one of the two X chromosomes in females [12-14]. In worms, both hermaphrodite X chromosomes are downregulated by the action of the dosage compensation complex (DCC) [3,4,15]. DCC activity leads to the enrichment of H4K20me1 [16,17] and the depletion of H4K16ac on the X [17], which is required for X chromosome compaction [18]. These DCC-mediated chromatin

changes then lead to decreased levels of RNA Polymerase II (Poll II) [19]. However the main question of how DCC-mediated changes in X chromosome structure lead to changes in RNA Polymerase recruitment remains unresolved.

Unlike mammals and flies in which the assembly and establishment of X inactivation and the MSL complex have been well characterized [10,11,20-31], how the DCC is targeted to the X chromosome as opposed to the autosome is not fully understood. In worms, the DCC is thought to be recruited and bind to the X at a number of randomly located recruitment loci, known as *rex* (recruitment element on X) sites, then spread in *cis* to neighboring sites, *dox* (dependent of X) sites, that are unable to recruit the DCC on their own [19,32]. It is believed that the targeting of the DCC involves a sequence element known as the MEX (motif enrichment on X) motif, which is slightly enriched on the X and at *rex* sites [19,32]. Additionally RNA Pol II transcription is important for the spreading of the complex across the X chromosome. The DCC is correlated with transcriptional activity, and is found to disengage from repressed genes and recruit to active genes during development. [33]. However, not all *rex* sites contain the MEX motif and there are copies of the MEX motifs on the autosomes and MEX sites of the X that do not bind the DCC [32,34]. Therefore it is believed that the MEX motif is not the only factor involved in DCC recruitment and it is hypothesized that chromatin may also play a role in DCC localization. For instance, it is known that the histone variant HTZ-1 (H2A.Z) restricts DCC binding to the X chromosome and acts as a barrier element to DCC binding on autosomes [35]. However, no additional chromatin changes have been implicated to play a role in DCC targeting.

We already know that chromatin plays a role in DCC recruitment [35]. Therefore, we investigated novel chromatin regulators function in the process. We examined the function HATs have on X chromosome structure and DCC recruitments, by studying three different *C. elegans* HATs: MYS-1, MYS-4 and CBP-1. These HATs fall under two of the three major HAT families, the MYST family and the CBP/p300 family, and are often correlated with active transcription [36]. MYS-1 is the *C. elegans* ortholog of mammalian protein Tip60 or yeast Esa1, a MYST family HAT [37]. Tip60 has been shown to function in several cellular processes, such as cell cycle progression, DNA repair, cell signaling and apoptosis [38]. The direct homolog of MYS-4 has not been resolved but it is believed to be a member of the MOZ/MORF subfamily of MYSTs [39]. Lastly CBP-1 encodes a homolog of the mammalian global transcriptional coactivator proteins CBP and p300 [36,40]. We find that the depletion of these HATs leads the decondensation of the X chromosome, which contradicts the belief that histone acetylation is correlated with decondensed chromatin configuration. HAT depletions do not lead to a decrease in DCC protein levels however they disrupt DCC localization to the X chromosome. Our data suggests that the DCC requires the action of HAT proteins for proper X chromosome localization. In addition, the proper targeting of the DCC may be responsible for maintaining a compact X chromosome structure.

RESULTS

HAT depletions have disrupted X chromosome structure

To determine if histone acetyltransferases affects X chromosome structure we performed X chromosome paint fluorescence *in situ* hybridization (FISH) in the various

HAT knockdowns. We deleted different HATs by feeding worms bacteria expressing double stranded RNA corresponding to the HAT of interest. Additionally, worms were fed bacteria carrying an empty vector as a control. In wild type worms the X chromosome is compact due to the DCC [18], however in the absence of certain HATs X chromosome compaction is lost (Figure 5.1A and B). When depleting MYS-1, MYS-4 or CBP-1, the X chromosome territories look decondensed compared to wild type, whereas MYS-2 has no effect in X chromosome compaction (Figure 5.1A). We then quantified chromosome territories, as in [18]. X chromosome volume quantifications showed that in MYS-1, MYS-4 and CBP-1 depletions the X chromosome territory where decondensed, occupying 17.11±2.66%, 16.39±2.45%, and 18.64±3.39% respectively. This was significantly larger than the 9.41±2.21%, occupied by wild type X chromosome territories ($p<0.001$, Student's t-test, for MYS-1, MYS-4 and CBP-1 compared to wild type). The degree of decondensaton in these HAT depleted worms is equivalent to what is observed in DCC mutants and depletions, with DCC mutant X chromosome territories occupying an average of 17% [18]. The depletion of MYS-2 showed no significant change in X chromosome territories occupying 10.20±2.25% (Figure 5.1B). We also examined the histone variant HTZ-1 (H2A.Z) which activity restricts DCC binding to the X chromosome [35]. We observed that X chromosome territory was significantly decondensed when HTZ-1 is depleted and DCC localization is perturbed, with the X occupying 17.57±3.08% ($p<0.001$) (Figure 5.1A and B). We conclude that the X chromosome is decondensed to a significant degree in MYS-1, MYS-4 and CBP-1 depletions.

We next examined chromosome I territories to determine whether the decondensation phenotype is X specific in MYS-1, MYS-4 and CBP-1 depletions. Chromosome I was unaffected in HAT and HTZ.1 depletions with an average chromosome I occupancy of about 14%, which was comparable to the 14.14±2.70% observed in wild type worms (Figures 5.1C and D). These data demostrate that MYS-1, MYS-4 and CBP-1 are required for compaction of the X and suggests they may have an affect on dosage compensation.

MYS-1 acetylates H4K16, while CBP-1 acetylates H3K56

MYS-1 is homologous to human Tip60, which is known to acetylate H2AK5 and H4K5, K8, K12, and K16 *in vitro* [41-43]. CBP-1 is homologous to CBP/p300, which can acetylate all four core histones [44] but has also been shown to specifically acetylate H3K56ac in mammals and *Drosophila* [45]. To determine which histone marks MYS-1, MYS-4, and CBP-1 were acetylating we performed western blot analysis with antibodies specific to H4K16ac, H3K56ac, and H3K9ac in control vector worms and *mys(RNAi)*, *mys-4(RNAi)*, and *cbp-1(RNAi)* worms. In Chapter 4, we had found that MYS-1 is the major H4K16ac HAT in worms; similarly we see that H4K16ac is lost in MYS-1 depleted animals while the other acetylated marks show no reduction (Figure 5.2). H4K56ac appears to by mediated by CBP-1, as we see depleted levels of H4K56ac in *cbp-1(RNAi)* worms (Figure 5.2B and D). Additionally depleting CBP-1 also causes a slight decrease in of H4K16ac and H3K9ac levels which is consistent with data reporting that CBP can acetylate all four core histones (Figure 5.2A and Figure 5.2C-D) [44]. Lastly MYS-4 depletion did not appear to reduce any histone acetylation levels, however it did

lead to increased levels of H3K56ac (Figure 5.2). These results suggest that MYS-1 is the major H4K16ac HAT in worms, while CBP-1 is capable of acetylating many histone marks and has greater affects on H3K56ac. MYS-4 homology is unknown, therefore more histone marks need to be examined to determine MYS-4 acetylation capabilities.

HAT depletions do not lead to a decrease in DCC protein levels

The disruption of X chromosome structure in HAT depleted worms suggest that dosage compensation may also be affected. To explore whether MYS-1, MYS-4 or CBP-1 impact DCC protein levels we performed a western blot analysis of MYS-1, MYS-4 and CBP-1 depleted animals and examined DCC components DPY-27 [14] and CAPG-1 [46]. In HAT depleted animals we do not observe a large change in DCC protein levels compared to vector control worms (Figure 5.3). This indicates these HATs do not affect DCC expression. Our results suggest that, MYS-1, MYS-4 or CBP-1 depletion does not lead to defects in overall DCC protein levels and therefore may have a more direct role in dosage compensation by affecting DCC localization or function.

DCC localization is disrupted in HAT depleted animals

To test whether the HATs MYS-1, MYS-4, and CBP-1 affect DCC localization we used DPY-27 immunofluorescence (to mark the localization of the DCC) and FISH (to mark the X) to observe DCC localization in HAT depleted worms. We find the DCC is present at normal levels in HAT depleted worms, confirming that depleting MYS-1, MYS-4 or CBP-1 does not lead to a reduction in DCC protein levels. However, the DCC is dispersed and mislocalized from the X chromosome, and exhibits aberrant binding to the X and autosomes (Figure 5.4). This suggests that these HATs play a critical role in

proper DCC localization. To investigate whether HATs are required for the DCC to stably bind chromatin, we performed a detergent extraction prior to fixing the tissue to remove nucleoplasmic content. We found that in HAT depleted worms the mislocalized DCC signal was not sensitive to detergent extraction. This is in contrast to what we observe in the DCC mutant, DPY-30, where DCC signal is lost after detergent extraction, because DPY-30 is required for the complex to stably bind chromatin (Figure 5.5) [47]. This indicates that in HAT depleted animals, the DCC is stably bound to chromatin and mislocalized.

H4K20me1 enrichment is maintained and colocalizes with the DCC

We next asked whether DCC function is disrupted when it is mislocalized upon HAT depletion. Currently known molecular functions for the DCC include altering X chromosome topology [48], condensation of the X chromosome [18,49], and differential distribution of the histone modifications H4K20me1 and H4K16ac on the X [16,17]. The misloclization of the DCC clearly disrupts X chromosome structure (Figure 5.1), therefore we next examined whether depleting HATs alters the distribution of H4K20me1. To test this, we co-stained HAT depleted worms with antibodies to CAPG-1 (to mark the DCC) and H4K20me. H4K20me1 remained colocalized with the DCC, implying that the mislocalized DCC also leads to mislocalized H4K20me1 (Figure 5.6). Altogether our data demonstrates that ectopic DCC binding on autosomes alters X specific chromatin marks and titrates the complex away from the X chromosome thereby compromising X chromosome compaction.

DISCUSSION

The DCC is believed to be targeted by the MEX motif however several MEX motifs are on autosome or lack binding of the DCC on the X. Additionally not all of DCC *rex* binding sites contain the MEX motif [32,34]. Therefore it is believed that chromatin modifications also play a role in DCC targeting. In this study we sought to explore the role of histone acetyltransferases in DCC targeting and recruitment. We have previously provided some evidence in that the histone variant HTZ-1 is required for the specific binding of the DCC to the X chromosome [35,50]. Here we establish that depleting MYS-1, MYS-4 or CBP-1 also disrupts the compact X chromosome structure. In addition, these HATs are required for the proper localization of the DCC on the X.

Possible mechanism of HAT activity in dosage compensation

We suggest that HAT depletions leads to ectopic DCC binding to autosomes which reduces the amount of DCC binding to the X chromosomes. As a result the DCC is unable to properly compact the X chromosome and dosage compensation is impaired. MYS-1/Tip60 and CBP/p300 are often described as transcriptional coactivators. One possible mechanism for MYS-1, MYS-4, and CBP-1 activity is promoting expression of DCC components or other genes that positively regulate dosage compensation, however we find that MYS-1, MYS-4, and CBP-1 are not acting by regulating DCC protein levels. Another possibility is that HATs activity is acting in transcription repression. Although histone acetylation is often associated with gene activation, there are instances of acetylation activity in transcriptional repression. In yeast the MYST family HATs Sas2 and Sas3 function in the silencing of mating type loci

and telomeres [51]. Additionally Tip60 transcriptionally represses genes in mouse ES cells. The depletion of Tip60 results in the upregulation of genes involved in differentiation and embryonic development and the downregulation of cell cycle regulators. However more genes are upregulated than downregulated, suggesting a role in transcriptional repression [52]. Another yeast HAT, Rtt109, similar to that of p300, is responsible for acetylating H3K56, which has been found to be important for correct three-dimensional organization of chromosomes within the nucleus. Deletion of Rtt109 and lack of H3K56ac results in loss of telomere localization to the nuclear periphery, and the correct peripheral localization of the “chromosome-organizing clamp” locus [53]. Therefore, it is possible that, instead of activating genes, these HATs could act in dosage compensation by transcriptionally repressing X-linked dosage compensated genes.

Chromatin modifications and dosage compensation

In mammals and flies, chromatin modifications, such as histone modifications or histone variants, are key factors in dosage compensation and regulating the X chromosome. For example in flies, the two fold X upregulation in males is regulated by MOF-mediated H4K16ac [7-9], where as in mammals the formation of heterochromatin along the inactive X is key to reducing X expression in females [12-14]. Additionally DNA methylation and the replacement of canonical histones with histone variants play important roles in mammalian X inactivation [54-57]. *C. elegans* X chromosomes also retain a repressive chromatin confirmation to achieve two-fold repression. The repressive mark H4K20me1 is enriched on the X, while H4K16ac is depleted [16,17].

Additionally the histone variant HTZ-1 is required for specific X chromosome binding of the DCC [35]. We have found that histone modifying enzymes may also be involved in the recruitment, binding or function of the DCC. There is precedent for chromatin environment to influence the recruitment and spreading of dosage compensation components in mammals and flies. In mammals, Xist is able to spread across the inactive X chromosome by taking advantage of the three-dimensional structure of the chromosome [58]. In flies, the low occupancy of histone H3 at MSL complex binding sites (chromatin entry sites, CES) is believed to by a key defining characteristic of functional binding sites [59]. Overall, chromatin organization likely plays an important, and as yet incompletely understood, role in *C. elegans* dosage compensation.

MATERIALS AND METHODS

Strains

All strains were maintained on NG agar plates with *E. coli* (OP50) as a food source, using standard methods [76]. Strains include: N2 Bristol strain (wild type) and TY1936 *dpy-30(y228)* V/nT1 (*unc-?* (n754*) let-?*).

RNA interference

E. coli HT115 bacteria expressing double stranded RNA for *mys-1*, *mys-2, mys-4, cbp-1, htz-1*, or vector control (polylinker), were used for feeding RNAi using the Ahringer laboratory RNAi feeding library [60]. Two generation feeding RNAi was performed as follows; L1s were placed on RNAi plate and grown to adulthood. P_0 adults from one generation feeding RNAi were transferred to new RNAi plates to produce progeny for 24 hours. These progeny (F_1 generation) were grown to adulthood and

examined.

Fluorescence *in situ* hybridization (FISH)

To generate FISH probe templates, purified yeast artificial chromosome (YAC) DNA were amplified by degenerate oligonucleotide primed PCR [61,62]. The labeled chromosome-paint probes were prepared and FISH was preformed as previously described [18,62].

Microscopy and Image Analysis

Detailed description of image analysis was previously described [18]. To summarize masks were applied over an image for all nuclei for each channel. DAPI mask was used as the total volume of the nucleus. The percent nuclear volume was obtained by dividing the volume of the specific chromosome over the volume of the whole nucleus, taking the average over all nuclei for final mean percent.

Western blot analysis

Equal numbers of adult RNAi-treated worms were collected in M9 solution. Equal volume of sample buffer (0.1 M Tris pH 6.8, 7.5 M urea, 2% SDS, 100mM β-ME, 0.05% bromophenol blue) was added to worms. Lysates were prepared by 10 minute heating at 65°C, two 30 second bursts of sonication, 5 minute heating to 65°C, 5 minute heating to 95°C, then kept at 37°C until loading onto SDS-PAGE gel. Proteins were transferred to nitrocellulose and blotted with the following antibodies: rabbit anti-DPY-27 [46], goat anti-CAPG-1, and rabbit anti-beta tubulin (Novus NB600-936). Band intensities were quantified using ImageJ and protein levels for histone marks and DCC proteins were normalized to tubulin.

Immunofluorescence

Immunofluorescence experiments were performed as described [46]. Young adult worms were dissected in 1X sperm salts, fixed in 2% paraformaldehyde in 1X sperm salts for 5 minutes and frozen on dry-ice for 10 minutes. Then slides were washed three times in PBS before overnight incubation with diluted primary antibodies in a humid chamber, at room temperature. Slides were then washed three times for 10 minutes with PBST, incubated for 1 hour with diluted secondary antibody at 37°C, washed twice for 10 minutes with PBST, and once for 10 minutes with PBST plus DAPI. Slides were mounted with Vectashield (Vector Labs). Antibodies were used at the following concentrations: CAPG-1, 1:100; DPY-27, 1:100; H4K20me1, 1:500.

Detergent extraction

Detergent extraction of nucleoplasmic protein from dissected nuclei was performed by dissecting animals in 1X sperm salts plus 1% Triton detergent. Dissected animals were processed for FISH followed by IF.

ACKNOWLEDGEMENTS

I would like to thank Kevin Zhu for the contribution in the wild type lanes for H3K56ac and H3K9ac western blot analysis.

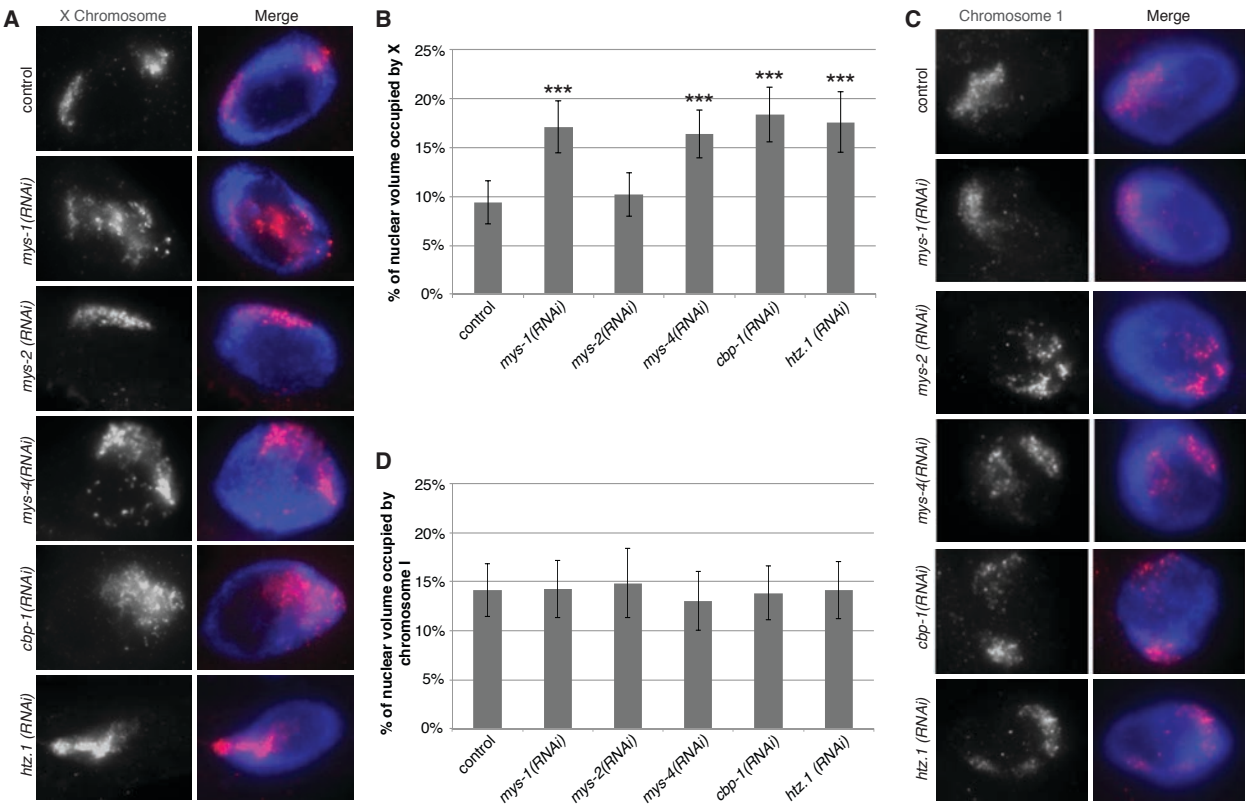

Figure 5.1 MYS-1, MYS-4, CBP-1 and HTZ-1 depletions have decondensed X chromosomes compared to wild type. (A-B) Adult hermaphrodite and HAT depleted intestinal nuclei stained with X-paint FISH (red) to label X chromosome territories and DAPI (blue) to label DNA. (A) Representative stained nuclei of wild type hermaphrodite and HAT depleted animals. (B) Quantification of the percentage of nuclear volume occupied by X in wild type (n = 40), *mys-1(RNAi)* (n = 36), *mys-2(RNAi)* (n = 45), *mys-4(RNAi)* (n = 40), *cbp-1(RNAi)* (n = 40), and *htz-1(RNAi)* (n = 37) hermaphrodites. Error bars indicate standard deviation. Asterisks indicate level of statistical significance by t-test analysis (***, $P < .001$). (C-D) Adult hermaphrodite and HAT depleted nuclei stained with chromosome I paint FISH (red) to label chromosome I territories and DAPI (blue) to label DNA. (C) Representative stained nuclei of wild type hermaphrodites and HAT depleted animals. (D) Quantification of the percentage of nuclear volume occupied by chromosome I in wild type (n = 20) *mys-2(RNAi)* (n = 21), *mys-4(RNAi)* (n = 40), *cbp-1(RNAi)* (n = 20), and *htz-1(RNAi)* (n = 20) hermaphrodites. Error bars indicate standard deviation.

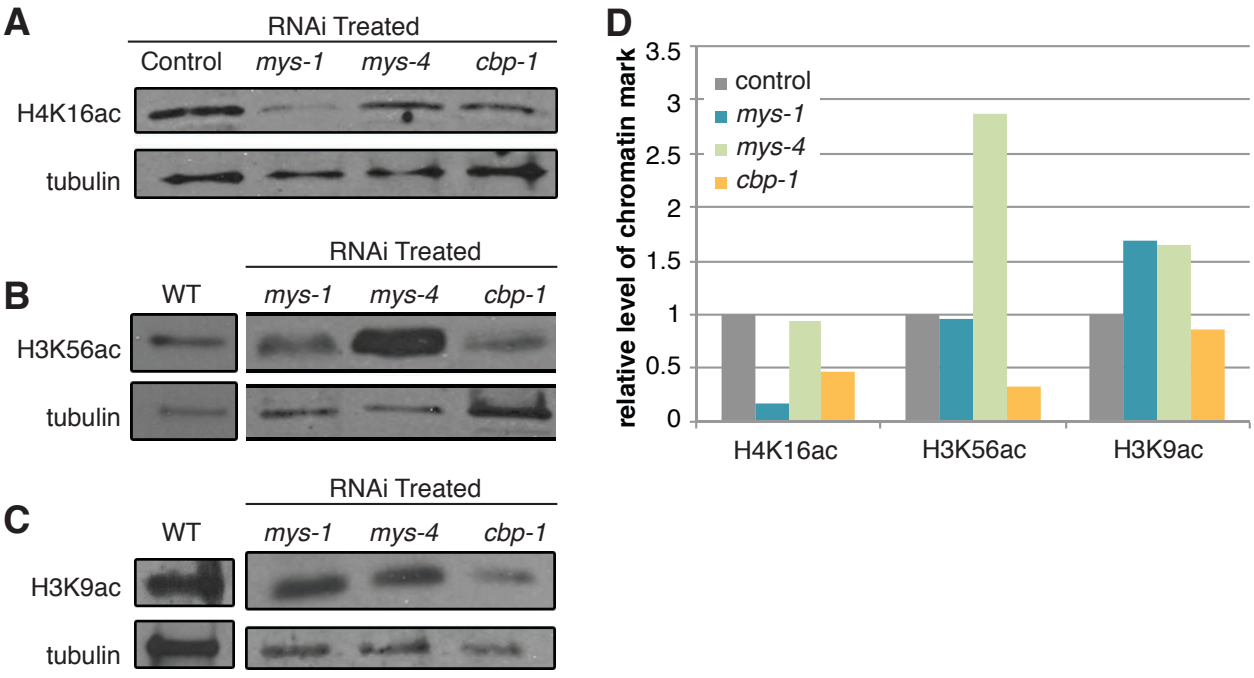

Figure 5.2 MYS-1 acetylates H4K16ac, while CBP-1 acetylates H3K56ac.
HAT levels were reduced be feeding RNAi in wild type worms. (A) H4K16ac, (B) H3K56ac, and (C) H3K9ac western blot analysis of adult RNAi treated worms. Tubulin is shown as a loading control. (D) Quantified band intensities normalized to tubulin.

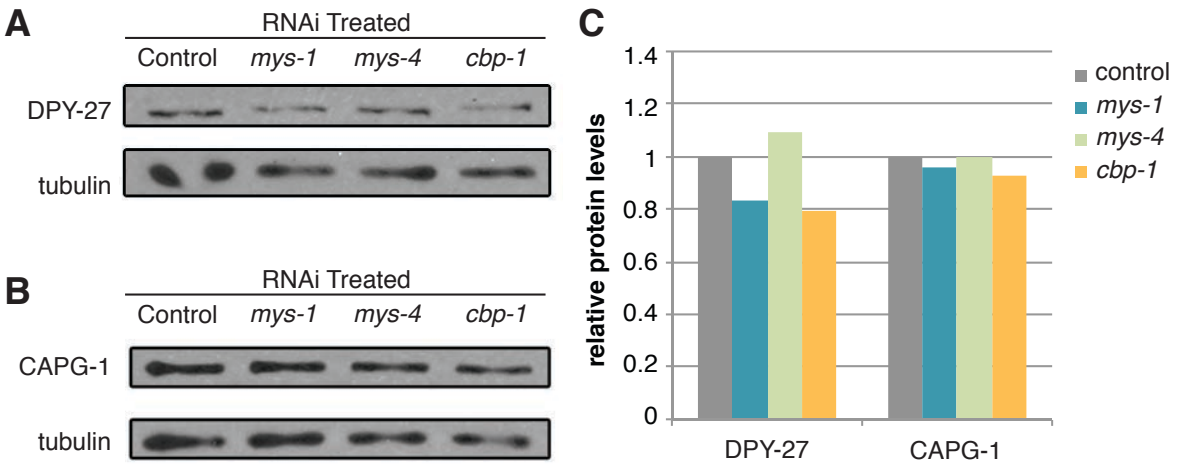

Figure 5.3 HAT depletions does not decrease DCC levels. HAT levels were reduced be feeding RNAi in wild type worms. An equal number of control vector, *mys-1(RNAi)*, *mys-4(RNAi)*, and *cbp-1(RNAi)* adult worms were collected for western blot analysis of observe levels of (A) DPY-21 and (B) CAPG-1 after RNAi depletion. Tubulin is shown as a loading control. (C) Quantified band intensities normalized to tubulin.

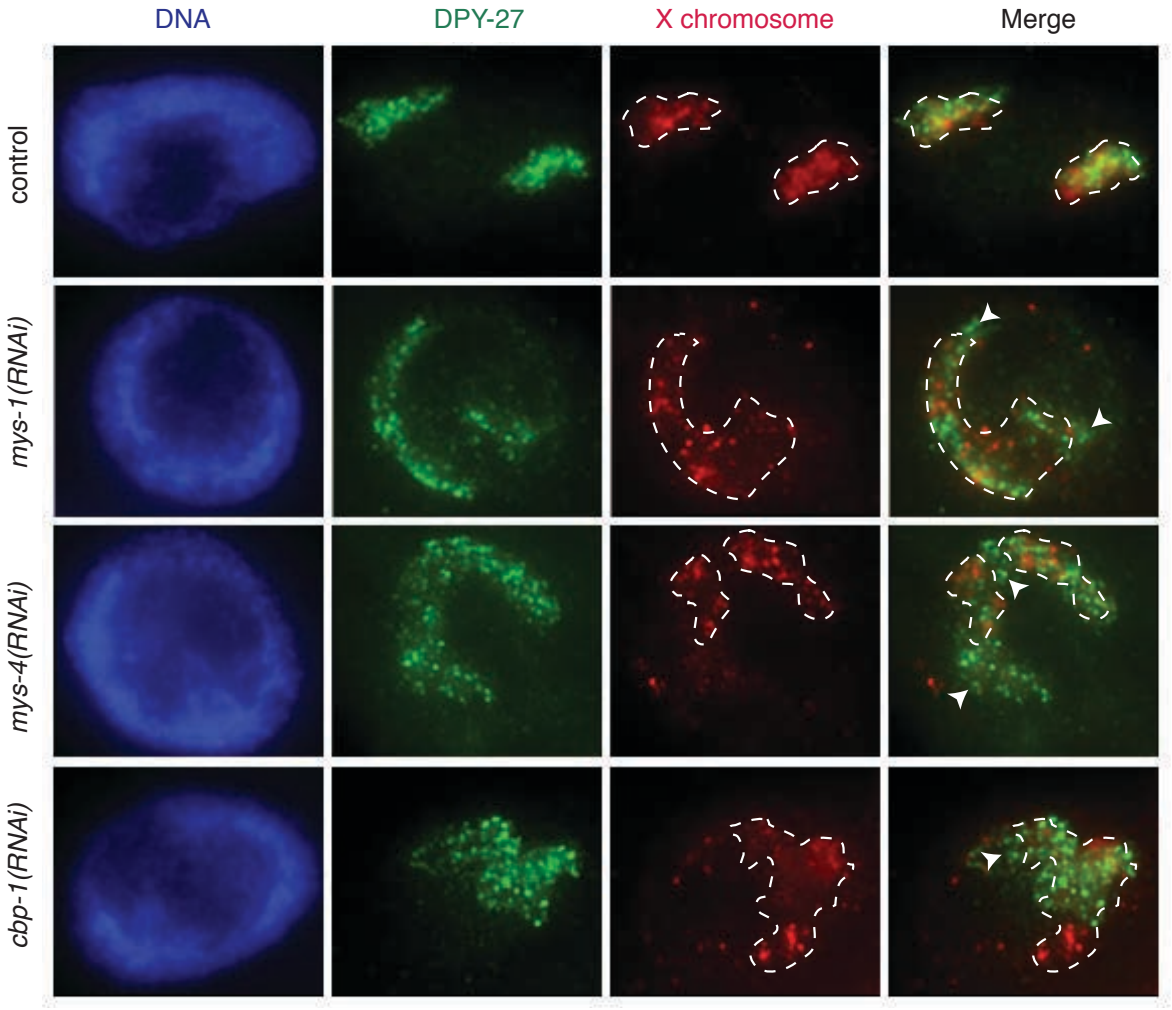

Figure 5.4 HATs depletion disrupts DCC restriction to the X chromosomes. Adult hermaphrodite and HAT depleted intestinal nuclei stained with DPY-27 (green) to label the DCC, X-paint FISH (red) to label X chromosome territories, and DAPI (blue) to label DNA. DCC localization to the X chromosome is disrupted in *mys-1(RNAi)*, *mys-4(RNAi)*, and *cbp-1(RNAi)* animals. White dashed lines outline the X chromosome. White arrowheads point out ectopic DPY-27 binding.

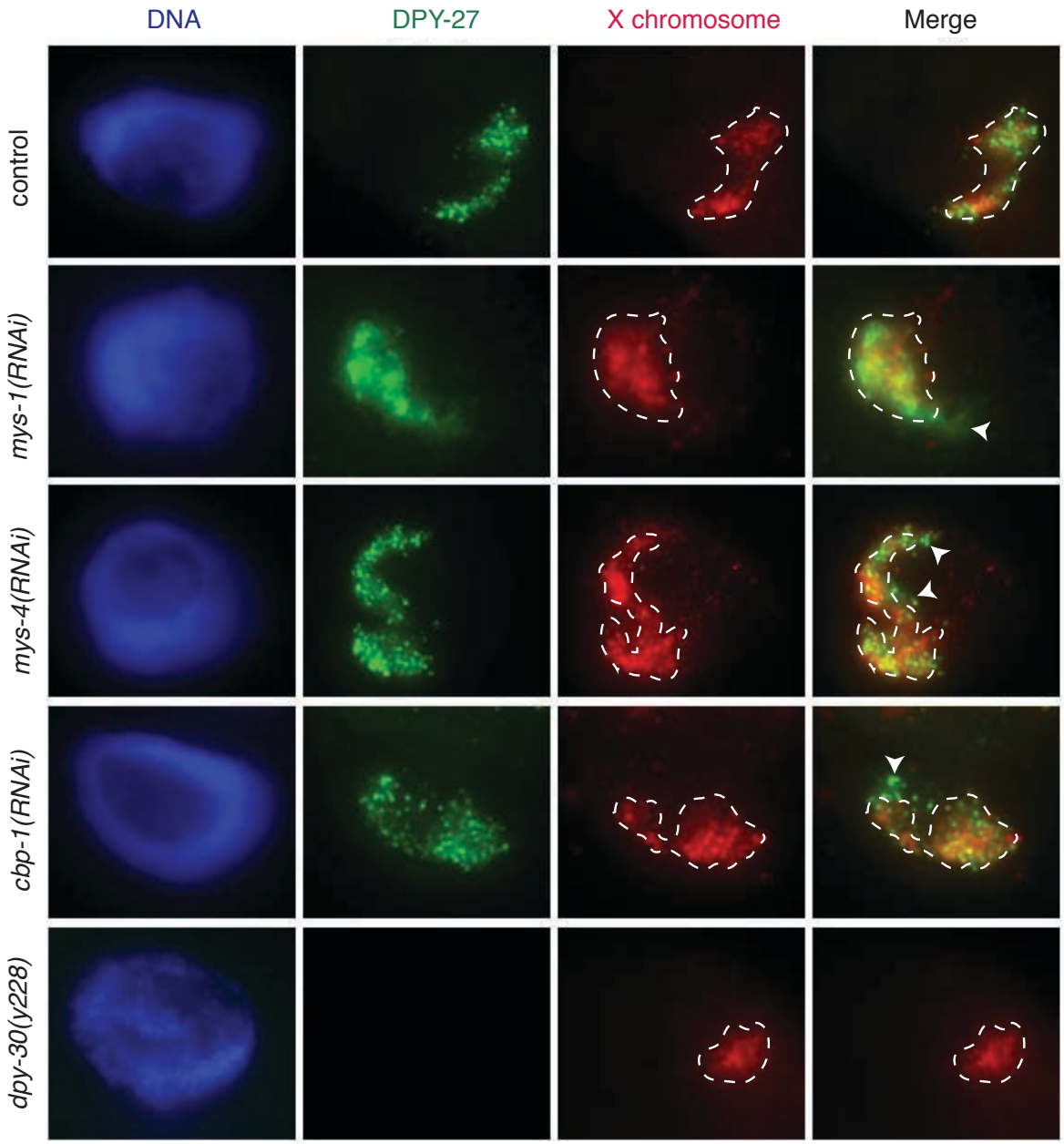

Figure 5.5 HATs are not required for the DCC to stably bind chromatin. DPY-27 (DCC) IF (green) and X-paint FISH (red) with detergent extraction in vector RNAi, *mys-1(RNAi)*, *mys-4(RNAi)*, *cbp-1(RNAi)*, and *dpy-30(y228)* hermaphrodite intestinal nuclei shows that DCC binding in HAT depletions are not sensitive to detergent treatment while *dpy-30* is sensitive. White dashed lines outline the X chromosome. White arrowheads point out ectopic DPY-27 binding.

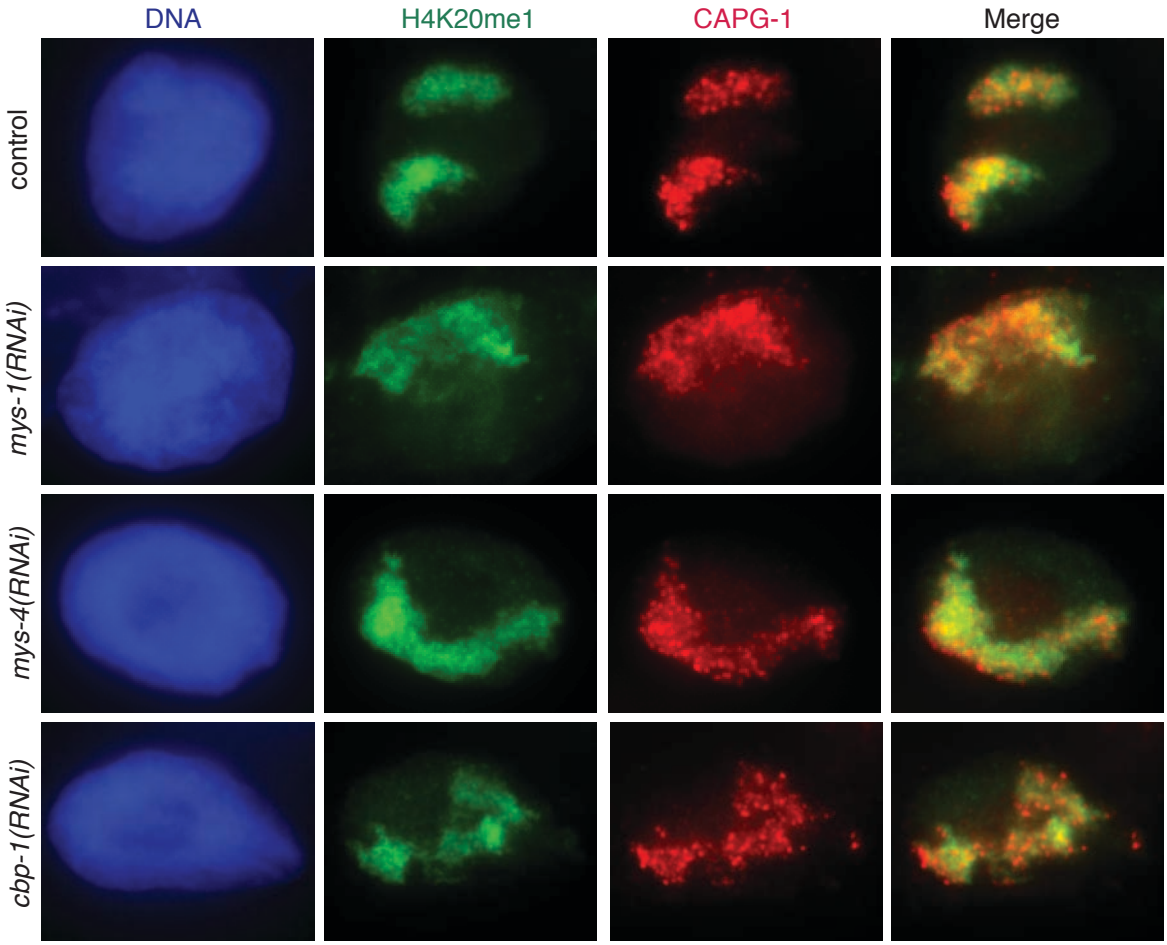

Figure 5.6 H4K20me1 enrichment is maintained and colocalizes with the DCC.
H4K20me1 IF (green) and CAPG-1 (DCC) IF (red) in vector RNAi, *mys-1(RNAi)*, *mys-4(RNAi)*, *cbp-1(RNAi)*, and hermaphrodite intestinal nuclei shows that H4K20me1 and DCC binding remains colocalized.

REFERENCES

1. Barakat TS, Gribnau J (2012) X chromosome inactivation in the cycle of life. Development 139: 2085-2089.
2. Conrad T, Akhtar A (2011) Dosage compensation in Drosophila melanogaster: epigenetic fine-tuning of chromosome-wide transcription. Nat Rev Genet 13: 123-134.
3. Lau AC, Csankovszki G (2015) Balancing up and downregulation of the C. elegans X chromosomes. Curr Opin Genet Dev 31: 50-56.
4. Meyer BJ (2010) Targeting X chromosomes for repression. Curr Opin Genet Dev 20: 179-189.
5. Leeb M, Wutz A (2010) Mechanistic concepts in X inactivation underlying dosage compensation in mammals. Heredity (Edinb) 105: 64-70.
6. Straub T, Becker PB (2011) Transcription modulation chromosome-wide: universal features and principles of dosage compensation in worms and flies. Curr Opin Genet Dev 21: 147-153.
7. Akhtar A, Becker PB (2000) Activation of transcription through histone H4 acetylation by MOF, an acetyltransferase essential for dosage compensation in Drosophila. Mol Cell 5: 367-375.
8. Smith ER, Pannuti A, Gu W, Steurnagel A, Cook RG, et al. (2000) The drosophila MSL complex acetylates histone H4 at lysine 16, a chromatin modification linked to dosage compensation. Mol Cell Biol 20: 312-318.
9. Akhtar A (2003) Dosage compensation: an intertwined world of RNA and chromatin remodelling. Curr Opin Genet Dev 13: 161-169.
10. Borsani G, Tonlorenzi R, Simmler MC, Dandolo L, Arnaud D, et al. (1991) Characterization of a murine gene expressed from the inactive X chromosome. Nature 351: 325-329.
11. Brockdorff N, Ashworth A, Kay GF, Cooper P, Smith S, et al. (1991) Conservation of position and exclusive expression of mouse Xist from the inactive X chromosome. Nature 351: 329-331.
12. Chaumeil J, Le Baccon P, Wutz A, Heard E (2006) A novel role for Xist RNA in the formation of a repressive nuclear compartment into which genes are recruited when silenced. Genes Dev 20: 2223-2237.
13. Zhao J, Sun BK, Erwin JA, Song JJ, Lee JT (2008) Polycomb proteins targeted by a short repeat RNA to the mouse X chromosome. Science 322: 750-756.
14. Hernandez-Munoz I, Lund AH, van der Stoop P, Boutsma E, Muijrers I, et al. (2005) Stable X chromosome inactivation involves the PRC1 Polycomb complex and requires histone MACROH2A1 and the CULLIN3/SPOP ubiquitin E3 ligase. Proc Natl Acad Sci U S A 102: 7635-7640.
15. Csankovszki G, Petty EL, Collette KS (2009) The worm solution: a chromosome-full of condensin helps gene expression go down. Chromosome Res 17: 621-635.
16. Vielle A, Lang J, Dong Y, Ercan S, Kotwaliwale C, et al. (2012) H4K20me1 contributes to downregulation of X-linked genes for C. elegans dosage compensation. PLoS Genet 8: e1002933.

17. Wells MB, Snyder MJ, Custer LM, Csankovszki G (2012) Caenorhabditis elegans dosage compensation regulates histone H4 chromatin state on X chromosomes. Mol Cell Biol 32: 1710-1719.
18. Lau AC, Nabeshima K, Csankovszki G (2014) The *C. elegans* dosage compensation complex mediates interphase X chromosome compaction. Epigenetics & Chromatin 7: 31.
19. Pferdehirt RR, Kruesi WS, Meyer BJ (2011) An MLL/COMPASS subunit functions in the C. elegans dosage compensation complex to target X chromosomes for transcriptional regulation of gene expression. Genes Dev 25: 499-515.
20. Lyon MF, Searle AG, Ford CE, Ohno S (1964) A Mouse Translocation Suppressing Sex-Linked Variegation. Cytogenetics 3: 306-323.
21. Lee JT, Davidow LS, Warshawsky D (1999) Tsix, a gene antisense to Xist at the X-inactivation centre. Nat Genet 21: 400-404.
22. Brown CJ, Ballabio A, Rupert JL, Lafreniere RG, Grompe M, et al. (1991) A gene from the region of the human X inactivation centre is expressed exclusively from the inactive X chromosome. Nature 349: 38-44.
23. Brown CJ, Hendrich BD, Rupert JL, Lafreniere RG, Xing Y, et al. (1992) The human XIST gene: analysis of a 17 kb inactive X-specific RNA that contains conserved repeats and is highly localized within the nucleus. Cell 71: 527-542.
24. Demakova OV, Kotlikova IV, Gordadze PR, Alekseyenko AA, Kuroda MI, et al. (2003) The MSL complex levels are critical for its correct targeting to the chromosomes in Drosophila melanogaster. Chromosoma 112: 103-115.
25. Gu W, Wei X, Pannuti A, Lucchesi JC (2000) Targeting the chromatin-remodeling MSL complex of Drosophila to its sites of action on the X chromosome requires both acetyl transferase and ATPase activities. EMBO J 19: 5202-5211.
26. Kelley RL, Wang J, Bell L, Kuroda MI (1997) Sex lethal controls dosage compensation in Drosophila by a non-splicing mechanism. Nature 387: 195-199.
27. Lyman LM, Copps K, Rastelli L, Kelley RL, Kuroda MI (1997) Drosophila male-specific lethal-2 protein: structure/function analysis and dependence on MSL-1 for chromosome association. Genetics 147: 1743-1753.
28. Palmer MJ, Richman R, Richter L, Kuroda MI (1994) Sex-specific regulation of the male-specific lethal-1 dosage compensation gene in Drosophila. Genes Dev 8: 698-706.
29. Morales V, Regnard C, Izzo A, Vetter I, Becker PB (2005) The MRG domain mediates the functional integration of MSL3 into the dosage compensation complex. Mol Cell Biol 25: 5947-5954.
30. Morales V, Straub T, Neumann MF, Mengus G, Akhtar A, et al. (2004) Functional integration of the histone acetyltransferase MOF into the dosage compensation complex. EMBO J 23: 2258-2268.
31. Richter L, Bone JR, Kuroda MI (1996) RNA-dependent association of the Drosophila maleless protein with the male X chromosome. Genes Cells 1: 325-336.
32. Jans J, Gladden JM, Ralston EJ, Pickle CS, Michel AH, et al. (2009) A condensin-like dosage compensation complex acts at a distance to control expression throughout the genome. Genes Dev 23: 602-618.

33. Ercan S, Dick LL, Lieb JD (2009) The C. elegans dosage compensation complex propagates dynamically and independently of X chromosome sequence. Curr Biol 19: 1777-1787.
34. Ercan S, Giresi PG, Whittle CM, Zhang X, Green RD, et al. (2007) X chromosome repression by localization of the C. elegans dosage compensation machinery to sites of transcription initiation. Nat Genet 39: 403-408.
35. Petty EL, Collette KS, Cohen AJ, Snyder MJ, Csankovszki G (2009) Restricting dosage compensation complex binding to the X chromosomes by H2A.Z/HTZ-1. PLoS Genet 5: e1000699.
36. Sterner DE, Berger SL (2000) Acetylation of histones and transcription-related factors. Microbiol Mol Biol Rev 64: 435-459.
37. Ceol CJ, Horvitz HR (2004) A new class of C. elegans synMuv genes implicates a Tip60/NuA4-like HAT complex as a negative regulator of Ras signaling. Dev Cell 6: 563-576.
38. Doyon Y, Selleck W, Lane WS, Tan S, Cote J (2004) Structural and functional conservation of the NuA4 histone acetyltransferase complex from yeast to humans. Mol Cell Biol 24: 1884-1896.
39. Cui M, Kim EB, Han M (2006) Diverse chromatin remodeling genes antagonize the Rb-involved SynMuv pathways in C. elegans. PLoS Genet 2: e74.
40. Shi Y, Mello C (1998) A CBP/p300 homolog specifies multiple differentiation pathways in Caenorhabditis elegans. Genes Dev 12: 943-955.
41. Ikura T, Ogryzko VV, Grigoriev M, Groisman R, Wang J, et al. (2000) Involvement of the TIP60 histone acetylase complex in DNA repair and apoptosis. Cell 102: 463-473.
42. Kimura A, Horikoshi M (1998) Tip60 acetylates six lysines of a specific class in core histones in vitro. Genes Cells 3: 789-800.
43. Smith ER, Eisen A, Gu W, Sattah M, Pannuti A, et al. (1998) ESA1 is a histone acetyltransferase that is essential for growth in yeast. Proc Natl Acad Sci U S A 95: 3561-3565.
44. Ogryzko VV, Schiltz RL, Russanova V, Howard BH, Nakatani Y (1996) The transcriptional coactivators p300 and CBP are histone acetyltransferases. Cell 87: 953-959.
45. Das C, Lucia MS, Hansen KC, Tyler JK (2009) CBP/p300-mediated acetylation of histone H3 on lysine 56. Nature 459: 113-117.
46. Csankovszki G, Collette K, Spahl K, Carey J, Snyder M, et al. (2009) Three distinct condensin complexes control C. elegans chromosome dynamics. Curr Biol 19: 9-19.
47. Petty E, Laughlin E, Csankovszki G (2011) Regulation of DCC localization by HTZ-1/H2A.Z and DPY-30 does not correlate with H3K4 methylation levels. PLoS One 6: e25973.
48. Crane E, Bian Q, McCord RP, Lajoie BR, Wheeler BS, et al. (2015) Condensin-driven remodelling of X chromosome topology during dosage compensation. Nature 523: 240-244.

49. Sharma R, Jost D, Kind J, Gomez-Saldivar G, van Steensel B, et al. (2014) Differential spatial and structural organization of the X chromosome underlies dosage compensation in C. elegans. Genes Dev 28: 2591-2596.
50. Pferdehirt RR, Meyer BJ (2013) SUMOylation is essential for sex-specific assembly and function of the Caenorhabditis elegans dosage compensation complex on X chromosomes. Proc Natl Acad Sci U S A 110: E3810-3819.
51. Reifsnyder C, Lowell J, Clarke A, Pillus L (1996) Yeast SAS silencing genes and human genes associated with AML and HIV-1 Tat interactions are homologous with acetyltransferases. Nat Genet 14: 42-49.
52. Fazzio TG, Huff JT, Panning B (2008) An RNAi screen of chromatin proteins identifies Tip60-p400 as a regulator of embryonic stem cell identity. Cell 134: 162-174.
53. Hiraga S, Botsios S, Donaldson AD (2008) Histone H3 lysine 56 acetylation by Rtt109 is crucial for chromosome positioning. J Cell Biol 183: 641-651.
54. Costanzi C, Pehrson JR (1998) Histone macroH2A1 is concentrated in the inactive X chromosome of female mammals. Nature 393: 599-601.
55. Weber M, Davies JJ, Wittig D, Oakeley EJ, Haase M, et al. (2005) Chromosome-wide and promoter-specific analyses identify sites of differential DNA methylation in normal and transformed human cells. Nat Genet 37: 853-862.
56. Cotton AM, Lam L, Affleck JG, Wilson IM, Penaherrera MS, et al. (2011) Chromosome-wide DNA methylation analysis predicts human tissue-specific X inactivation. Hum Genet 130: 187-201.
57. Wutz A (2011) Gene silencing in X-chromosome inactivation: advances in understanding facultative heterochromatin formation. Nat Rev Genet 12: 542-553.
58. Engreitz JM, Pandya-Jones A, McDonel P, Shishkin A, Sirokman K, et al. (2013) The Xist lncRNA exploits three-dimensional genome architecture to spread across the X chromosome. Science 341: 1237973.
59. Alekseyenko AA, Peng S, Larschan E, Gorchakov AA, Lee OK, et al. (2008) A sequence motif within chromatin entry sites directs MSL establishment on the Drosophila X chromosome. Cell 134: 599-609.
60. Kamath RS, Ahringer J (2003) Genome-wide RNAi screening in Caenorhabditis elegans. Methods 30: 313-321.
61. Nabeshima K, Mlynarczyk-Evans S, Villeneuve AM (2011) Chromosome painting reveals asynaptic full alignment of homologs and HIM-8-dependent remodeling of X chromosome territories during Caenorhabditis elegans meiosis. PLoS Genet 7: e1002231.
62. Csankovszki G, McDonel P, Meyer BJ (2004) Recruitment and spreading of the C. elegans dosage compensation complex along X chromosomes. Science 303: 1182-1185.

CHAPTER 6

Conclusions and Future Directions

CONCLUSIONS

Changes in gene dosage and chromosome copy number can lead to diseases, developmental abnormalities and are largely detrimental to all organisms. Most differences in chromosome copy number are not tolerated and are lethal. There are incidences of aneuploidies that are viable, however these changes have a dramatic impact on the development, fitness ad reproductive abilities of the organism [1]. Interestingly, in many species sex is determined by a chromosome-based method, resulting in a difference in X chromosome copy number between heterogametic males (XY or XO) and homogametic females (XX), as well as a natural aneuploidy within the heterogametic sex [2]. Specific mechanisms, known as dosage compensation mechanisms, have evolved to restore the balance within the genome and between males and females.

Dosage compensation mechanisms vary among species. In flies, the single X in males is upregulated two-fold [3]. In mammals and the worm *C. elegans*, X upregulation is hypothesized to occur in both sexes [4-6]. Although hypothesized about 50 years ago [7], only recently has evidence begun to emerge. This upregulation process corrects the natural aneuploidy within males, but hyperactivates the X chromosome in females/

hermaphrodites. Therefore in mammals, one X chromosome in females is inactivated [8], and in *C. elegans* both X chromosomes in hermaphrodites are downregulated two-fold by the dosage compensation complex (DCC) [9]. The DCC contains a condensin-like complex (condensin I^{DC}) similar to the canonical condensins that regulate chromosome compaction, organization, and segregation in mitosis and meiosis [10], suggesting that worm dosage compensation may involve changes of the X chromosome architecture.

The overall goal of my thesis work has been to further explore the connection between dosage compensation and chromatin organization. We sought to expand on the current understanding of condensin function in gene regulation as well as the role chromatin in X upregulation. Studying *C. elegans* condensin I^{DC}'s function in dosage compensation will shed further light on how condensin affects interphase chromosome organization and how the activities involved differ from condensin's function in mitosis. Additionally I have focused my work on understanding how X chromatin architecture and histone acetylation is involved in dosage compensation and changes in X-linked gene expression.

This work has contributed to the wider field of condensin biology. Condensin complexes have emerged as important regulators of chromatin organization throughout the cell cycle. Recent studies have revealed that in addition to their role in mitotic chromosome condensation and segregation, condensin complexes function in diverse interphase activities [11]. Emerging evidence has begun to connect mitotic condensin-mediated condensation with epigenetic control of gene expression. Although there is

increasing understanding of the biological functions of condensins in mitosis, meiosis, and in interphase, the molecular mechanism of condensin activity is still poorly understood. Since most of our current knowledge of the molecular mechanisms of condensin comes from analysis of condensin I in mitosis, it will be important to examine the mechanistic similarities and differences between the activities of condensins I and II, both in mitosis and interphase. Our study of *C. elegans* condensin I^{DC}'s function in mediating interphase X chromatin compaction in dosage compensation has led to a new understanding of how condensin affects interphase chromosome organization and how the activities involved differ from condensin's function in mitosis.

I first centered my experiments around 3D florescence *in situ* hybridization (FISH) examining the chromosome structure of the X and the autosome, chromosome I, in hermaphrodite interphase nuclei, in search of differences in levels of compaction that might be an indication that condensin I^{DC} regulates interphase X chromatin structure. I found that in hermaphrodites the X chromosome is much more compact relative to the autosomes. This led us to examine worms mutant for or depleted of DCC protein members. I in fact saw that without the DCC the X chromosome was decondensed and no longer compact to the level of wild type hermaphrodite X chromosomes. This X chromosome compaction was both sex-specific and DCC-specific. I also identified that the compaction of the X chromosome is not only dependent on the presence of the DCC but also the DCC regulated histone modifiers SET-1, SET-4, and SIR-2.1. This work is consistent with the long standing hypothesis that dosage compensated X chromosomes maintain some characteristics associated with condensed mitotic chromosome.

In addition to DCC regulated compaction, we found that X chromosome compaction is also disrupted when the mechanisms that anchor heterochromatin to the nuclear lamina are disrupted. This led us to analyze subnuclear localization of the X, and found that the chromosome relocates centrally both in the absence of the DCC and in tethering mutants. We also analyzed how anchoring proteins' activity of tethering heterochromatic regions to the nuclear lamina can affect gene expression during dosage compensation. Upon further study, we found that the changes in X chromosome structure and subnuclear localization are accompanied by a slight derepression of X-linked gene expression. This led us to the hypothesis that the tethering of the left arm of the X chromosome to the nuclear lamina forms a compact X structure, in which the DCC then uses the heteochromatin anchors to compact the entire X chromosome and bring it to the nuclear periphery, overall contributing to lower X-linked gene expression levels. However, we find there is a slight disconnect between condensation and subnuclear localization compared to gene expression. The DCC and tethering mutants have comparable effects on compaction and subnuclear localization, but very different effects on gene expression. Together this data gives us a better understanding how X chromosome architecture plays a role in gene regulation in dosage compensation.

While studying X chromosome architecture, in addition to finding that the X chromosome is compact in hermaphrodites due to DCC activities, we found the male X is decondensed relative to genome content. This study led me to explore X-lined gene regulation in males. I wanted to better understand the role of X chromosome decondensation in X-linked gene regulation and further explore the long hypothesized

mechanism of X-upregulation. To do this, I performed a 3D FISH screen depleting different histone acetyltransferases (HATs) to test for a change in X chromosome structure compared to wild type. I found that depleting MYS-1, led to a loss of X chromosome decondensation in males, while other HAT depletions did not alter X chromosome structure. MYS-1 is homologous to Tip60, however also distantly related to MOF, a key regulator in fly male X upregulation and decondensation. This similarity raised the possibility that MYS-1 could also have a key role in upregulation X-linked genes. Upon further characterizing MYS-1's role in X chromosome decondensation we found that MYS-1 acts in the context of a Tip60/NuA4-like complex, rather than in the content of MOF-MSL-like complex or MOF-NSL-like complex. I found that depleting the putative worm Tip60/NuA4 complex members, MRG-1 or SSL-1, in males lead to a compact X chromosome phenotype, similar to males depleted or mutant for MYS-1. We discovered that MYS-1 acetylates H4K16ac, therefore we established that the acetylation of the same mark in flies contributes to X chromosome decondensation in worms, despite being regulated by a different HAT.

Although, the H4K16ac HAT is a key component of X-linked gene upregulation in flies, we find that in worms the role of the H4K16ac HAT is much more limited. Interestingly when examining correlations between acetylation, compaction, and gene regulation we find that on the X chromosome H4K16ac and chromosome decondensation seem to correlate, but not on the autosomes. This suggests that H4K16ac and chromatin compaction are not always correlated. Additionally chromatin compaction and gene expression also do not necessarily correlate, as we found a

greater degree of X chromosome compaction compared to change in X-linked gene expression in MYS-1 depleted XO worms. Overall we find a factor, MYS-1, plays a role in the highly debated hypothesis suggesting that X upregulation occurs in *C. elegans* males. Although the high degree of compaction in a MYS-1 mutant does not perfectly correlate with the low level of change in gene expression, I showed that MYS-1 along with other Tip60-like complex members decondenses the X chromosome in *C. elegans* males and I believe that this decondensation contributes to upregulation of gene expression on the male X. I also present the first endogenous chromosome-wide data separating chromosome decondensation from gene regulation.

This work has contributed greatly to our current understanding of X upregulation. Although X upregulation is highly studied in flies, little is known about this mechanism in mammals and worms. Only recently has evidence emerged supporting this mechanism [4-6]. My work shows that H4K16ac and chromosome decondensation influence regulation of the male X chromosome, however other mechanisms must also play a role. This leads to the exploration on many other possible mechanisms for X regulation. It is possibility that in addition to MYS-1 activity, X upregulation could be achieved through the interactions between the male X and nuclear pore proteins, or through nucleosome occupancy, as X-linked gene promoters have higher nucleosome occupancy compared to autosomes [12]. Additionally I present work that contradicts the belief that acetylation, decondensation and gene regulation are correlated, leading us to think differently about how these three processes can be related.

From here, we speculated that if MYS-1 is upregulating, while the DCC is downregulating, then a hermaphrodite defective of both processes should essentially by fine. However, when I sought to see how MYS-1 was functioning in hermaphrodites, this is not what I found, partly because MYS-1 only plays a partial role in upregulation, and partly because HATs also affect DCC localization. I found that the depletion of MYS-1, MYS-4 or CBP-1 disrupted the compact X chromosome structure. In addition these HATs do not affect DCC expression. I found that MYS-1, MYS-4 and CBP-1 are required for proper DCC localization to the X chromosome. In all, these results suggest that HAT proteins play a critical role in targeting the DCC to the X chromosome, by preventing the DCC from spreading to the autosomes. However, when the HATs are depleted the DCC ectopically binds to the autosomes, which reduces the amount of DCC binding to the X chromosomes.

In total, my thesis work illustrates the role of both condensin and chromatin in regulating X chromosome architecture and represents a greater understanding in our knowledge of *C. elegans* dosage compensation. My work utilizes a variety of genome-wide methods, both at a high resolution (ChIP-seq and RNA-seq) and at a low resolution (FISH and immunofluorescence), to explore DCC function and regulation. In full, I have provided evidence that changes in higher order organization of the X chromosome plays a role both condensin I^{DC} mediated repression and X upregulation.

PROPOSED FUTURE DIRECTION

My work has provided the first evidence linking condensin-mediated chromosome compaction to chromosome-wide repression of gene expression as well as presented

novel work that supports the long debated hypothesis of X-upregulation; however there is still a lot more to learn about chromatin's role in gene regulation and the mechanism driving X upregulation. In the following section I will briefly describe future experimental aims that can address some of the new questions my work on condensin and chromatin mediated X chromosome architecture has raised. Experiments done in the future will identify the machinery responsible for X decondensation in males. In Chapter 4, I have shown that MYS-1, MRG-1 and SSL-1 are all involved in decondensing the male X, however it will be important to determine whether these three proteins are acting in the same complex in males and if there are other proteins within this complex. In addition to the genetic evidence that MYS-1, MRG-1 and SSL-1 are involved in regulating the volume of the X chromosome in males, I have found that depleting MRG-1 leads to reduced levels of MYS-1, while depleting MYS-1 leads to reduced levels of MRG-1 (Figure 6.1). This provided more evidence that MYS-1 and MRG-1 may be acting in the same complex. I expect there would be positive interactions between the three proteins, as MYS-1, SSL-1 and MRG-1 homologs are present in a Tip60-like complex in other organisms. Overall this will give us more insight into the machinery responsible for decondensing the single male X chromosome. Additionally we know that MYS-1/Tip60 activity is not the only factor involved in X upregulation it would be interesting to see what other factors could also contribute to this process.

To further characterize the role HATs may have in DCC localization it will be important to examine DCC mislocalization by HAT knockdown, assayed at high-resolution genome wide. Results detailed in Chapter 5 suggest that HATs and histone

acetylation play an important role in DCC localization. Future experiments will reveal unique DCC binding sites in hermaphrodite worms depleted of MYS-1, MYS-4 or CBP-1 compared to wild type hermaphrodites. I suspect that in HAT knockdowns DCC binding will decrease at known binding sites on the X chromosome and increase at other sites specifically on the autosomes. In addition to DCC localization it would be important to analyze gene expression changes to determine whether there is a direct correlation between the X chromosome regions that lose DCC binding and expression changes on nearby genes. It would also be interesting to see whether the mislocalized ectopic DCC in the autosomes leads to lower levels of gene expression. Overall this study will give us a better understanding of whether DCC mislocalization in HAT knockdowns also leads to greater changes in gene expression.

In conclusion, my work has provided the first evidence for two separate predominant, in *C. elegans* dosage compensation. I have linked condensin-mediated chromosome compaction to chromosome-wide repression of gene expression and uncovered that changes in higher order organization of the X chromosome plays a role in both X upregulation and condensin I^{DC} mediated repression. I have also presented the first endogenous chromosome-wide data separating the degree of decondensation from the level of gene expression, challenging the paradigm that acetylation, chromosome architecture, and gene regulation are perfectly correlated.

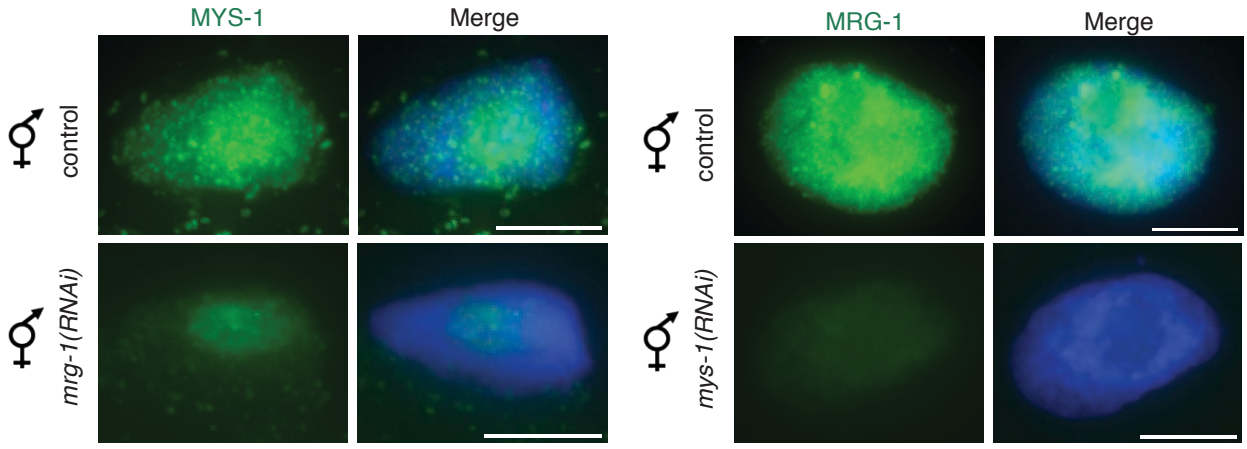

Figure 6.1 Depletion of MRG-1 leads to reduced levels of MYS-1 and vise versa. Hermaphrodite worms depleted of MRG-1 or MYS-1 stained by immunofluorescence with either MYS-1 or MRG-1 show reduced level of protein compared to control.

REFERENCES

1. Torres, E.M., Williams, B.R., and Amon, A. (2008). Aneuploidy: cells losing their balance. Genetics *179*, 737-746.
2. Deng, X., and Disteche, C.M. (2010). Genomic responses to abnormal gene dosage: the X chromosome improved on a common strategy. PLoS biology *8*, e1000318.
3. Conrad, T., and Akhtar, A. (2011). Dosage compensation in Drosophila melanogaster: epigenetic fine-tuning of chromosome-wide transcription. Nature reviews. Genetics *13*, 123-134.
4. Deng, X., Berletch, J.B., Ma, W., Nguyen, D.K., Hiatt, J.B., Noble, W.S., Shendure, J., and Disteche, C.M. (2013). Mammalian X upregulation is associated with enhanced transcription initiation, RNA half-life, and MOF-mediated H4K16 acetylation. Developmental cell *25*, 55-68.
5. Deng, X., Hiatt, J.B., Nguyen, D.K., Ercan, S., Sturgill, D., Hillier, L.W., Schlesinger, F., Davis, C.A., Reinke, V.J., Gingeras, T.R., et al. (2011). Evidence for compensatory upregulation of expressed X-linked genes in mammals, Caenorhabditis elegans and Drosophila melanogaster. Nature genetics *43*, 1179-1185.
6. Gupta, V., Parisi, M., Sturgill, D., Nuttall, R., Doctolero, M., Dudko, O.K., Malley, J.D., Eastman, P.S., and Oliver, B. (2006). Global analysis of X-chromosome dosage compensation. Journal of biology *5*, 3.
7. Ohno, S. (1967). Sex Chromosomes and Sex-Linked Genes. Berlin: Springer, 1-140.
8. Wutz, A. (2011). Gene silencing in X-chromosome inactivation: advances in understanding facultative heterochromatin formation. Nature reviews. Genetics *12*, 542-553.
9. Lau, A.C., and Csankovszki, G. (2015). Balancing up and downregulation of the C. elegans X chromosomes. Current opinion in genetics & development *31*, 50-56.
10. Csankovszki, G., Collette, K., Spahl, K., Carey, J., Snyder, M., Petty, E., Patel, U., Tabuchi, T., Liu, H., McLeod, I., et al. (2009). Three distinct condensin complexes control C. elegans chromosome dynamics. Current biology : CB *19*, 9-19.
11. Lau, A.C., and Csankovszki, G. (2014). Condensin-mediated chromosome organization and gene regulation. Frontiers in genetics *5*, 473.
12. Ercan, S., Lubling, Y., Segal, E., and Lieb, J.D. (2011). High nucleosome occupancy is encoded at X-linked gene promoters in C. elegans. Genome research *21*, 237-244.